3-D HYBRID EULERIAN-LAGRANGIAN / PARTICLE TRACKING MODEL FOR SIMULATING MASS TRANSPORT IN COASTAL WATER BODIES

by

Konstantina Dimou

Diploma, National Technical University, Athens
(1987)
S.M., Massachusetts Institute of Technology
(1989)

Submitted to the Department of Civil Engineering
in partial fulfillment of the requirements
for the degree of
DOCTOR OF PHILOSOPHY
at the
MASSACHUSETTS INSTITUTE OF TECHNOLOGY
May, 1992

Signature of Author _____.
Department of Civil Engineering
May 15, 1992

Certified by _____.
E. Eric Adams
Lecturer, Department of Civil Engineering
Thesis Supervisor

Accepted by _____.
Eduardo Kausel
Chairman, Departmental Committee on Graduate Students

3-D Hybrid
Eulerian-Lagrangian / Particle Tracking Model
for Simulating Mass Transport
in Coastal Water Bodies

by

Konstantina Dimou

Submitted to the Department of Civil Engineering
on May 15, 1992, in partial fulfillment of the
requirements for the degree of
Doctor of Philosophy

Abstract

The purpose of this research is the development and analysis of a three-dimensional finite-element Eulerian-Lagrangian / particle tracking model for the simulation of passive pollutant transport in coastal areas. Particular emphasis is given on the simulation of pollution sources (e.g. outfalls) whose spatial extend is small compared to that of the domain discretization. A hybrid particle tracking / Eulerian-Lagrangian method is developed and analyzed for the simulation of small scale sources: Mass discharge from the source is modeled by the release of particles. When the standard deviation of the particle distribution reaches a length scale of the order of the grid scale particle locations are mapped onto node concentrations and the calculations proceed in the Eulerian-Lagrangian mode. A technique for the interfacing of the particle tracking mode and the Eulerian-Lagrangian mode is developed. The developed method for the simulation of sources is applied for the simulation of outfalls in coastal water problems. The issue of consistently modeling the intermediate flow field around the diffuser is investigated. In order to demonstrate the performance of the developed model it is applied in Massachusetts Bay.

Thesis Supervisor: E. Eric Adams
Title: Lecturer

Acknowledgments

I am most thankful to my advisor Dr. E. Eric Adams for his constant help and support and for the educational opportunity, that he provided me. My sincere thanks goes to Professor Antonio M. Baptista and Professor Donald R. F. Harleman for their direction and many helpful suggestions through this work.

The Parsons Lab has been a most enjoyable work place. Pat Dixon takes all the praise for creating this warm environment. I especially thank my friends at the Lab Hari, Shawn and Maria, Nalin, John, Paul, Kaye, Lynn and Fernando for their support particularly during the last difficult months.

I would like to thank my sister, Christina, for undertaking these overseas trips, whenever I needed her presence. It is never easy to combine life at MIT with family life. To my husband, Kostas, who has seen me through five years at MIT from my first day here, I give my love and thanks and wish him success in his academic endeavors.

And to my parents Xenophon and Sia Dimou, words fall too short of expressing my appreciation. I hope that my son, George, will be as proud of me as I am of them.

This research was supported by the MIT Sea Grant College Program, National Oceanic and Atmospheric Administration, US Dept. of Commerce under Grant NA90AA-D-SG424.

Contents

List of Figures

List of Tables

Chapter 1

Introduction

1.1 Motivation-Objectives

In order to simulate the fate of passive pollutants in a water body two models must be used: a circulation or hydrodynamic model (HM), that simulates the movement of water, and a water quality model (WQM), that simulates the movement, transformation, and interaction of pollutants within the water. In order to make the system more flexible we can let the movement of the pollutant, i.e., advection, turbulent diffusion, and when spatial averaging is included, dispersion to be handled by a third model called a transport model (TM). According to the above we have the following framework (Fig 1-1):

- a HM that solves the continuity and momentum equations and the mass conservation equation for salinity and temperature
- a TM that accounts for advective/dispersive motion of passive constituents
- a WQM that accounts for transformation (or reactive) processes of all water quality parameters simulated. Transformation processes may be physical, chemical, or biological. Examples of these processes are the sedimentation and flocculation of organics, the assimilative capacity of a water body to receive an acid waste discharge, and the predator-prey relationship of zooplankton-

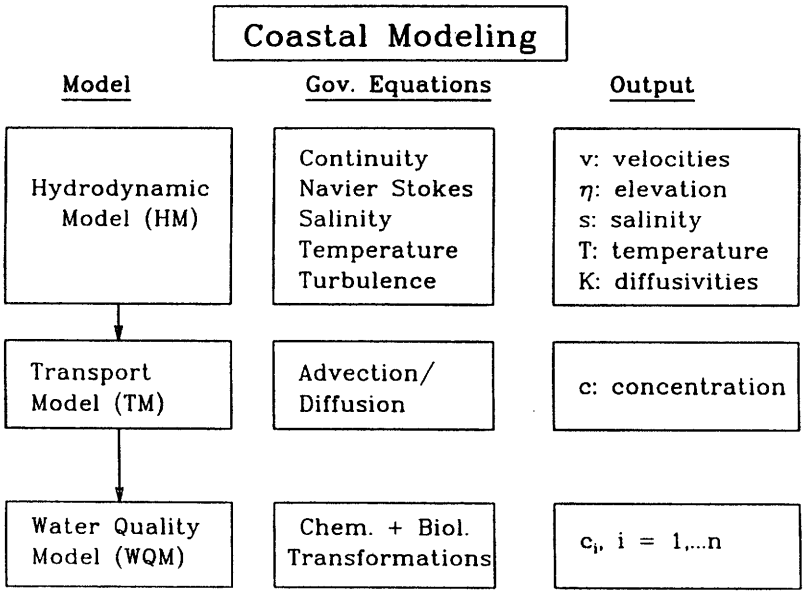

Figure 1-1: Modeling of Coastal Processes.

phytoplankton. In order to make the WQM as flexible as possible water quality processes should be represented in special subroutines so that easy substitution or addition of subroutines by the user is permitted.

Each of these models differs from the others in the physical and mathematical character of the equations it is solving and also in the numerical techniques it is using in solving these equations. The time and space scaling is different and as a result of that the required time- and space discretization in each of these models makes it difficult for them to be coupled. In order to have an efficient computational framework the following two criteria have to be met:

- accuracy and efficiency of each model
- efficient coupling of the models

Since the TM is in the middle of the model framework it bears the task of efficiently coupling itself to the HM and the WQM.

The objective of this study is the development and analysis of a TM, that would meet the requirements for modeling transport in surface water problems in an accurate and efficient way and also efficiently couple with a HM and a WQM.

The development and analysis of the TM focuses on two main issues, that constitute the characteristics of mass transport in coastal waters:

- the modeling of highly advective flows and
- the modeling of sources (e.g. outfalls) whose extent is small compared to the domain scale

The coupling issue between the TM and the HM is primarily related to the small time step used in the HM due to stability requirements. This results in

- high storage requirements and

- a need for incorporating the small time step velocity and turbulent diffusion coefficient output of the HM into the TM, that can use at least an order of magnitude larger time steps

This research includes a review of methods used in the past for interfacing a HM, that generates small time step velocity output with a TM, that can use larger timesteps. A method is proposed for efficiently coupling a HM with the developed TM.

1.2 Scope

Based on the objective of having a self-contained transport model, that would meet the requirement of accurate and computationally efficient modeling of coastal water mass transport processes and that would also be coupled with a HM and a WQM in an efficient manner, the following computational framework was chosen.

A 3-D hybrid particle tracking/Eulerian-Lagrangian finite element model was developed. The particle tracking approach is used for the simulation of outfalls or other pollution sources, whose extent is small compared to the discretization of the computational domain. The Eulerian-Lagrangian approach is justified by two reasons. First, by the fact that in surface water problems the modeler is dealing with highly advective flows, and so he is severely constrained by the Courant number requirement. Eulerian-Lagrangian models are based on the splitting of the operator into an advective and a diffusive component. The advective component is solved with the backwards method of characteristics, that allows for large Courant numbers, whereas the diffusive component results in a symmetric diagonally dominant system, that can easily be solved. The second reason is that the use of the backwards method of characteristics is ideal for coupling the TM with the HM and the WQM respectively. The small time step velocity output from the HM is averaged automatically by the model because of the Lagrangian character of the advection part, i.e., the model

automatically averages in a Lagrangian sense short time velocity data to compute the position of the characteristic lines. The separate treatment of the advective and diffusive component in the TM allows the user to efficiently model transformation processes (WQM) with different time scales. The finite element approach is justified by the fact that in surface water problems the modeler is dealing with highly irregular domains.

The computational strategy for simulating small scale sources (e.g. outfalls) is the following:

Sources and their extent are identified in the discretized domain used in the HM. When the extent of a source is of the order of several times the grid scale a certain concentration distribution is assigned in the region, where the source is located and the Eulerian-Lagrangian computational scheme is used. When the extent of a source is small compared to the grid scale the full hybrid particle tracking/Eulerian-Lagrangian finite element model is used. Sources are represented by the release of particles. The displacement of these particles consists of two components: an advective component and a diffusive/random walk component. The advective component results from the velocity field generated by the HM and the intermediate velocity field due to the presence of the source, which extends in a region of the order of several grid scales around the outfall. When the standard deviation of the particle distribution reaches a certain value particles are mapped onto nodal concentrations and the calculations continue in the Eulerian-Lagrangian computational scheme.

Due to the hybrid character of this model there are three main areas that deserve analysis:

- the Eulerian-Lagrangian mode
- the particle tracking mode
- the interfacing between the two modes

At every time step in the Eulerian-Lagrangian calculations three numerical calcu-

lation steps are taking place: backwards integration and interpolation that constitute the advection part and solution of the diffusion part. Each of these procedures generates a numerical error. Accuracy and efficiency of the ELM require minimization and balance of the errors. The numerical issues here are the selection of the integration scheme for the tracking, the interpolation functions, the order of the time discretization in the solution of the diffusion part, the numerical scheme for the solution of the diffusion part and the selection of the solver for the solution of the symmetric, positive definite system of linear equations resulting from the discretization of the diffusion equation.

In terms of the selection of the interpolation functions, the order of the time discretization, and the numerical scheme for the solution of the diffusion part, the choices made by Baptista in the two dimensional transport model ELA (Eulerian-Lagrangian Analysis; 1984) that were supported by the one dimensional analysis in Baptista (1987) were followed with slight modifications due to the three dimensionality of this model.

Previous studies (Zhang, 1990) have shown that by far the most expensive part in ELA (1984) is the tracking of the characteristic lines. This study thoroughly investigates the issue of strategy followed in the tracking part and draws useful conclusions. Due to the dimensionality of the developed TM the choice of the solver for the solution of the diffusion part is of particular importance from a cost point of view. After performing a brief cost analysis of direct methods the use of an iterative solver is preferred. Because of the three dimensionality of the problem the resulting matrix is strongly diagonal dominant and so a diagonal preconditioner is used.

The issue of interfacing the particle mode with the Eulerian-Lagrangian mode is very interesting. It is investigated from two points of view: as the general problem of interfacing a particle model with a concentration model and as the specific problem encountered in the hybrid model developed in this study. Methods of mapping particles onto node concentrations used by other researchers (e.g. Bagtzoglou et al.,

1991) are compared to the finite element method developed in this research. Part of the interfacing issue is also the question of when it should take place i.e., what should the value of the standard deviation of the particle distribution be in order to map particles onto node concentrations. This issue is very much related to the number of particles, that are employed and is thoroughly investigated in this study. This mixed particle tracking approach is compared to a concentration model approach in a 1-D case.

The final part of this study is devoted to the simulation of outfalls in realistic applications in coastal water regions. The general procedure described above is applied. One may define two flow regions around the diffuser: the near flow field, that extends in a region of the order of the water depth around the diffuser and where rapid mixing takes place, and the intermediate flow field, that extends in a region of the order of hundreds of meters around the diffuser equal to the extend of the resulting plume. A method is developed for simulating the intermediate flow field based on initial dilution S_{in} and trapping level z_{tr} from a near flow field model (e.g., EPA models, Muellenhoff et al, 1985). Apart from the fact that this method enables us to consistently represent the intermediate flow field it also allows us to model intermediate flow field processes e.g., the region of initial deposition of particles from sewage effluent or the vertical exchange of constituents such as nutrients.

In order to show how the model performs in a real world case the Massachusetts Bay application was chosen. It is used for demonstration purposes only and should not be regarded as an attempt to calibrate the model. The calibration of the model using collected data goes beyond the scope of this study and is part of the future work. The HM by Lynch et al (1991) was used to drive the Massachusetts Bay calculations. It is a 3-D harmonic, finite element model. The model is limited to the linearized equations with an externally specified density field. A linearized partial-slip condition is forced at the bottom. The spatial distribution of the viscosity and bottom stress coefficients is at the discretion of the user. The use of this particular HM imposed certain constraints on the use of the developed TM i.e. harmonic velocity input,

sigma coordinate system and diagnostic density field. Considerable effort was made to develop a robust TM that could easily be modified in order to be used with other HM i.e. stepping models, HM that use cartesian coordinates etc.

1.3 Organization of Study

This work is organized in seven chapters including the introductory chapter.

Chapter 2 gives a general overview of transport models and discusses in detail the coupling between a TM and a HM. The equations governing transport in coastal waters are presented. In the first part the transport equation is presented, an overview of numerical techniques used for the solution of the transport equation is given and their compatibility to coastal transport problems is discussed. The choice of the coordinate system (i.e Cartesian vs. sigma coordinate system) is also discussed. In the second part the coupling issue between the circulation model and the transport model is discussed. A general overview of coupling methods is presented. The methods of tidal dispersion coefficients, Lagrangian residual currents and Eulerian-Lagrangian approach are described and compared. Particular emphasis is given to the comparison between the Lagrangian residual currents method and the Eulerian-Lagrangian method. The Lagrangian residual currents method was used in the recent 3-D application in Cheasapeake Bay (Dortch, 1990). The Eulerian-Lagrangian approach as a method to couple the TM with the HM has never been used before and is proposed by this research as the optimal method for this purpose.

In Chapter 3 the 3-D Eulerian-Lagrangian model developed in this study is analyzed. The main issues associated with the solution of the advective part (i.e., the integration scheme for the tracking, the interpolation functions, the order of the time discretization) and the diffusive part (i.e., the choice of the basis functions and the solver) are presented and the choices made in this study are justified. The choice of an optimal time step is also addressed.

In Chapters 4 and 5 a methodology is presented for representing sources that are small compared to the grid discretization. The methodology entails using a hybrid particle tracking/concentration model, in which mass released from sources is represented by particles at earlier stages and is then mapped onto node concentrations when the standard deviation of their distribution exceeds a certain value. Chapter 4 includes a general discussion of the method and compares the model to a concentration based model. Criteria for selecting the number of particles, the size of the time step and the time of transition between particle and concentration mode are addressed. In Chapter 5 different techniques for mapping particles onto node concentrations are considered and a new approach based on a finite element error minimization is presented. Chapters 4 and 5 constitute independent papers and therefore have parts in common.

In Chapter 6 the methodology developed in this study for simulating outfalls in coastal water problems is applied in two applications involving Massachusetts Bay. The method developed in this study for the representation of the intermediate flow field based on data from the near flow field is presented and analyzed. A demonstration application of the model to Massachusetts Bay is presented.

Chapter 7 concludes the thesis summarizing the major findings and contributions of this work.

1.4 REFERENCES

1. Bagtzoglou, A. C., A. B. Tompson, D. E. Dougherty. Projected functions for particle grid methods. Num. Meth. for Partial Diff. Equations (to appear). 1991.

2. Baptista, A. M. Solution of advection-dominated transport by Eulerian-Lagrangian methods using the backwards method of characteristics. Ph. D. thesis. Dept. of Civil Engineering. MIT. 1987.

3. Dortch, M. S., R. S. Chapman. 1989. Interfacing time-varying, three-dimensional

hydrodynamic model output for Cheasapeake Bay water quality model. Proc. Estuarine and Coastal Modeling 1989, ASCE.

4. Lynch, D. R., F. E. Werner, D. A. Greenberg, J. W. Loder. Diagnostic model for baroclinic, wind-driven and tidal circulation in shallow seas. Continental Shelf Research. 1991 (to appear).

5. Muellenhof, W. P., et al. Initial mixing characteristics of muicipal ocean discharges Volume 1: Procedures and applications. Pacific Division Environmental Research Laboratory, Narragansett Office of Research and Development, U. S. EPA, Newport, Oregon 97365. EPA -600/3-85-073a. 1985.

Chapter 2

Overview of Transport Models - Coupling Issue between Transport Model and Hydrodynamic Model

2.1 General

This chapter acts as a general overview chapter. As mentioned in Chapter 1 the transport model (TM) depends for input on the hydrodynamic model (HM). According to this in developing a TM one is interested not only in the TM itself but also in coupling it with the HM. This chapter overviews TMs and also discusses in detail the coupling issue with the HM.

In the first part the transport equation and its features are described. A general overview of transport models is given and the particular reasons, that lead to the choice of an Eulerian-Lagrangian model are described. Because of the presence of a moving water surface boundary the choice of the coordinate system is of particular importance. The σ coordinate system with its advantages and disadvantages is presented.

In the second part of this chapter a general overview of hydrodynamic models

is given. The interfacing of the two models is investigated. The main issue here is how to incorporate the small time step velocity output of the HM into the TM, that can use an order of magnitude larger time steps. The methods of tidal dispersion coefficients, Lagrangian residual currents and Eulerian-Lagrangian methods are described and compared. Particular emphasis is given to the comparison between the Lagrangian residual currents method and the Eulerian-Lagrangian method. The Lagrangian residual currents method was used in the only known 3-D application to Chesapeake Bay (Dortch, 1990). The Eulerian-Lagrangian approach as a method to couple the TM with the HM has never been used before and is proposed by this research as the optimal method for this purpose.

2.2 Transport Model - Governing Equations

A transport model (TM) solves a form of the following equation:

$$\frac{\partial c}{\partial t} + \nabla \cdot \mathbf{v}c = \nabla \cdot \mathbf{K} \cdot \nabla c + Q \tag{2.1}$$

where c(x,t) is the concentration, $\mathbf{v}$(x,t) is the velocity vector, $\mathbf{K}$(x,t) is the diffusivity tensor and Q represents point sources/sinks.

There are two main problems associated with the solution of this equation:

- The upper vertical boundary of the problem (surface) is moving and so a moving boundary condition has to be implemented.
- The advective terms are often more important than the diffusive terms .

2.3 Types of Transport Models

2.3.1 Concentration versus Particle Tracking Models

Transport models can be classified into two main categories:

- Concentration models, where Eqn 2.1 is directly solved. Here the dependent variable of concentration is advected and diffused. Concentration models can be classified as Eulerian, Lagrangian and Eulerian-Lagrangian. A thorough literature review is given by Neuman (1981) and Baptista (1987). Nguyen and Martin (1988) review concentration models used specifically for the simulation of transport in estuary and coastal waters. In this chapter (Sections 2.3.2, 2.3.3, 2.3.4) a short review on the use of concentration models in surface water problems is given with a particular emphasis on Eulerian-Lagrangian models.

- Particle tracking models, where mass is represented by discrete particles. At each time step the displacement $\Delta \mathbf{x}$ of each particle consists of an advective, deterministic component and an independent, random Markovian component given by the equation (Gardiner, 1985; Tompson and Gelhar, 1990)

$$\Delta \mathbf{x} = \mathbf{X}^n - \mathbf{X}^{n-1} = \mathbf{A}(\mathbf{X}^{n-1}, t)\Delta t + \mathbf{B}(\mathbf{X}^{n-1}, t)\sqrt{\Delta t}\mathbf{Z} \tag{2.2}$$

where $\mathbf{A}$ and $\mathbf{B}$ are given by the expressions:

$$\mathbf{v} = \mathbf{A} - \nabla(\frac{1}{2}\mathbf{B}\mathbf{B}^T) \quad , \tag{2.3}$$

$$\mathbf{K} = \frac{1}{2}\mathbf{B}\mathbf{B}^T \tag{2.4}$$

Δt is the time step, $\mathbf{Z}$ is a vector of three independent random numbers with zero mean and unit variance (Tompson et al, 1988).

Eqn 2.2 is equivalent to Eqn 2.1 in the limit of large number of particles N_p and small Δt .

In Chapter 4 a thorough review of particle tracking models is presented.

A third category of hybrid models has also been developed (e.g., Pinder and Cooper, 1970; Konikow and Bredehoft, 1978; Neuman, 1981) where mass is represented by a large collection of particles, each of which is assigned a "value" of concentration. This procedure is somewhat awkward and suffers from mass conser-

vation problems that arise from the conversion of particle concentrations to node concentrations.

2.3.2 Eulerian Models

In the Eulerian method the equation is solved on a fixed grid by techniques such as finite differences, Galerkin or Petrov-Galerkin finite elements, and collocation. We see that scalar transport is the combination of two different processes: advection by the flow and diffusion due to turbulent velocity fluctuations. The numerical simulation technique used must therefore be suited to the nature of these two processes (Nguyen and Martin, 1988). Leonard (1979) gives a thorough review on methods used to accomodate diffusion or advection dominated processes. Diffusion has a tendency to smooth scalar distributions in all directions while advection propagates all scalar quantities in the direction of the flow, without deforming their initial distribution. When diffusion dominates, standard Eulerian numerical techniques, whose nature relies on the smoothness of the computing results, can be used to solve the problem. This means that in the case of finite differences, central difference schemes can be used whereas in the case of finite elements symmetric basis functions can be used.

Whenever advection is relatively strong, which is the case in transport in coastal areas, application of these techniques may provoke oscillations resulting in overshoot, undershoot, and negative values in the vicinity of high gradients of the scalar values (Glass and Rodi, 1982). The existense of these wiggles is associated with the use of finite Δx in the discretization: The solution of the linear Eqn 2.1 can be expressed as a superposition of individual Fourier modes:

$$c = \sum c_k e^{ikx} \tag{2.5}$$

where

k $= \frac{2\pi}{L_k}$ is the wavenumber

L_k is the wavelength

In the pure advective case i.e. $\mathbf{K} = 0$ all waves propagate at the same speed $\mathbf{u}$, i.e. the packet of waves maintaines its shape.

There are two effects due to finite Δx. First, the grid can not distinguish waves with wavelength $L_k < 2\Delta x$, i.e. waves with wavelength $L_k < 2\Delta x$ appear as a constant (aliasing error). Second, even though the grid distinguishes $L_k > 2\Delta x$ the higher modes do not travel at the right speed (e.g. $L_k = 2\Delta x$ is stationary in center differences schemes) and that causes dispersion errors, that appear as wiggles (i.e., high wavenumber modes lagging relative to the accurate long wavelenghts). In order to avoid wiggles researchers have used dissipative schemes, e.g. upwind finite differences (Raithby and Torrance, 1974) that result in damping errors. If we think of this numerical problem as a boundary layer problem we can say, that the length scale of the resulting boundary layer Δx_{bl} is

$$\Delta x_{bl} \sim \frac{K}{u} \tag{2.6}$$

and since the grid cannot distinguish waves with wave length $L_k < 2\Delta x$ the grid Peclet number $Pe_{gr} = \frac{u\Delta x}{K}$ should satisfy the relation

$$Pe_{gr} \leq 2 \tag{2.7}$$

This restriction eliminates the first problem. In order to eliminate the second problem higher-order approximations in space must be used.

On the other hand stability requirements of explicit methods enforce a restriction on the Courant number $Cu = \frac{u\Delta t}{\Delta x}$ i.e. $Cu \leq 1$ (Roache, 1976). This means high computational cost in highly transient flows. The use of implicit methods removes this restriction, but results to the costly solution of non symmetric matrices.

In order to overcome these errors higher-order approximations in space, time, or both have been used. QUICK i.e. Quadratic Upstream Interpolation for Convective Kinematics and QUICKEST i.e Quadratic Upstream Interpolation for Convective

Kinematics with Estimated Streaming Terms (Leonard, 1979), a popular transport model for coastal water applications, belongs to this category of higher-order upwind schemes. Since the main 3-D application in Chesapeake Bay (Dortch, 1990) used the QUICKEST scheme the two schemes (i.e. QUICK and QUICKEST) are described here in order to be later compared to the Eulerian Lagrangian approach developed in this research.

A control volume approach is used i.e. the spatially discretized form of Eqn 2.1 is written for the 1-D case as

$$\frac{\partial \bar{c}}{\partial t} = [u_l c_l - u_r c_r + K_r(\frac{\partial \bar{c}}{\partial x})_r - K_l(\frac{\partial \bar{c}}{\partial x})_l]/\Delta x_c \tag{2.8}$$

where the bars represent control volume averages (Fig 2-1). The wall cell values c_l and c_r are written in terms of a quadratic interpolation using in any one direction the two adjacent nodal values together with the value at the next upstream node i.e.

$$c_r = \frac{1}{2}(c_C + c_R) - \frac{1}{8}(c_L + c_R - 2c_C) \tag{2.9}$$

$$c_l = \frac{1}{2}(c_L + c_C) - \frac{1}{8}(c_{FL} + c_C - 2c_L) \tag{2.10}$$

$$(\frac{\partial \bar{c}}{\partial x})_r = \frac{c_R - c_C}{\Delta x_r} \tag{2.11}$$

$$(\frac{\partial \bar{c}}{\partial x})_l = \frac{c_C - c_L}{\Delta x_l} \tag{2.12}$$

The QUICKEST scheme is used in the case of variable velocity to ensure the upwinding. The wall values are weighted by Cu. (Fig 2-2) shows the stability range for the QUICKEST scheme. α is given by

$$\alpha = \frac{K\Delta t}{\Delta x^2} \tag{2.13}$$

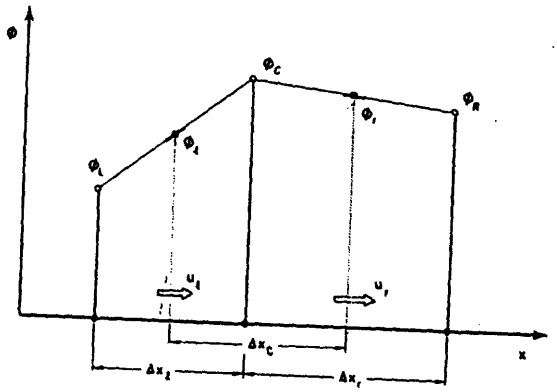

Fig. 1. Central differencing uses linear interpolation for cell wall values and the corresponding gradients.

(a)

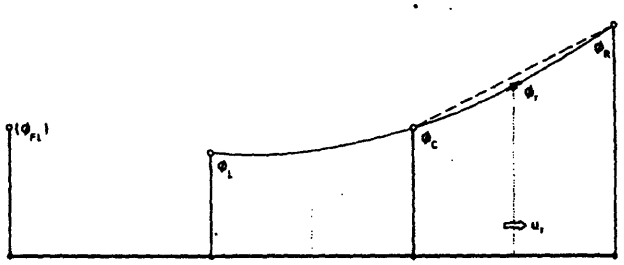

Fig. 8. Quadratic upstream interpolation for ϕ_r and $(\partial\phi/\partial x)_r$.

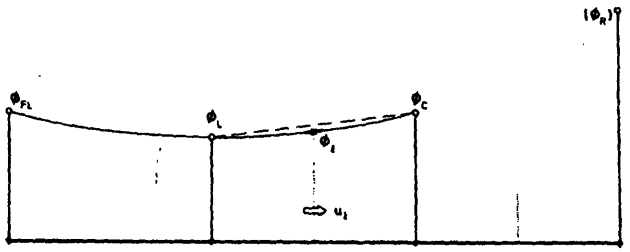

Fig. 9. Quadratic upstream interpolation for ϕ_l and $(\partial\phi/\partial x)_l$.

(b)

Figure 2-1: QUICK scheme.(a) Control volume approach. (b) Quadratic upstream interpolation for c_l, $\frac{\partial \bar{c}}{\partial x})_l$, c_r, $\frac{\partial \bar{c}}{\partial x})_r$ (from Leonard, 1979) (Substitute ϕ with c in the figures

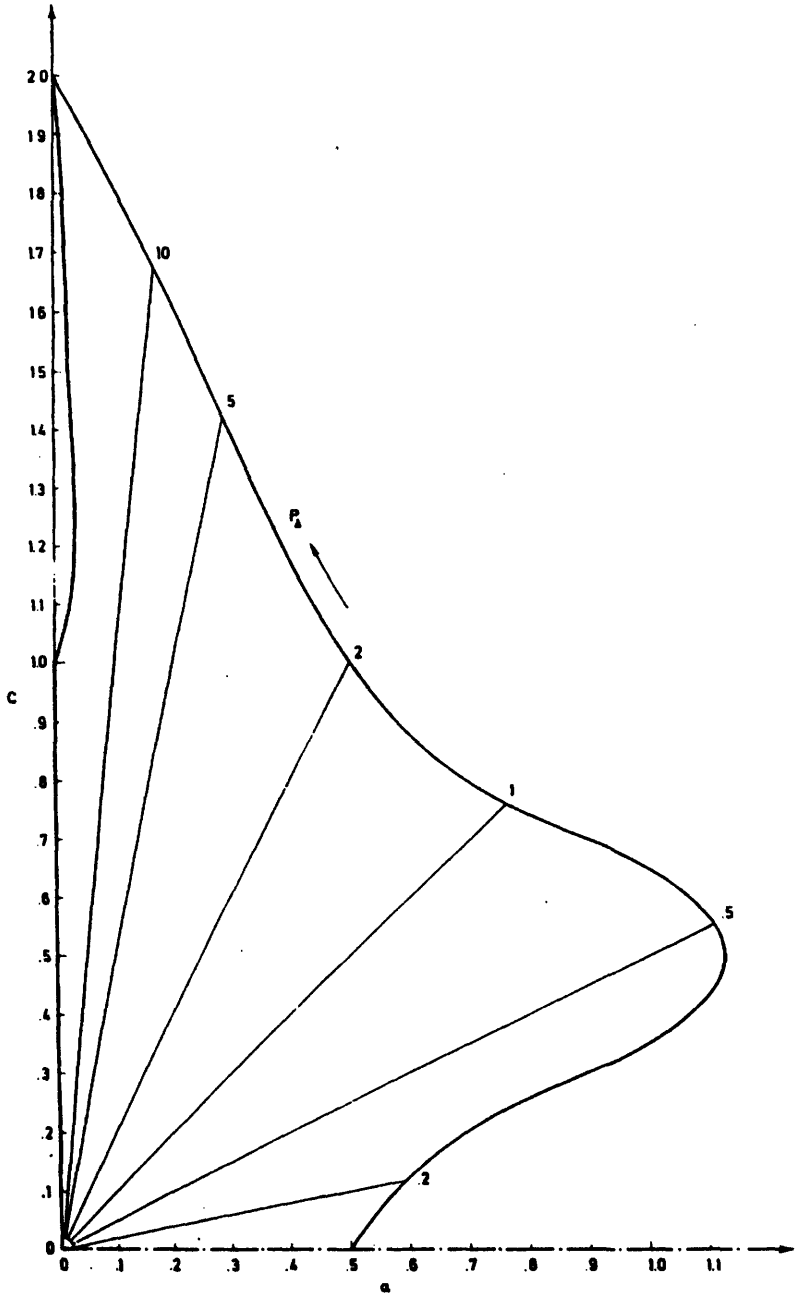

Figure 2-2: Stability range for QUICKEST scheme $\alpha = \frac{K\Delta t}{\Delta x^2}$, $C = Cu = \frac{u\Delta t}{\Delta x}$.

It is interesting to note that for $Pe \rightarrow \infty$ the stability criterion is given by $Cu = 1$.

In the case of finite elements in order to eliminate oscillations and numerical diffusion high-order schemes in space and/or time must be used (Christie et al., 1976; van Genuchten, 1977; van Genuchten and Gray, 1978; Hughes, 1978; Hughes and Brooks, 1979,1982; Hughes and Tezduyar, 1984; Celia et al., 1989; Westerink and Shea, 1990). The problem with higher-order schemes is that they still have to satisfy the Courant number criterion, which requires small time steps in advection-dominated problems.

2.3.3 Lagrangian Methods

Lagrangian methods (O'Neill and Lynch, 1980) are able to deal with steep concentration gradients while utilizing large time steps. However, the lack of a fixed grid, or fixed coordinates may cause difficulties such as mesh tangling, that become especially acute in non-uniform domains with multiple sources and complex boundary conditions.

2.3.4 Eulerian-Lagrangian Methods

Mixed Eulerian-Lagrangian methods attempt to eliminate such difficulties by combining the simplicity of a fixed Eulerian grid with the computational power of a Lagrangian approach. Most commonly, they split the transport equation into a pure advection part, that is solved by the backwards method of characteristics and a pure diffusion part, that is solved by some conventional global discrete element technique, e.g., finite elements or finite differences (Baptista, 1987). Eulerian-Lagrangian methods are called by a variety of names (Celia et al., 1989) including transport diffusion method (Benque and Ronat, 1982; Pironneau, 1982; Herevouet, 1986), method of characteristics (MOC) (Cooper and Pinder, 1970), modified method of characteristics (MMOC) (Ewing et al., 1984; Russell, 1985; Douglas and Russell, 1982), operator splitting methods (Espedal and Ewing, 1987; Dahle et al., 1988; Wheeler and Dawson, 1988), localized adjoint methods (Celia et al., 1989), and semi-Lagrangian

(Williamson and Rasch, 1989; McDonald, 1984; Ritchie, 1985; Robert, 1981). Because of their similarity to particle tracking methods Baptista (1987) calls the latter also an Eulerian-Lagrangian method and makes a distinction between ELM/C (Eulerian-Lagrangian concentration model), ELM/P (Eulerian-Lagrangian particle tracking method), and ELM/PC referring to the hybrid methods that use forward tracking close to high concentration gradients. From now on ELM/C will be referred as ELM.

ELM have been extensively used in many disciplines in order to solve transport problems with advection (i.e. hyperbolic) dominating terms (i.e., groundwater, petroleum engineering, surface water transport, meteorology). With ELM the problem of small Courant and Peclet numbers is eliminated. Eqn 2.1 is transformed into its nonconservative form

$$\frac{\partial c}{\partial t} + \mathbf{v} \cdot \nabla c = \nabla \cdot \mathbf{K} \cdot \nabla c + Q \tag{2.14}$$

According to the most common approach Eqn 2.14 is discretized in time according to

$$\frac{c^n - c^{n-1}}{\Delta t} + [\mathbf{v} \cdot \nabla c]^{n-1} = [\nabla \cdot \mathbf{K} \cdot \nabla c]^n \tag{2.15}$$

By defining an auxiliary variable c^f Eqn 2.15 can be split into two components due to its linearity i.e.

a pure advective component

$$\frac{c^f - c^{n-1}}{\Delta t} + [(\mathbf{v} - \nabla \cdot \mathbf{K}) \cdot \nabla c]^{n-1} = 0 \tag{2.16}$$

and a pure diffusive component

$$\frac{c^n - c^f}{\Delta t} = [\mathbf{K} \cdot \nabla^2 c]^n \tag{2.17}$$

Eqn 2.16 states that the concentration c remains constant along characteristic lines defined by

$$\frac{d\mathbf{x}}{dt} = (\mathbf{v} - \nabla \cdot \mathbf{K}) \tag{2.18}$$

According to Eqn 2.18, Eqn 2.16 is solved by tracking characteristic lines backwards from time n to time n-1 from every node (Fig 2-3). The concentrations c^f at time n are determined by spatial interpolation. Eqn 2.17 is solved by using finite differences (Nguyen and Martin, 1988) or finite elements (Baptista, 1987; Russell, 1985; Hasbani et al., 1983).

Mass conservation in transport models is guarantied by using a mass conservative velocity field and a mass conservative numerical scheme in the transport model. The drawback of the advective treatment in ELM is that second condition is not satisfied, i.e., it makes them not inherently mass conservative. In Eulerian methods conservation may be guaranteed by using difference equations which can be related to the species conservation equation applied to discrete control volumes defined with respect to the grid cells (Glass and Rodi, 1982). When these methods are applied to extended regions sharp gradients resulting from advection-dominated flows are simulated with severe damping. In ELM this problem is overcome by relaxing the requirement for inherent conservation and describing the advection by a point-to-point transfer by using the nonconservative form of the transport equation . In order to resolve this problem very accurate tracking schemes for the solution of Eqn 2.18 must be used. This need is particularly imperative in the case of highly variable velocity fields. Tests for various two-dimensional flows (Glass and Rodi, 1982; Baptista, 1987) have shown that because of the accuracy of the tracking schemes used, the transported scalar field is very nearly conserved. It is important to note, that a necessary condition for mass conservation in a TM is a mass conserving flow field.

The main issues in an ELM are the selection of

- the integration scheme for the tracking

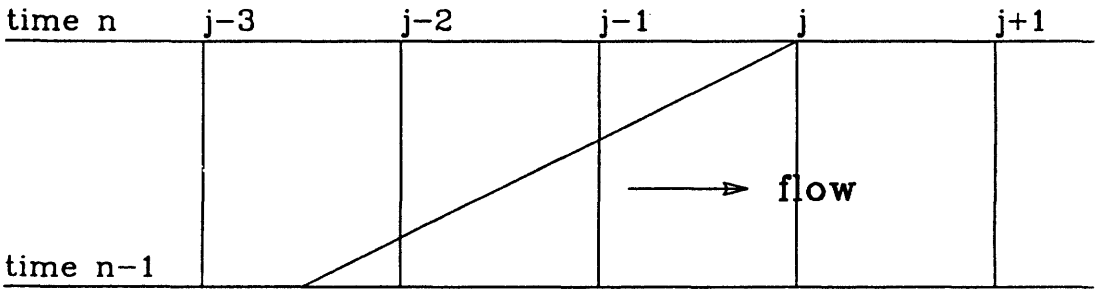

Figure 2-3: Illustration of the backwards method of characteristics.

- the interpolation functions
- the numerical scheme for the solution of the diffusion equation
- the order of the time discretization

  Related to the 3-D character of the ELM is
- the selection of a solver for the solution of the symmetric, positive definite system of linear equations resulting from the diffusion equation.

In the next chapter the 3-D Eulerian-Lagrangian model developed in this study will be presented and all the above issues will be addressed.

2.4 σ Coordinate System

The choice of the coordinate system is left to the HM since the TM uses output from the HM and the use of different coordinate systems would require interpolations and extrapolations of data, that introduce errors in the calculations. In this study a sigma coordinate system is used in the transport model because of compatibility with the available HM. The model can also accept Cartesian coordinate hydrodynamic input.

It has been noted, that the cartesian x, y, z coordinate system has certain disadvantages due to the fact that in surface water problems we are dealing with a moving upper boundary. In order to resolve this problem a new coordinate system (σ coordinate system) was introduced, that transforms both the surface and the bottom into a coordinate surface (Philips, 1957). The σ coordinate system is obtained by replacing the vertical coordinate z by the independent variable σ

$$\sigma = \frac{z - \eta}{H + \eta} = \frac{z - \eta}{D} \tag{2.19}$$

where

η is the free surface elevation,

H is the depth from $z = 0$, and

$D = H + \eta$ is the total depth (Fig 2-4).

Following the procedure described by Phillips, and using principal axis the mass transport equation with new coordinate system x, y, σ, t is

$$\frac{\partial(cD)}{\partial t} + \frac{\partial(cUD)}{\partial x} + \frac{\partial(cVD)}{\partial y} + \frac{\partial(c\omega)}{\partial \sigma} = DQ \tag{2.20}$$

where U, V are the x and y velocity components respectively and ω is given by

$$\omega = W - U[\sigma\frac{\partial D}{\partial x} + \frac{\partial \eta}{\partial x}] - V[\sigma\frac{\partial D}{\partial y} + \frac{\partial \eta}{\partial y}] - [\sigma\frac{\partial D}{\partial t} + \frac{\partial \eta}{\partial t}] \tag{2.21}$$

where W is the z velocity component

$$\begin{aligned} DQ \;=\; & \frac{\partial q_x}{\partial x} - \frac{\partial}{\partial \sigma}[(\frac{\sigma}{D}\frac{\partial D}{\partial x} + \frac{1}{D}\frac{\partial \eta}{\partial x})q_x] \\ & + \frac{\partial q_y}{\partial y} - \frac{\partial}{\partial \sigma}[(\frac{\sigma}{D}\frac{\partial D}{\partial y} + \frac{1}{D}\frac{\partial \eta}{\partial y})q_y] \\ & + \frac{\partial q_\sigma}{\partial \sigma} \\ & + \frac{\partial q_{xy}}{\partial x} - \frac{\partial}{\partial \sigma}[(\frac{\sigma}{D}\frac{\partial D}{\partial x} + \frac{1}{D}\frac{\partial \eta}{\partial x})q_{xy}] \\ & + \frac{\partial q_{yx}}{\partial y} - \frac{\partial}{\partial \sigma}[(\frac{\sigma}{D}\frac{\partial D}{\partial y} + \frac{1}{D}\frac{\partial \eta}{\partial y})q_{yx}] \\ & + \frac{\partial q_{x\sigma}}{\partial x} - \frac{\partial}{\partial \sigma}[(\frac{\sigma}{D}\frac{\partial D}{\partial x} + \frac{1}{D}\frac{\partial \eta}{\partial x})q_{x\sigma}] \\ & + \frac{\partial q_{\sigma x}}{\partial \sigma} - \frac{\partial}{\partial \sigma}[K_{zx}\frac{\partial c}{\partial \sigma}(\frac{\sigma}{D}\frac{\partial D}{\partial x} + \frac{1}{D}\frac{\partial \eta}{\partial x})] \\ & + \frac{\partial q_{y\sigma}}{\partial y} - \frac{\partial}{\partial \sigma}[(\frac{\sigma}{D}\frac{\partial D}{\partial y} + \frac{1}{D}\frac{\partial \eta}{\partial y})q_{y\sigma}] \\ & + \frac{\partial q_{\sigma y}}{\partial \sigma} - \frac{\partial}{\partial \sigma}[K_{zy}\frac{\partial c}{\partial \sigma}(\frac{\sigma}{D}\frac{\partial D}{\partial y} + \frac{1}{D}\frac{\partial \eta}{\partial y})] \end{aligned} \tag{2.22}$$

$$q_x = K_x[\frac{\partial(cD)}{\partial x} - \frac{\partial}{\partial \sigma}(\sigma\frac{\partial D}{\partial x} + \frac{\partial \eta}{\partial x})c] \tag{2.23}$$

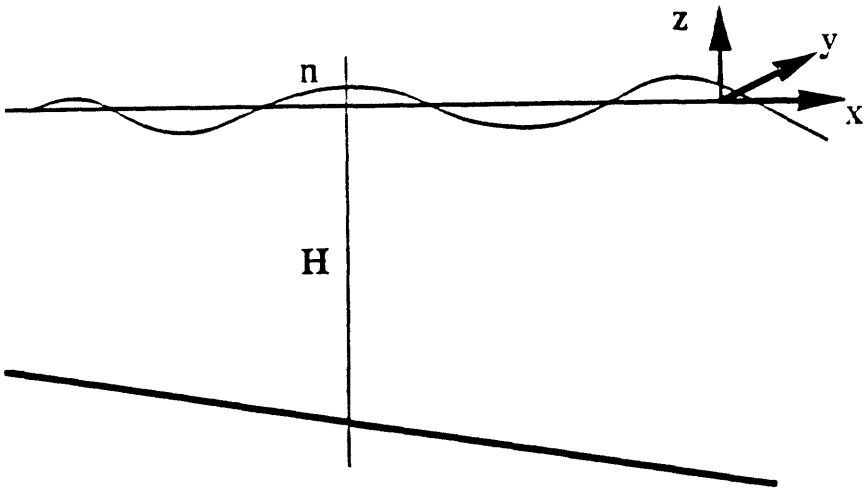

Figure 2-4: Cartesian-Coordinate System.

$$q_y = K_y[\frac{\partial(cD)}{\partial y} - \frac{\partial}{\partial \sigma}(\sigma\frac{\partial D}{\partial y} + \frac{\partial \eta}{\partial y})c] \tag{2.24}$$

$$q_\sigma = \frac{K_z}{D}\frac{\partial c}{\partial \sigma} \tag{2.25}$$

$$q_{xy} = K_{xy}[\frac{\partial(cD)}{\partial x} - \frac{\partial}{\partial \sigma}(\sigma\frac{\partial D}{\partial x} + \frac{\partial \eta}{\partial x})c] \tag{2.26}$$

$$q_{yx} = K_{yx}[\frac{\partial(cD)}{\partial y} - \frac{\partial}{\partial \sigma}(\sigma\frac{\partial D}{\partial y} + \frac{\partial \eta}{\partial y})c] \tag{2.27}$$

$$q_{x\sigma} = \frac{K_{xz}}{D}\frac{\partial c}{\partial \sigma} \tag{2.28}$$

$$q_{\sigma x} = \frac{K_{zx}}{D}\frac{\partial c}{\partial \sigma} \tag{2.29}$$

$$q_{y\sigma} = \frac{K_{yz}}{D}\frac{\partial c}{\partial \sigma} \tag{2.30}$$

$$q_{\sigma y} = \frac{K_{zy}}{D}\frac{\partial c}{\partial \sigma} \tag{2.31}$$

Vertical diffusivities are well parameterized using turbulence closure schemes. The horizontal length scale of most problems is large relative to the vertical scale and so horizontal diffusivity terms should be negligible compared with vertical diffusivity terms. However, for most larger-scale numerical applications horizontal grid elements are generally much larger than the smallest horizontal dominant scales and so these small unresolved mesoscale motions require modelers to use horizontal, sub-gridscale, diffusive terms much larger than the small-scale vertical diffusivities. According to Mellor and Blumberg (1985) vertical diffusivities resulting from turbulence closure schemes are $O(10^{-2}m^2s^{-1})$, while horizontal diffusivities may be $O(10^2m^2s^{-1})$ depending on horizontal resolution. Mellor and Blumberg (1985) have shown that

Eqn 2.23 and Eqn 2.24 are physically incorrect near sloping bottoms, when the horizontal diffusivity is larger than the vertical diffusivity. They suggested an alternative formulation, which makes it possible to model realistically bottom boundary layers over sharply sloping bottoms. In the rest of this section their approach is applied.

Consider the three coordinate systems shown in Fig 2-5. For simplicity principal axis will be used. The net diffusive flux for coordinate system (a) is

$$Q = \frac{\partial q_x}{\partial x} + \frac{\partial q_y}{\partial y} + \frac{\partial q_z}{\partial z} \tag{2.32}$$

where

$$q_x = K_x \frac{\partial c}{\partial x} \tag{2.33}$$

$$q_y = K_y \frac{\partial c}{\partial y} \tag{2.34}$$

$$q_z = K_z \frac{\partial c}{\partial z} \tag{2.35}$$

At the ocean surface there is no problem with Eqn 2.23 and Eqn 2.24 because the diffusive flux normal to the surface is q_z and although K_x, K_y may be much larger than K_z as stated before $\frac{\partial q_z}{\partial z}$ is generally still much larger than the horizontal flux terms. At the bottom there can be a problem when the bottom slope $\frac{\partial H}{\partial x}$ or $\frac{\partial H}{\partial y}$ is significantly non zero. In this case the diffusive flux normal to the bottom considering $\frac{\partial H}{\partial x} \neq 0$ and $\frac{\partial H}{\partial y} = 0$ is

$$q_n = q_z - q_x \frac{\partial H}{\partial x} = K_z \frac{\partial c}{\partial z} - K_x \frac{\partial c}{\partial x} \frac{\partial H}{\partial x} \tag{2.36}$$

assuming that c changes over a distance δ in the vertical and over a distance Δx in the horizontal direction we get

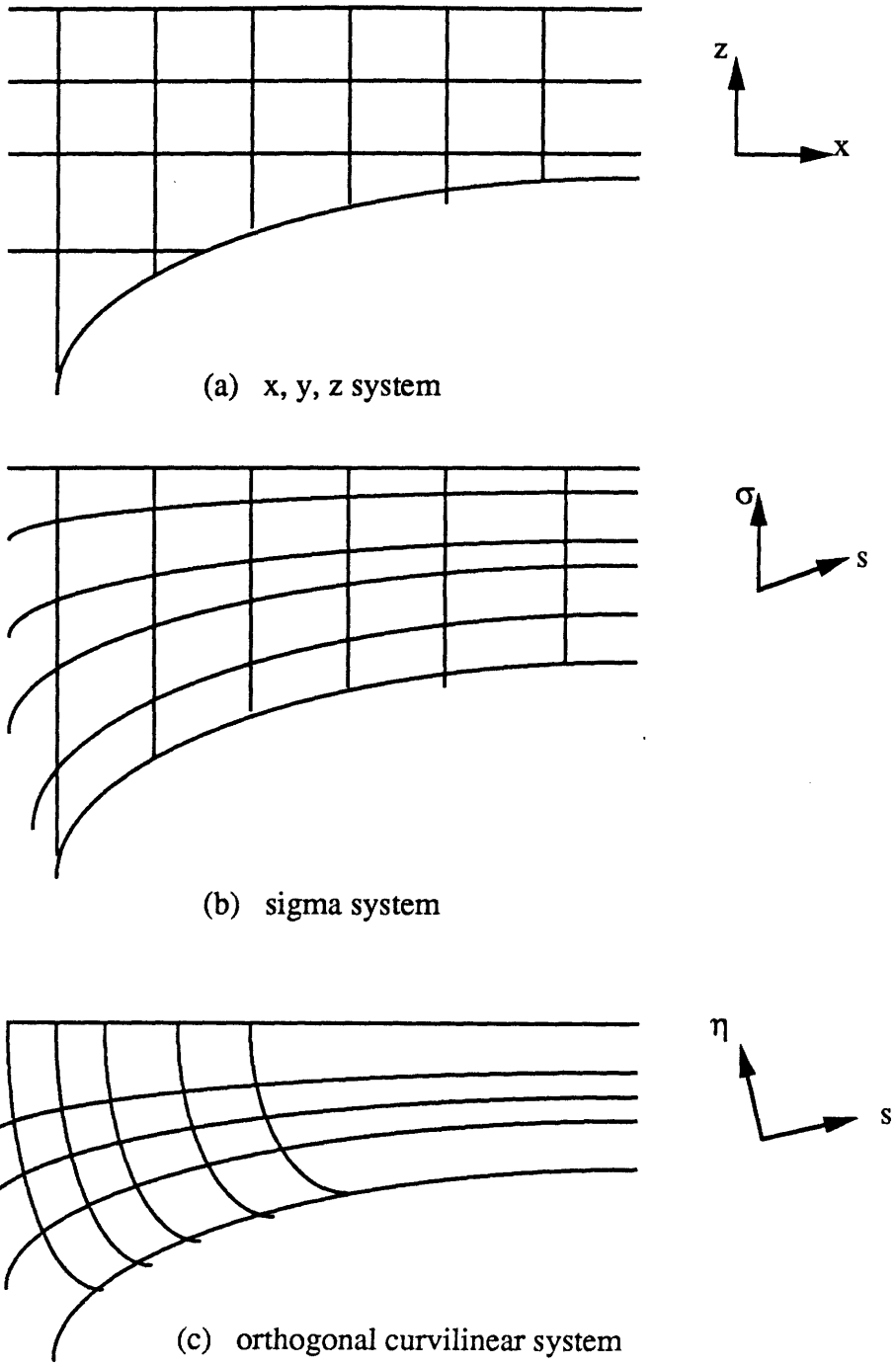

Figure 2-5: Three coordinate systems.

$$q_n \approx [K_z \frac{\Delta c}{\delta}][1 - \frac{K_x}{K_z}\frac{\partial H}{\partial x}\frac{\delta}{\Delta x}] \tag{2.37}$$

Suppose $\delta = 5\text{m}$, $\Delta x = 5\text{km}$, $\frac{\partial H}{\partial x} = -10^2$, $K_x = 10^4 m/s^2$, and $K_z = 10^{-2} m/s^2$ we get

$$q_n \approx [K_z \frac{\Delta c}{\delta}][1 + 20] \tag{2.38}$$

In order to develop a model valid near the bottom Eqn 2.23 and Eqn 2.24 must be replaced by equations that do not include a component containing horizontal diffusivities K_x, K_y for representing diffusive fluxes vertical to the bottom.

Considering coordinates s and m parallel to the bottom and n normal to the bottom (Fig 2-5) a new constitutive relation in the curvilinear orthogonal system can be written as

$$q_s = K_x \frac{\partial c}{\partial s} \tag{2.39}$$

$$q_m = K_y \frac{\partial c}{\partial m} \tag{2.40}$$

$$q_n = K_z \frac{\partial c}{\partial n} \tag{2.41}$$

In order to transform q_s, q_m, q_n to q_x, q_y, q_σ we use the fact that bottom slopes are small numbers, i.e., $\frac{\partial D}{\partial x} = 0.1$ is an upper limit. If $\phi_x \sim sin\phi_x - \sigma(\frac{\partial D}{\partial x})$ it can be shown that

$$q_x \approx q_s \tag{2.42}$$

and similarly $q_y \approx q_m, q_\sigma = q_n$. According to this formulation the complete equation for net mass diffusion by using principal axes is

$$q = \frac{1}{D}\frac{\partial(Dq_x)}{\partial x} + \frac{1}{D}\frac{\partial(Dq_y)}{\partial y} + \frac{1}{D}\frac{\partial(q_\sigma)}{\partial \sigma} \tag{2.43}$$

where

$$(q_x, q_y, q_\sigma) = (K_x\frac{\partial c}{\partial x}, K_y\frac{\partial c}{\partial y}, \frac{K_z}{D}\frac{\partial c}{\partial \sigma}) \tag{2.44}$$

In the general case (e.g., not using principal axes) and neglecting the cross terms $K_{xz}, K_{yz}, K_{zx}, K_{xy}$ we end up with the following mass transport equation.

$$\begin{aligned}
&\frac{\partial(cD)}{\partial t} + \frac{\partial(cUD)}{\partial x} + \frac{\partial(cVD)}{\partial y} + \frac{\partial(c\omega)}{\partial \sigma} = \\
&\quad \frac{\partial}{\partial x}[DK_x\frac{\partial c}{\partial x}] + \frac{\partial}{\partial x}[DK_{xy}\frac{\partial c}{\partial y}] + \\
&\quad + \frac{\partial}{\partial y}[DK_y\frac{\partial c}{\partial y}] + \frac{\partial}{\partial y}[DK_{yx}\frac{\partial c}{\partial x}] + \\
&\quad + \frac{\partial}{\partial \sigma}[\frac{K_z}{D}\frac{\partial c}{\partial \sigma}]
\end{aligned} \tag{2.45}$$

As mentioned before the choice of the coordinate system is left to the HM. In the remaining of this section the advantages and disadvantages of each coordinate system are mentioned and some suggestions for an efficient method to deal with the problem of the choice of a coordinate system are proposed.

The main advantages of the sigma coordinate system are:

- It eliminates the moving boundary condition in the HM by introducing another unknown η in the governing equations. Because in existing HMs the surface elevation is found for reasons of computational efficiency by using the vertically averaged equations this advantage of the sigma coordinate system is not an issue. With the evolution of computers a fully 3D circulation model may be the next step in modeling surface waters and that would make the sigma coordinate system necessary. The elimination of the moving upper boundary

is very important in 3-D TM. In the cartesian coordinate systems the use of "wet" and "dry" nodes is necessary to accomodate the moving boundary. In finite elements the size of the upper element has to change at every time step. This treatment of the upper boundary is very detrimental from an accuracy point of view (i.e. mass conservation errors) particularly in cases where mass is close to the surface.

The main disadvantages of the sigma coordinate system are:

- Because the same number of layers has to be used throughout the domain we end up having an unnecessarily big resolution in shallow waters and a coarse resolution in deep waters.

- The bottom layer in one column communicates with the bottom layer in an adjacent column and so when depth changes are coarsely resolved, channel stratification can not be maintained. Leendertse (1990) showed (Fig 2-6) that in a staggered grid as usually used in coastal waters HM the near-horizontal fluxes and the vertical transformed fluxes are not at the same location and so with a cross current component water with lower density is moved from the shallow area immediately into a lower level of the channel, before the vertical transformed flux takes effect. So the transition from low to high salinity is not horizontal but becomes vertical or near vertical.

- The problem associated with vertical transformed diffusive fluxes resulting from the use of high horizontal diffusion coefficients was addressed by Mellor and Blumberg (1985) and is presented at the beginning of this section. The antidote is to ignore horizontal diffusion in the calculation of the vertical diffusive fluxes.

2.5 Hydrodynamic Models-Overview

A HM involves the solution of the following equations:

- the continuity equation

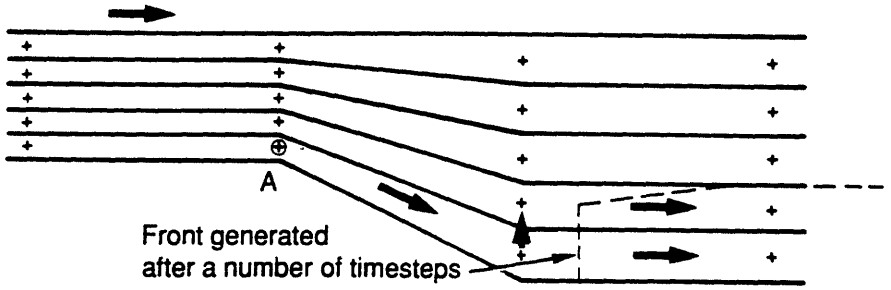

Figure 2-6: Pathway of Advective Salinity Transport Originating from Point A after 2 Time Steps. (from Leendertsee, 1990).

- the momentum equations
- the salinity equation
- the temperature equation
- a constitutive equation giving the density as a function of salinity and temperature

By making the simplifying assumptions of (i) hydrostatic variation of pressure in the vertical and (ii) Boussinesq approximations so that density variations are only important in the gravity terms the system of these equations becomes (Blumberg and Mellor, 1987).

- the continuity equation

$$\nabla \cdot \mathbf{V} + \frac{\partial W}{\partial z} = 0 \tag{2.46}$$

- the x-momentum equation

$$\frac{\partial U}{\partial t} + \mathbf{V} \cdot \nabla U + W\frac{\partial U}{\partial z} - fV = -\frac{1}{\rho}\frac{\partial P}{\partial x} + \frac{\partial}{\partial z}(K_M \frac{\partial U}{\partial z}) + F_x \tag{2.47}$$

- the y-momentum equation

$$\frac{\partial V}{\partial t} + \mathbf{V} \cdot \nabla V + W\frac{\partial V}{\partial z} + fU = -\frac{1}{\rho}\frac{\partial P}{\partial y} + \frac{\partial}{\partial z}(K_M \frac{\partial V}{\partial z}) + F_y \tag{2.48}$$

- the z-momentum equation

$$\rho g = -\frac{\partial P}{\partial z} \tag{2.49}$$

According to Eqn 2.49 the pressure P is given by

$$P(x, y, z, t) = P_{atm} + g\rho_\circ \eta + \int_z^0 \rho(x, y, z', t)dz' \tag{2.50}$$

- the conservation equation for salinity

$$\frac{\partial S}{\partial t} + \mathbf{V} \cdot \nabla S + W\frac{\partial S}{\partial z} = \frac{\partial}{\partial z}(K_H \frac{\partial V}{\partial z}) + F_S \tag{2.51}$$

- the conservation equation for temperature

$$\frac{\partial \Theta}{\partial t} + \mathbf{V} \cdot \nabla \Theta + W\frac{\partial \Theta}{\partial z} = \frac{\partial}{\partial z}(K_H \frac{\partial V}{\partial z}) + F_\Theta \tag{2.52}$$

where

V is the horizontal velocity with components (U,V)

W is the vertical velocity

ρ_0 is the reference density

ρ is the in situ density

g is the gravitational acceleration

P is the pressure

K_M is the vertical eddy diffusivity of vertical momentum

K_H is the vertical eddy diffusivity for mixing

f is the Coriolis parameter

Θ is the temperature

F_x, F_y and $F_{\Theta,S}$ are given by the expressions

$$F_x = \frac{\partial}{\partial x}[2A_M\frac{\partial U}{\partial x}] + \frac{\partial}{\partial y}[A_M(\frac{\partial U}{\partial y} + \frac{\partial V}{\partial x})] \tag{2.53}$$

$$F_y = \frac{\partial}{\partial y}[2A_M\frac{\partial V}{\partial y}] + \frac{\partial}{\partial x}[A_M(\frac{\partial U}{\partial y} + \frac{\partial V}{\partial x})] \tag{2.54}$$

$$F_{\Theta,S} = \frac{\partial}{\partial x}A_H\frac{\partial(\Theta,S)}{\partial x} + \frac{\partial}{\partial y}A_H\frac{\partial(\Theta,S)}{\partial y} \tag{2.55}$$

The horizontal diffusivities A_M and A_H are meant to parametarize subgrid scale processes but are usually used to damp oscillations. In the Chesapeake Bay application (Johnson et al, 1990) A_M and A_H were set to zero because the model was insensitive to their variation. The vertical mixing coefficients are found by using a

turbulence closure scheme.

The boundary conditions at the free interface $z = \eta(x, y)$ are

$$\rho_0 K_M(\frac{\partial U}{\partial z}, \frac{\partial V}{\partial z}) = (\tau_{ox}, \tau_{oy}) \tag{2.56}$$

$$\rho_0 K_H(\frac{\partial \Theta}{\partial z}, \frac{\partial S}{\partial z}) = (\dot{H}, \dot{S}) \tag{2.57}$$

and the kinematic boundary condition

$$W = U\frac{\partial \eta}{\partial x} + V\frac{\partial \eta}{\partial y} + \frac{\partial \eta}{\partial t} \tag{2.58}$$

The boundary conditions at the bottom are $(z = -H)$:

$$\rho_0 K_M(\frac{\partial U}{\partial z}, \frac{\partial V}{\partial z}) = (\tau_{bx}, \tau_{by}) \tag{2.59}$$

and the kinematic boundary condition

$$W_b = -U_b\frac{\partial H}{\partial x} - V_b\frac{\partial H}{\partial y} \tag{2.60}$$

For open boundaries the values of velocities, elevations, temperature and salinity need to be imposed.

The main issues associated with the solution of Eqn 2.46 - Eqn 2.52 are

- The moving surface boundary
- The cost of the numerical calculation
- The turbulence closure scheme
- The modeling of the bottom shear

The treatment of the moving upper boundary is associated with the choice of the coordinate system (σ vs. cartesian coordinate system) and it is analyzed in Section 2.4. The choice of the turbulence closure scheme and the modeling of the bottom shear are important for the HM but do not affect the numerical choices in the TM. Of particular importance to the TM is the numerical scheme used in the HM that is dictated by the cost of the numerical calculations.

2.5.1 Cost

3-D HM can be split into two categories:

- harmonic models (Lynch and Werner, 1987) that make the assumption that all dependent variables are harmonic functions of time - either single functions or the superposition of multiple functions.
- stepping models

The high cost of the numerical calculations is associated with the fact that in order to resolve free surface gravity waves the Courant - Friedrichs - Levy condition has to be satisfied i.e. the minimum allowed time step Δt_{gr} in the 1-D case is given by

$$\Delta t_{gr} = \Delta x / \sqrt{gH} \tag{2.61}$$

In the vertical direction the minimum allowed time step Δt_{ver} is dictated by the rate momentum diffuses i.e.

$$\Delta t_{ver} = H^2 / K_H \tag{2.62}$$

which is in most cases much less restrictive than Eqn 2.61.

In order to take advantage of the different time scales in the vertical and in the horizontal a mode splitting technique has been used. According to the splitting technique that they use the "3-D" circulation models can be classified into the following categories:

- 2D - 1D models: (Nihoul and Desjandis, 1987; Davies 1988). They make the additional assumption of negligible vertical density variations and so neglect the vertical velocities. The solution consists of two parts: (i) the external mode i.e. the depth averaged equations, that are solved with the highly restrictive Δt_{gr} and retains the nonlinearities and (ii) the internal mode that results from subtracting the vertically-integrated equations from the original equations and disregarding nonlinear terms.

- 2D - 3D models: (Blumberg and Mellor, 1987; Casulli and Cheng, 1992; Lynch and Werner, 1990). These models differ from the previous ones in the internal mode where the full 3D equation is solved. It is interesting to note here that in an application by Blumberg and Mellor (1989) the time step of the external and internal mode were 10sec and 10min respectively. The CH3D (Curvilinear Hydrodynamics in Three Dimensions) model (Johnson et al, 1990) used in the Chesapeake Bay study uses the same technique except that the internal mode consists of the solution of the depth averaged equations in each layer.

- 2D - 1D - 3D models (Lynch et al, 1991). They resemble the first category except that the 3D continuity equation is used to solve for the vertical velocity. This model was used in this study to drive the TM.

2.6 Interface between HM and TM

For reasons related to the physics of the problem i.e. the motions, that have to be resolved have time scales of the order of a tidal cycle and to the numerics i.e. the stability requirements the time step used in a HM Δt_{HM} is small e.g. of the order of 10min. Table 2.1 shows Δt_{HM} used in studies with 3D time-stepping HM. On the other hand mass concentrations are either steady state or slowly time-varying for periods of the order of a tidal cycle and so a TM could use time steps of the order of a tidal cycle if the numerical scheme so permits. Since the TM depends on the HM for hydrodynamic information (e.g. velocities and turbulent diffusivities) this difference

Table 2.1: Time steps Δt_{HM} used in sample 3-D HM studies

Study	by	Δt_{HM}	Δx_{HM}
Chesapeake Bay	Johnson et al(1990)(internal)	10min	5000m
San Fransisco Bay	Casulli and Cheng (1992)	15min	500m
Venice Lagoon	Casulli and Cheng (1992)	15min	100m

in time steps causes problems. A brute force solution could be to use the small time step of the HM in the TM as well. This would unnecessarily burden our calculations in terms of computational time and storage requirements. A better approach is to use a technique for averaging the small time step HM output over the TM time step Δt_{TM}. This would involve averaging both velocities and turbulent diffusivities. Concerning turbulent diffusivities the simple approach of averaging their values over Δt_{TM} has been followed so far (Dortch, 1990). In 3-D coastal water problems we are often dealing with advection dominated flows and so the problem of incorporating small time step velocity output is by far a more important problem. Section 2.6 includes a literature review of methods used in the past for incorporating the small time step velocity input and it also proposes a method based on the Eulerian-Lagrangian approach.

Three methods can be used to incorporate the small time step input of the HM into the TM.

- Tidal dispersion coefficients
- Lagrangian Residuals
- Eulerian-Lagrangian methods

This study will primarily focus on the last two approaches. The first approach is only described for historical reasons because its physical meaning and generation mechanism is not well understood (Feng et al, 1986). The only three dimensional application where the issue of time averaging of the HM output has been addressed is the Chesapeake Bay application (Dortch and Chapman, 1989; Dortch, 1990) where the

Lagrangian residuals method was used. In this research a 3-D Eulerian-Lagrangian approach is developed and applied. From a physical and mathematical point of view we believe, that an Eulerian-Lagrangian approach is ideal for incorporating the small time step HM output in the larger time step TM. The Eulerian-Lagrangian approach is contrasted to the Lagrangian residuals approach used in the Chesapeake Bay study and its advantages are highlighted. The application of the Eulerian-Lagrangian method in the coupling of the HM to the TM is beyond the scope of this study and so the brief analysis that follows will hopefully serve as a starting point for further investigating the coupling issue of the HM to the TM using the Eulerian-Lagrangian approach.

2.6.1 Tidal dispersion coefficients

If we call p a variable in the TM we can decompose p into two components: a tidally averaged component $\overline{p}$ and a tidally varying component p' e.g.

$$p = \overline{p} + p' \tag{2.63}$$

where

$$\overline{p} = \frac{1}{T}\int_{t_0}^{t_0+T} p dt \tag{2.64}$$

$$\overline{p'} = 0 \tag{2.65}$$

with T being the averaging period

If we use the notation given by Eqn 2.63 for all variables in the transport equation , substitute and average over a tidal cycle we get the following expression in Einstein notation:

$$\frac{\partial \overline{c}}{\partial t} + \frac{\partial(\overline{U_i}\overline{c})}{\partial x_i} + \frac{\partial(\overline{U_i' c'})}{\partial x_i} = \frac{\partial(\overline{D_{ij}}\frac{\partial \overline{c}}{\partial x_j})}{\partial x_i} \tag{2.66}$$

The mean velocities $\overline{U_i}$ are called Eulerian residual velocities (Officer, 1976) U_E. The third term which is the non-zero correlation between the tidal velocity and concentration fluctuations can be modeled by using the tidal dispersion coefficient D_T e.g.

$$D_{Tij}\frac{\partial \overline{c}}{\partial x_j} = -\overline{U_i' c'} \tag{2.67}$$

In transport models that use this approach D_T is used to represent tidal dispersion, turbulent diffusion and shear dispersion (for depth averaged models) and so Eqn 2.66 takes the form:

$$\frac{\partial \overline{c}}{\partial t} + \frac{\partial (U_{E_i}\overline{c})}{\partial x_i} = \frac{\partial (\overline{D_{T_{ij}}\frac{\partial c}{\partial x_j}})}{\partial x_i} \tag{2.68}$$

This approach has been used quite extensively in the past (Awaji, 1982). In a water quality study of Boston Harbor (Hydroscience Inc., 1971) dispersion coefficients were used to represent tidal flows. As advective flows U_E only the flows from the tributaries were considered that represent 10% of the tidal velocities. Its main drawback is that an advective process is lumped into Fickian diffusion terms resulting in an unrealistic representation.

2.6.2 Lagrangian Residuals

Using this technique the velocities in Eqn 2.68 are replaced by Lagrangian mean velocities of first or second order depending on the degree of nonlinearity of the system. Lagrangian mean velocities are defined as the net displacement of a marked particle over one or more tidal cycles divided by the displacement time (Feng, 1987). This treatment eliminates the need to include the tidal dispersion coefficient at least for weakly nonlinear systems.

The intertidal 3-D mass transport equation has been derived by Feng (1987) by using a small parameter perturbation technique (van Dyke, 1964) with κ as the small

parameter

$$\kappa = \frac{\zeta_c}{h_c} = \frac{l_c}{L_c} \tag{2.69}$$

where ζ_c is the tidal amplitude, h_c the water depth, l_c the tidal excursion and L_c the basin horizontal length scale.

Using a second-order solution (Feng et al, 1986) the Lagrangian velocity U_L is given by

$$U_L = U_E + U_S + \kappa U_{LD} + 0(\kappa^2) \tag{2.70}$$

where U_E is the Eulerian residual velocity, U_S is the Stokes drift velocity, U_{LD} is the Lagrangian drift velocity and κ is a measure of system nonlinearity.

When the system is very weakly nonlinear then the first order approximation for Lagrangian residuals i.e. only the Stokes drift is sufficient.

Dortch (1990) provides a very thorough literature review of studies, where first or second order residual currents have been calculated or used as input in a TM. Since the purpose of this section is to compare the residual currents approach to the Eulerian-Lagrangian method a very brief description of the residual currents approach will be given. The first order Lagrangian residual approach, e.g. Stoke's drift will be described for two reasons: First, for simplicity and second, because this approach was used in the major 3-D study where residual currents were used in the TM e.g. the Chesapeake Bay study (Dortch, 1991). This approach is developed by Longuet-Higgins(1969).

Using a first order Taylor series expansion for the Eulerian velocity field the velocity of a particle is given by:

$$U(\mathbf{x}, t) = U(\mathbf{x_0}, t) + \Delta\mathbf{x} \cdot \nabla U(\mathbf{x_0}, t) \tag{2.71}$$

If $\Delta \mathbf{x}$ is small compared to the total length scale of the velocity field we may use the following approximation:

$$\Delta \mathbf{x} = \int_{t_0}^{t} U(\mathbf{x_0}, t) dt \tag{2.72}$$

Substituting Eqn 2.72 into Eqn 2.71 and averaging we get

$$\overline{U(\mathbf{x}, t)} = \overline{U(\mathbf{x_0}, t)} + \overline{\int_{t_0}^{t} U(\mathbf{x_0}, t) dt \cdot \nabla U(\mathbf{x_0}, t)} \tag{2.73}$$

with the Stokes velocity U_S given by:

$$U_S = \overline{\int_{t_0}^{t} U dt \cdot \nabla U} = \overline{\int_{t_0}^{t} U' dt \cdot \nabla U'} \tag{2.74}$$

Using an alternative formulation that guarantees mass conservation U_S can be written as:

$$U_S = \nabla \times \mathbf{B} \tag{2.75}$$

where

$$B_x = \overline{v' \int w' dt} \tag{2.76}$$

$$B_y = \overline{w' \int u' dt} \tag{2.77}$$

$$B_z = \overline{u' \int v' dt} \tag{2.78}$$

In order to avoid storing all velocities in the averaging interval Δt in order to compute $\mathbf{B}$ Dortch (1991) uses the following technique. Taking as an example term B_z it can be written in the following form:

$$B_z = \overline{u'\eta'} \tag{2.79}$$

where η' is the cumulative displacement vector resulting from the velocity deviation v'

By expanding Eqn 2.79 and taking averages we get:

$$B_z = \overline{u}\overline{\eta} - \overline{u}\overline{t}\overline{v} \tag{2.80}$$

As mentioned before this method was applied in the Chesapeake Bay study (1990). Chesapeake Bay is a partially mixed estuary approximately 300km long, 50km wide at its widest point and with an average depth of about 8m. The tidal range reaches a maximum value of 0.8m and so κ takes the value of 0.05 which allows the use of a first order approximation (i.e. Stokes drift) for the Lagrangian residuals. Intratidal (i.e. averaging time step is less than a tidal period) and intertidal (i.e. averaging time step is greater than a tidal period) tests were conducted during the September 1983 and the 1985 simulation periods. A sensitivity analysis was conducted to investigate the effect of the length of the averaging period. The QUICKEST scheme was used in the TM. The main conclusions are the following:

- The storage requirement decreases significantly (i.e. at least an order of magnitude) by using intertidal averaging.
- The computational effort also decreases significantly by using intertidal averaging.
- The size of the TM time step is restricted by the presence of non tidal forcings (e.g. wind).
- Due to the use of the Eulerian scheme QUICKEST the Courant number restriction has to be satisfied. As a result of that QUICKEST fails to accomodate intertidal time steps and so in the TM calculations the intertidal time step Δt_{TM}

is subdivided in n_{TM} time steps δt_{TM} so that $\Delta t_{TM} = n_{TM}\delta t_{TM}$. Over the time interval Δt_{TM} the same velocity field resulting from the Eulerian average plus the Stokes drift over Δt_{TM} is used. This use of a Lagrangian velocity in an Eulerian scheme is conceptually not correct.

2.6.3 Eulerian-Lagrangian methods

As described in Section 3.4 Eulerian-Lagrangian methods are based on the decomposition of the transport equation into an advective and diffusive part. The advective part is solved with the backwards method of characteristic lines, e.g. using the Lagrangian approach, whereas the diffusive part is solved using an Eulerian technique. This approach solves the problem of modeling Lagrangian transport in a natural way. The backwards method of characteristics provides a direct means of computing Lagrangian residual circulation. The methodology is the following: Over each interval Δt_{TM} the characteristic lines are tracked backwards and so the small Δt_{HM} is incorporated in the calculations (Fig 2-7). In terms of storage cost, that means that the HM velocities at the interval Δt_{TM} would have to be saved and postprocessed by the backtracking subroutine. If we take a 12h averaging period and $\Delta t_{HM} = 10min$ with a common domain of 25000 nodes (e.g. Massachusetts Bay) the storage of the three velocity components translates to a storage requirement of $O(40Mb)$ which is reasonable for a workstation.

The Eulerian-Lagrangian approach has the following advantages compared to the Lagrangian residuals approach used in the Chesapeake Bay application:

- There is no Courant number restriction hence Δt_{TM} can be chosen quite large. The problem of subdividing Δt_{TM} in order to accomodate the Courant number restriction is not an issue here.

- In cases where the nonlinearity parameter κ is large i.e. San Fransisco Bay, North Sea (Dortch, 1990) one has to also compute the Lagrangian drift velocity using the Lagrangian residuals approach whereas in Eulerian-Lagrangian

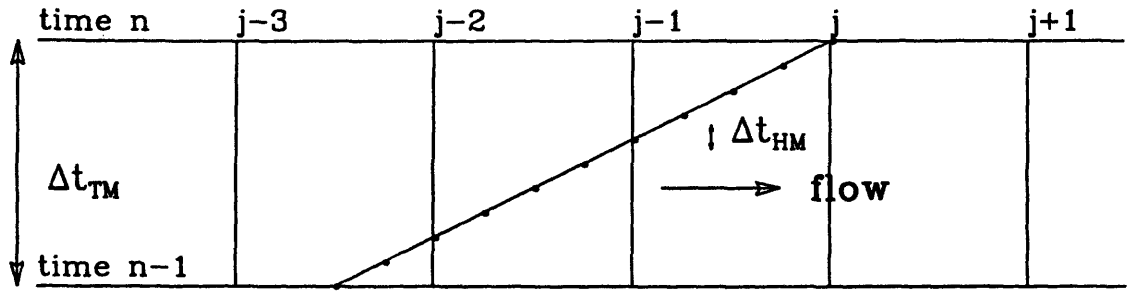

Figure 2-7: Eulerian-Lagrangian approach for coupling the HM with the TM.

methods the approach remains the same regardless of κ.

- There are cases where the finite amplitude approximation (Eqn 2.70) does not hold, e.g. flow close to headlands and so the Lagrangian velocities can not be computed from the Eulerian velocities (Signell,1987). The Eulerian-Lagrangian approach does not depend on κ.

- The coupling of the TM with the HM does not add in terms of computational cost as is the case in the computation of the Stokes drift, because it is part of the solution of the advective part.

In conclusion one can claim that the Eulerian-Lagrangian approach is ideal for incorporating the small time step HM input into the TM from an accuracy and cost point of view. It is also more robust since it can be used in all applications regardless of the value of κ. The next step as mentioned in Chapter 7 would be to apply this method in a case study preferably a case study where the Lagrangian residuals method has been applied (i.e. Chesapeake Bay) and compare the performance of the two methods.

2.7 REFERENCES

1. Awaji, T. Water mixing in a tidal current and the effect of turbulence on tidal exchange through a strait. J. Phys. Oceanogr. 12(6), 501-514. 1982.

2. Baptista, A. M., E. E. Adams, and K. D.Stolzenbach. Eulerian-Lagrangian analysis of pollutant transport in shallow water. Tchnical Report No. 296. MIT. 1984.

3. Baptista, A. M. Solution of advection-dominated transport by Eulerian-Lagrangian methods using the backwards method of characteristics. Ph. D. thesis. Dept. of Civil Engineering. MIT. 1987.

4. Benque, J. P., and J. Ronat. Quelques difficultes des modeles numeriques en hydraulique. In Computing methods in applied sciences and engineering. V. Glowinski

and Lions, eds., North-Holland, 471-494. 1982.

5. Blumberg, A. F., and G. L. Mellor. A description of a three-dimensional coastal ocean circulation model. Three-Dimensional Coastal Ocean Models, ed. by N. S. Heaps. AGU. Washington D.C. 1-16. 1987.

6. Casulli V. and R. T. Cheng. A semi-implicit finite difference model for three-dimensional tidal circulation. Proc. 2nd International Conference on Estuarine and Coastal Modeling. Nov. 1991. Tampa, FL. 1992.

7. Celia, M. A., I. Herrera, and E. T. Bouloutas. Adjoint Petrov-Galerkin methods for multi-dimensional flow problems. Finite element analysis in fluids. Chung and Karr, eds. UAH Press, 965-970. 1989.

8. Christie, I. D. F. Griffiths, and A. R. Mitchell. Finite element methods for second order differential equations with significant first derivatives. Int. J. Num. Meth. Engrg. 10:1389-1396. 1976.

9. Dahle, K. H., and M. S. Espedal, and R. E. Ewing. Characteristic Petrov-Galerkin subdomain method for convection diffusion problems. In IMA v. 11, Numerical simulation in oil recovery. M. F. Wheeler, ed. Springer-Verlag, 77-88. 1988.

10. Dortch, M. S., and R. S. Chapman. Interfacing time-varying, three-dimensional hydrodynamic model output for Cheasapeake Bay water quality model. Proc. Estuarine and Coastal Modeling 1989, ASCE. 1989.

11. Dortch, M. S. Three-Dimensional, Lagrangian Residual Transport Computed from an Intratidal Hydrodynamic Model. Technical Report EL-90-11, US Army Engineer Waterways Experiment Station, Vicksburg, MS. 1990.

12. Douglas, J., Jr., and T. F. Russell. Numerical methods for convection-dominated diffusion problems based on combining the method of characteristics with finite element or finite difference procedures. SIAM J. Num. Analysis 19:871-885. 1982.

13. Espedal, M. S., and R. E. Ewing. Characteristic Petrov-Galerkin subdomain

methods for two-phase immiscible flow. Comp. Meth. Appl. Mech. Engrg. 64:113-135. 1987.

14. Ewing, R. E., T. F. Russell, and M. F. Wheeler. Convergence analysis of an approximation of miscible displacement in porous media by mixed finite elements and a modified method of characteristics. Comp. Meth. Appl. Mech. Engrg. 47:73-92. 1984.

15. Feng S., R. T. Cheng and P. Xi. 1986. On Tide - Induced Residual Current and Residual Transport, 2. Residual Transport with Application in South San Francisco Bay, California. Water Resources Research. Vol 22(2) 1635-1646.

16. Feng, S. A Three-Dimensional Weakly Nonlinear Model of Tide-Induced Lagrangian Residual Current and Mass-Transport, with an Application to the Bohai Sea. Three-Dimensional Models of Marine and Estuarine Dynamics. Elsevier Oceanography Series. Ed. by J. C. J. Nihoul and B. M. Jamart, Vol. 45, Amsterdam, pp. 471-488. 1987.

17. Gardiner, C. W. Handbook of stochastic methods for physics, chemistry, and the natural sciences. Second ed., Springer Verlag. 1985.

18. Glass, J., and W. Rodi. A higher order numerical scheme for scalar transport. Computer Methods in Applied Mechanics and Engineering 31:337-358. 1982.

19. van Genuchten, M. T., W. G. Gray. Finite elements in water resources. W. G. Gray, G. F. Pinder, C. A. Brebbia, eds. pp1.71-1.90. Pentech. 1977.

20. Hasbani, Y., E. Livne, and M. Bercovier. Finite elements and characteristics applied to advection-diffusion equations. Computer and Fluids 11(2):71-83. 1983.

21. Hervouet, J. M. Application of the method od characteristics in their weak formulation to solving two-dimensional advection equations on mesh grids. Computational techniques for fluid flow. Recent advances in numerical methods in fluids, v. 5, Taylor et al., eds., Pineridge Press, 149-185. 1986.

22. Hughes, T. J. R., and A. Brooks. A multidimensional upwind scheme with no crosswind diffusion. Finite element methods for convection dominated flows. Hughes, ed., AMD v. 34, ASME. 1979.

23. Hughes, T. J. R., and T. E. Tezduyar. Finite element methods for first-order hyperbolic systems with particular emphasis on the compressible Euler equations. Comp. Meth. Appl. Mech. Engrg. 45:217-284. 1984.

24. Hydroscience, Inc. Final Report. Development of water quality model of Boston Harbor. Publ. Number: 6763(227-44-5-73-CV). Commonwealth of Massachusetts. Water Resources Commission. Boston. Massachusetts. 1971.

25. Johnson, B. H., K. W. Kim, Y. P. Sheng, and R. E. Heath. Development of Three-Dimensional Hydrodynamic Model of Chesapeake Bay. Procedings of Conference on Estuarine and Coastal Modeling. ASCE. Nov 15-17, 1989. Newport, RI. 1990.

26. Konikow, L. F., J. D. Bredehoft. Computer model of two-dimensional solute transport and dispersion in groundwater. Book 7, Ch. 2, U.S. Geological Survey. 1978.

27. Leendertse, J. J. Turbulence Modeling of Surface Water Flow and Transport: Part IV: Discussion. J. Hydr. Div., ASCE, 116(4), 603-606. 1990.

28. Leonard, B. P. A stable and accurate convective modeling procedure based on quadratic upstream interpolation. Comp. Meth. Appl. Mech. Engrg. 19:59-98. 1979.

29. Longuet-Higgins, M. S. On the Transport of Mass by Time-Varying Ocean Currents. Deep-Sea Research and Oceanographic Abstracts, Vol. 16, pp. 431-447. 1969.

30. Lynch, D. R., and F. E. Werner. Three-dimensional hydrodynamics on finite elements. Part I: Linearized harmonic model. Int. J. Numerical Meth. in Fluids. 7, 871-909. 1987.

31. Lynch, D. R., and F. E. Werner. Three-dimensional hydrodynamics on finite

elements. Part II: Nonlinear time-stepping model. Int. J. Numerical Meth. in Fluids. 1990.

32. McDonald, A. Accuracy of multiply-upstream, semi-Lagrangian advective schemes. Monthly Weather Review 112:1267-1275. 1984.

33. Mellor, G. L., and A. F. Blumberg. Modeling vertical and horizontal diffusivities and the sigma coordinate system. Monthly Weather Review 113:1379-1383. 1985.

34. Neuman, S. P. An Eulerian-Lagrangian scheme for the dispersion-convection equation using conjugate space-time grids. J. Comp. Physics 41:270-279. 1981.

35. Neuman, S. P. Adaptive Eulerian-Lagrangian finite element method for advection-dispersion. Int'l. J. Numerical Methods in Engineering 20:317-337. 1984.

36. Nguyen, K. D., and J. M. Martin. A two-dimensional fourth-order simulation for scalar transport in estuaries and coastal seas. Estuarine, Coastal and Shelf Science 27:263-281. 1988.

37. Officer, C. B. Physical Oceanography of Estuaries. John Wiley and Sons, Inc., New York, NY. 1976.

38. O' Neill, K., and D. R. Lynch. In Proceedings, 3rd Intl. Conf. on Finite Elements in Water Resources, Univ. of Mississippi, Oxford, 1:3.67-3.76. 1980.

39. Phillips, N. A. A coordinate system having some special advantages for numerical forecasting. J. Meteorol. 14:184-185. 1957.

40. Pinder, G. F., and H. H. Cooper. A numerical technique for calculating the transient position of the last water front. Wat. Resources Res. 6(3):875. 1970.

41. Pironneau, O. On the transport diffusion algorithm and its application to the Navier-Stokes equations. Numer. Meth. 38:309-332. 1982.

42. Price, H. S., R. S. Varga, and J. R. Warren. J. Math. Phys. 45:301-311. 1966.

43. Raithby, G. D. and K. E. Torrance. Upstream-weighted schemes and their application to elliptic problems involving fluid flow. Computers and Fluids 2:191-206. 1974.

44. Ritchie, H. Application of a semi-Lagrangian integration scheme to the moisture equation in a regional forecast model. Monthly Weather Review 113:424-435. 1985.

45. Roache, P. J. Computational fluid dynamics. Hermosa. 1972.

46. Robert, A. A stable numerical integration scheme for the primitive meteorological equations. Atmos. Ocean. 19:35-46. 1981.

47. Russell, T. F. Time stepping along characteristics with incomplete iteration for a Galerkin approximation of miscible displacement in porous media. SIAM J. Num. Analysis 22:970-1013. 1985.

48. Signell R. P. Tidal rectification and Lagrangian drift around coastal headlands. Thesis Proposal. Woodshole Oceanographic Institute. 1987.

49. Tompson, A. F. B., E. G. Vomvoris, L. W. Gelhar. Numerical simulation of solute transport in randomly heterogeneous porous media: Motivation, model development and application. Report No. MIT-316. 1988.

50. Tompson, A. F. B., L. W. Gelhar. Numerical simulation of solute transport in three-dimensional randomly heterogeneous porous media. Water Resources Research 26(10):2541-2562. 1990.

51. Westerink, J. J., D. Shea. Consistent higher degree Petrov-Galerkin methods for the solution of the transient convection-diffusion equation. Int. J. Num. Meth. in Eng. Accepted. 1990.

52. Wheeler, M. F., C. N. Dawson. An operator-splitting method for advection-diffusion-reaction problems. MAFELAP Proceedings VI, J. A. Whiteman, ed. Academic Press, 463-482. 1988.

53. Williamson, D. L., P. J. Rasch. Two-dimensional semi-Lagrangian transport with shape-preserving interpolation. Monthly Weather Review 117:102-129. 1989.

Chapter 3

3-D Eulerian-Lagrangian Mass Transport Model

3.1 General

A transport model solves the following equation in the (x, y, z) coordinate system:

$$\frac{\partial c}{\partial t} + \nabla \cdot \mathbf{v}c = \nabla \cdot \mathbf{K} \cdot \nabla c + Q, \tag{3.1}$$

where c(x,t) is the concentration, v(x,t) is the velocity vector, K(x,t) is the diffusivity tensor, Q represents point sources/sinks

To complete the formulation initial and boundary conditions must be imposed. Such conditions are of the form (Fig 3-1)

$$\begin{aligned} c(\mathbf{x},t) &= c_0(\mathbf{x}) \quad at \quad t=0 \quad in \quad \Omega \\ c(\mathbf{x},t) &= \bar{c}(\mathbf{x},t) \quad at \quad t>0 \quad on \quad \Gamma_1 \\ q_n(\mathbf{x},t) &= \bar{q_n}(\mathbf{x},t) \quad at \quad t>0 \quad on \quad \Gamma_2 \end{aligned} \tag{3.2}$$

where q_n represents the flux normal to the boundary defined as

$$q_n = -K_j \frac{\partial c}{\partial x_j} cos(\hat{n}, \hat{x}_i) \tag{3.3}$$

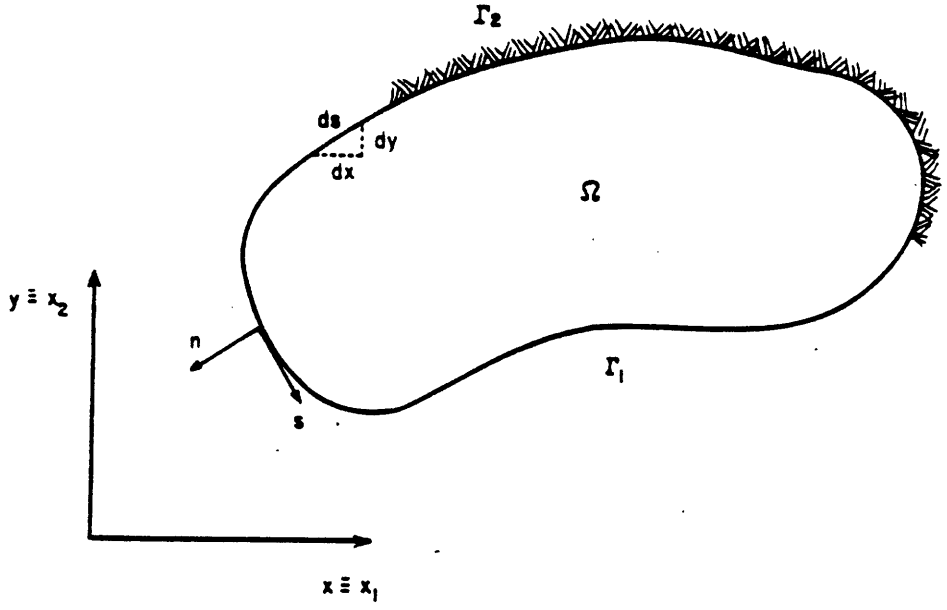

Figure 3-1: Boundary Conditions in Transport Problem.

As mentioned in Chapter 2 the major difficulties associated with the solution of this equation in coastal water problems are the facts, that the flow is highly advection dominated and the presence of a moving upper boundary and sometimes a highly irregular bottom boundary. In order to resolve the first problem an Eulerian-Lagrangian scheme was used. In order to resolve the representation of the upper and bottom boundary and for reasons of compatibility with an available hydrodynamic model (Lynch et al, 1991) a σ coordinate system was used.

The developed 3-D transport model is based on the 2-D Eulerian-Lagrangian transport model (ELA) developed by Baptista et al (1984) and on an extensive analysis by Baptista (1987) on the issues of convergence, consistency and stability. In this study particular emphasis is given on the cost issue and the choice of the optimal timestep based on cost/accuracy analysis. Because of the dimensionality of the problem the choice of the solver is also of particular importance.

3.2 Eulerian-Lagrangian Methods

Mixed Eulerian-Lagrangian methods attempt to eliminate difficulties related to highly advective problems by combining the simplicity of a fixed Eulerian grid with the computational power of a Lagrangian approach. Most commonly, they split the transport equation into a pure advection part, that is solved by the backwards method of characteristics and a pure diffusion part, that is solved by some conventional global discrete element technique, e.g., finite elements or finite differences (Baptista,1987). Eulerian-Lagrangian methods are called by a variety of names (Celia et al., 1989) including transport diffusion method (Benque and Ronat, 1982; Pironneau, 1982; Herevouet, 1986), method of characteristics (MOC) (Cooper and Pinder, 1970), modified method of characteristics (MMOC) (Ewing et al., 1984; Russell, 1985; Douglas and Russell, 1982), operator splitting methods (Espedal and Ewing, 1987; Dahle et al., 1988; Wheeler and Dawson, 1988), localized adjoint methods (Celia et al., 1989), and semi-Lagrangian (Williamson and Rasch, 1989; McDonald, 1984; Ritchie, 1985; Robert, 1981).

ELM have been extensively used in many disciplines in order to solve transport problems with hyperbolic dominating terms (i.e., groundwater, petroleum engineering, surface water transport, meteorology). With ELM the problem of small Courant and Peclet numbers is eliminated. The general procedure used is the following. Eqn 3.1 is transformed into its nonconservative form

$$\frac{\partial c}{\partial t} + \mathbf{v} \cdot \nabla c = \nabla \cdot \mathbf{K} \cdot \nabla c + Q \tag{3.4}$$

According to the most common approach Eqn 3.4 is discretized in time according to

$$\frac{c^n - c^{n-1}}{\Delta t} + [\mathbf{v} \cdot \nabla c]^{n-1} = [\nabla \cdot \mathbf{K} \cdot \nabla c]^n \tag{3.5}$$

The initial and boundary conditions of the problem are written in discretized form as:

$$\begin{array}{lcllll} c & = & c^{n-1} & at & n-1 & in \quad \Omega \\ c^n & = & \bar{c} & at & n & on \quad \Gamma_1 \\ q_n^n & = & \bar{q_n} & at & n & on \quad \Gamma_2 \end{array} \tag{3.6}$$

By defining an auxiliary variable c^f Eqn 3.5 can be split into two components due to its linearity, i.e. a pure advective component

$$\frac{c^f - c^{n-1}}{\Delta t} + [(\mathbf{v} - \nabla \cdot \mathbf{K}) \cdot \nabla c]^{n-1} = 0 \tag{3.7}$$

and a pure diffusive component

$$\frac{c^n - c^f}{\Delta t} = [\mathbf{K} \cdot \nabla^2 c]^n \tag{3.8}$$

Using the auxiliary variable c^f the discretized form of the initial and boundary conditions is decomposed into two parts i.e.

$$\left.\begin{array}{lllllll} c & = & c^{n-1} & at & n-1 & in & \Omega \\ c^f & = & \bar{c} & at & n & on & \Gamma_1 \end{array}\right\} advection \quad part \tag{3.9}$$

$$\left.\begin{array}{lllllll} c & = & c^f & at & n-1 & in & \Omega \\ c^n & = & c^f & at & n & on & \Gamma_1 \\ q_n^n & = & \bar{q}_n & at & n & on & \Gamma_2 \end{array}\right\} diffusion \quad part \tag{3.10}$$

Eqn 3.7 states that the concentration c remains constant along characteristic lines defined by

$$\frac{d\mathbf{x}}{dt} = \mathbf{v}^* \tag{3.11}$$

with $\mathbf{v}^*$ given in the (x,y,z) coordinate system by

$$\mathbf{v}^* = (\mathbf{v} - \nabla \cdot \mathbf{K}) \tag{3.12}$$

According to Eqn 3.11, Eqn 3.7 is solved by tracking characteristic lines backwards from time n to time n-1 from every node (Fig 3-2). The concentrations c^f at time n are determined by spatial interpolation. Eqn 3.8 is solved by using centered finite differences (i.e., Nguyen and Martin, 1988) or finite elements (i.e. Baptista, 1987; Russell, 1985; Hasbani et al., 1983).

Using the analysis presented in Chapter 2 the mass transport equation in the (x,y,σ) coordinate system is given by:

$$\begin{aligned} &\frac{\partial(cD)}{\partial t} + \frac{\partial(cUD)}{\partial x} + \frac{\partial(cVD)}{\partial y} + \frac{\partial(c\omega)}{\partial \sigma} = \\ &\quad \frac{\partial}{\partial x}[DK_x \frac{\partial c}{\partial x}] + \frac{\partial}{\partial x}[DK_{xy} \frac{\partial c}{\partial y}] + \\ &\quad \frac{\partial}{\partial y}[DK_y \frac{\partial c}{\partial y}] + \frac{\partial}{\partial y}[DK_{yx} \frac{\partial c}{\partial x}] + \frac{\partial}{\partial \sigma}[\frac{K_z}{D} \frac{\partial c}{\partial \sigma}] \end{aligned} \tag{3.13}$$

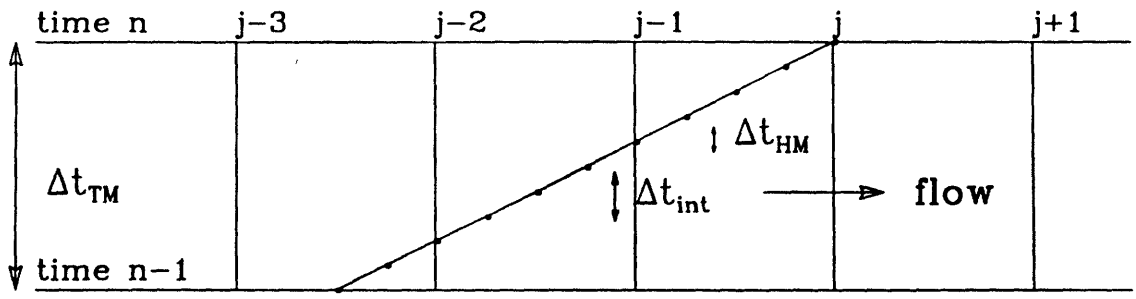

Figure 3-2: Definition of timesteps for different solution phases.

The non-conservative form of Eqn 3.13 is:

$$D\frac{\partial c}{\partial t} + uD\frac{\partial c}{\partial x} + vD\frac{\partial c}{\partial y} + \omega\frac{\partial c}{\partial \sigma} = \frac{\partial}{\partial x}[DK_x\frac{\partial c}{\partial x}] + \frac{\partial}{\partial x}[DK_{xy}\frac{\partial c}{\partial y}] + \frac{\partial}{\partial y}[DK_y\frac{\partial c}{\partial y}] + \frac{\partial}{\partial y}[DK_{yx}\frac{\partial c}{\partial x}] + \frac{\partial}{\partial \sigma}[\frac{K_z}{D}\frac{\partial c}{\partial \sigma}] \tag{3.14}$$

Eqn 3.14 can be written as:

$$\frac{\partial c}{\partial t} + u^*\frac{\partial c}{\partial x} + v^*\frac{\partial c}{\partial y} + \omega^*\frac{\partial c}{\partial \sigma} = K_x\frac{\partial^2 c}{\partial x} + K_{xy}\frac{\partial^2 c}{\partial x} + K_y\frac{\partial^2 c}{\partial y} + K_{yx}\frac{\partial^2 c}{\partial y} + \frac{K_z}{D^2}\frac{\partial^2 c}{\partial \sigma} \tag{3.15}$$

where

$$u^* = u - \frac{1}{D}\frac{\partial D}{\partial x}K_x - \frac{1}{D}\frac{\partial D}{\partial y}K_{yx} - \frac{\partial K_x}{\partial x} - \frac{\partial K_{yx}}{\partial y} \tag{3.16}$$

$$v^* = v - \frac{1}{D}\frac{\partial D}{\partial y}K_y - \frac{1}{D}\frac{\partial D}{\partial x}K_{xy} - \frac{\partial K_y}{\partial y} - \frac{\partial K_{xy}}{\partial x} \tag{3.17}$$

$$\omega^* = \frac{\omega}{D} - \frac{\partial(\frac{K_z}{D^2})}{\partial \sigma} \tag{3.18}$$

For reasons of compatibility with the available HM a σ coordinate system was used in this research. In the case of a cartesian coordinate system particular emphasis should be given to the fact that the upper boundary is moving. In order to accomodate the moving upper boundary the z-coordinates at the upper boundary must be a function of time. The developed model has the option of using a cartesian coordinate

system with fixed z- coordinates at the upper boundary equal to the mean water level (i.e. $z = 0$).

The main issues in an ELM are the selection of

- the integration scheme for the tracking
- the interpolation functions
- the numerical scheme for the solution of the diffusion equation
- the order of the time discretization

Related to the 3-D character of the ELM is

- the selection of a solver for the solution of the symmetric, positive definite system of linear equations resulting from the diffusion equation

3.3 Form of Errors / Optimal Timestep Issue

The size of the timestep is dictated by the physics (chemistry or biology) and by the numerics of the problem; i.e., if we designate as Δt_{ph} the critical timestep dictated by the physics (chemistry or biology) and as Δt_{num} the critical timestep dictated by the numerics then the timestep Δt_{TM} used in the model must satisfy the relation

$$\Delta t_{TM} = min(\Delta t_{ph}, \Delta t_{num}) \tag{3.19}$$

Baptista (1987) developed a generalized Fourier method in order to investigate the stability of the backwards method of characteristics for cases of higher order interpolation functions. He used this method to also look at consistency and convergence issues related to the use of different interpolation functions and time integration schemes in 1-D cases. He used the results of his 1-D analysis in the developed 2-D depth averaged finite element model ELA and found that they also applied to the

2-D case. This work involves the development of a 3-D Eulerian-Lagrangian model based on the 2-D Eulerian-Lagrangian transport model developed by Baptista (1984). The results of previous investigations (Baptista, 1897; Zhang, 1990) are verified in the 3-D model. This study focuses primarily on the issue of cost vs accuracy of an Eulerian-Lagrangian model in a 3-D case.

Due to the existence of the different treatment of the two components i.e. advection and diffusion the total truncation error ϵ_{tot} can be expressed as:

$$\epsilon_{tot} = \epsilon_{adv} + \epsilon_{dif} \tag{3.20}$$

where

ϵ_{adv} is the truncation error in the solution of the advection component

ϵ_{dif} is the truncation error in the solution of the diffusion component

The truncation errors ϵ_{adv} and ϵ_{dif} can be further decomposed as

$$\epsilon_{adv} = \underbrace{\epsilon_{adv}^{svel} + \epsilon_{adv}^{tvel}}_{\epsilon_{adv}^{vel}} + \epsilon_{adv}^{tr} + \epsilon_{adv}^{int} \tag{3.21}$$

where ϵ_{adv}^{vel} is the error due to the velocity interpolation. It may be further divided into two components: ϵ_{adv}^{svel} associated with the spatial interpolation of velocities and ϵ_{adv}^{tvel} associated with the temporal interpolation of velocities.

ϵ_{adv}^{tr} is the truncation error due to the tracking

ϵ_{int} is the error in the interpolation of concentrations at the feet of characteristic lines

and

$$\epsilon_{dif} = \epsilon_{dif}^{sd} + \underbrace{\epsilon_{dif}^{tmd} + \epsilon_{dif}^{tdf}}_{\epsilon_{dif}^{td}} \tag{3.22}$$

where

ϵ_{dif}^{sd} is the error due to the space discretization of the dispersion operator

ϵ_{dif}^{td} is the error due to the time discretization of the dispersion operator along the characteristic lines. It may be divided into two components: ϵ_{dif}^{tmd} asociated with the time dicretization along parallel characteristic lines defined by a mean flow; and ϵ_{dif}^{tdf} that accounts for the fact that characteristic lines may come closer or further away from each other as time progresses due to flow non-uniformity (Baptista, 1987).

The existence of the different numerical schemes combined with the fact that the TM depends on input from HM results to the use of the following timesteps in the numerical simulation (Fig 3-2):

Δt_{HM} : the timestep used in the HM

Δt_{int} : the timestep used in the tracking of the characteristic lines

Δt_{TM} : the timestep of the TM i.e. the timestep of Eqn 3.5 which also designates how often the concentration interpolations are computed.

Since Δt_{HM} is defined in the HM , in order to achieve an accurate and cost efficient algorithm one has two degrees of freedom: Δt_{int} and Δt_{TM}. The error due to the velocity interpolation also depends partly on the HM.

In this study we are primarily concerned with the choice of Δt_{int} and Δt_{TM} so that ϵ_{adv}^{tr}, ϵ_{adv}^{int} and ϵ_{dif} become of comparable magnitude. Fig 3-3 shows qualitatively the balance between ϵ_{adv}^{int} and ϵ_{dif} when $\epsilon_{adv}^{tr} = 0$. We see that for a pure advective case ($\epsilon_{dif} = 0$) ϵ_{tot} increases as Δt_{TM} decreases whereas in the pure diffusion case the contrary holds. The solution of the diffusion part becomes a major issue in 3-D problems because of the high cost associated with it. Fig 3-4 shows qualitatively the balance between ϵ_{adv}^{int} and ϵ_{adv}^{tr} in a pure advective case. We see that unless a balance between the two errors is achieved unnecessary CPU time may be wasted on overly accurate tracking or on an overly high order interpolation functions. Apart from the issue of error balance the issue of designing the code (e.g. tracking strategy, recognition of boundaries etc) becomes of particular importance in a 3-D case where cost is a major issue. A thorough investigation of the integration scheme and the tracking strategy is conducted in this study.

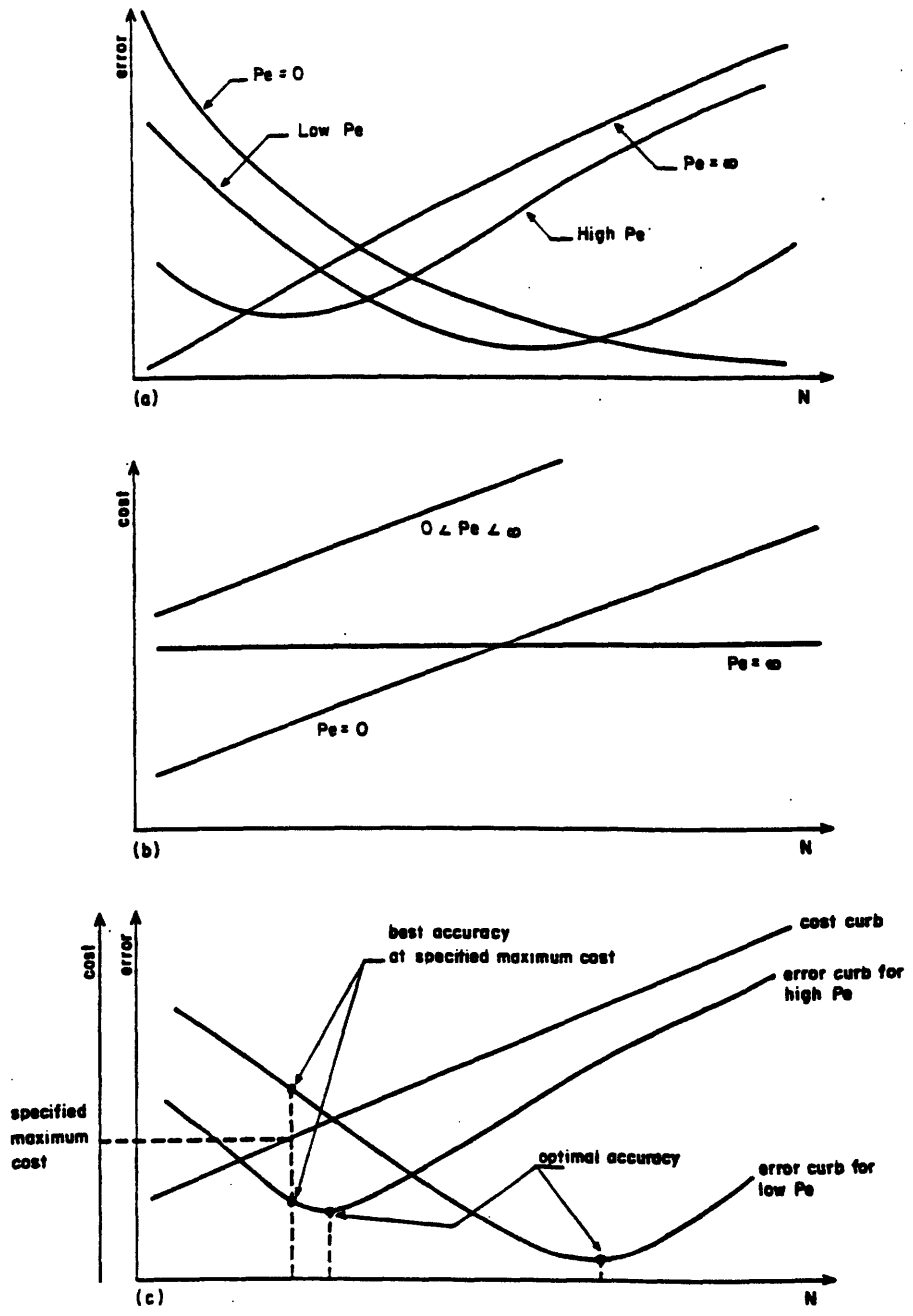

Figure 3-3: Δt_{TM} vs. error = ϵ_{adv}^{int} and ϵ_{dif} (from Baptista, 1985).

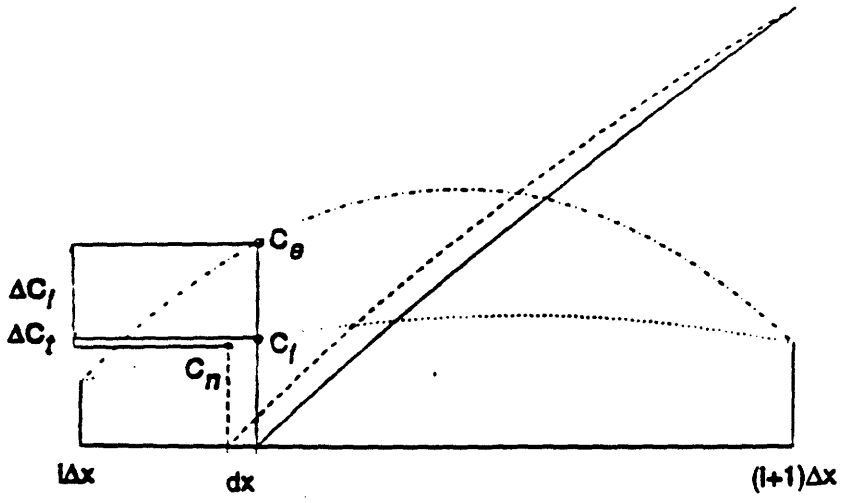

(a)

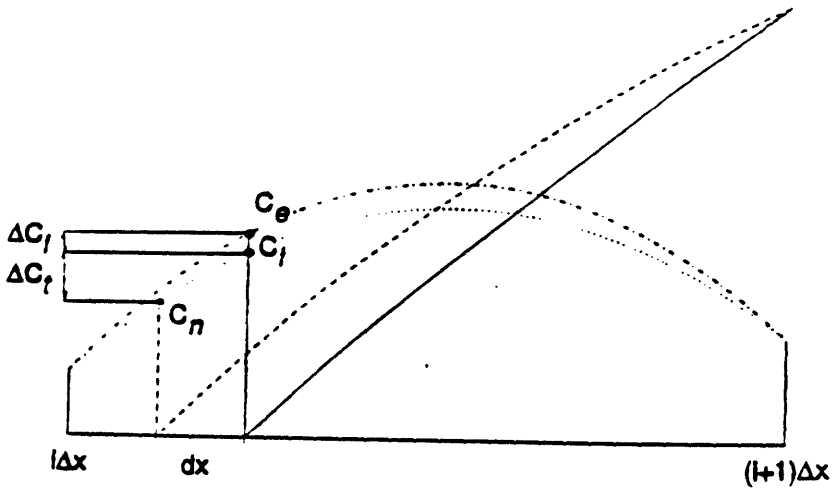

(b)

Figure 3-4: ϵ_{adv}^{int} vs ϵ_{adv}^{tr}. (a)ϵ_{adv}^{int} dominates. (b) ϵ_{adv}^{tr} dominates. (from Zhang, 1990) .

3.4 Advective Part

3.4.1 Integration scheme for tracking

In order to resolve the fact that ELM are not inherently mass conservative highly accurate tracking techniques must be used. Two alternatives have been followed by researchers.

- Use of low-order schemes and small timesteps Δt_{int}
- Use of high-order schemes, that allow for larger timesteps Δt_{int}

The main higher order schemes used are Euler predictor corrector methods (Glass and Rodi, 1982; Nguyen and Martin, 1988), second order Runge-Kutta methods (Hasbani et al., 1983), fourth-order Runge-Kutta methods (Ahsan and Bruno, 1989), and the fifth order Runge-Kutta method, i.e. fourth-order Runge-Kutta method with adaptive timestep (Baptista, 1984). Russell(1985) approximates the characteristics by a sequence of line segments corresponding to sub-timesteps and each of these segments is determined by a predictor corrector method, that keeps expected error below a tolerance.

Making the assumption of very accurate tracking or tracking with controlled error in order to decrease the total error the number of interpolations has to decrease also i.e., the size of the timestep Δt_{TM} has to increase.

Cost analysis of the existing 2 - D Eulerian-Lagrangian model (Zhang, 1990) has shown that by far the most expensive part in a simulation is the tracking part. In order to understand how to control this cost a full description of how the tracking algorithm works has to be presented.

Backtracking of the characteristic lines involves solution of the equation

$$\frac{d\mathbf{x}}{d\tau} = \mathbf{v}^*(\mathbf{x}(\tau), \tau) \quad (n-1)\Delta t_{TM} \leq \tau < n\Delta t_{TM} \tag{3.23}$$

In order to complete the integration using the chosen integration method we start with an initial timestep Δt_{int} with

$$\Delta t_{int} \leq \Delta t_{TM} \tag{3.24}$$

and continue until the integration is completed. Fig 3-5 shows a flowchart of the backtracking algorithm.

The fifth order Runge Kutta method is used in this research (Press et al., 1986). It is a fourth order integration scheme combined with step doubling to monitor the truncation error. The step doubling works as follows: Suppose tracking is being performed from time t to time $t - \delta t$ where $x(t - \delta t)$ is the exact solution and the two approximate solutions are x_1 (one step of size δt) and x_2 (two steps of size $\frac{\delta t}{2}$). If we define $\Delta = x_2 - x_1$ and ϵ as an accuracy control parameter then ϵ_{adv}^{int} can be controlled by requiring

$$\Delta \leq \epsilon\sqrt{(\delta x)^2 + (\delta y)^2 + (\delta z)^2} \tag{3.25}$$

where δx, δy, δz are the distances transversed during the step interval Δt_{int}. According to this the tracking error is

$$\epsilon_{adv}^{int} = 0(\epsilon u \Delta t_{int}) \tag{3.26}$$

After completing the integration along Δt_{int} the algorithm starts searching for the element, where the foot of the characteristic line (FCL) is located. The searching proceeds as follows (Fig. 3-6). The element from which the integration started is searched first and if the FCL is not in this element the searching continues with the next group of surrounding elements until a certain limit of searched elements N_{max} is searched. The computational effort for searching these N_{max} elements becomes extremely expensive as N_{max} increases.

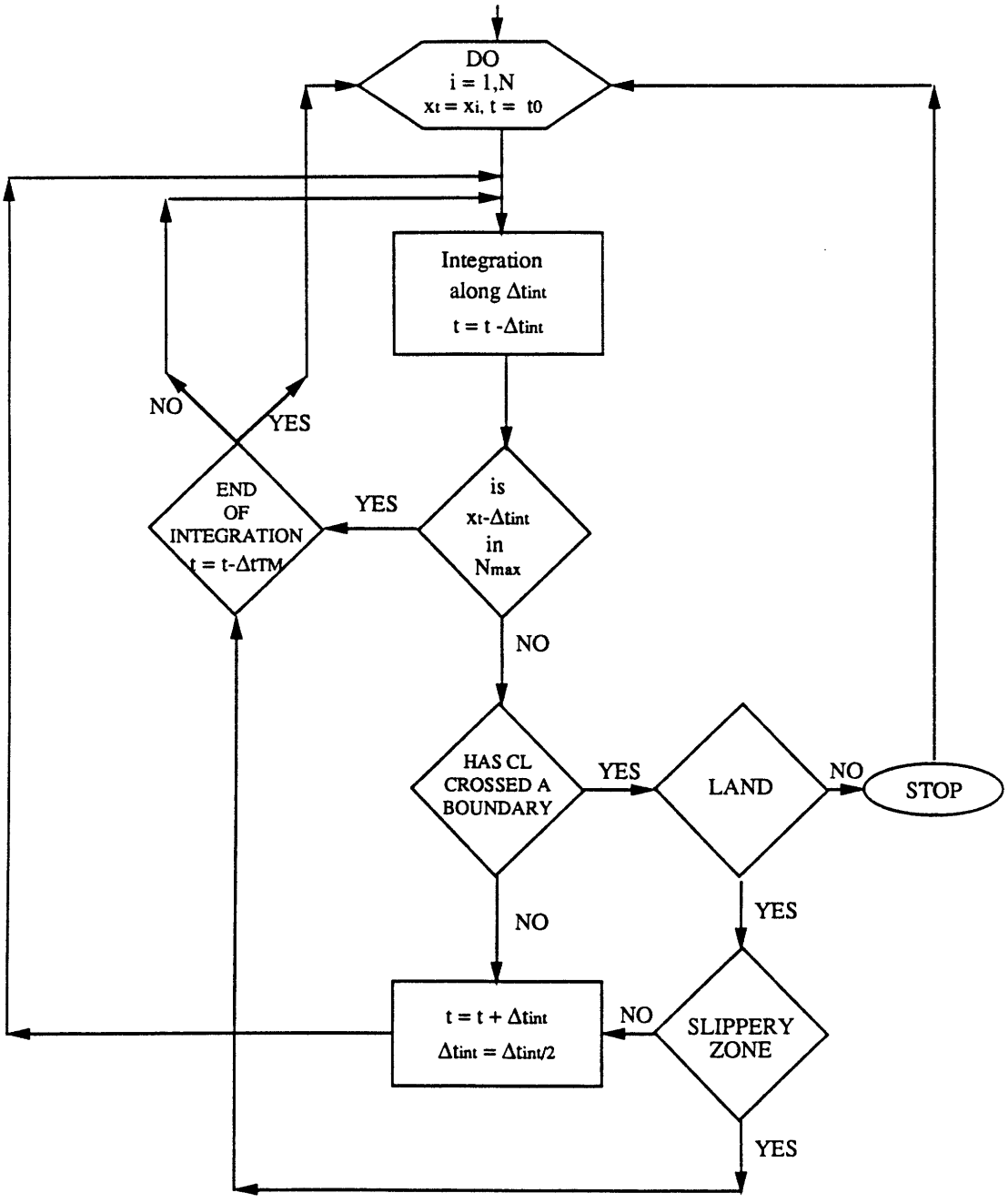

Figure 3-5: Flowchart of Backtracking Algorithm.

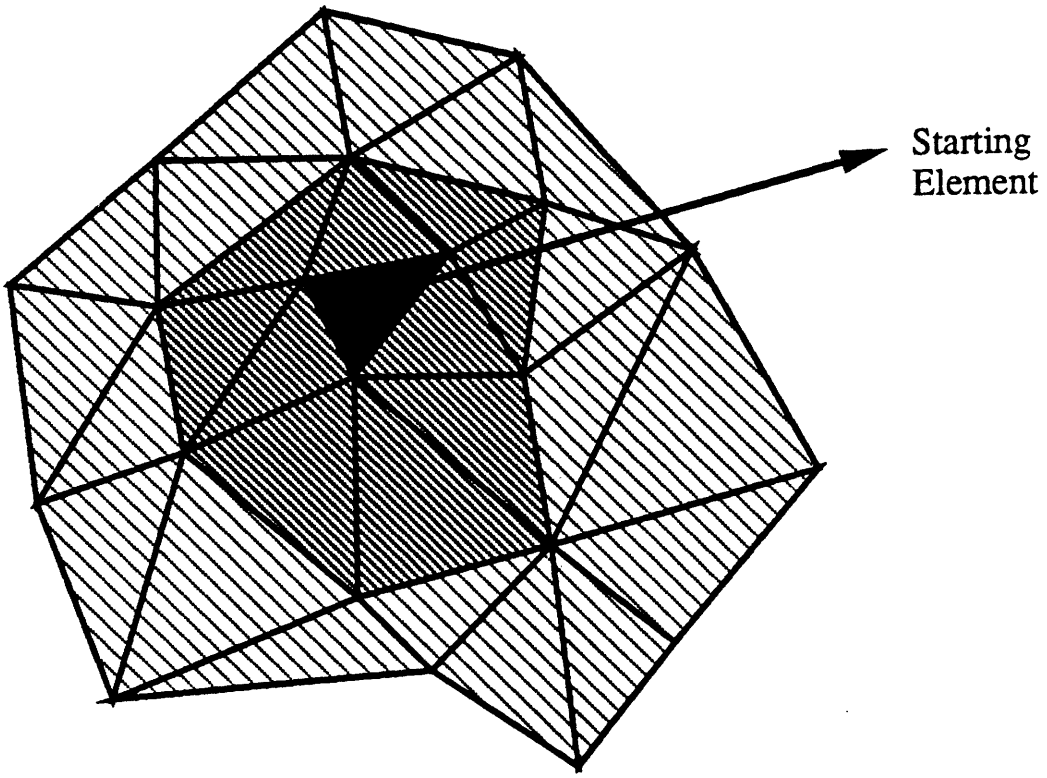

Figure 3-6: Searching method.

If the FCL is found in any of the adjacent elements in the case of an adaptive timestep integration technique like the fifth order Runge Kutta method used in this research a truncation error test described in this section is conducted. If the truncation error does not pass this test the integration timestep Δt_{int} is subdivided.

If FCL has not been found in the N_{max} elements the next thing to be checked is whether it has crossed a boundary. The same searching technique as before is used but now the question is whether it has crossed a boundary and whether this element is part of an open or land boundary.

Because of inaccuracies in the flow field a FCL may cross a land boundary. Instead of stopping the tracking exactly at the edge of the grid system the tracking routine allows the particle to move within a small 'slippery zone' (Fig. 3-7) defined as a thin band just outside of every element which forms part of the boundary. The width of the slippery zone is controlled by a parameter δ so the

$$\delta \leq \frac{l_{sl}}{l_{el}} \tag{3.27}$$

where l_{sl} is he length of the slippery zone and l_{el} is a characteristic length scale of the boundary element. The value of $\delta = 0.03$ is used in this study. If the FCL has crossed an open boundary the exact point the open boundary was crossed has to be found in order to assign to it the correct concentration according to the boundary conditions.

If the FCL is not in any of the adjacent elements N_{max} and none of them is a boundary element then the integration timestep Δt_{int} is subdivided and the same procedure is repeated.

If we designate as Cu_{int} the Courant number of the integration step i.e.,

$$Cu_{int} = \frac{u\Delta t_{int}}{\Delta x} \tag{3.28}$$

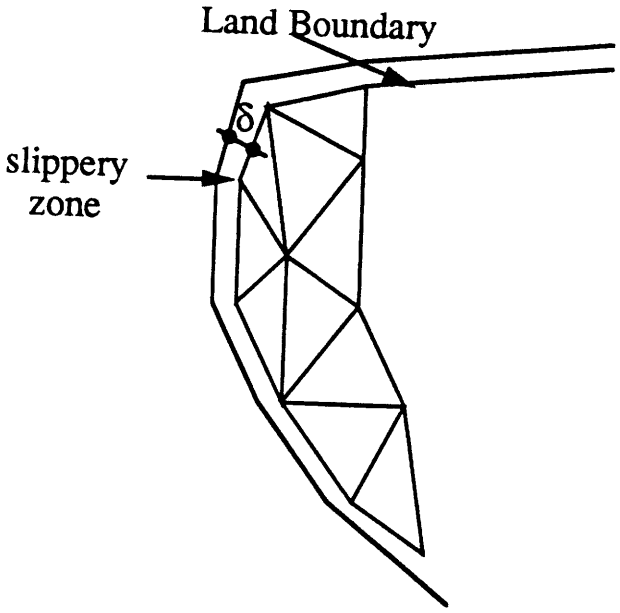

Figure 3-7: Slippery zone.

According to the above in the case of a fifth order Runge Kutta method described before Cu_{int} is prescribed by N_{max} or ϵ whichever is more restrictive. In the case of a tracking method without an error control mechanism Cu_{int} is prescribed by N_{max} only.

As seen from the above the backtracking of the characteristic lines consists of three parts:

- the actual tracking part by which the (x,y,z) location of the FCL at the end of each integration step is determined and
- the searching part by which the element where point (x,y,z) is located is determined or whether the FCL has reached an open or land boundary is determined.
- the accuracy control part by which Δt_{int} is adjusted to the desired accuracy level using the tolerance parameter ϵ as the criterion.

We investigate in this section the combined effect of

- The type of the tracking method used (the second and the fifth order Runge-Kutta method are compared)
- N_{max}
- Δt_{TM}
- ϵ

on the accuracy and cost of the backwards method of characteristics. Prismatic, triangular quadratic elements are used (Fig. 3-8). The interpolation functions are the same as the finite element basis functions.

The following error measures were used:

- Discrete $L-2$ error norm normalized by the total mass

$$\phi_D = \frac{1}{M}\{[\sum_i (c_i^{nu} - c_i^{ex})^2]^{\frac{1}{2}}\} \tag{3.29}$$

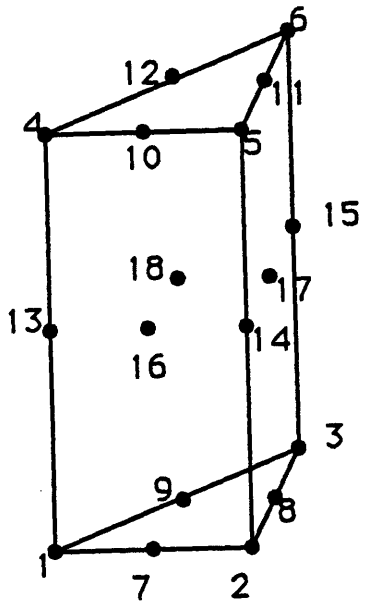

Figure 3-8: Prismatic Triangular Quadratic Finite Element.

- Error in the peak concentration normalized by the exact peak concentration

$$\epsilon(t) = \frac{c^{ex}_{max}(t) - c^{nu}_{max}(t)}{c^{ex}_{max}(t)} \tag{3.30}$$

The rigid body rotation test case was used as an example. A $32 \times 32 \times 32$ grid was used with $x, y \in [-2000, 2000]$, $z \in [-1, 0]$. The velocities were given by

$$u = -\omega_1 y, \quad v = \omega_1 x, \quad w = w_0 sin(\omega_2 t) \tag{3.31}$$

with $\omega_1 = \frac{2\pi}{3000}$, $\omega_2 = \frac{2\pi}{1000}$ $w_0 = 0.0002$ and uniform depth D = 1. The simulation time is 3000. A Gaussian cloud with $x_0 = 0.$, $y_0 = -1000$ and $z_0 = -0.5$, $\sigma_x = \sigma_y = 1\Delta x = 125$, and $\sigma_z = 1\Delta z = 0.03125$ is imposed as initial condition. Zero concentration conditions are imposed at the boundaries.

Fig. 3-12 shows the normalized error as a function of the timestep in a pure advection case. As seen the error increases as Δt_{TM} decreases but reaches a plateau as $\Delta t_{TM} \rightarrow 0$ which proves the consistency of the method (Baptista, 1987). Fig. 3-9 - Fig. 3-11 show the concentration field and the absolute error at $z = -0.5$. Negative concentration appeared in these runs and were of the order of one percent the maximum concentration. In Fig. 3-13 and Fig. 3-14 $K_x = K_y = 6.4$, $K_z = .8 * 10^{-6}$ and $K_x = K_y = 15.3$, $K_z = 2. * 10^{-6}$ were used respectively that correspond to Pe of 57 and 24. For estimating Pe the velocity at the location of the peak concentration at $t = 0$ is considered. We see that as expected the optimal timestep shifts to the left as Pe increases. In 3 - D transport problems in coastal waters the Peclet number is large and so the error introduced by the diffusion part is not decisive in choosing the size of the timestep.

Tracking Method

For the rigid body rotation example in a pure advection case Fig. 3-15 and Fig. 3-16 show the normalized error vs. N_{max} by using the second and fifth order Runge-Kutta

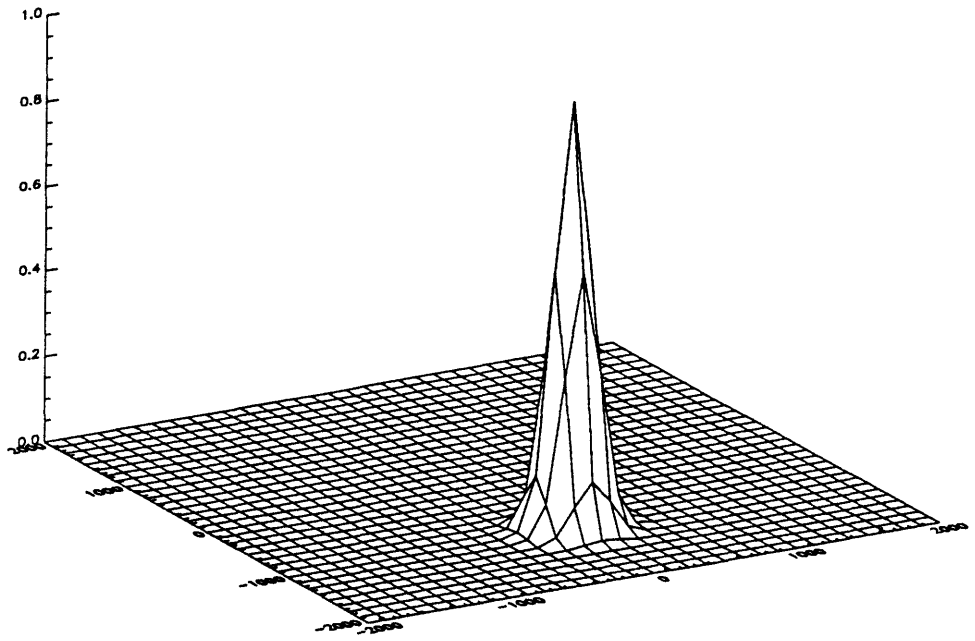

Figure 3-9: Pure rotation of a Gaussian cloud at $z = 0$ at time $t = 3000$ with $\Delta t = 3000$ (no numerical error)

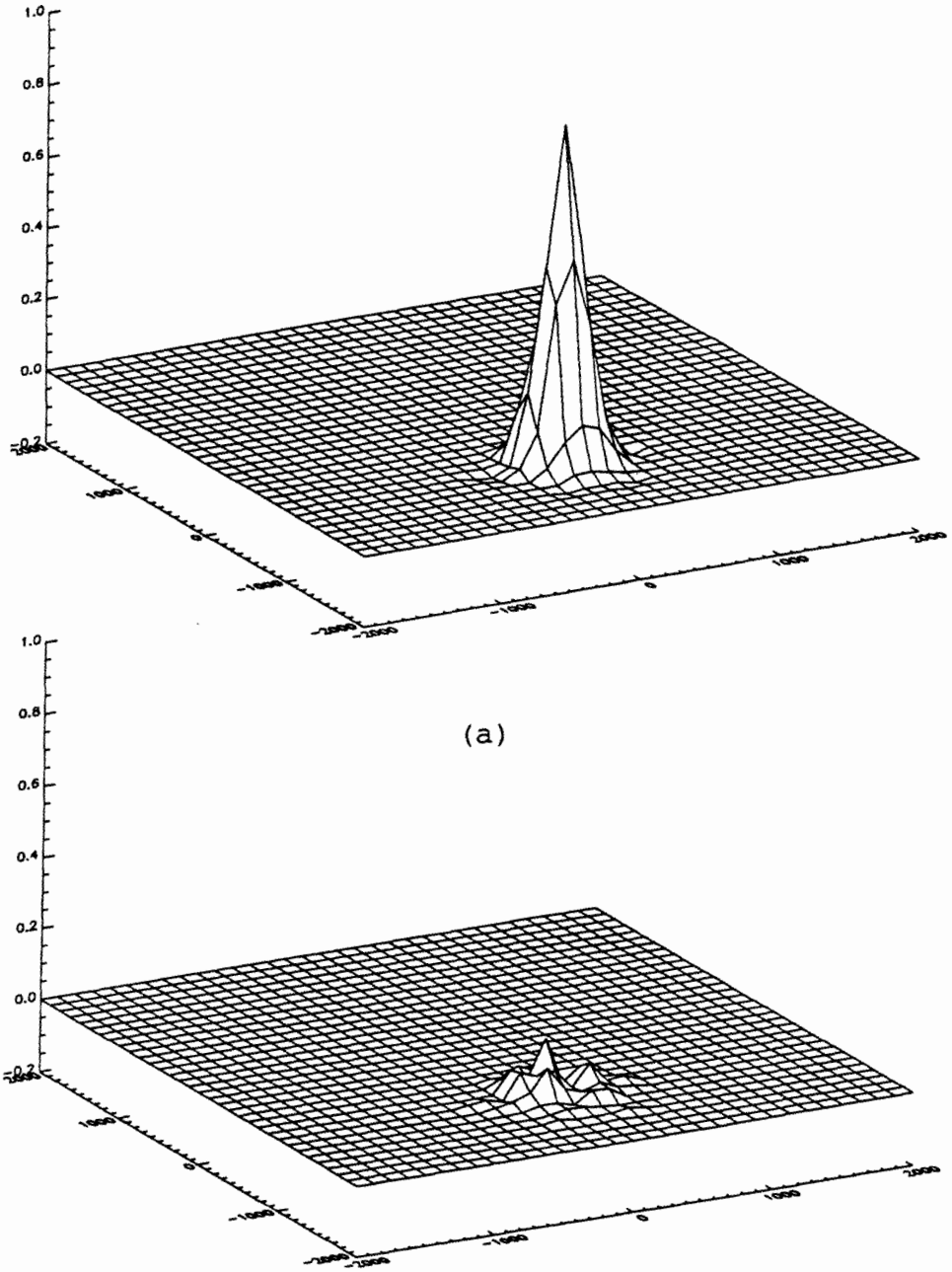

Figure 3-10: Pure rotation of a Gaussian cloud at $z = 0$ at time $t = 3000$ with $\Delta t = 1000$ (a) concentation field (b) absolute numerical error

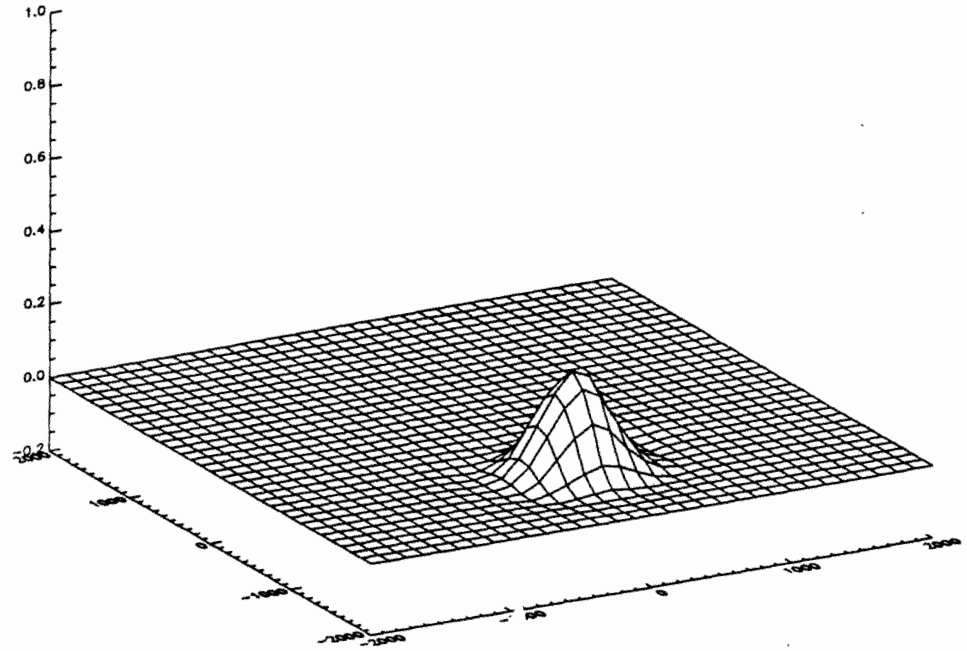

(a)

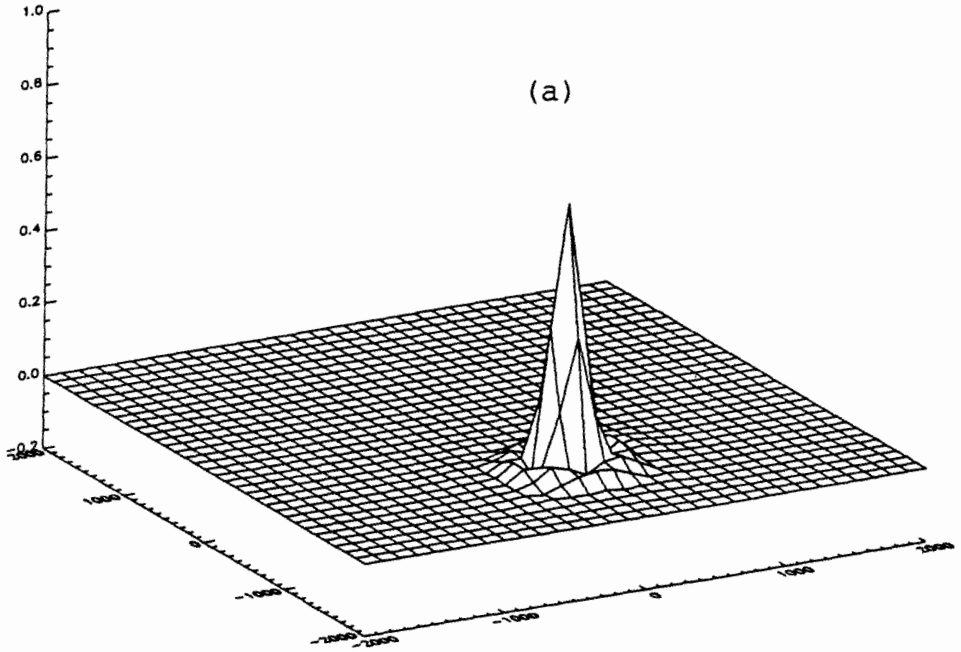

(b)

Figure 3-11: Pure rotation of a Gaussian cloud at $z = 0$ at time $t = 3000$ with $\Delta t = 100$ (a) concentation field (b) absolute numerical error

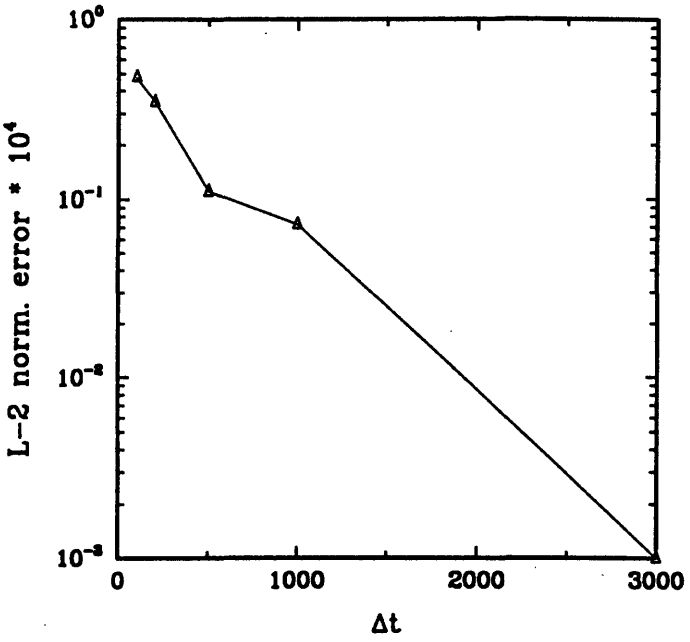

(a)

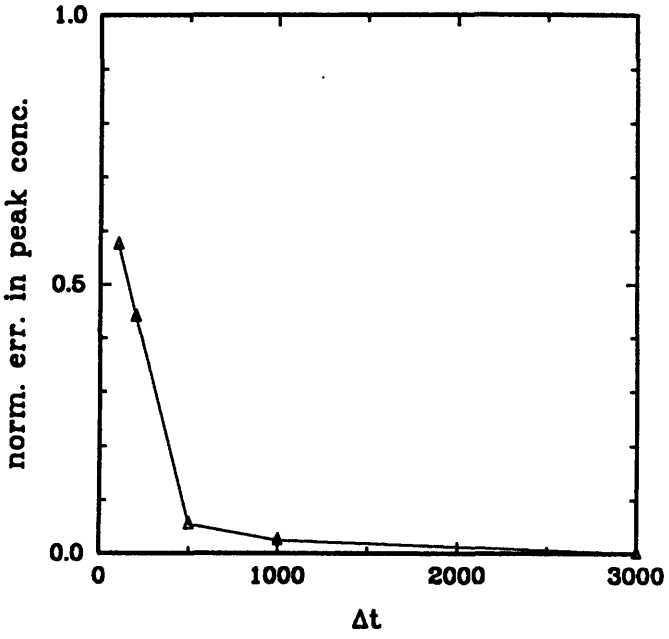

(b)

Figure 3-12: (a) L-2 error vs Δt (b) error in peak concentration vs Δt for $Pe = \infty$.

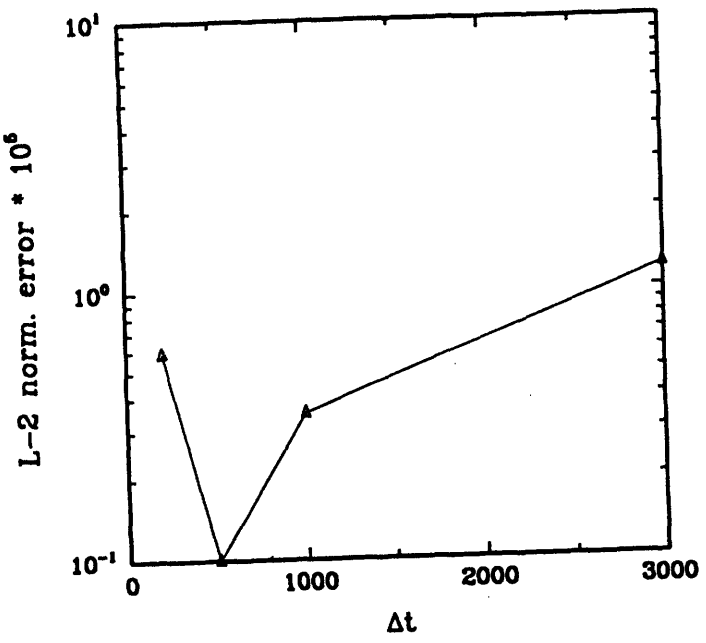

(a)

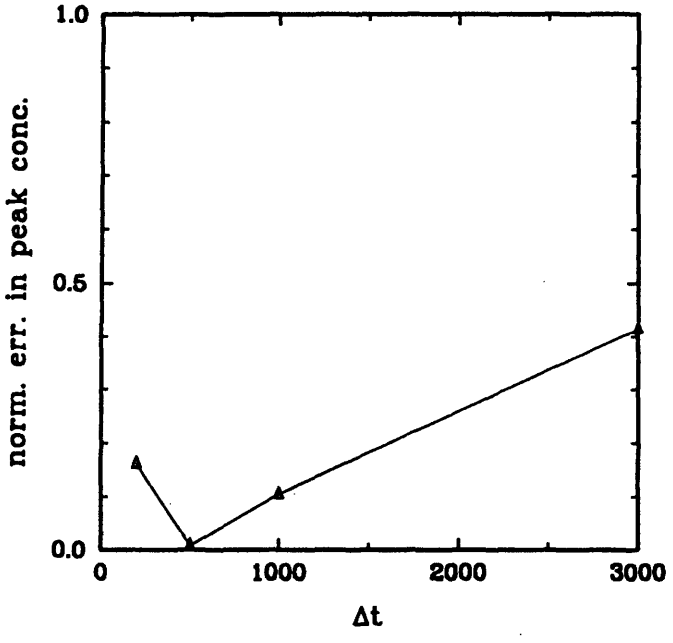

(b)

Figure 3-13: (a) L-2 error vs Δt (b) error in peak concentration vs Δt for $Pe = 57$.

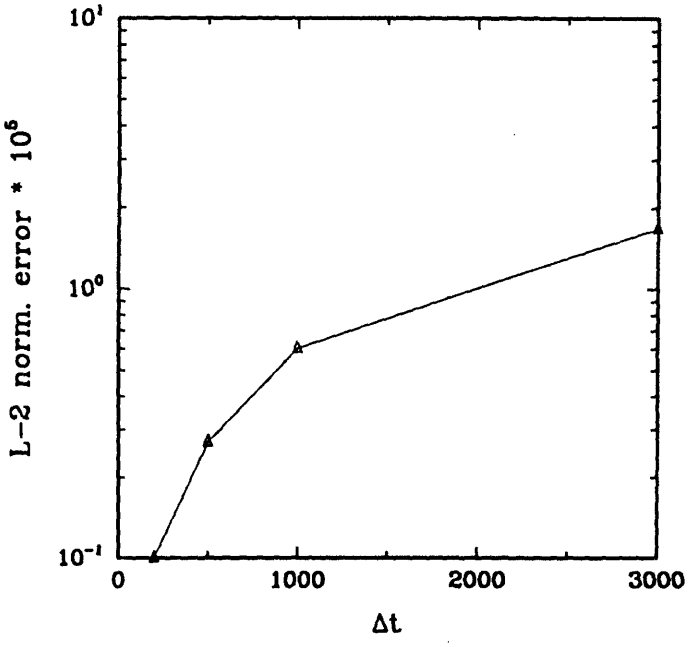

(a)

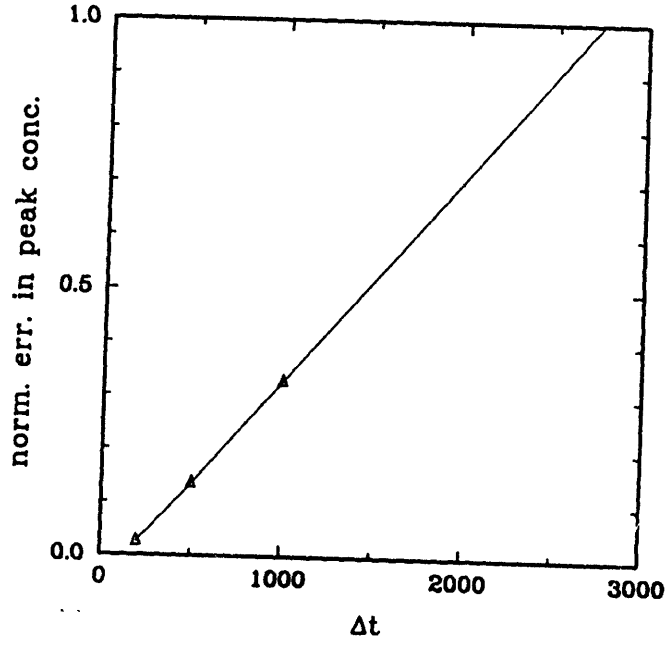

(b)

Figure 3-14: (a) L-2 error vs Δt (b) error in peak concentration vs Δt for $Pe = 24$.

method respectively. The second order Runge-Kutta method gives in all cases considerably higher error than the fifth order Runge-Kutta method with means that in the second order Runge-Kutta method the tracking error always exceeds the interpolation error. So the use of a fifth order Runge-Kutta method is suggested. In the second order Runge-Kutta method the error is an increasing function of N_{max}, which is easily explained by the fact that in the absence of a control error mechanism N_{max} plays the role of one. Fig. 3-17 and Fig. 3-18 show CPU time vs. N_{max} . We also see that the CPU time is in both cases a strongly decreasing function of N_{max}.

ϵ vs. N_{max}

Zhang(1990) investigated the issue of balancing the interpolation error with the tracking error for quadratic interpolation functions and a fifth order Runge Kutta tracking method by varying the tolerance parameter ϵ and concluded that the optimal timestep corresponds to $Cu_{int} = 0(1)$. Since the searching part must proceed the accuracy part N_{max} must be chosen, so that it matches the desired Cu_{int}. If N_{max} corresponds to a larger Cu_{int} than the one prescribed by accuracy, CPU time is wasted on unneccesary searching. On the other hand if N_{max} corresponds to a smaller Cu_{int} more than necessary CPU time is spent on tracking. In this case a lower order tracking method could have been used and resulted to the same level of accuracy. Since according to Zhang(1990) the optimum value for Cu_{int} in the case of a fifth order Runge-Kutta method is of 0(1) the use of $N_{max} = 0(10)$ for 3-D applications is recommended so that all the elements, that have common nodes with the element, where the tracking starts are included.

3.4.2 Interpolation functions

If $\mathbf{x}(n\Delta t)$ is the solution of the differential equation (see also Eqn 3.11)

$$\frac{d\mathbf{x}}{d\tau} = \mathbf{v}(\mathbf{x}(\tau), \tau) \quad (n-1)\Delta t \leq \tau < n\Delta t \tag{3.32}$$

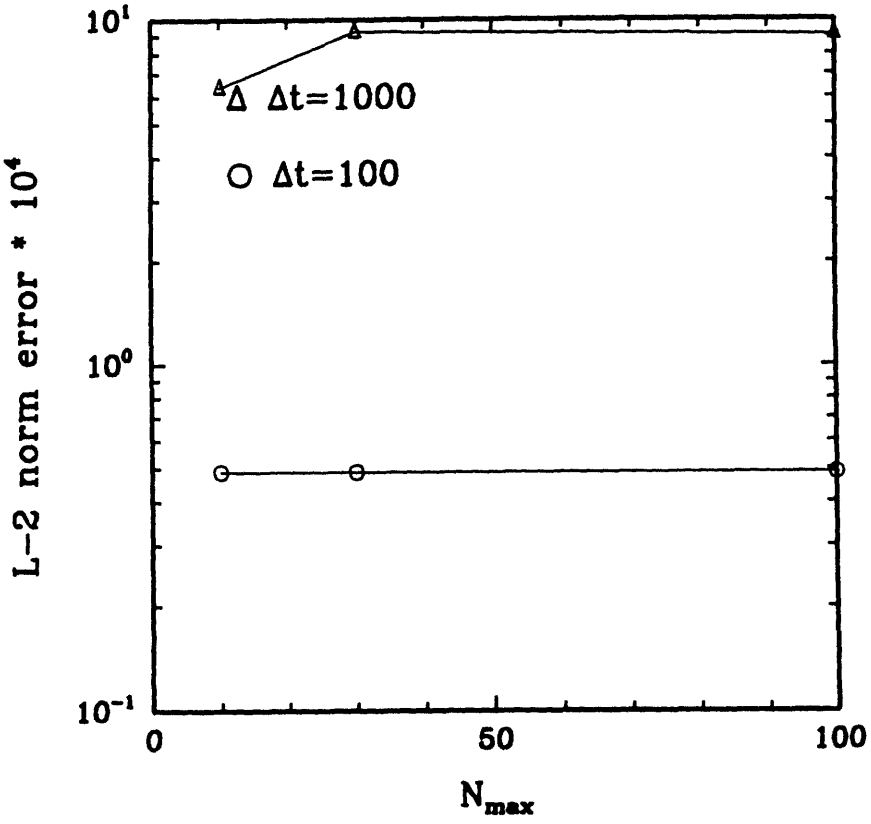

Figure 3-15: L-2 error vs. N_{max} using the 2nd order Runge Kutta method.

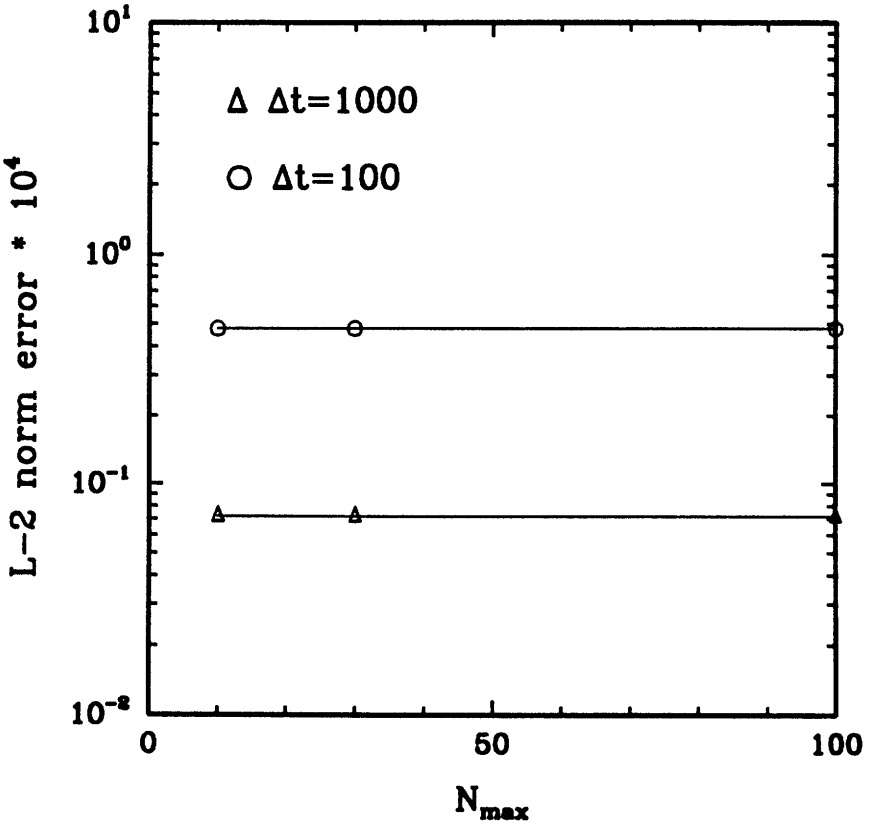

Figure 3-16: L-2 error vs. N_{max} using the 5th order Runge Kutta method.

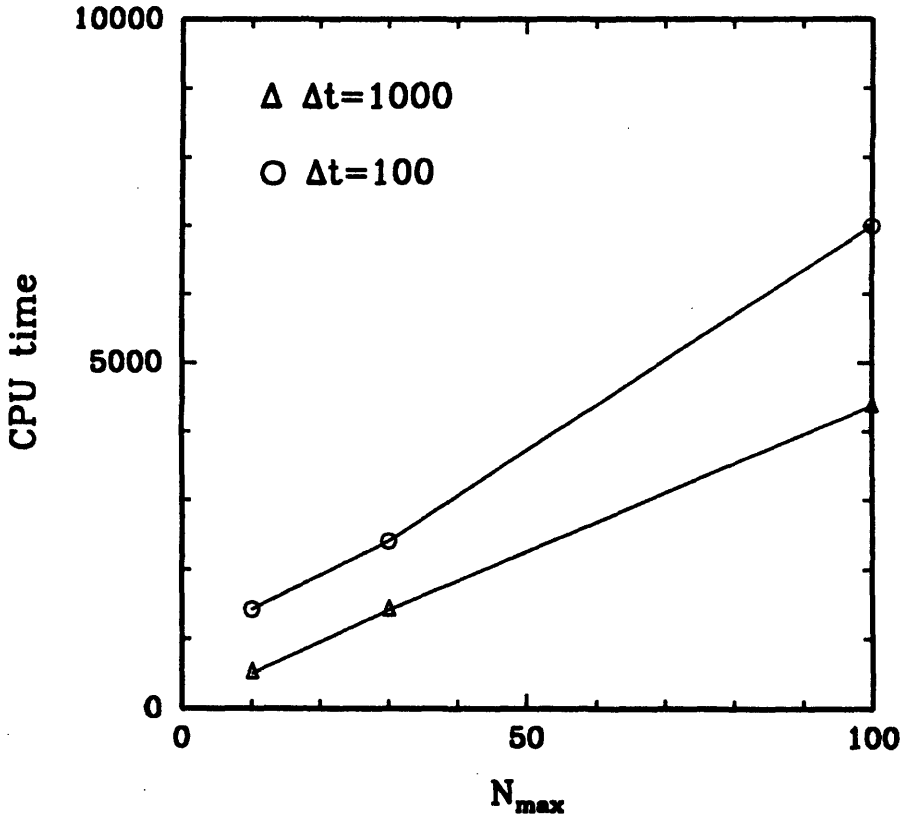

Figure 3-17: CPU (sec) in a DEC-3000 workstation vs. N_{max} using the 2nd order Runge Kutta method.

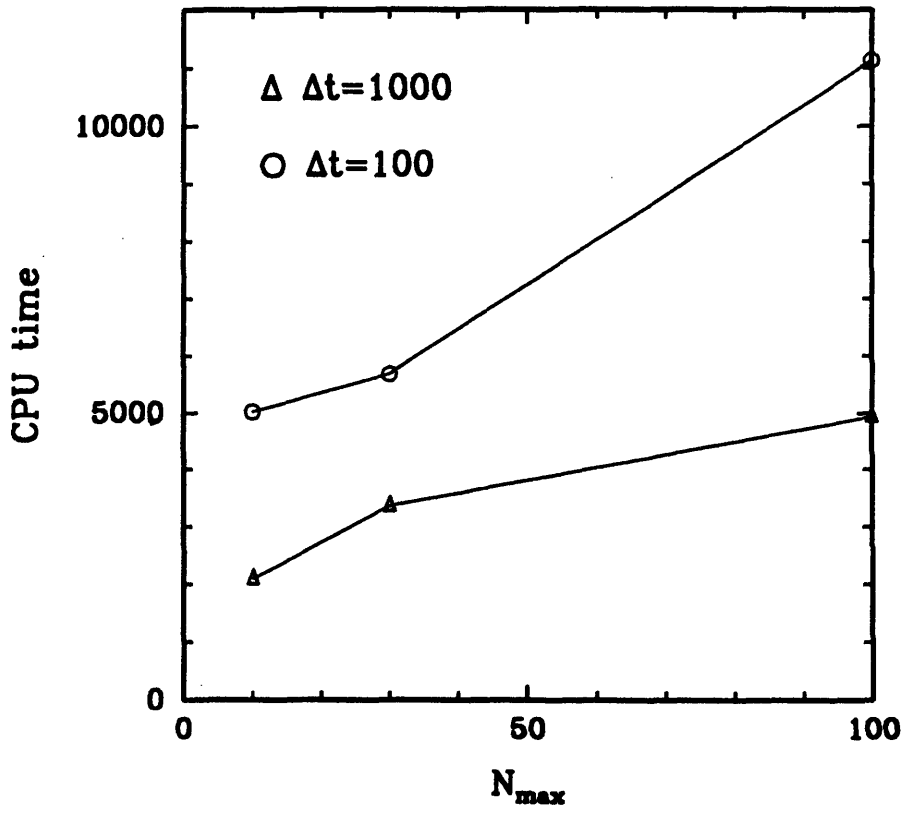

Figure 3-18: CPU (sec) in a DEC-3000 workstation vs. N_{max} using the 5th order Runge Kutta method.

then we define as $c^*(\mathbf{x})$ the function given by the Lagrangian step

$$c^*(\mathbf{x}) = c^{n-1}(\mathbf{x}(\mathbf{x}, n\Delta t; (n-1)\Delta t) \tag{3.33}$$

Two procedures have been followed after finding $c^*(\mathbf{x})$

- Project $c^*(\mathbf{x})$ on the grid in order to find c^f and then proceed with Eqn 3.8.
- Use $c^*(\mathbf{x})$ instead of c^f and then proceed with Eqn 3.8.

The first approach is mostly used when finite differences are used for the diffusion component (Glass and Rodi, 1982; Holly and Preissmann, 1977; Holly and Polatera, 1984; Ahsan and Bruno, 1989; Branski and Holley, 1986; Nguyen and Martin, 1988). Baptista (1987) use this approach with finite elements.

Baptista (1987) does a thorough analysis on different interpolators. He distinguishes among compact and non-conpact interpolation according to whether they use node values only from one element or from its immediate neighborhood. He also distinguishes interpolation according to their continuity; i.e., C^0 vs C^1 interpolators. Cubic Hermite interpolators are the most accurate interpolators used (Holly and Preissmann, 1977; Glass and Rodi, 1982; Holly and Polatera, 1984) but their use impacts the cost of not only the interpolation procedure but also that of the tracking and the diffusion step. This is due to the extra work asociated with the additional concentration gradients, that have to be calculated i.e., c_x in 1 - D (one additional variable), c_x, c_y and c_{xy} in 2 - D (three additional variables), and c_x, c_y, c_z, c_{xy}, c_{yz} and c_{xz} in 3 - D (six additional variables). Among C^0 compact interpolators there is a trade off between numerical diffusion and instability. Linear interpolators resemble upwind differences in terms of numerical diffusion. Quadratic Lagrange interpolators (Baptista, 1987) are more appropriate in most problems of practical interest in surface waters but they can not handle steep gradients. Higher-order compact interpolators are slightly unstable and that may cause problems in long simulations. Non-compact interpolators are practical because linear elements can be used but they

cause problems in irregular grids.

According to the second option the diffusion equation (Eqn 3.8) is solved according to the scheme

$$\int_{\Omega_e} c_j^n \phi_j \phi_i dx + \Delta t \int_{\Omega_e} \mathbf{K} \nabla c_j^n \phi_j \nabla \phi_i dx = \int_{\Omega_e} c_j^f \phi_j \phi_i dx + boundary \quad terms \quad (3.34)$$

where ϕ is the weighting function in the finite element formulation.

After using integration by parts Eqn 3.34 becomes

$$\int_{\Omega_e} c_j^n \phi_j \phi_i dx + \Delta t \int_{\Omega_e} \mathbf{K} \nabla c_j^n \phi_j \nabla \phi_i dx = \int_{\Omega_e} c_j^f \phi_j \phi_i dx + boundary \quad terms \quad (3.35)$$

In the case of 1 - D linear elements the order of the approximation is Δx^2 (Hasbani et al., 1983) which is one order higher than by using linear interpolation in the previous approach. As we go to higher dimensions the integral $\int_{\Omega_e} c_j^* \phi_j \phi_i d\mathbf{x}$ has to be calculated numerically and the order of accuracy of the approximation depends on the accuracy of the integration scheme. Hasbani et al. (1983) are using 4x4 Gauss-Legendre interpolation. Russell (1985) is using bilinear finite elements and a Lobatto quadratic rule. This approach has the advantage of having accuracy of one degree higher than the degree of the interpolation-basis functions. Its drawbacks are the cost resulting from the integration of the term $\int_{\Omega_e} c_j^* \phi_j \phi_i d\mathbf{x}$ and the fact that it can be slightly unstable.

In this research the use of prismatic triangular quadratic finite elements was used. The interpolation functions were chosen to be the same as the finite element basis functions i.e. quadratic triangular in the horizontal plane with quadratic functions in the z-direction i.e. 18 points in each element. The reasons for this choice were:

- The cost associated with the evaluation of the term $\int_{\Omega_e} c_j^* \phi_j \phi_i d\mathbf{x}$
- By using a particle tracking model for the simulation of sources (see Chapters 4 and 5) the concentration model does not need to handle steep gradients and

so quadratic interpolation functions are sufficient.

- The use of triangular elements in the horizontal facilitates the tracking part because using the functions it is easy to determine whether the FCL lies within an element.

3.4.3 Time discretization scheme

Crank-Nicolson is the most often used scheme ((Hasbani et al., 1983; Holly and Polatera, 1984). Russell(1985) uses a third-order Euler backwards time scheme. Baptista (1987) is using a first-order Euler backwards scheme.

As mentioned before in 3 - D transport problems the Peclet numbers are large and so the diffusion part is by far less important compared to the advection part and so the first order Euler backwards scheme was used.

3.5 Diffusion Part

3.5.1 General

Using the finite element discrete representation the concentration $c(\mathbf{x}, t)$ is approximated by:

$$c(\mathbf{x}, t) = \sum_{j=1}^{N_p} c_j(t)\phi_j(\mathbf{x}) \tag{3.36}$$

where

$c_j(t)$ are unknown coefficients

$\phi_j(\mathbf{x})$ are the basis functions

N_p is the number of nodes in the domain

Substituting Eqn 3.36 into Eqn 3.8 , applying the weighted residuals formulation and using integration by parts we get

$$\int_{\Omega_e} \phi_j \phi_i dx + \Delta t \int_{\Omega_e} \mathbf{K} \nabla \phi_j \nabla \phi_i dx = \int_{\Omega_e} c_j^f \phi_j \phi_i dx - \int_{\Gamma_2} \bar{q}_n \phi_i dx \qquad (3.37)$$

or in matrix form

$$(H_1 + H_2 \Delta t)c = H_1 c^f + P \qquad (3.38)$$

with

$$H_1 = \int_{\Omega_e} \phi_j \phi_i dx \quad (geometric \quad matrix) \qquad (3.39)$$

$$H_2 = \int_{\Omega_e} \mathbf{K} \nabla \phi_j \nabla \phi_i dx \quad (diffusion \quad matrix) \qquad (3.40)$$

$$P = \int_{\Gamma_2} \bar{q}_n \phi_i dx \qquad (3.41)$$

H_1 is always a symmetric, time independent matrix. H_2 is time dependent if $\mathbf{K}$ is time dependent. It can be symmetric if $\mathbf{K}$ is constant over each element. In this research $\mathbf{K}$ is time dependent but a uniform value over each element is chosen in order to solve a symmetric system of equations. This treatment of $\mathbf{K}$ may cause numerical problems if $\mathbf{K}$ has a strong spatial variability. In this research $\mathbf{K}$ was chosen to be a spatially and temporally uniform due to the lack of a turbulence closure scheme in the HM.

According to the above the solution of the diffusion part boils down to the solution of Eqn 3.8 i.e. the solution of the linear system of equations

$$\mathbf{Hx} = \mathbf{b} \qquad (3.42)$$

where $\mathbf{H}$ is a NxN matrix where N is the number of nodes with entries

$$h_{ij} = \int_{\Omega_e} \phi_j \phi_i dx + \Delta t \int_{\Omega_e} \mathbf{K} \nabla \phi_j \nabla \phi_i dx \qquad (3.43)$$

and $\mathbf{b}$ is a vector with entries

$$b_i = \int_{\Omega_e} c_j^f \phi_j \phi_i dx + boundary \quad terms \tag{3.44}$$

The cost of the solution to the advective part of the transport equation is proportional to the number of nodes, so the computational time spent by going from the two- to the three-dimensional case would increase by a factor equal to the number of layers in the vertical direction. The diffusion step on the other hand becomes a major problem in terms of computational cost and memory requirements in the 3 - D case because of its global character (i.e., it involves all the grid nodes simultaneously), which implies that large systems of equations must be solved at each time step.

Alternate-direction implicit (ADI) methods are favorable if we can split the problem into three one-dimensional problems, i.e., the equation is first solved along the x-direction with y and z constant to allow x diffusion, then along the y-direction with x and z constant to allow y diffusion and finally along the z-direction with y and x constant to allow z diffusion (Ahsan and Bruno, 1989; Pepper and Baker, 1979). In the case of an NxNxN grid this method requires $0(N^3)$ operations (Carey and Oden, 1986). In our case we can not split the equation in three one-dimensional problems because of the irregular geometry in the horizontal plane. If we want to still use an ADI technique only the combination of one two-dimensional (horizontal sweep) and one one-dimensional (vertical sweep) is possible. In this case the number of operations for the horizontal sweeps is of order N $0(N^3) \approx 0(N^4)$, where $0(N^3)$ is the number of operations for the two-dimensional problem using a conjugate gradient method (CG) (Patera, 1988). In the case of timely invariant or periodically changing coefficients an LU-backwards substitution method (direct method) could be used (Baptista, 1987). In this case the number of operations for the horizontal sweep (backwards substitution step) is N $0(N^3) \approx 0(N^4)$, i.e., the same as for the iterative CG method. The number of operations for the vertical sweep is N^2 $0(N) \approx 0(N^3)$, i.e., the horizontal sweep dominates as expected in terms of computational time. In the case of variable coefficients the LU decomposition has to be done at every timestep and so the cost

increases to $0(N^7)$ at each timestep.

Instead of using an implicit method one could use an explicit methos. In this case the stability criterion must apply i.e.

$$\Delta t \leq \frac{1}{2max(K_x, K_y, K_z)(\frac{1}{\Delta x^2} + \frac{1}{\Delta y^2} + \frac{1}{\Delta z^2})} \tag{3.45}$$

This criterion can be very restrictive and force the user to use small timesteps and not take advantage of the Eulerian-Lagrangian approach. Since the horizontal diffusion terms are typically much smaller than the vertical diffusion terms Casulli and Cheng, 1992 adopted a semi-implicit scheme where the horizontal diffusion terms are treated explicitely whereas the vertical diffusion term is treated implicitely.

The stability criterion for the scheme then is

$$\Delta t \leq \frac{1}{2max(K_x, K_y)(\frac{1}{\Delta x^2} + \frac{1}{\Delta y^2})} \tag{3.46}$$

A second alternative is the implementation of ADI with three 1 - D sweeps for non-rectangular regions (Hayes, 1980). According to this method the element isoparametric maps can be used to define a global transformation to a rectangular domain in the horizontal plane. This results in the solution of a series of three one-dimensional problems through an ADI approach. The limitation of this approach is that the finite element grid must be isoparametrically equivalent to a unit of rectangles in plan view. The basis functions must be tensor products on the master element, i.e., $\phi_{i(x,y)} = \phi_{(x)} \cdot \phi_{(y)}$ where $\phi_{i(x,y)}$ is the basis function. These are the standard four-node linear, nine-node quadratic, and sixteen-node cubic quadrilaterals.

The number of operations for solving the fully three-dimensional equation using CG is $0(N^4)$ without any preconditioning (Patera, 1988), which is equal to the number of operations using ADI (2-D and 1-D sweep).

The computational cost could be further reduced by using a preconditioning CG

Table 3.1: Operations Count for Diffusion Operator

Method	Cost	Stabil. Criterion	Elem. Restriction
ADI(2-D,1-D)	$0(N^4)$	no	no
LU	$0(N^7)$	no	no
ADI(1-D,1-D,1-D)	$0(N^3)$	no	yes
semi-implicit	$0(N^3)$	yes	yes
CG	$0(N^4)$	no	no
PCG	$0(N^m)$ $3 \prec m \prec 4$	no	no

scheme, i.e., Jacobi conjugate gradient (JCG), successive overrelaxation conjugate gradient (SSOR-CG), or incomplete factorization conjugate gradient (ICCG) (Axelson and Barker, 1984). The number of operations using ICCG is $0(N^{3.5})$

In this research a conjugate gradient solver with a diagonal preconditioner was used. The reason for using a conjugate gradient solver instead of another iterative solver (i.e. SOR, SSOR) was the robustness of the method, e.g. whereas the performance of other iterative solvers is highly dependent on parameter choice. The diagonal preconditioner was chosen instead of other preconditioners, i.e. incomplete Cholesky ICCG or least squares for the following reasons. First in a 3-D diffusion problem the resulting conductivity matrix is highly diagonal dominant and so the use of more complicated preconditioners is not required. Second as pointed out by Pini and Gambolati (1990) the diagonal scaling is the most efficient preconditioning scheme for supercomputer applications.

Table 3.1 summarizes the operations count of each method per timestep.

3.5.2 Conjugate Gradient Solver with Diagonal Preconditioner

In order to solve system (19) the conjugate gradient solver uses the following algorithm

Given $\mathbf{x}^{(0)}$

set $\mathbf{r}^{(0)} = \mathbf{b} - \mathbf{H}\mathbf{x}^{(0)}$

$\mathbf{p}^{(0)} = \mathbf{r}^{(0)}$

for $k = 0, 1, 2, ...$

If $\|\mathbf{r}^{(k)}\|/\|\mathbf{r}^{(0)}\| < \epsilon$ set $\mathbf{x} = \mathbf{x}^{(k-1)}$ and quit

else

$\alpha_k = (\mathbf{r}^{(k)}, \mathbf{r}^{(k)})/(\mathbf{p}^{(k)}, \mathbf{H}\mathbf{p}^{(k)})$

$\mathbf{x}^{(k+1)} = \mathbf{x}^{(k)} + \alpha_k \mathbf{p}^{(k)}$

$\mathbf{r}^{(k+1)} = \mathbf{r}^{(k)} - \alpha_k \mathbf{H}\mathbf{p}^{(k)}$

$\beta_k = (\mathbf{r}^{(k+1)}, \mathbf{r}^{(k+1)})/(\mathbf{r}^{(k)}, \mathbf{r}^{(k)})$

$\mathbf{p}^{(k+1)} = \mathbf{r}^{(k+1)} + \beta_k \mathbf{p}^{(k)}$

When **H** is a symmetric positive definite matrix the conjugate gradient method is guaranteed to converge after at most N iterations (Golub and van Loan, 1983). The rate of convergence of the conjugate gradient method depends on the distribution of the eigenvalues of **H**. The residual after k iterations is bounded by (Axelson and Barker, 1984)

$$\|\mathbf{r}^{(k)}\|_H \leq 2\|\mathbf{r}^{(0)}\|_H \left(\frac{1-\sqrt{\kappa_H}}{1+\sqrt{\kappa_H}}\right)^k \approx 2\|\mathbf{r}^{(0)}\|_H (1 - 2\sqrt{\kappa_H})^k \tag{3.47}$$

where κ_H is the spectral condition number of **H** defined as the ratio of the largest to the smallest eigenvalue of **H**,

$$\kappa_H = \frac{\lambda_{max}(\mathbf{H})}{\lambda_{min}(\mathbf{H})} \tag{3.48}$$

and $\|\cdot\|_H$ the norm defined by

$$\|\mathbf{x}\|_H = (\mathbf{x}^T \mathbf{H}\mathbf{x})^{\frac{1}{2}} \tag{3.49}$$

According to Eqn 3.49 the maximum number of iterations k_{max} to achieve an ϵ - error tolerance in the H-norm of the residual is given by

$$k_{max} = \frac{1}{2}\sqrt{\kappa_H} ln(\frac{2}{\epsilon}) + 1 \tag{3.50}$$

As seen in Eqn 3.50 in order to reduce the number of iteration steps required to obtain a good approximation κ_H has to be reduced. In order to achieve this a preconditioner is used. The basic idea behind a preconditioner is to solve the transformed system

$$(\mathbf{C}^{-1}\mathbf{H}\mathbf{C}^{-1})\mathbf{C} = \mathbf{C}^{-1}\mathbf{b} \tag{3.51}$$

where $\mathbf{C} \in R^{N\times N}$ is a nonsingular symmetric matrix so that the matrix $\tilde{\mathbf{H}} = \mathbf{C}^{-1}\mathbf{H}\mathbf{C}^{-1}$ has an improved condition number and possibly eigenvalue clustering. On the other hand the solution of the system

$$\mathbf{C}^2\mathbf{z} = \mathbf{r} \tag{3.52}$$

should be computationally inexpensive to obtain. $\mathbf{M} = \mathbf{C}^2$ is called the preconditioning matrix.

The algorithmic form of the preconditioned conjugate gradient method is (Golub and van Loan, 1983)

Given $\mathbf{x}^{(0)}$

set $\mathbf{r}^{(0)} = \mathbf{b} - \mathbf{H}\mathbf{x}^{(0)}$

$\mathbf{p}^{(0)} = \mathbf{r}^{(0)}$

$\mathbf{z}^{(0)} = \mathbf{M}^{-1}\mathbf{r}^{(0)}$

for $k = 0, 1, 2, ...$

. If $\|\mathbf{r}^{(k)}\|/\|\mathbf{r}^{(0)}\| < \epsilon$ set $\mathbf{x} = \mathbf{x}^{(k-1)}$ and quit

else

$\alpha_k = (\mathbf{z}^{(k)}, \mathbf{r}^{(k)})/(\mathbf{p}^{(k)}, \mathbf{H}\mathbf{p}^{(k)})$

$\mathbf{x}^{(k+1)} = \mathbf{x}^{(k)} + \alpha_k\mathbf{p}^{(k)}$

$\mathbf{r}^{(k+1)} = \mathbf{r}^{(k)} - \alpha_k\mathbf{H}\mathbf{p}^{(k)}$

$$\mathbf{z}^{(k+1)} = \mathbf{M}^{-1}\mathbf{r}^{(k+1)}$$
$$\beta_k = (\mathbf{z}^{(k+1)}, \mathbf{r}^{(k+1)})/(\mathbf{r}^{(k)}, \mathbf{r}^{(k)})$$
$$\mathbf{p}^{(k+1)} = \mathbf{z}^{(k+1)} + \beta_k \mathbf{p}^{(k)}$$

Because the resulting matrices in 3-D applications are strongly diagonally dominant a diagonal preconditioner was used in this research. Diagonal preconditioning is the simplest form of preconditioning. It involves the scaling of the rows and columns of **H** with the diagonal i.e.

$$M = D \tag{3.53}$$

The diagonal preconditioning is trivially implemented since $M^{-1} = D^{-1} = \frac{1}{d_{ii}}$ i = 1, ... N where N is the number of nodes.

Fig 3-19 shows the convergence rate for a 3-D application involving the diffusion of a gaussian cloud. Fig 3-20 shows the CPU time on the MIT Cray as a function of N for the solution of the resulting linear system of equations. We see that the slope is 1.14.

3.6 REFERENCES

1. Ahsan, A. K. M. Q., and M. S. Bruno. Three-dimensional modeling of plooutant transport in coastal waters. Proc. Estuarine and Coastal Modeling 1989, ASCE. 1989.

2. Axelsson, O., and V. A. Barker. Finite element solution of boundary value problems. Academic Press, Orlando. 1984.

3. Baptista, A. M., E. E. Adams , and K. D. Stolzenbach. Eulerian-Lagrangian analysis of pollutant transport in shallow water. Tchnical Report No. 296. MIT.

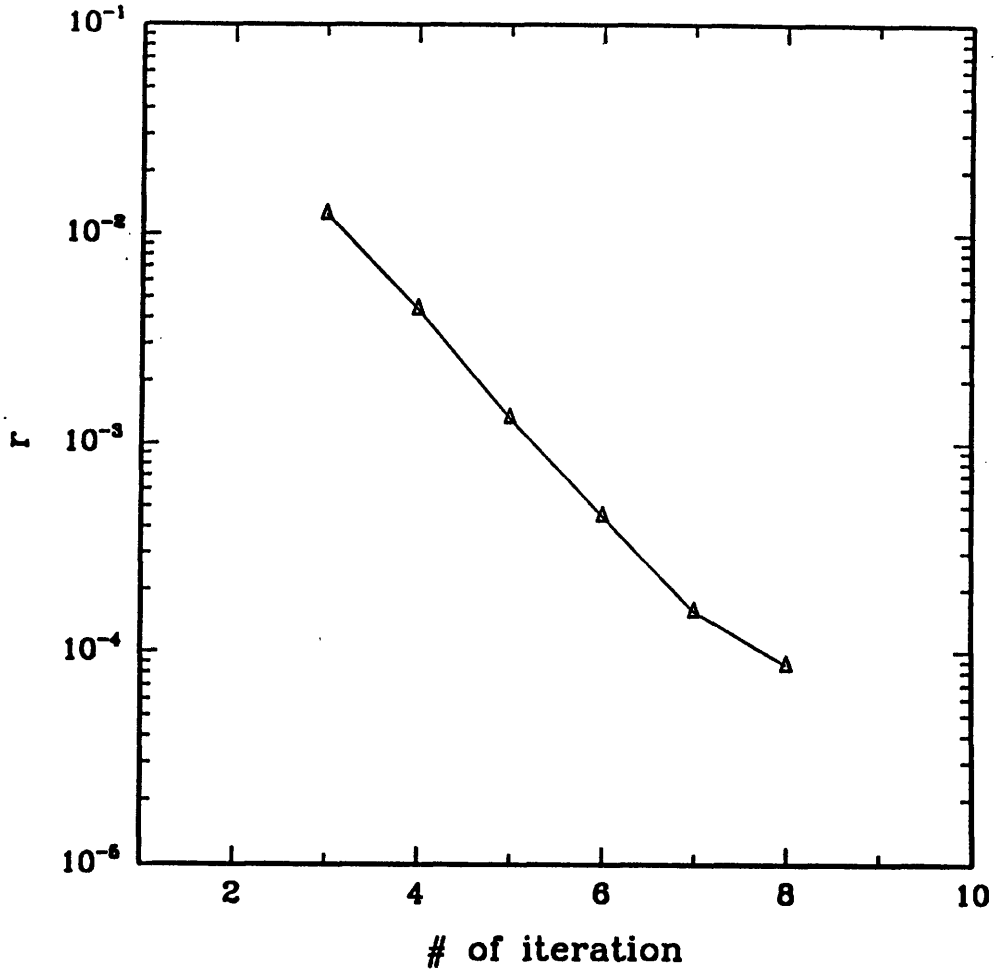

Figure 3-19: Convergence rate of the diagonal preconditioner.

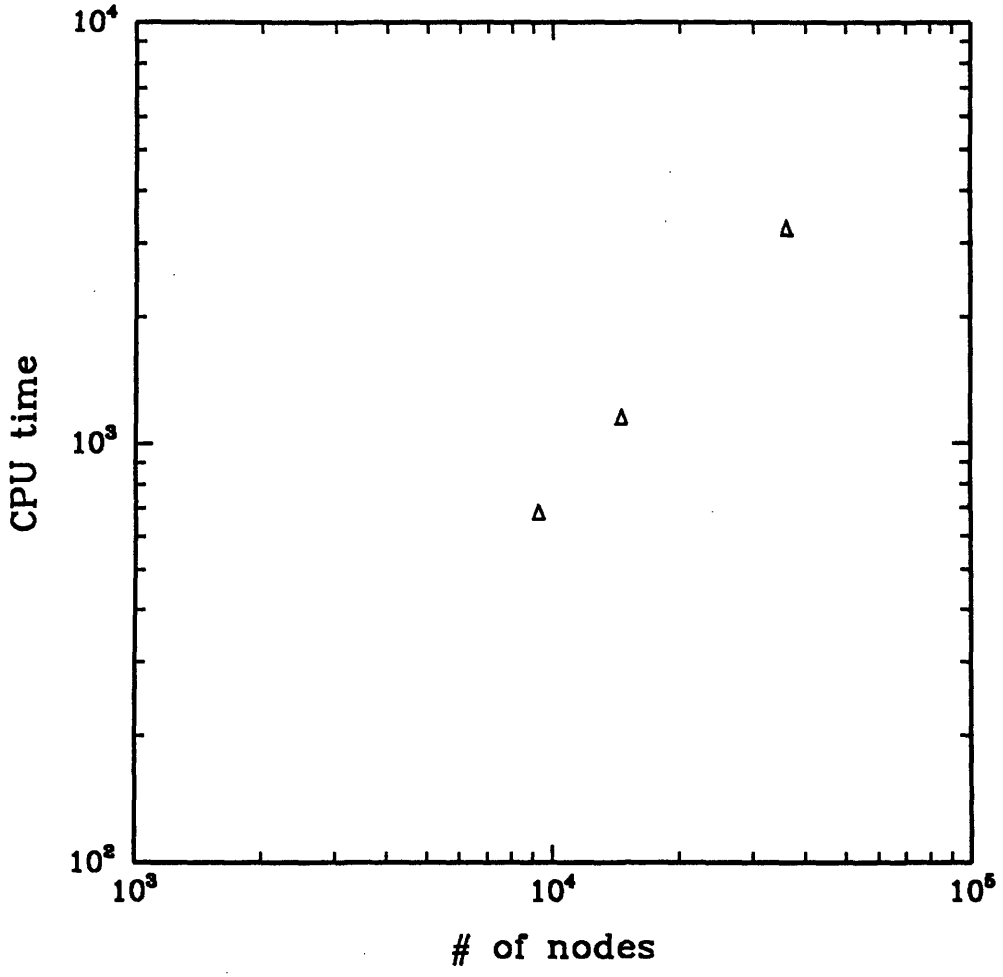

Figure 3-20: CPU time in the MIT Cray vs. the number of nodes.

1984.

4. Baptista, A. M. Solution of advection-dominated transport by Eulerian-Lagrangian methods using the backwards method of characteristics. Ph. D. thesis. Dept. of Civil Engineering. MIT. 1987.

5. Baptista, A. M., P. Gresho, and E. E. Adams. Reference problems for the convection-diffusion forum. Seventh Int'l. Conf. on Computational Methods in Water Resources. Cambridge. Mass. 1988.

6. Benque, J. P., and J. Ronat. Quelques difficultes des modeles numeriques en hydraulique. In Computing methods in applied sciences and engineering. V. Glowinski and Lions, eds., North-Holland, 471-494. 1982.

7. Branski, J. M., and E. R. Holley. Advection calculations using spline schemes. Water Forum '86. 1986.

8. Carey, G. F., and J. T. Oden. Finite elements. Prentice Hall. 1982.

9. Casulli V., and R. T. Cheng. A semi-implicit finite difference model for three-dimensional tidal circulation. Proc. 2nd International Conference on Estuarine and Coastal Modeling. Nov. 1991. Tampa, FL. 1992.

10. Celia, M. A., I. Herrera, and E. T. Bouloutas. Adjoint Petrov-Galerkin methods for multi-dimensional flow problems. Finite element analysis in fluids. Chung and Karr, eds. UAH Press, 965-970. 1989.

11. Dahle, K. H., M. S. Espedal, and R. E. Ewing. Characteristic Petrov-Galerkin subdomain method for convection diffusion problems. In IMA v. 11, Numerical simulation in oil recovery. M. F. Wheeler, ed. Springer-Verlag, 77-88. 1988.

12. Douglas, J., Jr., and T. F. Russell. Numerical methods for convection-dominated diffusion problems based on combining the method of characteristics with finite element or finite difference procedures. SIAM J. Num. Analysis 19:871-885. 1982.

13. Espedal, M. S., and R. E. Ewing. Characteristic Petrov-Galerkin subdomain methods for two-phase immicible flow. Comp. Meth. Appl. Mech. Engrg. 64:113-135. 1987.

14. Ewing, R. E., T. F. Russell, and M. F. Wheeler. Convergence analysis of an approximation of miscible displacement in porous media by mixed finite elements and a modified method of characteristics. Comp. Meth. Appl. Mech. Engrg. 47:73-92. 1984.

15. Glass, J., and W. Rodi. A higher order numerical scheme for scalar transport. Computer Methods in Applied Mechanics and Engineering 31:337-358. 1982.

16. van Genuchten, M. T., and W. G. Gray. Finite elements in water resources. W. G. Gray, G. F. Pinder, C. A. Brebbia, eds. pp1.71-1.90. Pentech. 1977.

17. Golub G. H., and C. F. van Loan. Matrix Computations. John Hopkins University Press. Baltimore. 1989.

18. Hasbani, Y., E. Livne, and M. Bercovier. Finite elements and characteristics applied to advection-diffusion equations. Computer and Fluids 11(2):71-83. 1983.

19. Hayes, L. J. Impementation of finite element alternating direction methods on nonrectangular regions. Int. J. Num. Meth. in Eng. 16:35-49. 1980.

20. Hervouet, J. M. Application of the method of characteristics in their weak formulation to solving two-dimensional advection equations on mesh grids. Computational techniques for fluid flow. Recent advances in numerical methods in fluids, v. 5, Taylor et al., eds., Pineridge Press, 149-185. 1986.

21. Holley, F. M., and A. Preissman. Accurate calculation of transport in two dimensions. J. Hydr. Div., ASCE 103:1259-1277. 1977.

22. Holley, M. F., and J. M. Usseglio-Polatera. Dispersion simulation in two-dimensional tidal flow. J. Hydr. Div., ASCE 110:905-926. 1984.

23. McDonald, A. Accuracy of multiply-upstream, semi-Lagrangian advective schemes. Monthly Wather Review 112:1267-1275. 1984.

24. Neuman, S. P. An Eulerian-Lagrangian scheme for the dispersion-convection equation using conjugate space-time grids. J. Comp. Physics 41:270-279. 1981.

25. Neuman, S. P. Adaptive Eulerian-Lagrangian finite element method for advection-dispersion. Int'l. J. Numerical Methods in Engineering 20:317-337. 1984.

26. Nguyen, K. D., and J. M. Martin. A two-dimensional fourth-order simulation for scalar transport in estuaries and coastal seas. Estuarine, Coastal and Shelf Science 27:263-281. 1988.

27. Patera, A. 1988. Notes from class: Computational Fluid Dynamics.

28. Pepper, D. W., and A. J. Baker. A high order accurate numerical algorithm for three-dimensional transport prediction. Computers and Fluids 8:371-390. 1980.

29. Pinder, G. F., and H. H. Cooper. A numerical technique for calculating the transient position of the last water front. Wat. Resources Res. 6(3):875. 1970.

30. Pini and Gambolatti. Is a simple diagonal scaling the best preconditioner for conjugate gradients on supercomputers? Adv. Water Resources. Vol. 13. No. 3. 1990.

31. Pironneau, O. On the transport diffusion algorithm and its application to the Navier-Stokes equations. Numer. Meth. 38:309-332. 1982.

32. Press, W. H. Numerical recopes: the art of scientific computing. Cambridge. 1986.

33. Ritchie, H. Application of a semi-Lagrangian integration scheme to the moisture equation in a regional forecast model. Monthly Weather Review 113:424-435. 1985.

34. Robert, A. A stable numerical integration scheme for the primitive meteorological equations. Atmos. Ocean. 19:35-46. 1981.

35. Russell, T. F. Time stepping along characteristics with incomplete iteration for a Galerkin approximation of miscible displacement in porous media. SIAM J. Num. Analysis 22:970-1013. 1985.

36. Wheeler, M. F., and C. N. Dawson. An operator-splitting method for advection-diffusion-reaction problems. MAFELAP Proceedings VI, J. A. Whiteman, ed. Academic Press, 463-482. 1988.

37. Williamson, D. L., and P. J. Rasch. Two-dimensional semi-Lagrangian transport with shape-preserving interpolation. Monthly Weather Review 117:102-129. 1989.

38. Zhang, X. Control of tracking error in numerical solution of advection diffusion equation by Eulerian-Lagrangian method. S. M. thesis. Dept. of Civil Engineering. MIT. 1990.

Chapter 4

Representation of Sources in a 3-D Transport Model

4.1 Introduction/Background

A transport model (TM) solves the following equation:

$$\frac{\partial c}{\partial t} + \nabla \cdot \mathbf{v}c = \nabla \cdot \mathbf{K} \cdot \nabla c + Q \tag{4.1}$$

where c(x,t) is the concentration, $\mathbf{v}$(x,t) is the velocity vector, $\mathbf{K}$(x,t) is the diffusivity tensor and Q represents sources/sinks.

Transport models solve Eqn 4.1 using different techniques. According to the form of Eqn 4.1 that they solve, they can be classified into two main categories:

- Concentration models, where Eqn 4.1 is directly solved. Here the dependent variable of concentration is advected and diffused. Concentration models can be classified as Eulerian (EM), Lagrangian (LM), and Eulerian-Lagrangian (ELM). Literature reviews are given by Neuman (1981), Baptista (1987), and Celia et al. (1990).

- Particle tracking models, where mass is represented by discrete particles. At each timestep the displacement $\Delta\mathbf{x}$ of each particle consists of an advective,

deterministic component and an independent, random Markovian component given by the equation (Gardiner, 1985; Tompson and Gelhar, 1990)

$$\Delta \mathbf{x} = \mathbf{X}^n - \mathbf{X}^{n-1} = \mathbf{A}(\mathbf{X}^{n-1}, t)\Delta t + \mathbf{B}(\mathbf{X}^{n-1}, t)\sqrt{\Delta t}\mathbf{Z} \tag{4.2}$$

where $\mathbf{A}$ and $\mathbf{B}$ are given by the expressions:

$$\mathbf{v} = \mathbf{A} - \nabla(\frac{1}{2}\mathbf{B}\mathbf{B}^T) \tag{4.3}$$

$$\mathbf{K} = \frac{1}{2}\mathbf{B}\mathbf{B}^T \tag{4.4}$$

Δt is the timestep, $\mathbf{Z}$ is a vector of three independent random numbers with zero mean and variance one (Tompson et al, 1988). Eqn 4.2 is equivalent to Eqn 4.1 in the limit of large number of particles N_p and small Δt (Tompson and Gelhar, 1990).

Particle tracking models have been extensively used in modeling one-, two-, and three-dimensional solute transport in groundwater (e.g., Ahlstrom et al., 1977; Prickett et al., 1981; Ackerer and Kinzelbach, 1985; Uffink, 1987; Tompson and Gelhar, 1990) but fewer applications have been done in surface waters (e.g., Bugliancello and Jackson, 1964; Ahn and Smith, 1972; Jeng and Holly, 1986; Mas-Gallic and Raviart, 1987; Jolles and Huberson, 1988; Dimou and Adams, 1990; Pearce et al., 1990). The main reason for using particle tracking models in groundwater problems is the fact that we encounter small scale variability, that can be modeled without grid resolution expense. In surface waters the main motivation appears to be the simulation of advection-dominated transport problems.

The representation of sources forms a severe limitation for concentration models because they can not resolve concentration fields, whose spatial extent is small compared to that of the discretization, whereas sources can easily be simulated in a particle tracking model by simply introducing particles in the domain. ELM can use this advantage of particle tracking methods by implementing forward particle tracking

close to sources. For example Adams et al. (1986) generated continuous point-source plumes by superimposing a series of small Gaussian clouds or puffs. Each of these clouds is transported by simply solving a relative diffusion problem analytically. Each cloud has a size consistent with the width of the plume. Adjacent clouds overlap such that a smooth concentration distribution is obtained. The puffs are tracked analytically until they are large enough to be resolved on the finite element grid and there computations proceed with a concentration model. This representation works well in relatively uniform flow fields (e.g, 2-D flow offshore) but it encounters difficulties near shore and it would fail completely if we acknowledge the 3-D density exchange flow near an outfall discharging to a stratified ocean.

Neuman (1984) proposed a hybrid model in which the advective component of steep concentration fronts is tracked forward with the aid of moving particles clustered around each front. Away from such fronts the advection problem is handled by the backwards method of characteristics. When a front dissipates with time, its forward tracking stops automatically and the corresponding cloud of particles is eliminated. The shortcomings of this method are the way it detects sharp gradients, and the procedure it uses for mapping concentrations from particles to the nodes of the fixed grid each time step, previous to the solution of the diffusion equation by the Eulerian-Lagrangian finite element formulation.

These drawbacks could be eliminated by using a complete particle tracking model instead of an ELM. The big question here is computational cost. The computational cost in particle tracking models is proportional to the number of particles N_p used whereas in concentration models with N_g nodes the computational cost is proportional to $N_g^{1+\eta}$ where $0 < \eta \leq 1$ (Tompson and Gelhar, 1990). The exponent η depends on the type of solver that one is using. Several attempts have been made to improve the computational efficiency of algorithms by taking advantage of vector and parallel machines both for particle tracking models (Martin and Brown, 1987; Torney and Warnock,1987) and concentration models (Melhem and Garmon, 1987) with particle tracking models having the advantage of being better suited to the capabilities of

parallel machines because of the independent nature of the calculations. If we do not take the role of the computational machine into account and we assume an efficient solver, the computational cost of the two methods would be comparable when the number of particles used is of the same order as the number of grid points. Since we are generally interested in concentration and not particle locations at the end of our calculations, we are computing concentration by sampling the mass concentration of particles, a process, that is strongly dependent on sample size. If N_s is the number of samples over which particles are located and N_{ps} is the number of particles per sample required to achieve the desired accuracy, then the necessary number of particles is $N_s \cdot N_{ps}$. If mass is spread over the whole domain, as is the case when the Peclet number is small, then N_s is of the order of N_g and so the particle tracking model becomes computationally inefficient. On the other hand when we are dealing with elongated plumes (large Peclet numbers) N_s is much smaller than N_g and so the particle tracking model becomes competitive.

Similarly, for short periods of time following release from a source (instantaneous or continuous), mass is concentrated near the source. This means that the number of samples using a particle tracking model can be small whereas a very fine discretization around the source is required if a concentration model is used. So at early times $N_s \ll N_g$ and we would expect a particle tracking model to be more efficient representing sources than a concentration model. At later times, when mass has spread out over the domain, a concentration model would be more efficient.

4.2 Procedure

In this research sources are simulated by the introduction of particles. For an instantaneous source, particles are advected and diffused independently for several timesteps until their distribution becomes smooth enough to be mapped onto the numerical grid by identifying the particle density (concentration) associated with each node (Fig 4-1). Computations then proceed with an Eulerian-Lagrangian concentration model. For continuous sources, node concentrations resulting from particles will be added

to existing node concentrations from the Eulerian-Lagrangian scheme and calculations will proceed in the concentration mode. For continuous source this procedure is repeated every timestep.

According to the above, two modes are used at the same time:

- The particle mode for particles, that have a spatial distribution whose standard deviation has not reached the minimum value of σ_{min}. In the case of an instantaneous source particles are released only once and after the standard deviation of their distribution reaches the value of σ_{min} they are mapped onto node concentrations and the rest of the model computations continue in the concentration mode only. In the case of a continuous source a certain number of particles is released every timestep. Each batch of particles is mapped onto node concentrations when the standard deviation of its distribution has exceeded σ_{min}. The advective displacement of each particle is solved by using a fifth order Runge-Kutta integration scheme whereas the random walk displacement due to the presence of the random number is solved using a first order scheme.

- The concentration mode for the domain. In this research a 3-D finite element Eulerian-Lagrangian model was developed. The main advantage of using an Eulerian-Lagrangian model is that one can use large Courant numbers, a feature particularly important in surface waters, where we are dealing with advection dominated flows. In this case the use of ELM is compatible with the use of a particle tracking model, where forward tracking of particles is used instead of backward tracking of characteristic lines.

The general procedure is the following. Eqn 4.1 is transformed into its nonconservative form

$$\frac{\partial c}{\partial t} + \mathbf{v} \cdot \nabla c = \nabla \cdot \mathbf{K} \cdot \nabla c + Q \tag{4.5}$$

Since the sources are modeled in the particle mode they are not included in the

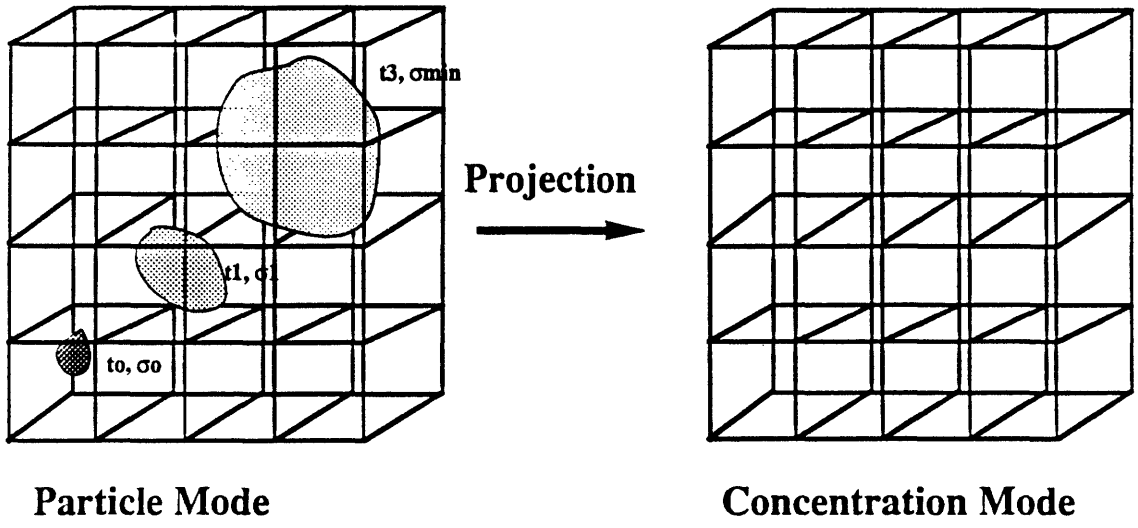

Figure 4-1: Representation of sources.

concentration mode. Eqn 4.5 is discretized in time according to

$$\frac{c^n - c^{n-1}}{\Delta t} + [\mathbf{v} \cdot \nabla c]^{n-1} = [\nabla \cdot \mathbf{K} \cdot \nabla c]^n \tag{4.6}$$

and then split into a pure advective

$$\frac{c^f - c^{n-1}}{\Delta t} + [\mathbf{v} \cdot \nabla c]^{n-1} = 0 \tag{4.7}$$

and a pure diffusive component

$$\frac{c^n - c^f}{\Delta t} = [\nabla \cdot \mathbf{K} \cdot \nabla c]^n \tag{4.8}$$

Eqn 4.7 states that the concentration c remains constant along characteristic lines defined by

$$\frac{d\mathbf{x}}{dt} = \mathbf{v} \tag{4.9}$$

According to Eqn 4.9, Eqn 4.7 is solved by tracking characteristic lines backwards using a fourth-order Runge-Kutta method from time n to time n-1 from every node. The concentration c^f at time n are determined by spatial interpolation. The interpolation functions were chosen to be the same as the basis functions. Eqn 4.8 is solved by using quadratic triangular prismatic finite elements. A conjugate gradient solver with a diagonal preconditioner was used (Golub and van Loan, 1989).

There are several important considerations in coupling the two models.

- How will particles be mapped onto node concentrations? This issue is thoroughly investigated in Chapter 5, and will be summarized in the following section.

- How does the developed hybrid model compare with a concentration model in simulating transport from small sources. This question is investigated in Section 4.4 in a 1-D case.

- What is the number of particles necessary for achieving the expected accuracy? What is an appropriate criterion for particle elimination, (i.e., when does a front of particles become smooth enough to justify projecting the particles) ? How does the size of the timestep affect accuracy?

  The first two questions will be investigated in Section 4.5 on 1-D and 3-D test cases respectively involving an instantaneous source in a quiescent fluid. The third question is investigated using a 2-D test case involving an instantaneous source with a radially variable diffusion coefficient.

4.3 Mapping Particles onto Node Concentrations

A basic part of particle tracking models is the transformation of particle locations to node concentrations at the end of the calculations. This is necessary because we are usually more interested in conveying concentration contours than mere particle locations. The issue becomes more important for a hybrid model, where calculations continue in the concentration mode after particles have been projected. We want to be as accurate as possible because the error in the procedure of mapping particles onto node concentrations will carry over to the rest of our computations.

The issue of mapping particle locations onto node concentrations is even more important in the case of reactive transport (Tompson and Dougherty, 1991; Bagtzoglou et al., 1991) and in cases where the velocity field is concentration dependent (Araktingi and Orr,1990). In these cases the problem becomes more complicated because periodically one switches back and forth between particle mode and concentration mode and so the use of a particle tracking model becomes more involved.

In this research a method designed particularly for irregular finite element grids is developed and applied. The methodology is the following. Element concentrations c_{el}^{i} are found first using

$$c_{el}^{i} = \frac{m}{N_p}\frac{N_{el}^{i}}{V_{el}} \tag{4.10}$$

where M is the total mass in the system, N_{el} is the number of particles in V_{el} and V_{el} is the volume of each element. Then element concentrations are mapped onto node concentrations using the mass conservation principle, i.e., the following expression has to be minimized.

$$min[\int c d\mathbf{x} - \int c_{el} d\mathbf{x}]^2 \tag{4.11}$$

The finite element representation, i.e.,

$$c = \sum c_j \phi_j \tag{4.12}$$

where c_j are the concentrations at the nodes and ϕ_j are the basis functions and the variational formulation leads to

$$\int c_j \phi_j \phi_i d\mathbf{x} - \int c_{el} \phi_i d\mathbf{x} = 0 \tag{4.13}$$

In the interfacing step between the particle tracking model and the Eulerian/Lagrangian model two equations have to be solved.

- Eqn 4.13 that transforms element concentrations to node concentrations. Let us call c^1 the solution of this equation.
- The diffusion part of the finite element formulation

$$\int_{\Omega_e} c_j^n \phi_j \phi_i d\mathbf{x} + \Delta t \int_{\Omega_e} \mathbf{K} \nabla c_j^n \phi_j \nabla \phi_i d\mathbf{x} = \int_{\Omega_e} c_j^f \phi_j \phi_i d\mathbf{x} + boundary \quad terms \tag{4.14}$$

Let us call c^2 the solution of Eqn 4.14. The total concentration c in the domain (excluding mass near the source, which has not yet been projected) is then $c = c^1 + c^2$

Since Eqn 4.13 and Eqn 4.14 are linear we can add them and then solve the system

in order to be computationally efficient. This proves to be cost efficient in the case of continuous sources where Eqn 4.13 would have to be solved at every timestep after the standard deviation of the distribution of the first batch of particles has reached the value of σ_{min}.

4.4 Comparison between the developed hybrid model and a concentration model in a 1-D test case

The developed hybrid model was compared with a pure concentration model in a 1-D test case involving an instantaneous mass release of standard deviation σ_0 in an infinite domain. The analytical solution to this problem in the case of a quiescent fluid and a conservative pollutant is

$$c = \frac{M}{(2\pi(\sigma_0^2 + 2K_x t))^{\frac{1}{2}}} exp\{-\frac{1}{2}[\frac{(x - x_o)^2}{(\sigma_0^2 + 2K_x t)}]\} \tag{4.15}$$

where M is the mass released, (x_o is the coordinate of the release point, K_x is the diffusion coefficient and t is the elapsed time.

A 1-D finite element grid $x \in [-100, 100]$ with spacing Δx_{grid} was used with model parameters ($K_x = 0.1$ and $\sigma_0 = 2$. The following error measures were used (Baptista et al, 1988)

- 0th moment of the concentration profile normalized by the exact value (integral measure of mass preservation)

$$\mu_o(t) = \frac{1}{m(t)} \int_\Omega c^{nu}(x, t) dx \tag{4.16}$$

Table 4.1: Dependence of concentration model on Δx_{grid} , $\Delta t = 5$, t = 500, $\sigma_0 = 2$

Δx_{grid}	μ_o
1	1
2	1
4	1.21
8	0.43

- Discrete $L-2$ error norm normalized by the total mass

$$\phi_D = \frac{1}{M}\{[\sum_i (c_i^{nu} - c_i^{ex})^2]^{\frac{1}{2}}\} \tag{4.17}$$

- Error in the peak concentration normalized by the exact peak concentration

$$\epsilon(t) = \frac{c_{max}^{ex}(t) - c_{max}^{nu}(t)}{c_{max}^{ex}(t)} \tag{4.18}$$

Fig 4-2 shows the ensemble average values of $\epsilon < \epsilon >$ after 50 Monte Carlo runs ($\Box$) in comparison with the concentration model (Δ) as a function of Δt. In the hybrid model $N_p = 2000$ and $\sigma_{min} = 8$ is used. The dashed band around $< \epsilon >$ is a measure of the noise for 50 Monte Carlo runs and is given by

$$< \epsilon > \pm \sigma \tag{4.19}$$

where $\sigma^2 =< \epsilon^2 > - < \epsilon >^2$. Fig 4-2 indicates, that the particle tracking model is not sensitive to the timestep and this enables us to use large timesteps and save on computational time. On the other hand the concentration model is very sensitive to Δt depending on the temporal discretization (Euler backwards in this case).

Table 4.1 presents further results suggesting, that in a concentration model $\frac{\Delta x_{grid}}{\sigma_0}$ has to be less than one in order to avoid severe mass concentration errors, whereas in a particle tracking model we never encounter mass conservation errors.

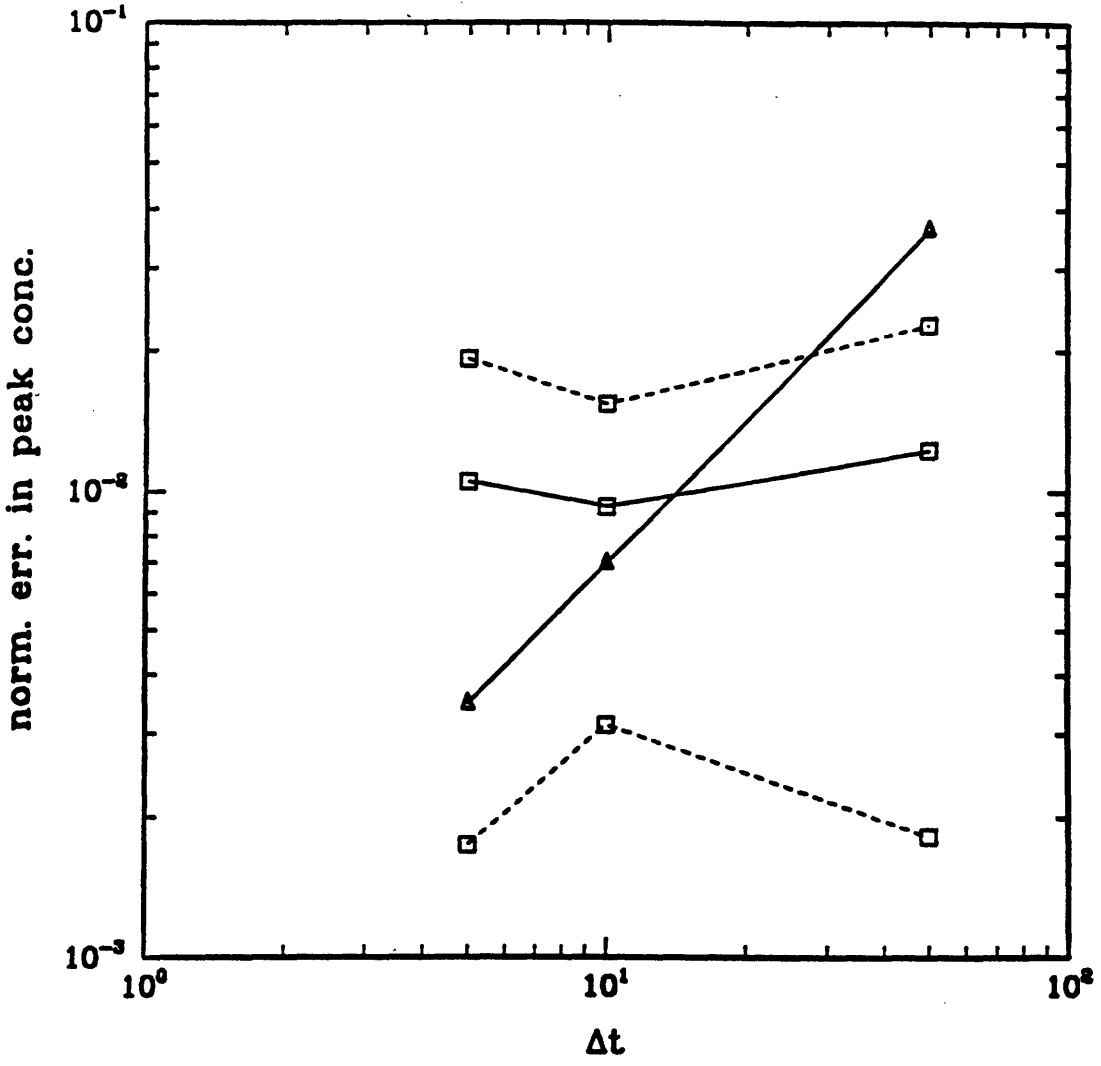

Figure 4-2: Comparison between a concentration model (Δ) and the developed hybrid model ($\square$); solid line represents the mean concentrations; dashed lines represent the mean concentratins $\pm$ standard deviation for 50 Monte Carlo runs in a 1-D case ($\sigma_0 = 2, t = 500, \sigma_{min} = 8$) $\Delta x_{grid} = 1$.

4.5 Dependence of accuracy on N_p, $\frac{\sigma_{min}}{\Delta x_{grid}}$ and Δt

In this section issues related to the use of the developed hybrid particle tracking / Eulerian-Lagrangian model are investigated. The issues investigated include the number of particles necessary for achieving the desired accuracy, the appropriate criterion for particle elimination and the size of the timestep.

- Test Case 1: (instantaneous 1 - D point source in a quiescent fluid)

The grid used in Section 4.4 was also used here. For the particle tracking model 50 Monte Carlo runs were used. In Fig 4-3 and Fig 4-4 we see the ensemble average values of ϕ_D and ϵ respectively as a function of $\frac{\sigma_{min}}{\Delta x_{grid}}$. Fig 4-5 shows the ensemble average values of $\phi_D \pm$ one standard deviation as a function of $\frac{\sigma_{min}}{\Delta x_{grid}}$. As expected accuracy increases as N_p increases up to a limit, where the errors due to the interfacing and to the concentration mode become more important and so increasing N_p does not improve the accuracy. Increased N_p results in decreased variability between runs (i.e., decreased standard deviation of error in ensemble average).

If we call $\frac{\sigma_{min}}{\Delta x_{grid}}_{opt}$ the value of $\frac{\sigma_{min}}{\Delta x_{grid}}$, that minimizes the error, Fig 4-3 and Fig 4-4 show that $\frac{\sigma_{min}}{\Delta x_{grid}}_{opt}$ is an increasing function of N_p. This is explained by the balance between numerical error of the particle tracking mode and the concentration mode. As the gradient of the initial concentration field i.e., $\frac{\sigma_{min}}{\Delta x_{grid}}$ increases the error in the concentration mode decreases. On the other hand as $\frac{\sigma_{min}}{\Delta x_{grid}}$ increases the dimensions of the plume increase and occupy more sample volumes and so an increased N_p is required.

It is important to understand the balance between numerical error of the particle tracking mode and the concentration mode. Fig 4-6 shows the amplification factor Λ as a function of $\frac{L_k}{\Delta x}$, where L_k is the wavelength, resulting from the von Neuman stability analysis of the pure diffusion case using a first order Euler backwards scheme in time and quadratic finite elements in space. Fig 4-7 shows the Fourier transform of a Gaussian hill. The use of small $\rho = \frac{K\Delta t}{\Delta x^2}$ (i.e. use of small Δt for given Δx) decreases

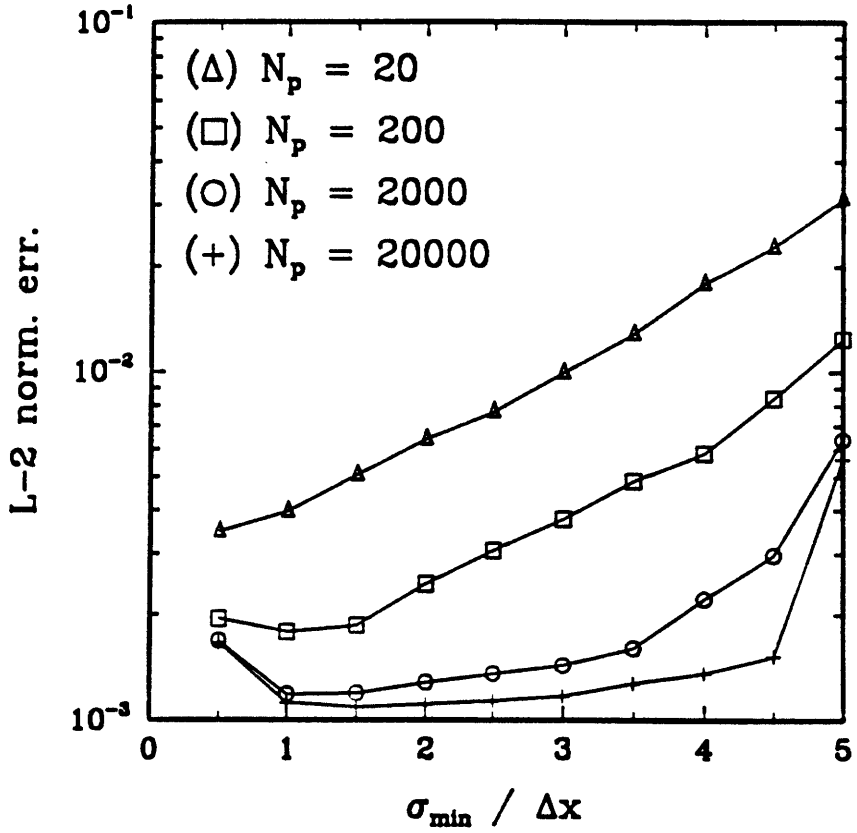

Figure 4-3: Discrete normalized L-2 error vs. $\sigma_{min}/\Delta x_{grid}$ in 1-D case for $N_p = 20$ ($\triangle$), $N_p = 200$ ($\diamond$), $N_p = 2000$ ($\times$) and $N_p = 20000$ ($\square$). Ensemble average values of 50 Monte Carlo simulations.

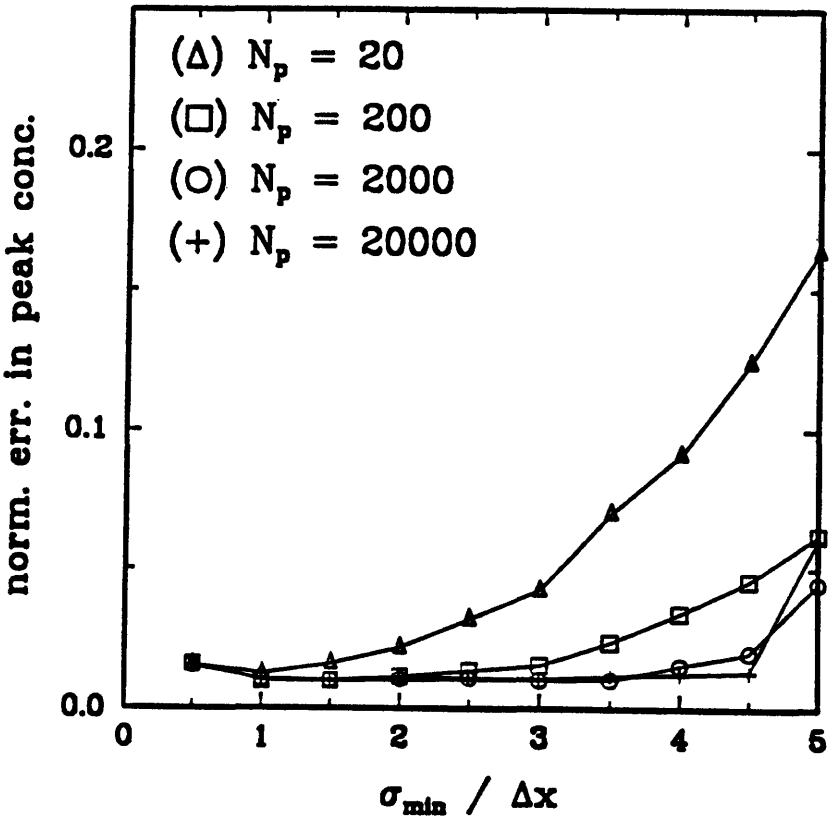

Figure 4-4: Normalized error in the peak concentration vs. $\sigma_{min}/\Delta x_{grid}$ in 1-D case for $N_p = 20$ ($\triangle$), $N_p = 200$ ($\diamond$), $N_p = 2000$ ($\times$) and $N_p = 20000$ ($\square$). Ensemble average values of 50 Monte Carlo simulations.

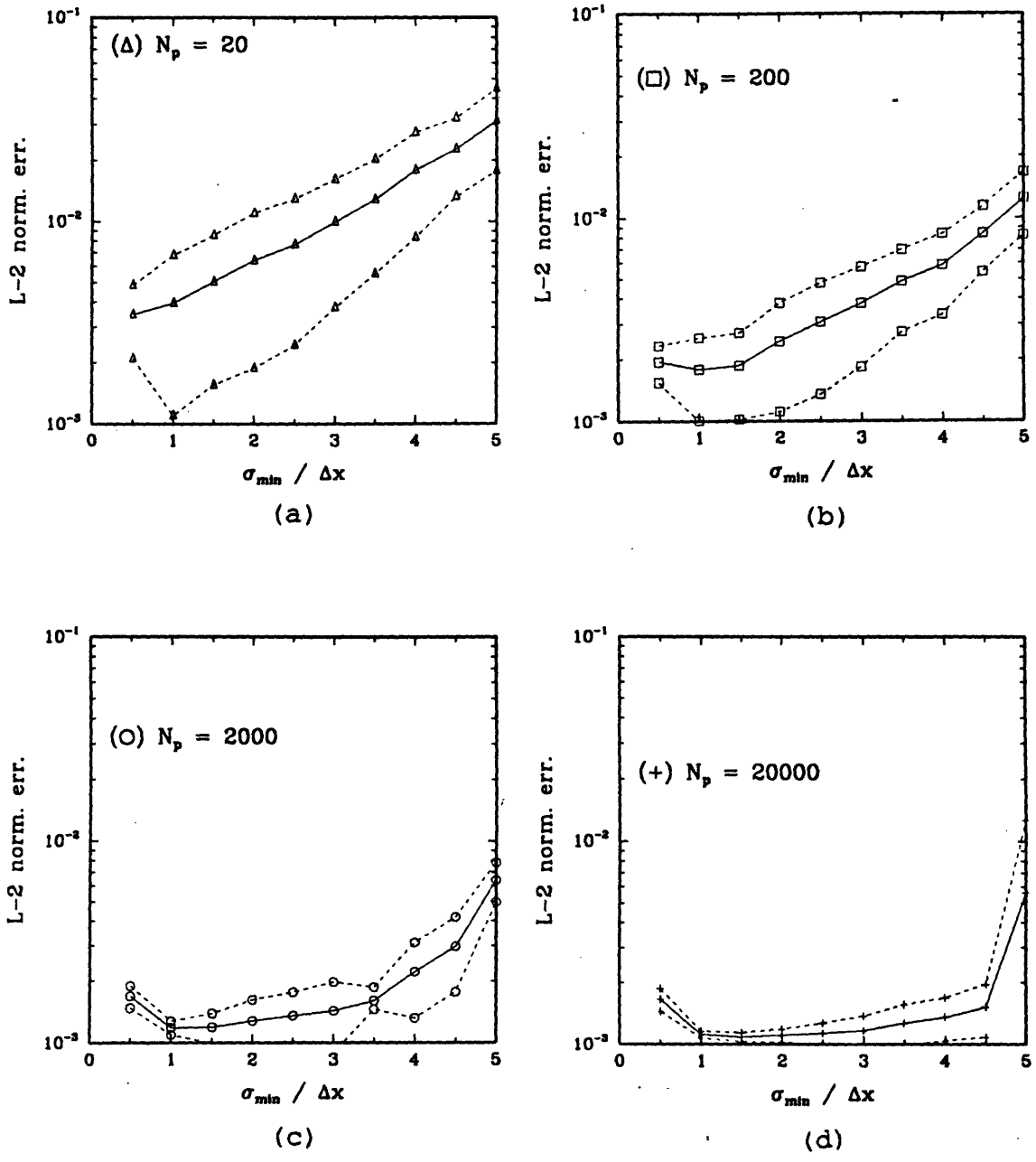

Figure 4-5: Discrete normalized L-2 error vs. $\sigma_{min}/\Delta x_{grid}$ in 1-D case for (a) $N_p = 20$ ($\triangle$) (b) $N_p = 200$ ($\diamond$), (c) $N_p = 2000$ ($\times$) and (d) $N_p = 20000$ ($\square$). Ensemble average values $\pm$ standard deviation of 50 Monte Carlo simulations.

Table 4.2: Dependence on N_p , $\Delta t = 1000$.

Run	N_p	$\frac{\sigma_{min}}{\Delta x_{grid}}$	t	ϕ_D	$\epsilon(t)$
1	200	3	20000	0.26106×10^{-5}	0.2371
2	2000	3	20000	0.10486×10^{-5}	0.04205
3	20000	3	20000	0.07106×10^{-5}	0.0397

the error in the concentration mode (for $\frac{L_k}{\Delta x}$ larger than three there is negligible numerical error). By using large Δt, $\frac{\sigma_0}{\Delta x}$ has to increase to avoid numerical error caused by the concentration mode, due to the misrepresentation of high wavenumbers. As $\frac{\sigma_0}{\Delta x}$ increases the number of particles N_p has to increase in order to decrease the numerical error in the particle mode.

- Test Case 2: (instantaneous 3 - D point source in a quiescent fluid)

The sensitivity of the numerical solution to Δt, N_p, and σ_{min} was tested on a test case involving an instantaneous point source in an infinite 3-D domain. The analytical solution to this problem in the case of a quiescent fluid and a conservative pollutant is

$$c = \frac{M}{(4\pi t)^{\frac{3}{2}}(K_x K_y K_z)^{\frac{1}{2}}} exp\{-\frac{1}{4t}[\frac{(x-x_o)^2}{K_x} + \frac{(y-y_o)^2}{K_y} + \frac{(z-z_o)^2}{K_z}]\} \qquad (4.20)$$

where M is the mass released, (x_o, y_o, z_o) are the coordinates of the release point, (K_x, K_y, K_z) are the diffusion coefficients and t is the elapsed time.

A domain of 21x21x21 nodes in the x, y, and z directions respectively was used with $x, y \in [-2000, 2000]$, $z \in [-1, 1]$, $K_x = K_y = 10, K_z = 0.25x10^{-5}, M = 1$ x 10^5.

From Table 4.2 it is clear that the number of particles affects the results. The average values of the error measurements from 5 Monte Carlo runs are presented.

Fig 4-8 and Fig 4-9 show ϕ_D and $\epsilon(t)$ versus $\frac{\sigma_{min}}{\Delta x_{grid}}$ at time $t = 20000$, which corresponds to the time when the standard deviation of the concentration distribution

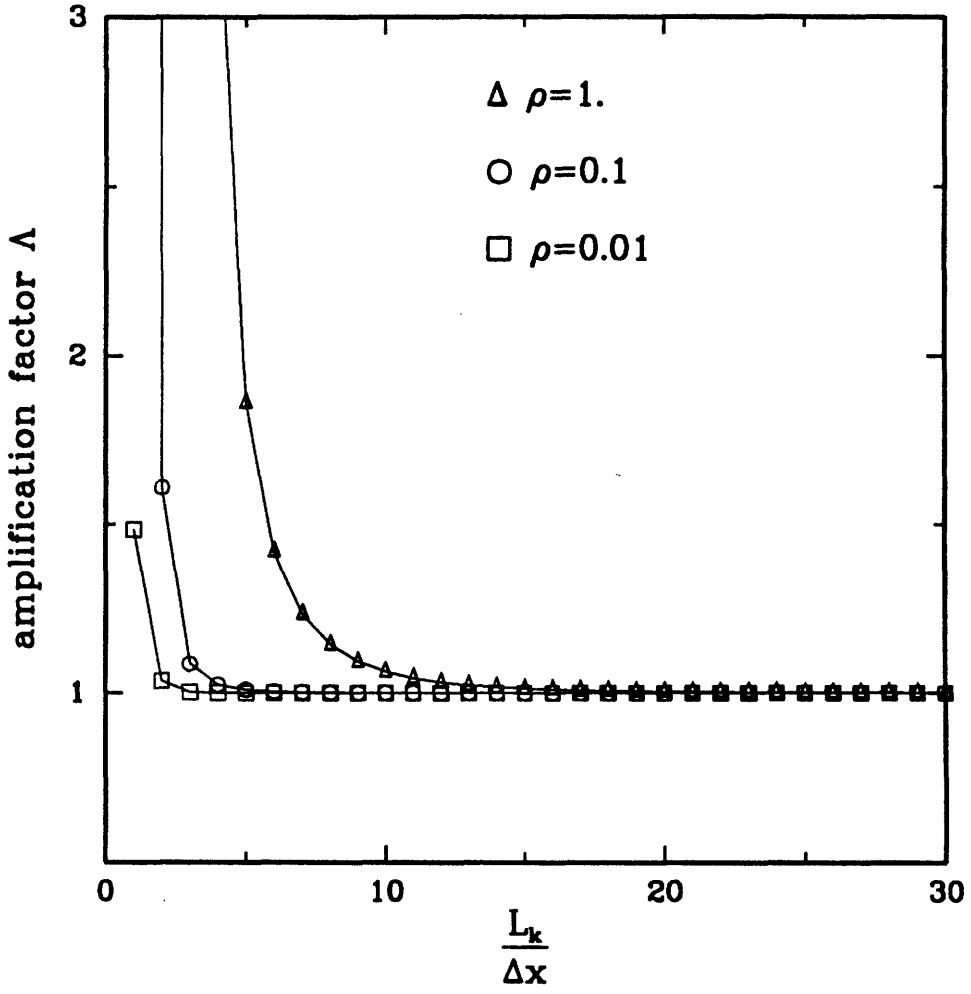

Figure 4-6: Amplification factor Λ vs. $\frac{L_k}{\Delta x}$ for the pure diffusion case using the first order Euler backwards scheme in time and quadratic finite elements in space ($\rho = \frac{K\Delta t}{\Delta x^2}$)

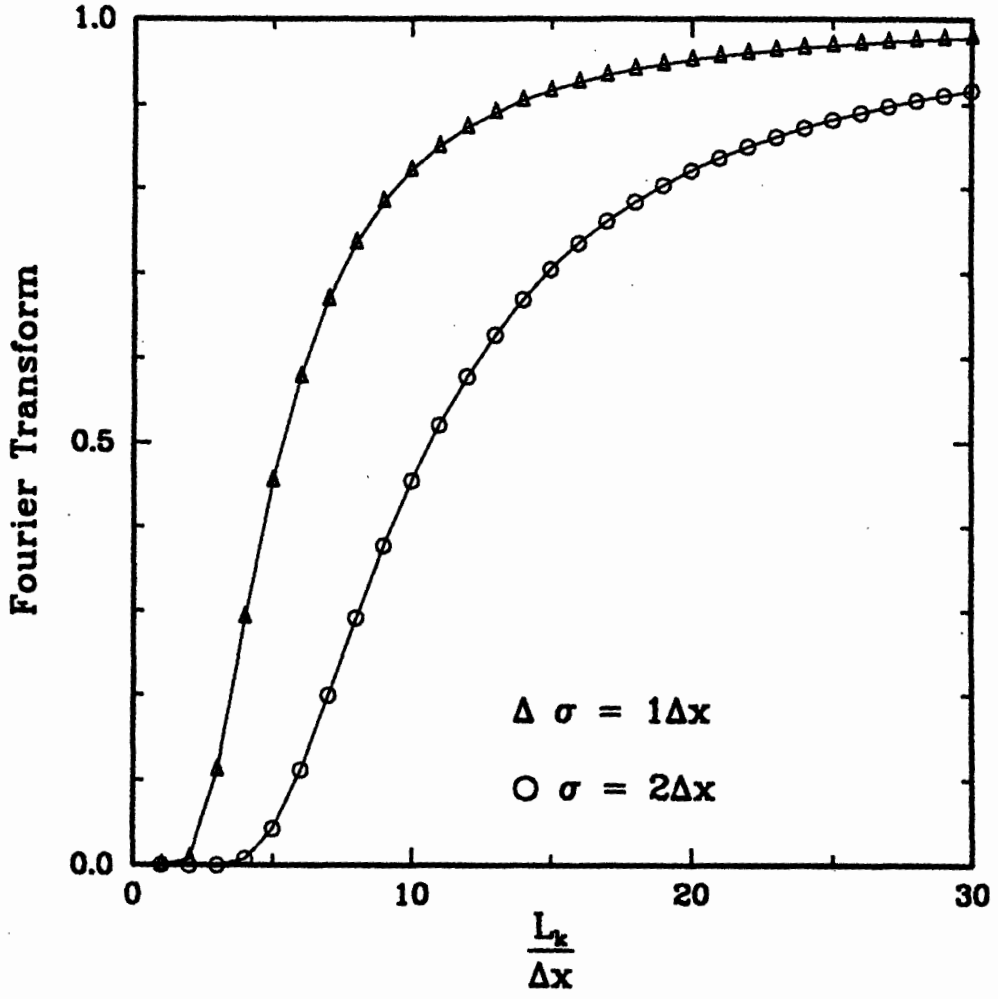

Figure 4-7: Fourier Transform of the Gaussian distribution

is approximately $3\Delta x_{grid}$ in all three directions. All runs are made with $\Delta t = 1000$ and four values of N_p. We see, that as σ_{min} increases the number of particles N_p necessary to achieve the expected accuracy increases substantially. As stated previously, this is because of counting errors due to decreasing particle density with increasing σ_{min}.

As a general rule of thumb one might suggests the use of $N_p = O(1000)$ with $\frac{\sigma_{min}}{\Delta x_{grid}} = 0(1)$.

- Test Case 3: (instantaneous line source with variable diffusion coefficient in a quiescent fluid)

Test case 3 investigates the choice of the timestep. In the case of highly variable velocity fields and/or non constant diffusion coefficients large Δt result in overshot errors. Tompson and Gelhar (1990) propose the use of a Δt so that $V_{max}\Delta t \ll \Delta x_{grid}$. This resembles a Courant number restriction. Tompson and Dougherty (1988) also propose the use of higher order schemes for the integration of the deterministic component **A** in Eqn 4.2. This may lead to problems in cases where diffusion is important, because of the different numerical treatment of the two components: **A** and **B**. In the case of advection-dominated flows, a higher order scheme (i.e., second or fourth order Runge-Kutta method) can be used for the deterministic part **A** without significant loss of accuracy. In this research a fourth order Runge-Kutta method with adaptive timestep was used for the deterministic part **A**.

Test case 3 demonstrates the influence of Δt in the case of variable diffusion coefficient. An instantaneous line source with variable diffusion coefficient was used. The same grid as in test case 1 was used with $K_x = K_y = K_r = a_1 r = a_1\sqrt{x^2+y^2}$, $a_1 = 1$. The analytical solution is given by Joseph and Sender (1958).

$$c = \frac{M}{2\pi h a_1^2 t^2} exp[-\frac{\sqrt{x^2+y^2}}{a_1 t}] \tag{4.21}$$

According to Section 4.2 for the particle tracking model we would have

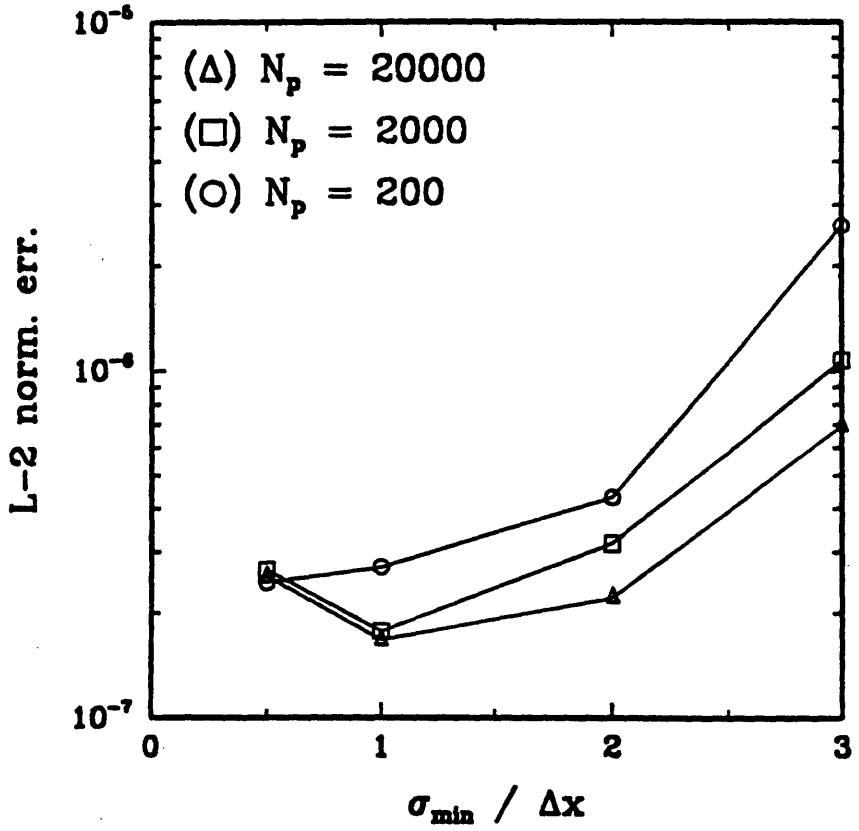

Figure 4-8: Discrete normalized L-2 error vs. $\sigma_{min}/\Delta x_{grid}$ in a 3-D case for $N_p = 200$ ($\diamond$), $N_p = 2000$ ($\times$) and $N_p = 20000$ ($\Box$).

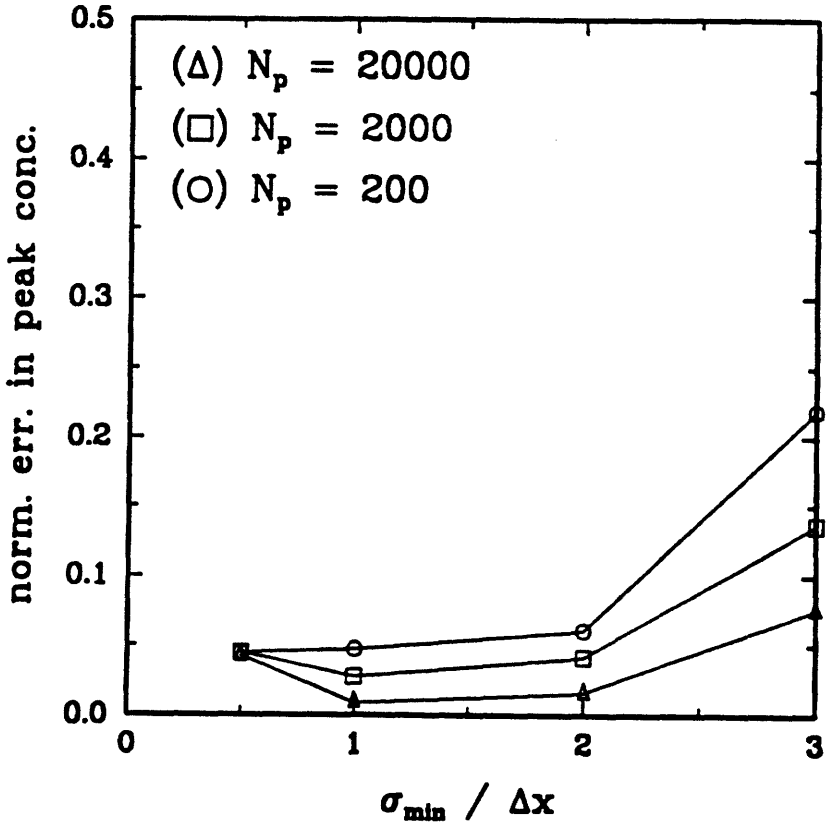

Figure 4-9: Normalized error in the peak concentration vs. $\sigma_{min}/\Delta x_{grid}$ in a 3-D case for $N_p = 200$ ($\diamond$), $N_p = 2000$ ($\times$) and $N_p = 20000$ ($\square$).

Table 4.3: Dependence on Δt , $\frac{\sigma_{min}}{\Delta x_{grid}} = 3$, $N_p = 20000$, $t = 450$.

Run	Δt	ϕ_D	$\epsilon(t)$
1	10	0.17×10^{-5}	0.241
2	50	0.18×10^{-5}	0.401
3	150	0.22×10^{-5}	0.477

$$\mathbf{A} = \begin{matrix} a_1 x(x^2+y^2)^{\frac{-1}{2}} \\ a_1 y(x^2+y^2)^{\frac{-1}{2}} \end{matrix} \tag{4.22}$$

$$\mathbf{B} = \begin{pmatrix} \sqrt{2a_1}(x^2+y^2)^{\frac{1}{4}} & 0 \\ 0 & \sqrt{2a_1}(x^2+y^2)^{\frac{1}{4}} \end{pmatrix} \tag{4.23}$$

In Table 4.3 the effect of the size of the timestep Δt is shown. The particles were mapped onto node concentrations at $t = 450$, when the standard deviation of the particle distribution in the x- and y- direction is approximately $3\Delta x_{grid}$. We can clearly see that the size of the timestep is decisive in the case of a variable diffusion coefficient.

4.6 Summary - Conclusions

A efficient method for simulating pollution sources in 3-D transport models was introduced. According to this method sources are simulated by particles that advect and diffuse independently until they have dispersed enough to be mapped onto the numerical grid by identifying the particle density (concentration) associated with each node. Questions which have been addressed relate to the number of particles N_p, the minimum standard deviation σ_{min} before the particles should be mapped onto node concentrations, and how N_p and σ_{min} are related. Fourier series analysis and numerical experiments suggest that as σ_{min} increases, accuracy increases up to a value of $(\sigma_{min})_{opt}$ that is an increasing value of N_p. This supports the notion that particle tracking models become less efficient as particles spread over larger areas of the domain. The question of how the size of the timestep affects the accuracy of the

solution is investigated on a 2-D test case ,that involves a radially variable diffusion coefficient. As expected the accuracy deteriorates with increased Δt.

4.7 REFERENCES

1. Ackerer, Ph., W. Kinzelbach. Modelisation de transport de conteminant par le methode de march au hasard: Influence des variation de champ d' ecoulement au cours de temps sur la dispersion. International Symposium on the Stochastic Approach to Subsurface Flow, Proceedings, Montrillargemme, France. 1985.

2. Adams, E.E., R. Kossik, A. E. M. Baptista. Source representation in a numerical model. In Finite Elements in Water Resources (ed. A. Sá da Costa et al.) pp589-598. Proc. of 6th Int. Conf. Lisboa, Portugal, 1986.

3. Ahlstrom, S.W., H. P. Foote, R.C. Arnett, C. R. Cole, R. J. Serne. Multicomponent mass transport model: Theory and numerical implementation. Report BNWL 2127, Battelle, Pacific Northwest Laboratories, Richland, Wash. 1977.

4. Ahn, S. A., P. F. Smith. The first report of a study to forecast nuclear power plant effects on coastal zones. EG G Document No. ESTR3-72 submitted to U.S. Atomic Energy Commission. 1972.

5. Araktingi, U. G., F. M. Orr, Jr. Viscous fingering, gravity segregations, and reservoir heterogeneity in miscible displacements i nvertical cross sections. SPE/DOE 20176 presented at the SPE/DOE 7th Symp. on Enhanced Oil Recovery, Tulsa. 1990.

6. Bagtzoglou, A. C., A. F. B. Tompson, D. E. Dougherty. Projected functions for particle grid methods. Num. Meth. for Partial Diff. Equations (to appear). 1991.

7. Baptista, A. E. M. Solution of advection-dominated transport by Eulerian-Lagrangian methods using the backwards method of characteristics. Ph. D. thesis. Dept. of Civil Engineering. MIT. 1987.

8. Baptista, A. E. M., P. Gresho, E. E. Adams. Reference problems for the convection-diffusion forum. Seventh Int'l. Conf. on Computational Methods in Water Resources. Cambridge. Mass. 1988.

9. Bugliarello, G., E. D. Jackson III. Random walk study of convective diffusion. Journal of Engineering Mechanics Division, ASCE 90(Em4):49-77. 1964.

10. Celia M. A., T. F. Russell, I. Herrera and R. E. Ewing. An Eulerian-Lagrangian localized adjoint method for the advection - diffusion equation. Advances in Water Resources. 1990. (to appear).

11. Dimou, K. N. and E. E. Adams. 2-D particle tracking model for estuary mixing. Proc. ASCE Estuarine and Coastal Modeling Conference. 15-17 Nov 1989. Newport. RI. 1990.

12. Dimou, K. N., E. E. Adams, A. E. M. Baptista. Interface between particle tracking and concentration model. 1992. (to be submitted).

13. Gardiner, C. W. Handbook of stochastic methods for physics, chemistry, and the natural sciences. Second ed., Springer Verlag. 1985.

14. Golub, G. H., C. F. van Loan. Matrix computations. Johns Hopkins Univ. Press. 1989.

15. Hockney, R. W., J. W. Eastwood. 1988. Computer simulation using particles. Adam Hilger. 1988.

16. Jeng, S. W., E. Holley. Two-dimensional random walk model for pollutant transport in natural rivers.Report. Dept. of Civil Engineering. Univ. Texas at Austin. 1986.

17. Jolles, A., S. Huberson. Clouds in cell method. Submitted to convection-diffusion forum. Seventh Int'l. Conf. on Computational Methods in Water Resources. Cambridge. Mass. 1988.

18. Joseph, J., H. Sendner. Uber die horizontale Diffusion im Meere. Deut. Hydrogr. Zeit. 11(2):49-77. 1958.

19. Martin, W. R., F. B. Brown. Status of vectorized Monte Carlo for particle transport analysis. Int. J. Supercomputer Appl. 1(2):11. 1987.

20. Mas-Gallic, S., P. A. Raviart. Particle approximation of convection-diffusion problems. Publication Universite Paris 6. 1987.

21. Melhem, R., Ganman. Toward efficient implementation of preconditioned conjugate gradient methods in vector supercomputers. Int. J. Supercomputer Appl. 1:70-98. 1987.

22. Neuman, S. P. An Eulerian-Lagrangian scheme for the dispersion-convection equation using conjugate space-time grids. J. Comp. Physics 41:270-279. 1981.

23. Neuman, S. P. Adaptive Eulerian-Lagrangian finite element method for advection-dispersion. Int'l. J. Numerical Methods in Engineering 20:317-337. 1984.

24. Pearce, B. R., et al. Thermal plume study in the Delaware River: Prototype measurements and numerical simulation. Proc. of IAHR Int'l Conf. on Physical Modeling of Transport and Dispersion. Cambridge. Mass. pp13B.7-13B.12. 1990.

25. Prickett, T. A., et al. Random walk solute transport model for selected groundwater quality evaluation. Bulletin 65. Illinois State Water Survey. 1981.

26. Press, W. H. Numerical recopes: the art of scientific computing. Cambridge. 1986.

27. Raviart, P. A. Particle numerical models in fluid dynamics. Numerical Methods for fluid Dynamics II, K. W. Morton, M. J. Baines, eds., pp 231-253. 1986.

28. Tompson, A. F. B., E. G. Vomvoris, L. W. Gelhar. Numerical simulation of solute transport in randomly heterogeneous porous media: Motivation, model development and application. Report No. MIT-316. 1988.

29. Tompson, A. F. B., D. E. Dougherty. On the use of particle tracking methods for reacting flows in porous media. Computational Methods in Subsurface Water Resources, Vol 2, Numerical Methods for Transport and Hydrologic Processes, M. A. Celia et al. (eds.), 227-232. 1988.

30. Tompson, A. F. B., L. W. Gelhar. Numerical simulation of solute transport in three-dimensional randomly heterogeneous porous media. Water Resources Research 26(10):2541-2562. 1990.

31. Tompson, A. F. B., D. E. Dougherty. Particle-grid methods for reacting flows in porous media with application to Fisher's equation. SIAM J. Sc. St. Comp. (to appear). 1991.

32. Torney, D., T. Warnock. Computer simulation of diffusion-limited chemical reaction in three dimensions. Int. J. Supercomputer Appl. 1(2):33. 1987.

33. Uffink, G. Modeling of solute transport with the randem walk method. NATO Advanced Workshop on Advances in Analytical and Numerical Groundwater Flow and Quality Modeling. Lisbon, Portugal. 1987.

Chapter 5

Interface Between Particle Tracking and Concentration Model

5.1 Introduction/Background

The mass balance of a conservative tracer is given by the following equation:

$$\frac{\partial c}{\partial t} + \nabla \cdot \mathbf{v}c = \nabla \cdot \mathbf{K} \cdot \nabla c + Q \tag{5.1}$$

where c(x,t) is the concentration, $\mathbf{v}$(x,t) is the velocity vector, $\mathbf{K}$(x,t) is the diffusivity tensor and Q represents point sources/sinks.

Transport models solve Eqn 5.1 using different techniques. According to the form of Eqn 5.1, that they solve, they can be classified into two main categories:

- Concentration models, where Eqn 5.1 is directly solved. Here the dependent variable of concentration is advected and diffused. Concentration models can be classified as Eulerian (EM), Lagrangian (LM), and Eulerian-Lagrangian (ELM). Thorough literature reviews are given by Neuman (1981), Baptista (1987), and Celia et al. (1990).

- Particle tracking models, where mass is represented by discrete particles. At each time step the displacement $\Delta \mathbf{x}$ of each particle consists of an advective, deterministic component and an independent, random Markovian component given by the equation (Gardiner, 1985; Tompson and Gelhar, 1990)

$$\Delta \mathbf{x} = \mathbf{X}^n - \mathbf{X}^{n-1} = \mathbf{A}(\mathbf{X}^{n-1}, t)\Delta t + \mathbf{B}(\mathbf{X}^{n-1}, t)\sqrt{\Delta t}\mathbf{Z} \tag{5.2}$$

where $\mathbf{A}$ and $\mathbf{B}$ are given by the expressions:

$$\mathbf{v} = \mathbf{A} - \nabla(\frac{1}{2}\mathbf{B}\mathbf{B}^T) \tag{5.3}$$

$$\mathbf{K} = \frac{1}{2}\mathbf{B}\mathbf{B}^T \tag{5.4}$$

Δt is the time step, $\mathbf{Z}$ is a vector of three independent random numbers with zero mean and variance one (Tompson et al, 1988). Eqn 5.2 is equivalent to Eqn 5.1 in the limit of a large number of particles N_p and small Δt (Tompson and Gelhar, 1990).

The main advantage of particle tracking models is that they concentrate the computational effort in regions, where most particles are located, i.e. in regions with highest concentrations, whereas in concentration models all regions of the domain are treated equally in terms of computational effort. This feature of particle methods is particularly useful in the case of large Peclet numbers, where we are dealing with elongated plumes, that are confined in a small portion of the computational domain or in the case of source representation at early times after the mass release. Particle tracking models are also a better choice than concentration models in cases, where transport and fate processes are better described by attributes of the individual particles (i.e. settling processes) rather than their aggregation. On the other hand in cases, where mass is spread out over the whole domain, as is the case with small Peclet numbers, concentration models are preferred. Also, in the case of concentration dependent processes (i.e. reactive transport) there is a need for calculating node

concentrations. Finally from the point of presenting our results we are usually more interested in concentration contours than mere particle locations.

From the above we see that in order to use the advantages of both models one is sometimes compelled to use a computational framework that includes two modes: a particle tracking mode and a concentration mode. In Chapter 4 a 3-D hybrid particle tracking / Eulerian-Lagrangian model is developed for the representation of sources whose spatial extent is small compared to that of the discretization. Sources are simulated by the introduction of particles. Each particle advects and diffuses independently and when the particles have dispersed enough they are mapped onto the numerical grid by identifying the particle density (concentration) at each node. In Tompson and Dougherty (1991) in order to model reactive transport with a 3-D particle tracking model, one switches back and forth between the particle mode and the concentration mode. In these hybrid models the issue of interfacing the particle tracking mode with the concentration mode becomes of particular importance.

In Section 5.2 the particle tracking mode / concentration mode interface method developed in this research is described. This interfacing method was developed in order to interface the particle tracking mode with the Eulerian Lagrangian mode in a 3-D hybrid model for the representation of sources analyzed in Chapter 4. This method is particularly suitable for this model and so the model itself is briefly described. In Section 3 the developed method is compared to other methods for mapping particle locations onto node concentrations. Section 4 includes summary and conclusions.

5.2 Mapping Particles onto Node Concentrations

If we consider a set of N_g grid points at which the concentration $\tilde{\mathbf{c}}$ is to be evaluated, then we are looking for an operator $\mathbf{J}$ so that (Tompson and Dougherty, 1991)

$$\tilde{\mathbf{c}} \leftarrow \mathbf{J} \cdot \mathbf{m} \tag{5.5}$$

where $\tilde{\mathbf{c}}$ is a vector of N_g concentrations, $\mathbf{m}$ is a vector of N_p particle masses and $\mathbf{J}$ is an N_g x N_p weighting matrix

The particle mass density $\hat{\mathbf{c}}$ can be defined as

$$\hat{\mathbf{c}}(\mathbf{x},t) = \sum_{p \in N_p} m_p(t)\delta(\mathbf{x} - \mathbf{X_p}(t)) \tag{5.6}$$

where δ is the Dirac function, $m_p(t)$ is the mass that particle p represents at time t, and $\mathbf{X_p}(t)$ is the location of particle p at time t. Because this representation is discontinuous, smoothed approximations have been used in its place. In this research a method designed for finite element grids that is particularly suitable for irregular grids is developed and applied. The methodology is the following. Element concentrations c^i_{el} are found first using

$$c^i_{el} = \frac{m}{N_p}\frac{N^i_{el}}{V_{el}} \tag{5.7}$$

where M is the total mass in the system, N_{el} is the number of particles in V_{el} and V_{el} is the volume of each element. Then element concentrations are mapped onto node concentrations using the mass conservation principle, i.e., the following expression has to be minimized.

$$min[\int c d\mathbf{x} - \int c_{el} d\mathbf{x}]^2 \tag{5.8}$$

Since we are using finite element basis functions we can express c as

$$c = \sum c_j \phi_j \tag{5.9}$$

where c_j are the concentrations at the nodes and ϕ_j are the basis functions and so Eqn 5.8 becomes

$$min[\int c d\mathbf{x} - \int c_{el} d\mathbf{x}]^2 = min[\int (c_j\phi_j - c_{el})^2 d\mathbf{x}] \tag{5.10}$$

Using the Lagrange method Eqn 5.10 is solved by treating the following system of equations

$$\frac{\partial}{\partial c_i}[\int (c_j\phi_j - c_{el})^2 d\mathbf{x}] = 0 \quad i = 1, 2, \cdots, N_g \tag{5.11}$$

which leads to

$$\int c_j\phi_j\phi_i d\mathbf{x} - \int c_{el}\phi_i d\mathbf{x} = 0 \tag{5.12}$$

One disadvantage of this method is that one could get slightly negative concentrations at some nodes. This can be avoided by adding the constraint that

$$c_i \geq 0 \quad i = 1, 2, \cdots, N_g \tag{5.13}$$

By doing that, though, we relax on the mass conservation principle.

This interface method was developed in order to couple the concentration to the particle tracking mode in a 3-D hybrid model for the simulation of sources in surface water problems. Sources are simulated by the introduction of particles. These particles are advected and diffused independently for several time steps until their distribution becomes smooth enough to be mapped onto the numerical grid by identifying the particle density (concentration) associated with each node (Fig 5-1). Node concentrations resulting from particles are added to node concentrations from the Eulerian-Lagrangian scheme and calculations then proceed in the concentration mode. In the case of a continuous source this procedure is repeated every time step.

According to the above, we have the following two modes: the particle tracking mode and the concentration mode and the interface between the two modes.

- The particle mode: Sources are represented by particles. These particles are displaced according to Eqn 5.2. The advective displacement is calculated using a fourth order Runge-Kutta method with adaptive time step (Press, 1986), whereas the diffusive displacement is calculated using a first order method due

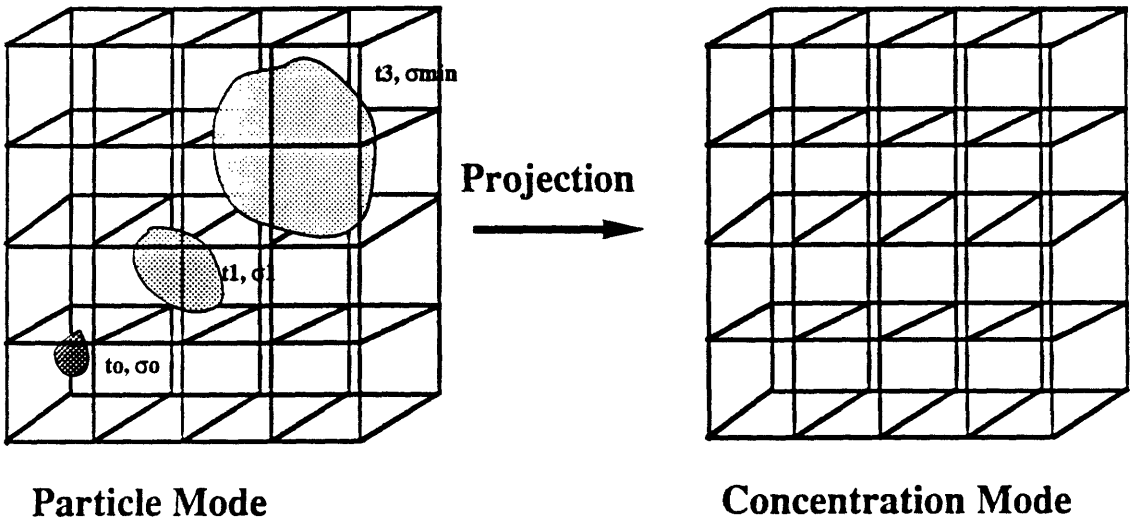

Figure 5-1: Representation of sources.

to the presence of a random number. This different numerical treatment of the two components is justified because of the higher accuracy required for advection in advection dominated flows. When the standard deviation of the particles' distribution reaches the value of σ_{min} the particle locations are mapped onto node concentrations. In the case of an instantaneous source particles are released only once and after the standard deviation of their distribution reaches the value of σ_{min} they are mapped onto node concentrations and the rest of the model computations continue in the concentration mode only. In the case of a continuous source a certain number of particles is released every time step. Each batch of particles is mapped onto node concentrations, when the standard deviation of its distribution has exceeded σ_{min}.

- The concentration mode: In this research a 3-D finite element Eulerian-Lagrangian model was developed. The main advantage of using an Eulerian-Lagrangian model is that one can use large Courant numbers, a feature particularly important in surface waters, where we are dealing with advection dominated flows. In this case the use of ELM is compatible with the use of a particle tracking model, where forward tracking of particles is used instead of backward tracking of characteristic lines.

The general procedure is the following. Eqn 5.1 is transformed into its nonconservative form

$$\frac{\partial c}{\partial t} + \mathbf{v} \cdot \nabla c = \nabla \cdot \mathbf{K} \cdot \nabla c + Q \tag{5.14}$$

Since the sources are modeled in the particle mode they are not included in the concentration mode. Eqn 5.14 is discretized in time according to

$$\frac{c^n - c^{n-1}}{\Delta t} + [\mathbf{v} \cdot \nabla c]^{n-1} = [\nabla \cdot \mathbf{K} \cdot \nabla c]^n \tag{5.15}$$

and then split into a pure advective

$$\frac{c^f - c^{n-1}}{\Delta t} + [\mathbf{v} \cdot \nabla c]^{n-1} = 0 \tag{5.16}$$

and a pure diffusive component

$$\frac{c^n - c^f}{\Delta t} = [\nabla \cdot \mathbf{K} \cdot \nabla c]^n \tag{5.17}$$

Eqn 5.16 states that the concentration c remains constant along characteristic lines defined by

$$\frac{d\mathbf{x}}{dt} = \mathbf{v} \tag{5.18}$$

According to Eqn 5.18, Eqn 5.16 is solved by tracking characteristic lines backwards using a fourth order Runge-Kutta method with adaptive time step (Press, 1986) from time n to time n-1 from every node. The concentration c^f at time n are determined by spatial interpolation. The interpolation functions were chosen to be the same as the basis functions. Eqn 5.17 is solved by using quadratic prismatic finite elements with triangular bases in the x-y plane. A conjugate gradient solver with a diagonal preconditioner was used (Golub and van Loan, 1989).

In the interfacing step between the particle tracking mode and the Eulerian/Lagrangian mode two equations have to be solved.

- Eqn 5.12 that transforms element concentrations to node concentrations. Let us call c^1 the solution of this equation.
- The diffusion part of the finite element formulation, which in its finite element representation takes the form:

$$\int_{\Omega_e} c_j^n \phi_j \phi_i d\mathbf{x} + \Delta t \int_{\Omega_e} \mathbf{K} \nabla c_j^n \phi_j \nabla \phi_i d\mathbf{x} = \int_{\Omega_e} c_j^f \phi_j \phi_i d\mathbf{x} + boundary \quad terms \tag{5.19}$$

Let us call c^2 the solution of Eqn 5.19. The concentration c in the domain (not including the vicinity of the source) is then $c = c^1 + c^2$

Since Eqn 5.12 and Eqn 5.19 are linear we can add them and then solve the system in order to be computationally efficient. This proves to be cost efficient in the case of continuous sources where Eqn 5.12 would have to be solved at every time step after the standard deviation of the distribution of the first batch of particles has reached the value of σ_{min}.

5.3 Comparison with other methods

Our method described above is designated as Method C, and is compared with two other types of smoothed approximations.

A first type of smoothing approximation (Method A) involves the selection of a symmetric region $\mathcal{V}$ around each grid point N_g and dividing the mass found within $\mathcal{V}$ by its volume V, i.e.,

$$c_{\mathcal{V}} = \frac{m}{N_p}\frac{N_{\mathcal{V}}}{V} \tag{5.20}$$

where M is the total mass in the system and $N_{\mathcal{V}}$ is the number of particles in $\mathcal{V}$. This method has been extensively utilized in regular grids (Tompson, 1988) but is difficult to apply in the case of irregular grids because the definition of $\mathcal{V}$ becomes cumbersome. Another drawback is that it is contaminated with random noise. It becomes more accurate as N_p increases but the error only decreases with ${N_p}^{1/2}$ (Ahlstrom et al., 1977). Moving averages (low pass filters) and Fast-Fourier-Transforms have been utilized by Ahlstrom et al. (1977) in order to improve the accuracy without the cost of adding more particles. However these filters are costly when applied in two or more dimensions (Ahlstrom et al., 1977).

The second method (Method B) involves the use of a cut-off function ζ (Hockney

and Eastwood, 1988, Tompson and Dougherty, 1991), i.e.,

$$\tilde{\mathbf{c}}(\mathbf{x},t) = \int_{\Omega_c} \hat{\mathbf{c}}(\mathbf{x}',t)\zeta(\mathbf{x}-\mathbf{x}')d\mathbf{x}' = \sum_{p\in N_p} m_p(t)\zeta(\mathbf{x}-\mathbf{X_p}(t)) \tag{5.21}$$

where Ω_c is the computational domain. For mass conservation purposes the weighting function ζ should satisfy the conditions (Raviart, 1986)

$$\int_{\Omega_c} \zeta d\mathbf{x} = 1 \tag{5.22}$$

If we define the weighting function ζ over a regularization parameter δ^d, where d is the dimensionality of the problem, then Raviart (1986) has shown that the interparticle distance h must be much smaller than δ in order to obtain satisfactory approximation results. For reasons of mass conservation, δ must be greater than a representative grid scale Δx_{grid} (Tompson and Dougherty, 1991) (Fig 5-2).

Essentially this method replaces the discontinuous representation $\hat{\mathbf{c}}$ by a function with finite support ζ. In terms of accuracy the choice of the weighting function ζ in terms of accuracy resembles the choice of a basis function in a finite element grid. Accordingly ζ must be at least $\in H^\circ$ in Ω_c, where H is the Sobolev space. The accuracy of the approximation increases with increasing m, where $\zeta \in H^m$.

Bagzoglou et al. (1991) investigate four types of ζ weighting functions for a one-dimensional case : the Nearest Grid Point (NGP), the Closed in Cell (CIC), the Triangular Shaped Cloud (TSC) and the Truncated Gaussian (TG) (Fig 5-3). NGP is equivalent to Method A. Bagzoglou et al. (1991) compared the above weighting functions and found that higher order ζ functions give more accurate results, but at an increased computational cost. Thus they concluded that CIC is the optimal ζ function. From now on we will refer to CIC as Method B1, to TSC as Method B2, to the Box Method as Method A and to the method developed in this research as Method C1, when linear basis functions are used and C2, when quadratic basis functions are used.

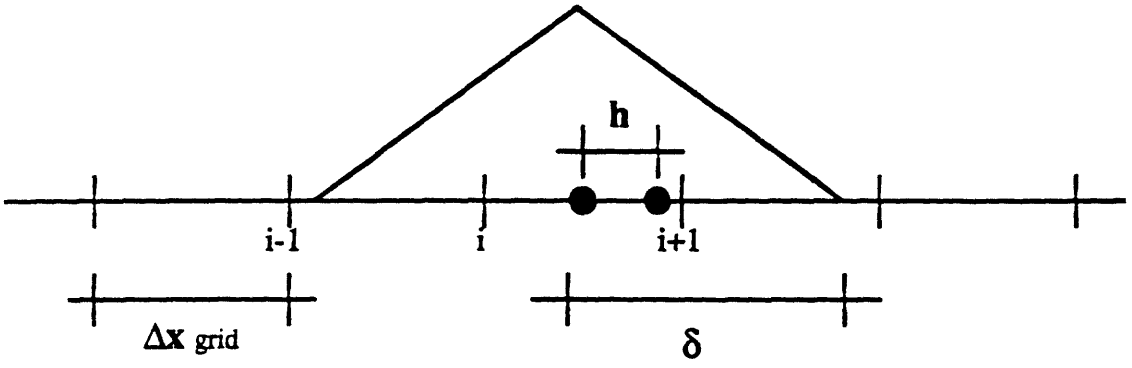

Figure 5-2: Projection functions.

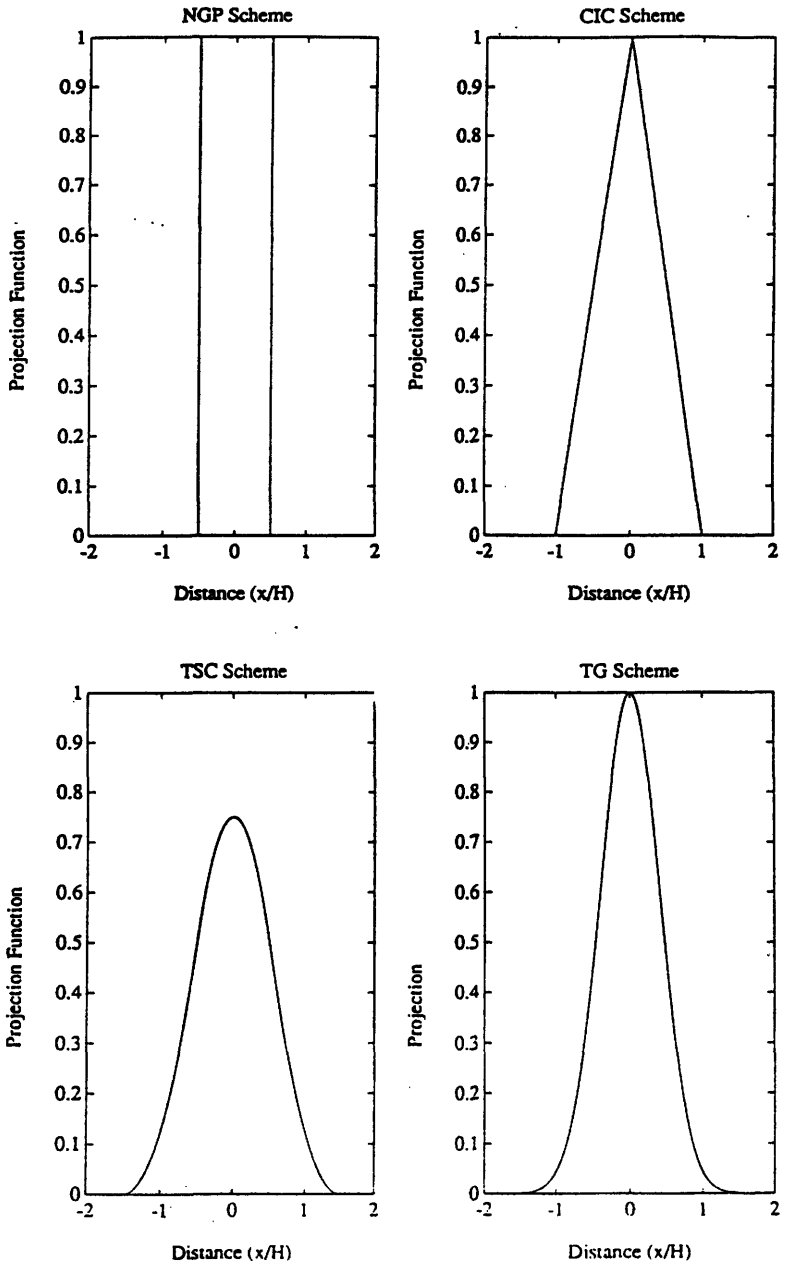

Figure 5-3: Types of ζ functions (from Bagtzoglou, 1991).

In the following the three methods A, B, and C are compared using a 1-D test case. Additional issues explored include the effect of the order of the method on accuracy, i.e. the choice of basis functions (C1 vs C2) and the choice of weighting functions (B1 vs B2), and performance on non-regular grids. The ratio $\frac{\delta}{\Delta x_{grid}}$ for method B is taken equal to one in all examples unless otherwise stated.

The following error measures are used

- Discrete $L-2$ error norm normalized by the total mass

$$\phi_D = \frac{1}{M}\{[\sum_i (c_i^{nu} - c_i^{ex})^2]^{\frac{1}{2}}\} \tag{5.23}$$

- Error in the peak concentration normalized by the exact peak concentration

$$\epsilon(t) = \frac{c_{max}^{ex}(t) - c_{max}^{nu}(t)}{c_{max}^{ex}(t)} \tag{5.24}$$

In all figures the ensemble average values of the error measurements after 50 Monte Carlo simulations are shown. The ensemble average of a variable a is defined as

$$< a >= \frac{1}{50}\sum a^i \tag{5.25}$$

where a^n is the value of a in realization i.

5.3.1 Basic comparison among three methods

In this section the simplest forms of each method are compared, i.e. method A, Method B1 and Method C1. In each case N_p particles are distributed on a 1-D grid x$\in$[-100,100] with spacing $\Delta x_{grid} = 1$ according to a Gaussian distribution with zero mean and variable $\frac{\sigma}{\Delta x_{grid}}$. Fig 5-4 shows plots of the normalized error as a function of N_p for the three different methods for different values of $\frac{\sigma}{\Delta x_{grid}}$.

We see that Method B1 performs better than the other two methods in the case of small N_p and $\frac{\sigma}{\Delta x_{grid}}$. It is interesting to see that Methods A and C1 are very

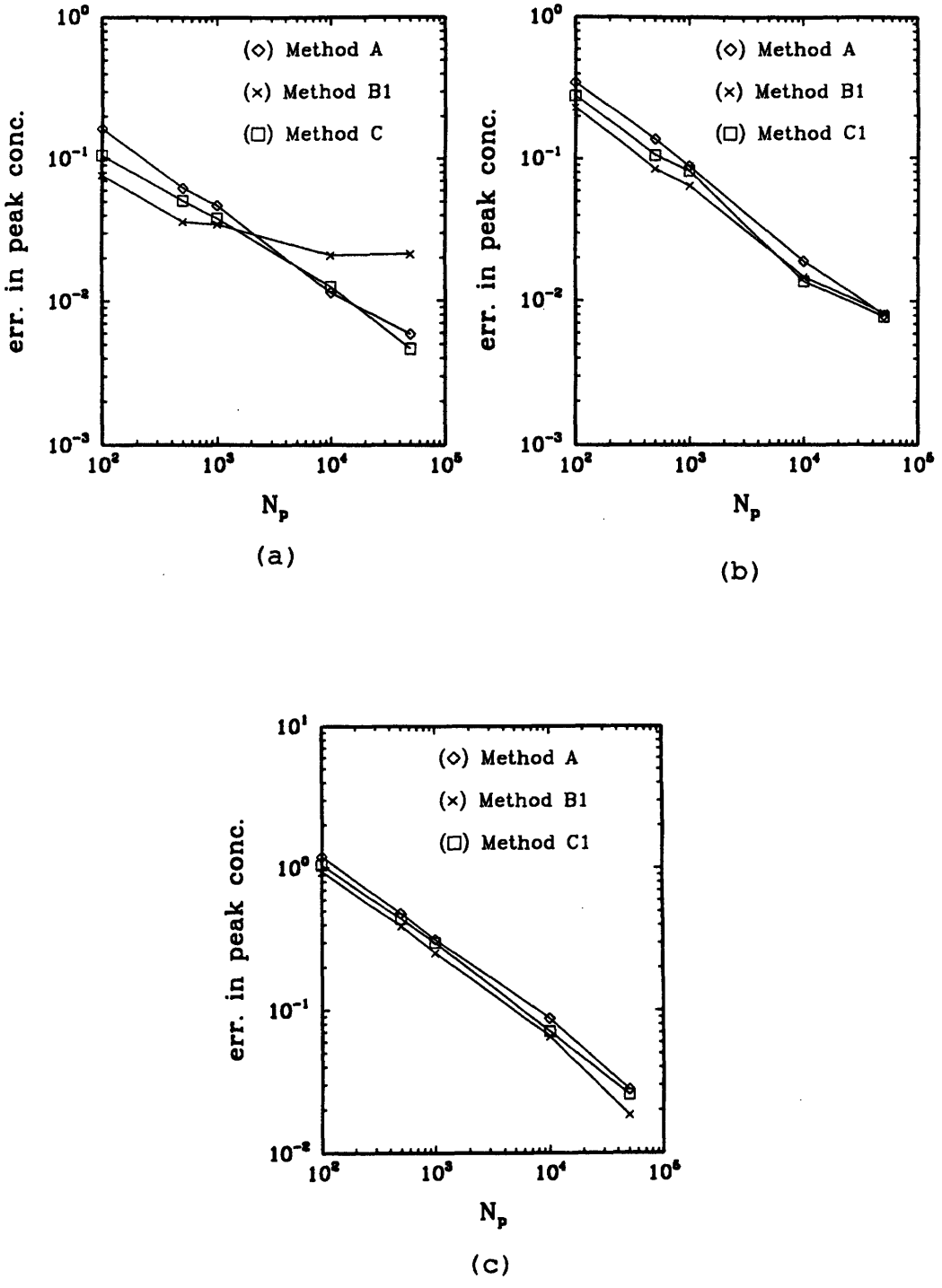

Figure 5-4: Error in peak concentration vs. N_p for a) $s_{dev} = 2\Delta x_{grid}$, b) $s_{dev} = 4\Delta x_{grid}$ and c) $s_{dev} = 15\Delta x_{grid}$ using Method A (◇),Method B1 (×), Method C1 (□).

sensitive to N_p, whereas Method B1 in the case of small $\frac{\sigma}{\Delta x_{grid}}$ is not sensitive to N_p. Also Method C1 always performs better than Method A. This is due to the smoothing effect that the finite element method has on the noise resulting from the use of Method A.

5.3.2 Comparison within methods

This section includes a comparison of Methods B1 and B2 (i.e. a test of the weighting function ζ) and a comparison of Methods C1 and C2 (i.e. a comparison of linear and quadratic basis functions). Fig 5-5 shows plots of ϵ as a function of N_p for the four schemes. In Fig 5-5a $\frac{\sigma}{\Delta x_{grid}} = 2$ and in Fig 5-5b $\frac{\sigma}{\Delta x_{grid}} = 4$. Regarding Method B we see that there is almost no difference in accuracy between Methods (B1) and (B2). Taking costs into consideration, our result supports the conclusion of Bagzoglou et al (1991), that CIC (B1) is optimal among the other functions in Method B. Regarding Method C, we note that $\Delta x_{grid} = 1$ is used in all cases, so the number of elements in the linear grid is twice the number of elements in the quadratic grid. Thus for the case of high gradients (Fig 5-5a), linear elements are better than quadratic elements, because averaging over the larger elements in the latter case causes a greater dilution of peak concentrations. For lower concentration gradients (Fig 5-5b), accuracy also depends on the number of particles N_p. For small N_p quadratic basis functions give significantly more accurate results than linear basis functions, whereas for large N_p linear basis functions behave better. This can be explained by the fact that, for large N_p, smoothness is not a significant source of error. Hence, by averaging over smaller elements peak concentrations are not diluted as much by the linear elements.

5.3.3 Effect of grid irregularity

In this section we compare Method A, Method B1 and Method C1 using non-uniform 1-D grids. Following Baptista (1986), the following grid was used:

$x_i = x_{i-1} + \Delta x_b$ if i odd

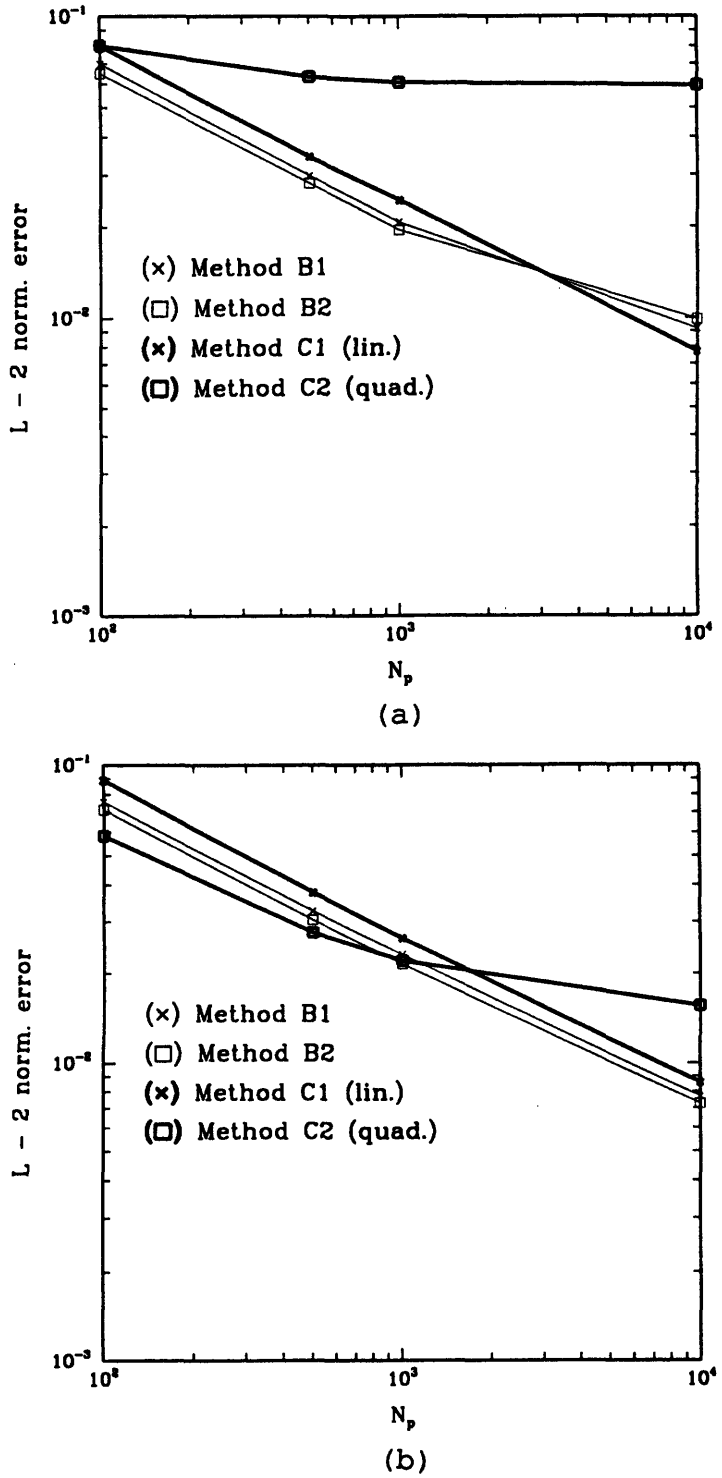

Figure 5-5: Discrete normalized L-2 error vs. N_p using Methods B1 (thin line $\times$), B2 (thin line $\square$), C1 (bold line $\times$) and C2 (bold line $\square$) basis functions. (a)$s_{dev} = 2\Delta x_{grid}$, (b) $s_{dev} = 4\Delta x_{grid}$.

$$x_i = x_{i-1} + \Delta x_a \quad \text{if i even with } \frac{\Delta x_b}{\Delta x_a} = s \geq 1$$

Fig 5-6 shows the influence of the grid irregularity parameter s on accuracy using the three methods for $N_p = 2000$ and $\frac{\sigma}{\Delta x_{grid}} = 8$. It is interesting to see how sensitive Method B1 is to the parameter δ. Method B1 behaves poorly and encounters mass conservation errors when $\delta = \Delta x_a$. This is an important consideration in highly irregular grids, where there is no fixed ratio s, so δ has to be chosen larger than the maximum grid scale. This adds computational effort in finely discretized areas, because ζ of each particle covers a large number of nodes. On the other hand Method C is not sensitive in terms of computational cost to the irregularity of the grid.

5.4 Summary - Conclusions

The issue of interfacing a particle tracking model with a concentration model, i.e. the issue of projecting particle locations onto node concentrations, is investigated in this research. A method based on the finite element methods, that is particularly suitable for irregular finite element grids is developed. The advantage of this method is that the added cost of the interfacing is reduced due to the linear character of the governing equations. The developed method (Method C) is compared with two other methods. In the first method (Method A) node concentrations are found by specifying a volume around each node and dividing the mass in this volume by the volume. In the second method (Method B) each particle is represented by a cut-off function ζ, that defines a concentration distribution.

For applications on irregular grids we conclude the following. Method A can not be used because of the difficulty in defining volume $\mathcal{V}$ in an irregular grid. Methods B and C have comparable results in terms of accuracy with the more accurate choice depending on issues such as $\frac{\sigma}{\Delta x_{grid}}$ and grid irregularity. However Method C is computationally more efficient in hybrid models involving finite element grids with calculations in both particle and concentration mode. This is because of the way node

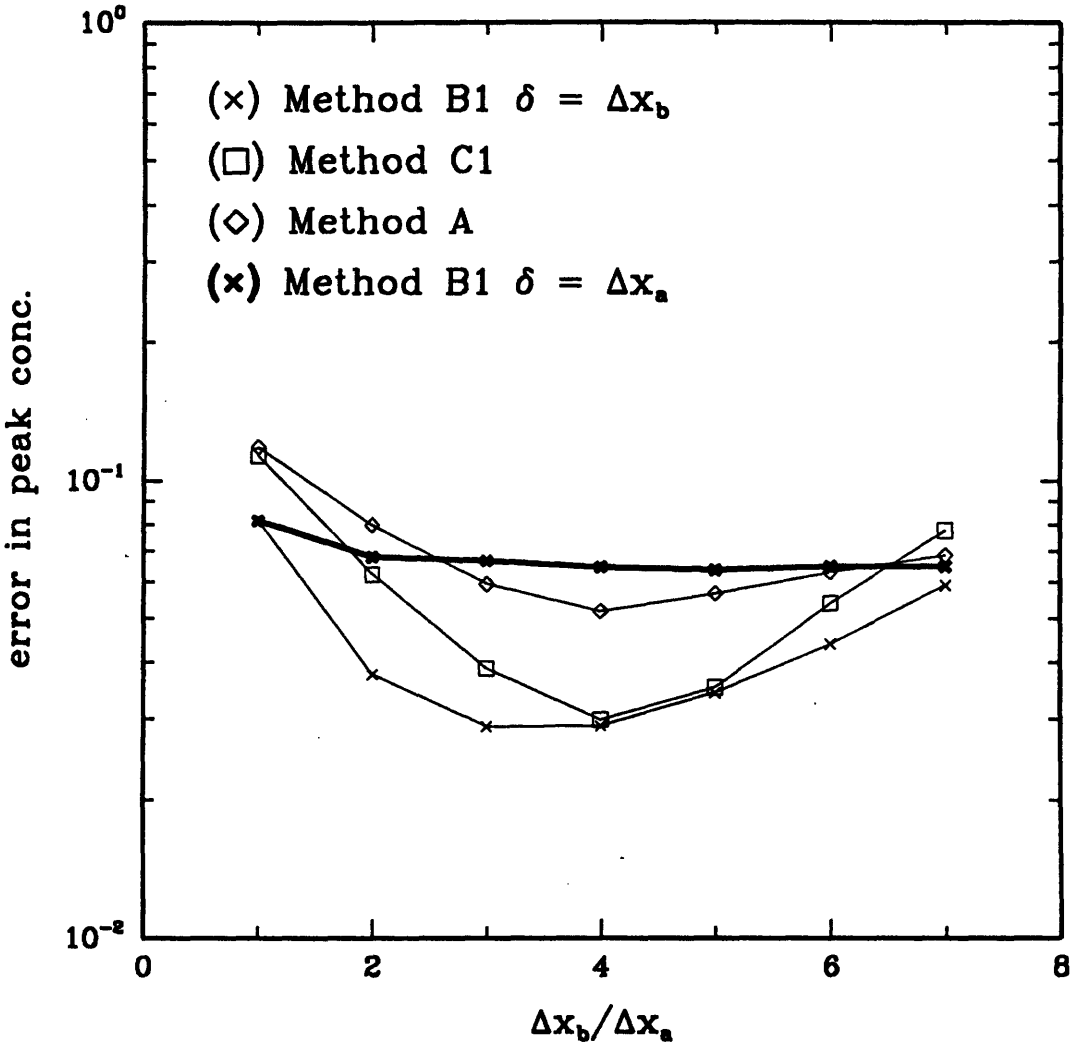

Figure 5-6: Error in peak concentration vs. the grid irregularity parameter $\frac{\Delta x_b}{\Delta x_a}$ for $N_p = 2000$ using Methods A(thin line $\diamond$), B1 with $\delta = \Delta x_b$ (thin line $\times$), B1 with $\delta = \Delta x_a$ (bold line $\times$) and C1 (thin line $\square$) with linear basis functions.

concentrations are calculated from particle locations allowed by the linear character of the governing equation . In addition the application of Method B could become cumbersome in 3-D irregular domains because of the difficulty in defining the zone of influence of a particle in an irregular grid.

5.5 REFERENCES

1. Ahlstrom, S.W., H. P. Foote, R.C. Arnett, C. R. Cole, R. J. Serne. Multicomponent mass transport model: Theory and numerical implementation. Report BNWL 2127, Battelle, Pacific Northwest Laboratories, Richland, Wash. 1977.

2. Bagtzoglou, A. C., A. F. B. Tompson, D. E. Dougherty. Projected functions for particle grid methods. Num. Meth. for Partial Diff. Equations (to appear). 1991.

3. Baptista, A. E. M. Accurate numerical modeling of advection-dominated transport of passive scalars. Ministerio do Equipamento Social. Laboratorio Nacional de Engenharia Civil Proc. 64/13/7398. 1986.

4. Baptista, A. E. M. Solution of advection-dominated transport by Eulerian-Lagrangian methods using the backwards method of characteristics. Ph. D. thesis. Dept. of Civil Engineering. MIT. 1987.

5. Baptista, A. E. M., P. Gresho, E. E. Adams. Reference problems for the convection-diffusion forum. Seventh Int'l. Conf. on Computational Methods in Water Resources. Cambridge. Mass. 1988.

6. Celia M. A., T. F. Russell, I. Herrera and R. E. Ewing. An Eulerian-Lagrangian localized adjoint method for the advection - diffusion equation. Advances in Water Resources. 1990. (to appear).

7. Dimou, K. 3-D hybrid Eulerian-Lagrangian / Particle tracking model for simulating mass transport in coastal water bodies. PhD thesis. Massachusetts Institute of Technology. Department of Civil Engineering. 1992.

8. Gardiner, C. W. Handbook of stochastic methods for physics, chemistry, and the natural sciences. Second ed., Springer Verlag. 1985.

9. Golub, G. H., C. F. van Loan. Matrix computations. Johns Hopkins Univ. Press. 1989.

10. Hockney, R. W., J. W. Eastwood. 1988. Computer simulation using particles. Adam Hilger. 1988.

11. Neuman, S. P. An Eulerian-Lagrangian scheme for the dispersion-convection equation using conjugate space-time grids. J. Comp. Physics 41:270-279. 1981.

12. Raviart, P. A. Particle numerical models in fluid dynamics. Numerical Methods for fluid Dynamics II, K. W. Morton, M. J. Baines, eds., pp 231-253. 1986.

13. Tompson, A. F. B., E. G. Vomvoris, L. W. Gelhar. Numerical simulation of solute transport in randomly heterogeneous porous media: Motivation, model development and application. Report No. MIT-316. 1988.

14. Tompson, A. F. B., D. E. Dougherty. On the use of particle tracking methods for reacting flows in porous media. Computational Methods in Subsurface Water Resources, Vol 2, Numerical Methods for Transport and Hydrologic Processes, M. A. Celia et al. (eds.), 227-232. 1988.

15. Tompson, A. F. B., L. W. Gelhar. Numerical simulation of solute transport in three-dimensional randomly heterogeneous porous media. Water Resources Research 26(10):2541-2562. 1990.

16. Tompson, A. F. B., D. E. Dougherty. Particle-grid methods for reacting flows in porous media with application to Fisher's equation. SIAM J. Sc. St. Comp. (to appear). 1991.

Chapter 6

Representation of Sea Outfalls - Application in Massachusetts Bay

6.1 Background

Oceans are used for wastewater disposal by many communities. The wastewater is typically carried to the offshore discharge point by a pipe laid on or buried in the ocean floor (outfall) or by a tunnel (Metcalf Eddy, 1991). The discharge occurs through a single port or multiport diffuser . As it is discharged the effluent rises in the water column due to the initial buoyancy and momentum to form a plume. As it rises it entrains ambient water. After it reaches the water surface or a trapping level z_{tr} (Fig 6-1) in the case of stratified ambient water it starts spreading in the radial direction.

We can distinguish three zones around the diffuser:

- The zone of the near flow field or zone of initial dilution ZID (Muellenhoff et al, 1985) that extends to a distance of the order of the water depth from any point of the diffuser (Tetra Tech, 1982). It is defined as the zone where rapid mixing takes place between the waste stream and ambient fluid entrained into this zone. Due to the entrainment an initial dilution S_{in} is reached in the near

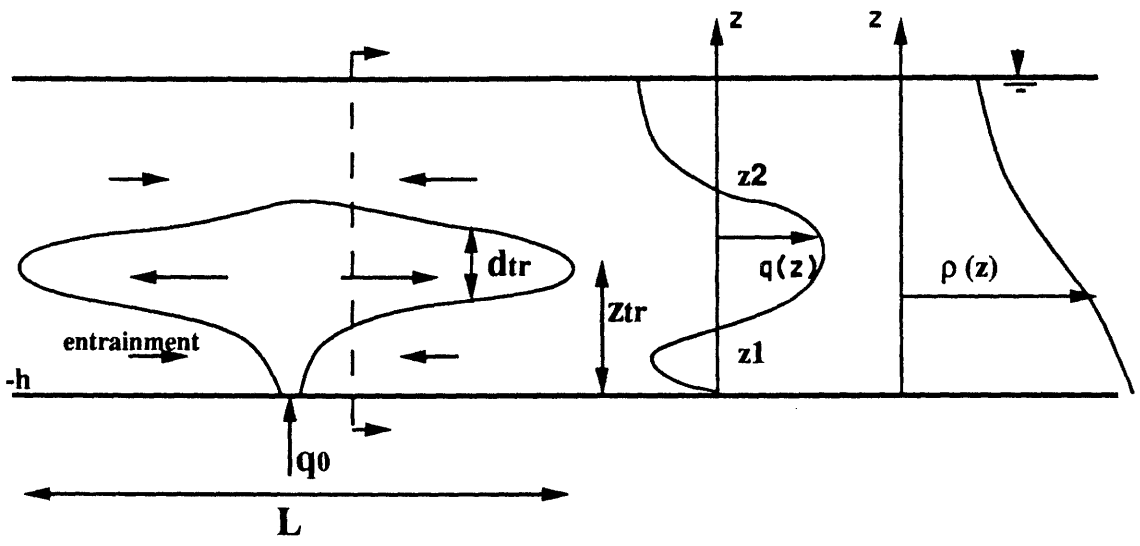

Figure 6-1: Near Flow Field.

field. As the mixed fluid from the plume moves away from the initial dilution zone further dilution takes place that depends on ambient oceanic processes.

- The far field zone where the formed wastewater field is carried away by ambient currents and further diluted by diffusion.

- The zone of the intermediate flow field defined in this research as the zone that extends beyond the near field zone and that is influenced by the presence of the outfall. It serves as a link between the near and far field zone.

Extended research in the form of experiments or mathematical modeling has been done for the near flow field zone. In Muellenhoff et al (1985) a thorough literature review of experimental work and simple analytical expressions resulting from this work are presented. CORMIX1 (Jirka and Doneker, 1991) and CORMIX2 (Jirka and Akar, 1991) are two microcomputer based expert system programs for single port and multiport discharges respectively. They include a classification scheme that provides a comprehensive quantitative description of the many possible flow configurations. They are based on experimental data and appear to be useful for practical applications: they are easy to use, guide the user on which predictive models to use in complicated cases and help him to eliminate undesirable design configurations. EPA models (Muellenhoff et al, 1985) constitute the main effort in the area of mathematical modeling of the near flow field zone. These models vary in terms of sophistication from a simple generalization of the analytical formulas of Roberts (1977; 1979) to a 3-D integral jet representation of the flow field that solves for the conservation of mass, energy, pollutant and momentum equations taking into account the effect of merging plumes (UDKHDEN).

In the case of large scale modeling one is primarily interested in two variables resulting from the near flow field modeling:

- Initial dilution S_{in} and

- trapping level z_{tr}

No attempt has been made so far to include the modeling of an outfall in a large scale 3-D TM. In the 2-D TM ELA (Baptista et al, 1984) the initial dilution S_{in} of the discharged fluid which is a user specified function is taken into consideration in the initial size of the "puff" originating from the outfall (Adams et al, 1986). Apart from the problem arising from modeling a point source with puffs described in Chapter 4 this method does not take into account the intermediate flow field. This results in the following inconsistency. Physically, S_{in} is due to the near field entrainment of ambient fluid into the plume. However, by not taken into account the intermediate field there is no general mechanism to guaranty that S_{in} is achieved in the far field.

In this research a method is developed for consistently modeling a single or multiport diffuser in a 3-D TM. The methodology involves the incorporation of near flow field model data into the developed large scale 3-D model by modeling the intermediate flow field. Apart from the fact that this method enables us to consistently represent an outfall in coastal waters it also allows us to model intermediate flow field processes i.e.

- the region of initial deposition of particles from sewage effluent
- the vertical exchange in the intermediate flow field from constituents such as nutrients.

6.1.1 Methodology

In order to represent the near flow field in the developed large scale model the following procedure is followed at every time step:

- Use of an initial mixing model (e.g., one of the EPA models) in order to specify values for S_{in} and z_{tr}. These calculations require a value for the ambient water current (magnitude and direction) at the location of the outfall, which is taken from the ambient velocity field. As seen in Fig 6-2 from Roberts (1989) S_{in} and z_{tr} are not influenced by the magnitude of the current u and its orientation in respect to the diffuser θ if $F = \frac{u^3}{b} < 0.1$ where

$b = \frac{g'_D Q_D}{L}$

L is the length of the diffuser

Q_D is the maximum discharge flowrate

$g'_D = g\frac{\Delta\rho_D}{\rho}$ is the discharge buoyancy

ρ is the ambient water density

$\Delta\rho_D$ is the discharge density difference

Thus for sufficiently small maximum currents, this step needs to be done only once.

- Generation of the intermediate flow field $\mathbf{u_{in}}$ by using results from the near flow field.

  For mass conservation purposes for an initial dilution S_{in} the resulting horizontal outflow rate i.e. $\int_A \mathbf{u_{in}^{out}} \vec{\eta} dA$ must satisfy the following conditions in any control volume that extends over the whole depth and includes the diffuser

$$\int_A \mathbf{u_{in}^{out}} \vec{\eta} dA = S_{in} q_0 \tag{6.1}$$

  where q_0 is the flow from the diffuser.

- Use of the developed 3-D Eulerian-Lagrangian / particle tracking mass transport model. The particles are put between levels z_1 and z_2, that are symmetric from z_{tr}, in the vertical (Fig 6-1), where outward flow is present.

In order to generate the intermediate flow field two methods have been considered.

In the first method the near velocity profile $q(z)$ (Fig 6-1) at the location of the diffuser is considered known from a near flow field model and so condition Eqn 6.1 is satisfied at the location of the diffuser. For example, the intermediate flow field could be generated by using an analytical potential flow solution with the near flow field as a vertically distributed source or sink .

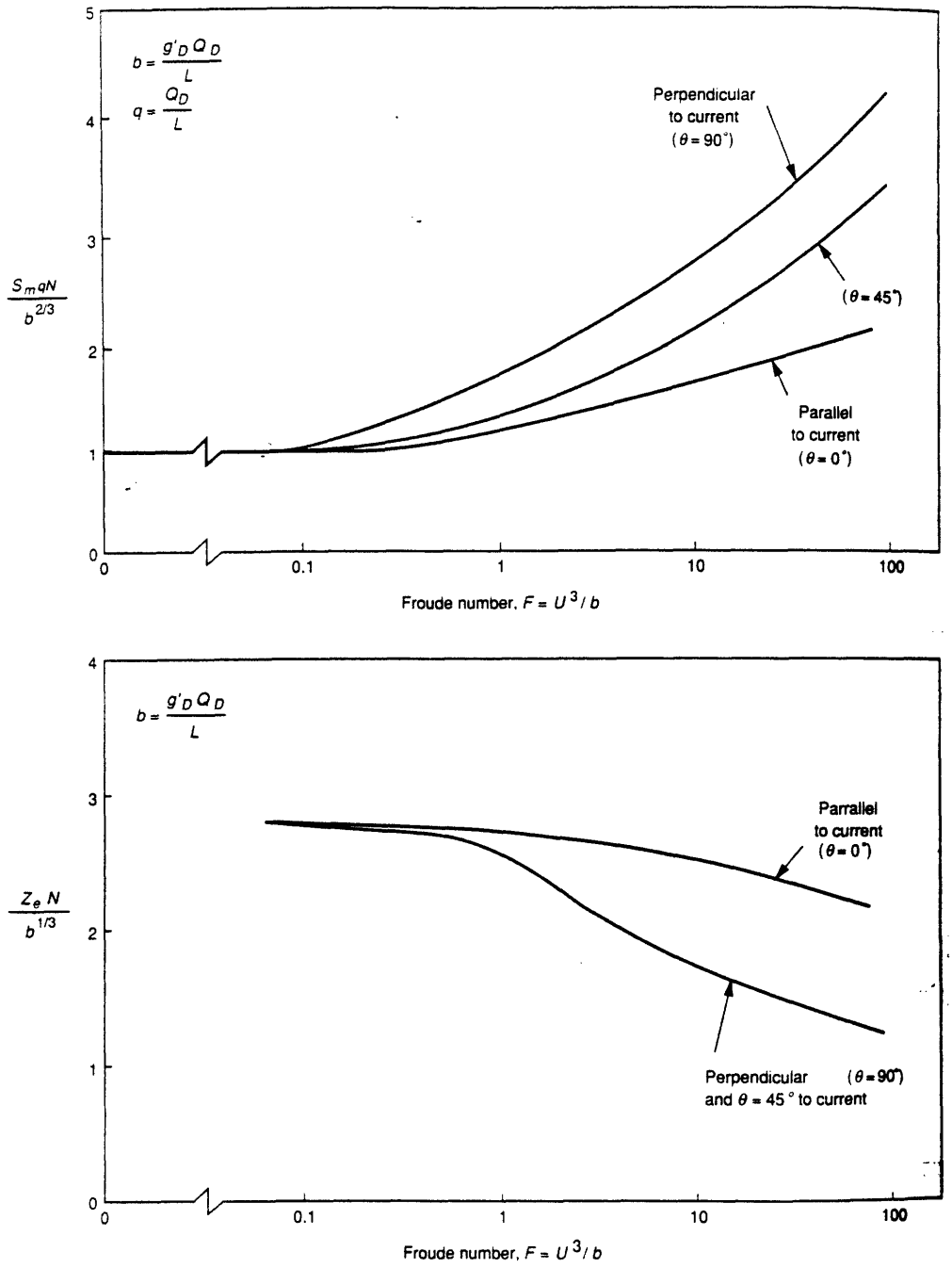

Figure 6-2: Influence of ambient current on S_{in} and z_{tr} (from Roberts et al, 1989).

In the case of a single port diffuser located at (x_0, y_0) the horizontal velocity u_r at a point x', y' is given by

$$u_r(x', y', z) = \frac{q(z)}{2\pi\sqrt{(x' - x_0)^2 + (y' - y_0)^2}} \tag{6.2}$$

where $q(z)$ is the flow per unit depth $(\frac{l^2}{t})$ sketched schematically in Fig 6-1. In the case of a multiport diffuser the horizontal velocity u_r at a point x', y' due to an infinitensimal source of extend dx_0 along the diffuser is given by

$$u_r(x', y', z; x_0) = \frac{q(z)dx_0}{2\pi\sqrt{(x' - x_0)^2 + y'^2}} \tag{6.3}$$

where in this case $q(z)$ is the flow per unit depth and length $(\frac{l}{t})$. The horizontal velocity field $\mathbf{u_{in}}$is found by integrating Eq(6.3) over $-\frac{L}{2} < x_0 < \frac{L}{2}$ (Fig 6-3).

In the second method only S_{in} and z_{tr} are required. The intermediate flow field is generated numerically by the density differences between the well mixed near flow field zone of thickness $d_{tr} = |z_2 - z_1|$ and the stratified ambient water.

In order to generate such a density-driven flow we used the density field for an idealized 2-D front in stratified shallow water used by Garrett and Loder (1981), with slight modifications to accomodate flow from a diffuser. The density field is given by (Fig 6-6)

$$\frac{\partial\rho}{\partial x} = \frac{1}{2}\frac{\partial\Delta\rho(x)}{\partial x}[-cos(\frac{\pi(z - z_1)}{d_{tr}})] \tag{6.4}$$

$$\frac{\partial\rho}{\partial y} = \frac{1}{2}\frac{\partial\Delta\rho(y)}{\partial y}[-cos(\frac{\pi(z - z_1)}{d_{tr}})] \tag{6.5}$$

$$\Delta\rho(x) = \Delta\rho(y) = \Delta\rho_s \quad r > L, \quad z > z_{tr} \quad or \quad z < z_{tr} - d_{tr} \tag{6.6}$$

$$u_r(x', y', z; x_0) = \frac{q(z)dx_0}{2\pi\sqrt{(x' - x_0)^2 + y'^2}}$$

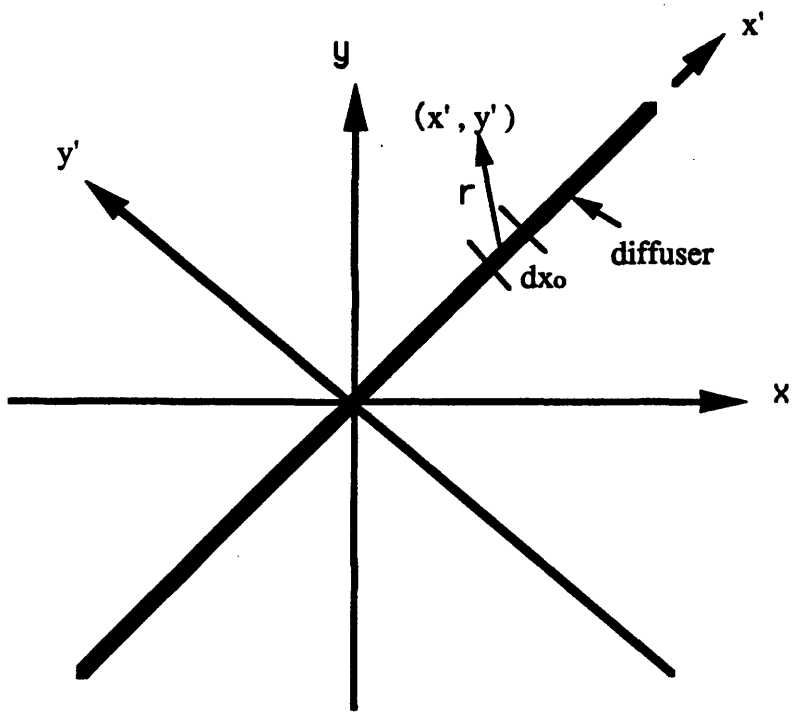

Figure 6-3: Potential Flow solution for multiport diffuser.

$$\Delta\rho(x) = \Delta\rho(y) = \frac{1}{2}\Delta\rho_s[1 + cos(\pi\frac{r-L}{L})] \quad 0 \leq r \leq L, \quad z_{tr} - d_{tr} \leq z \leq z_{tr} \qquad (6.7)$$

where d_{tr} is the thickness of the resulting plume, $\Delta\rho_s$ is the density difference between depths z_{tr} and $z_{tr} - d_{tr}$ in the stratified region, r is the radial distance from the diffuser, L is a length scale for the resulting plume, i.e. the length of the intermediate flow field zone (Fig 6-1). The magnitude of the generated flow depends on d_{tr} and in order to satisfy Eqn 6.1 the parameter d_{tr} has to be adjusted. Several iterations are required in order to specify d_{tr}.

For our applications the 3-D finite element model by Lynch et al. (1991) is used. As described in the following section, the model requires input of horizontal gradients of the density field, i.e. density driven flow is handled diagnostically.

Fig 6-4 shows an example of the values of S_{in} computed in the model changes as a function of d_{tr}. In this example a $29 \times 29 \times 21$ grid $x, y \in [-2800, 2800]$, $z \in [-25, 0]$ with uniform depth and vertical spacing $\Delta z = \frac{h}{20}$. Fig 6-5 shows a horizontal crossection of the grid . A diffuser with length $L_{dif} = 2000m$ is located in the middle of the grid parallel to the y-axis. The dimensional parameters $g = 9.806\frac{m}{s^2}$, $f = .9946 \times 10^{-4}s^{-1}$, h = 25m, $\Delta\rho_s = 0.002\frac{kg}{l}$, $q_0 = 25m^3/s$, $L = 2000m$, $k = 0.005m/s$ (see Eq 6.12), $N = 0.02m^2/s$ (see Eq 6.12). EPA's model ULINE with $q_0 = 25m^3/s$ and $\Delta\rho_s = 0.002\frac{kg}{l}$ results in $S_{in} = 50$ and $z_{tr} = -16.4m$. According to Fig 6-4 then d_{tr} is 13m. Fig 6-6 shows the density field at $y = 0$. Fig 6-7 shows a vertical profile of the x velocities at $x = 4000$, $y = 0$ (section (b) in Fig 6-6). Fig 6-8 shows a vertical profile of the density field in the ambient water.

One of the parameters in this model of the intermediate flow field is the horizontal length scale L. In the next section an analysis based on experimental studies for the specification of L is presented.

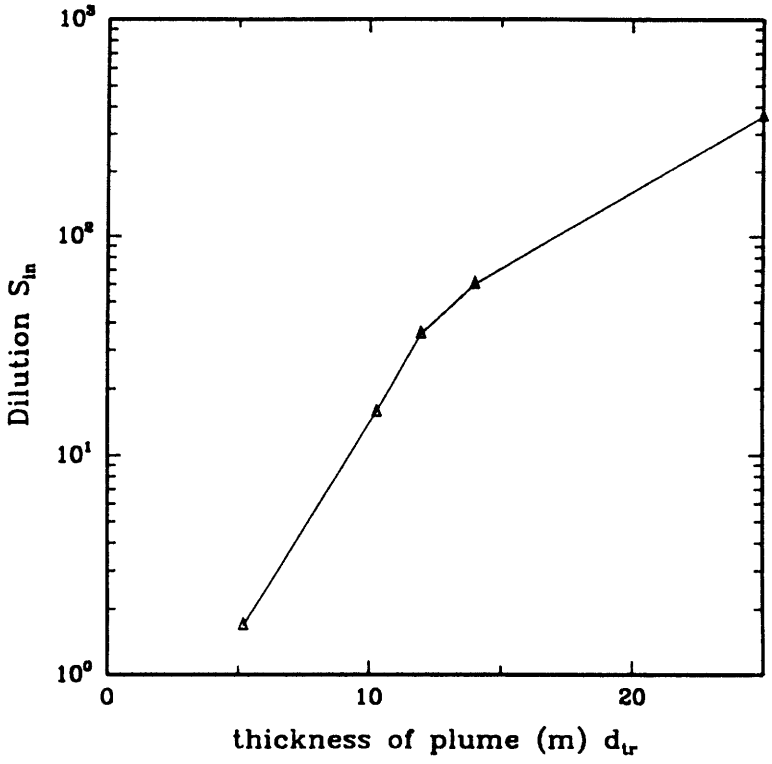

Figure 6-4: Variation of S_{in} as a function of d_{tr}.

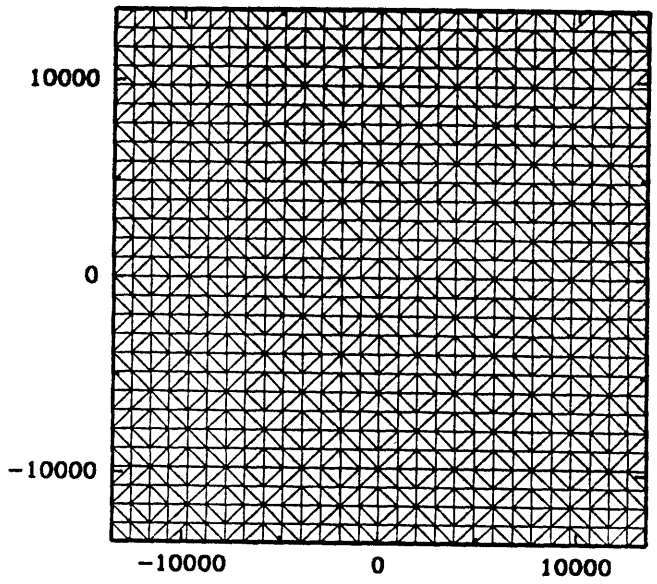

Figure 6-5: Horizontal crossection of grid.

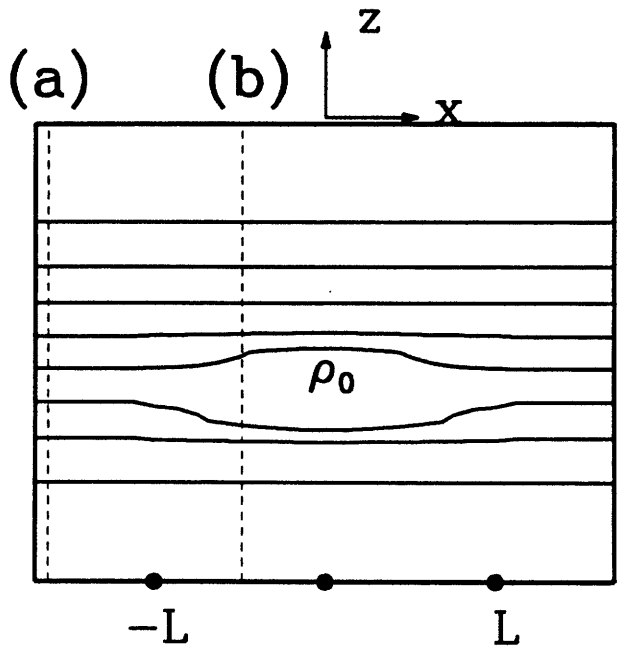

Figure 6-6: Density Field at $y = 0$.

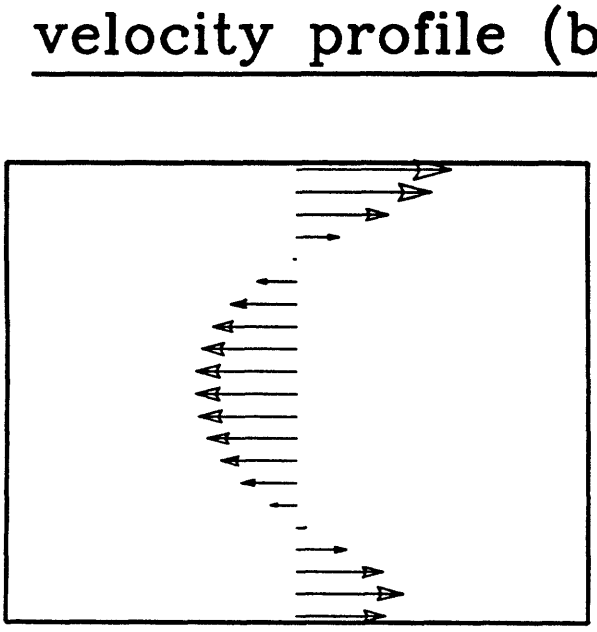

Figure 6-7: Vertical profile of velocity at $x = -4000$ $y = 0$.

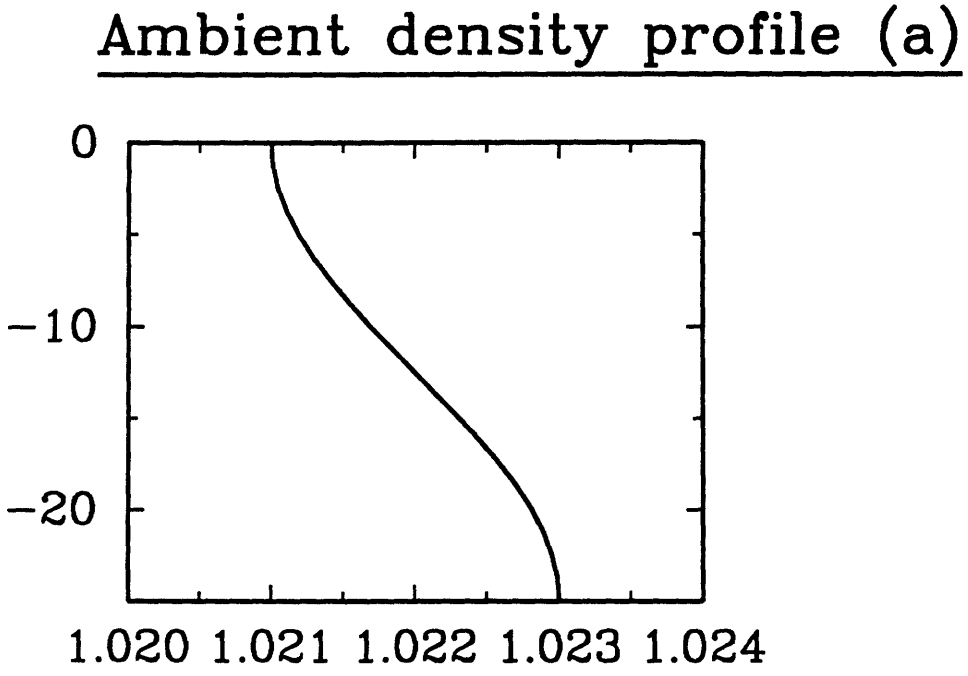

Figure 6-8: Vertical profile of ambient fluid density field.

In the application in Massachusetts Bay that follows the second method for the generation of the intermediate flow field is used because it is more physically based (e.g., it includes the effect of Coriolis force and computes flow by coupling both near field and far field consideration). However, we anticipate that for some applications, a potential flow solution may be attractive because it is easy to be implemented.

6.1.2 Specification of length scale L of the intermediate flow field

In order to specify a horizontal length scale L for the intermediate flow field the experimental study by Helfrich and Battisti (1991) was used. The purpose of this study was to examine the effects of rotation on the structure and stability of hydrothermal plumes. The study of hydrothermal plumes resulting from hot vents is similar to the study of wastewater plumes resulting from the discharge of wastewater from a diffuser. Fluid from a hot vent rises as a turbulent plume, entraining and mixing with ambient seawater as it rises. Because the ambient environment is stratified, the density of the plume is eventually increased to that of the ambient water at a neutral buoyancy level where the plume fluid slowly spreads laterally (Helfrich and Battisti, 1991). They found that the horizontal length scale L of the resulting eddies depends on the dimensionless number $\frac{N}{f}$ where N is the ambient buoyancy frequency f is the Coriolis frequency

N is given by:

$$N^2 = -\frac{g}{\rho_0}\frac{\partial \rho}{\partial z} \tag{6.8}$$

where

ρ_0 is the density of the source

$\rho(z)$ is the ambient density

Fig 6-9 shows $\frac{NH}{fL}$ versus tf. H is the thickness of the plume (d_{tr} in this study) and t represents time after the beginning of the release. We see that at steady state

$\frac{NH}{fL} \simeq 0(1)$

Let us try now to specify $\frac{NH}{f}$ for applications that are of interest in this study. In a typical application (e.g. Massachusetts Bay) we have $\rho_0 = 1.023$, $\frac{\partial \rho}{\partial z} \simeq \frac{(1.021-1.023)}{25}$ and $H \simeq 5m \Rightarrow \frac{N}{f} \simeq 280 \Rightarrow L \simeq 0(1300)$. We see that the length scale L of the intermediate flow field is of the order of the grid scale and so in order to represent the intermediate flow field there is no need for a finer resolution around the diffuser.

6.2 Testing of the Model in Massachusetts Bay

6.2.1 General

Model verification is necessary in order to establish its validity for describing the phenomena it has been developed for. With respect to numerical models, the first step in the verification process is an evaluation of the numerical approximation and involves comparison of the numerical results to analytical solutions. Chapter 3 and 4 contain comparisons with analytical solutions. These tests are restricted to problems involving simple geometry and flow conditions. To establish confidence in the predictive capability of a model, further verification, consisting of comparisons to real world cases is necessary.

In order to test the ability of the model to simulate real world applications, the model was applied in Massachusetts Bay. Two test cases were used:

- Application to the NOMES (New England Offshore Mining Environmental Study) experiment, that involves the simulation of an instantaneous source and comparison with the available data

- Demonstration - Application involving the continuous discharge of fine grained sediments from a diffuser located close to the proposed diffuser location. The results of this test were not compared to any field data. The main reason for this choice is the fact that it demonstrates the main features of our model i.e.

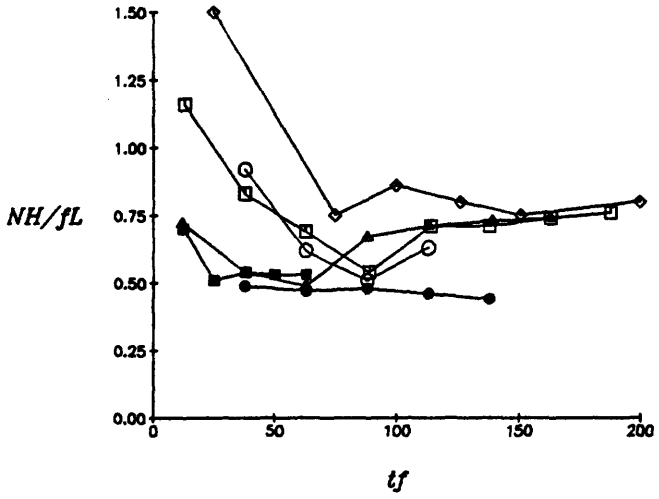

Fig. 3. NH/fL versus tf for $N/f = 0.67$, (solid circles), 1.42 (solid squares), 1.88 (diamonds), 3.11 (triangles), 4.28 (open circles), and 5.02 (open squares).

Figure 6-9: Specification of length scale L of the intermediate flow field(from Helfrich and Battisti).

modeling of advection dominated processes in coastal waters, representation of outfalls and modeling of processes that depend on the behavior of individual particles i.e. settling of fine-grained sediments.

6.2.2 Grid

The combined Massachusetts and Cape Cod Bays form a body of water enclosed by land along 75 percent of its perimeter. It is bounded on the north by Cape Ann and on the South by Cape Cod. It has an area of approximately $3600 km^2$ and depths of up to 90m.

The 2-D grid shown in Fig 6-10 was developed by Camp Dresser & McKee, Inc., for evaluating the impact of Combines Sewer Overflows on water quality in Boston Harbor (CDM, 1988) and was used in this study. It has a total of 2358 quadratic nodes and 1031 triangular elements in the horizontal plane. It was modified to a 3-D grid by adding 11 nodes in the vertical so that in each layer $\frac{z}{H}$ is constant and so the 3-D grid has 25938 quadratic nodes and 5155 prismatic triangular quadratic elements.

6.2.3 Application to the NOMES Experiment

In the context of the three year NOMES (New England Offshore Mining Environmental Study) project a major field experiment was carried out by NOAA in the Massachusetts Bay (Fig 6-11. The objective of the project was to study the environmental effects of offshore mining for sand and gravel in the coastal zone due mainly to fines discharged back into the water body. On the morning of June 11, 1973, 1000 lbs of fluorescent sphalerite (ZnS) particles (or approximately 2.95×10^5 particles) were introduced near the water surface, about 8 miles east of Boston Harbor. The time of the experiment was such that, although some stratification existed, the thermocline was not as distinct as it becomes later in the summer. The motion of the particles was tracked for more than a week, by means of samples taken throughout the water

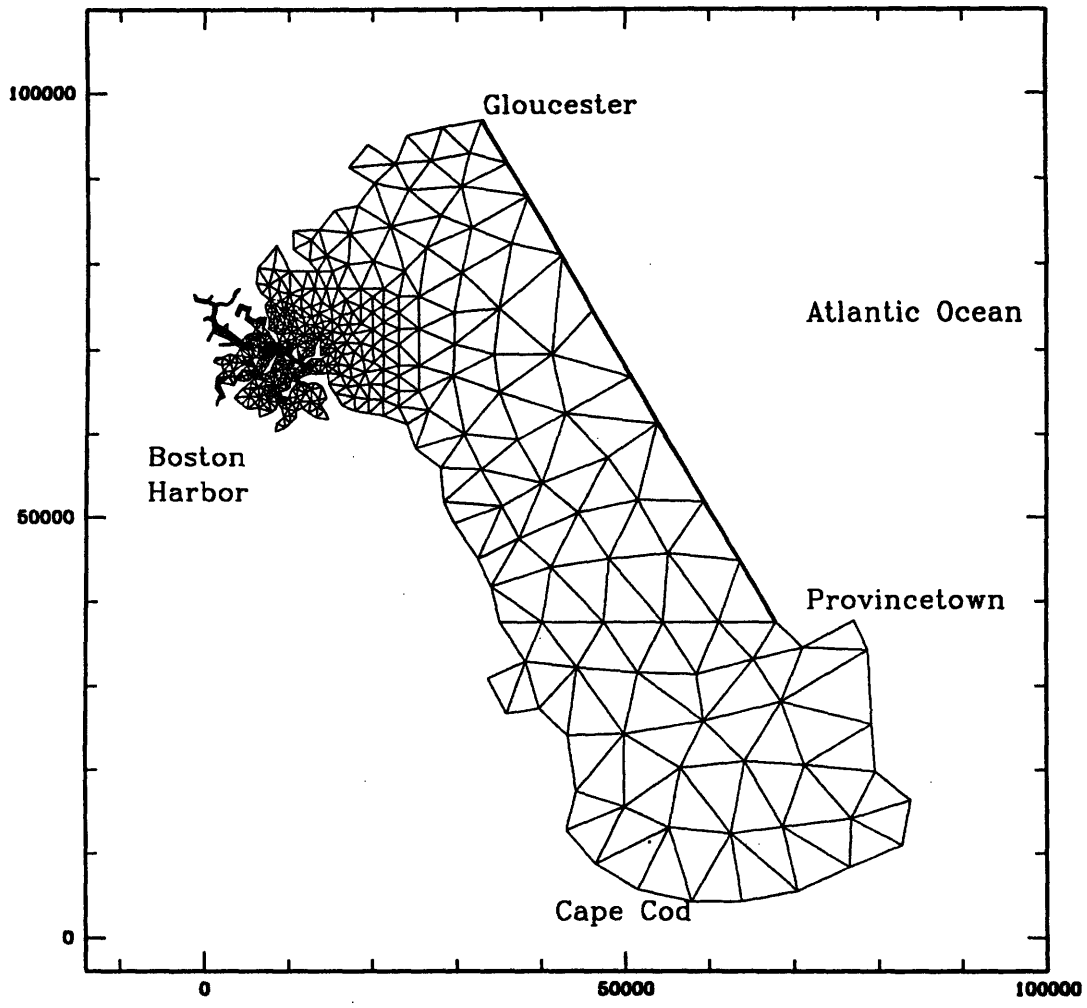

Figure 6-10: Massachusetts Bay Grid (a bold line is used for the open boundary).

column and from the bottom. A number of current meters were installed in several stations in the vicinity of the dump site to obtain current information. The sphalerite data are beleived to be of reasonable quality (Christodoulou et al, 1976).

Velocity Field

Currents in Massachusetts Bay are in large part tidally driven. The tides are primarily semi-diurnal, of the M2 type, with a period of 12.42h. Diurnal variations are also observed but with a much lower amplitude. The average tidal range is of the order of 2.6 meters along the Gloucester-Provincetown line which separates Massachusetts from the Gulf of Maine. In the proposed discharge sites area, the tidal currents are predominantly east-west with a maximum speed of the order of 10cm/s. Much higher velocities occur in some constricted passages such as President Roads and Nantasket Roads, with speeds of up to 60cm/s. Non-tidal currents in Massachusetts Bay have been the subject of several studies summarized by Butman and Fry (1990). Progressive vector plots indicate net drifts of varying direction and amplitude (MDC, 1984).

The hydrodynamic model by Lynch et al (1991) was used in this study to generate the velocity field. It is a linearized, harmonic, finite element, diagnostic, 3-D shallow water equation model with conventional hydrostatic and Boussinesq assumptions and eddy viscosity closure in the vertical. It uses the 2-D/1-D/3-D approach, i.e. the same technique as in 2D/1D models described in Section 2.5.1 is used with the additional solution of the 3D continuity equation in order to compute the vertical velocity.

The advantages of this model is that it is relatively simple (and thus useful for testing over 3-D TM), it uses finite elements and accepts baroclinic pressure gradients. Obviously, disandvantages arise from the fact that it is linear and so makes a number of approximations in solving the governing equations. For example due to the fact that the vertical velocity w is solved by using the continuity equation only the kinematic boundary condition at the free interface (Eq. 2.55) is not satisfied. According to Eq.

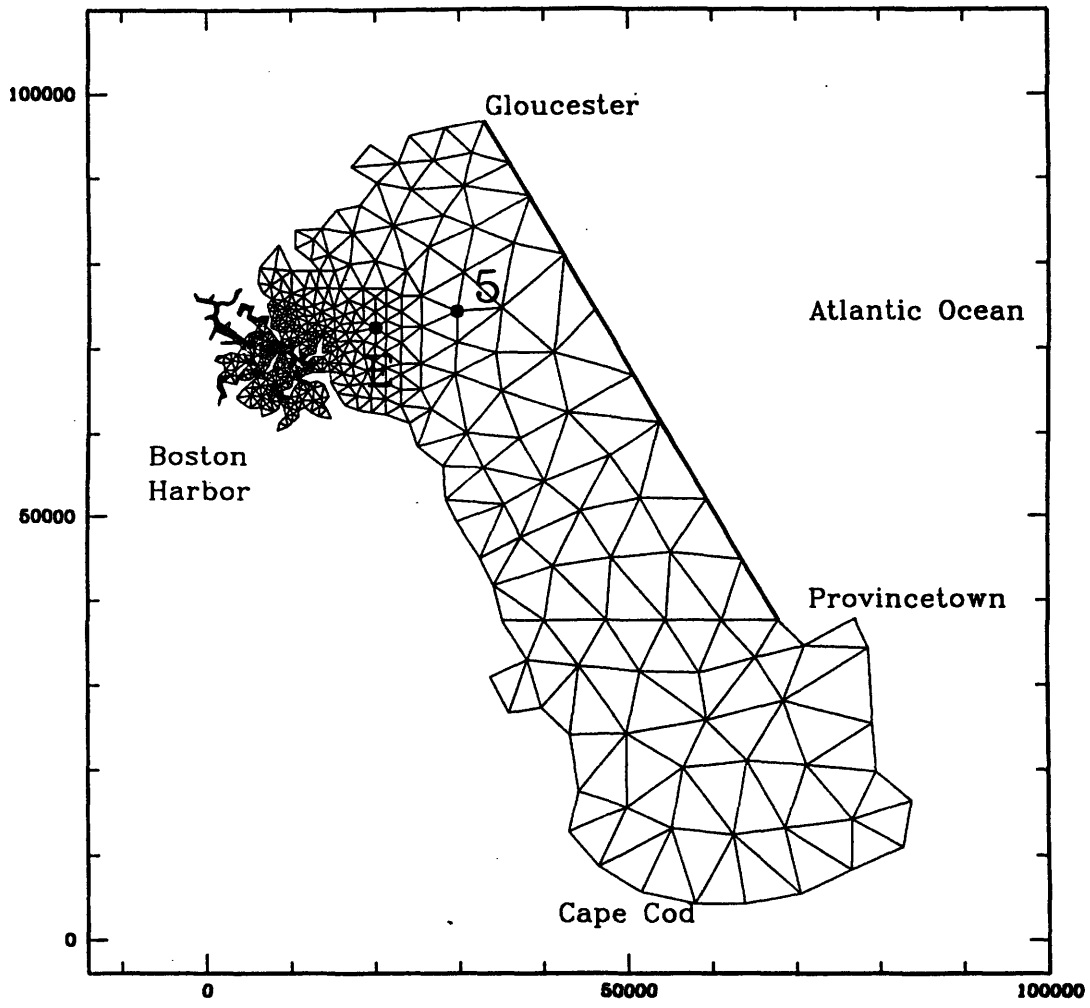

Figure 6-11: NOMES experiment. The discharge point (E) and Station 5 are depicted.

Table 6.1: Amplitude and lags of M2 components of water level measurements

	Gloucester	Provincetown
amplitude (m)	1.258	1.311
phase lag (min)	10.6	0.

2.55 the boundary condition at $z = \eta(x, y)$ is

$$W = U\frac{\partial \eta}{\partial x} + V\frac{\partial \eta}{\partial y} + \frac{\partial \eta}{\partial t} \tag{6.9}$$

Since the spacial gradients of the surface elevation are small compared to the other terms the vertical velocity at the surface is

$$w \approx \frac{\partial \eta}{\partial t} \tag{6.10}$$

Fig 6-12 shows how w and $\frac{\partial \eta}{\partial t}$ vary over one tidal period at locations close to the discharge point. We clearly see that the surface boundary condition is not satisfied. This causes severe mass conservation errors when mass is located close to the surface. In order to overcome this difficulty the particle mode was used throughout the calculations.

Two forcing constituents were superimposed:

- The semi-diurnal tidal constituent M2 with a period of 12.4 hrs. Table 6.1 (EPA, 1988) lists the amplitude and phase lags of Gloucester and Provincetown tides at the M2 frequency. Fig 6-13 - Fig 6-16 show the resulting velocity field at high tide at the bottom, middepth and surface.

- A steady baroclinic flow field generated by an elevation difference of 20cm at the open boundary is used . Field data have indeed shown the existence of this steady component. Fig 6-17 shows the resulting velocity field at middepth in the vicinity of the outfall.

The boundary conditions at the surface and bottom are given by:

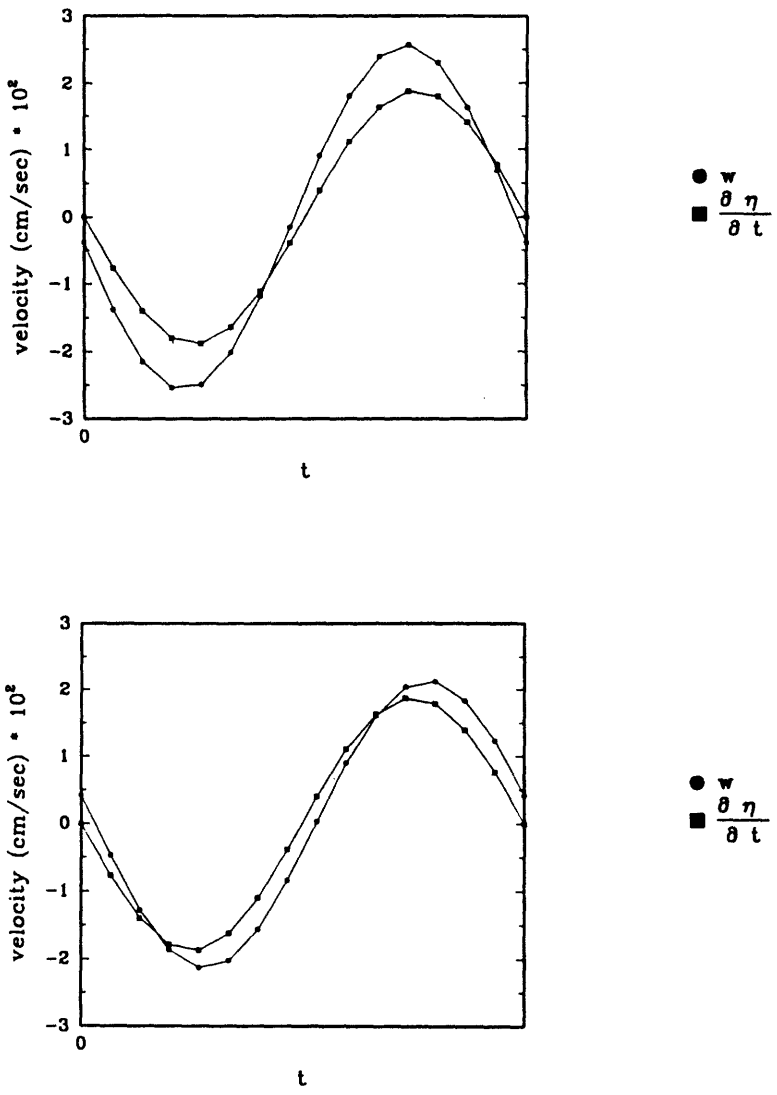

Figure 6-12: Variation of w and $\frac{\partial \eta}{\partial t}$ over a tidal period

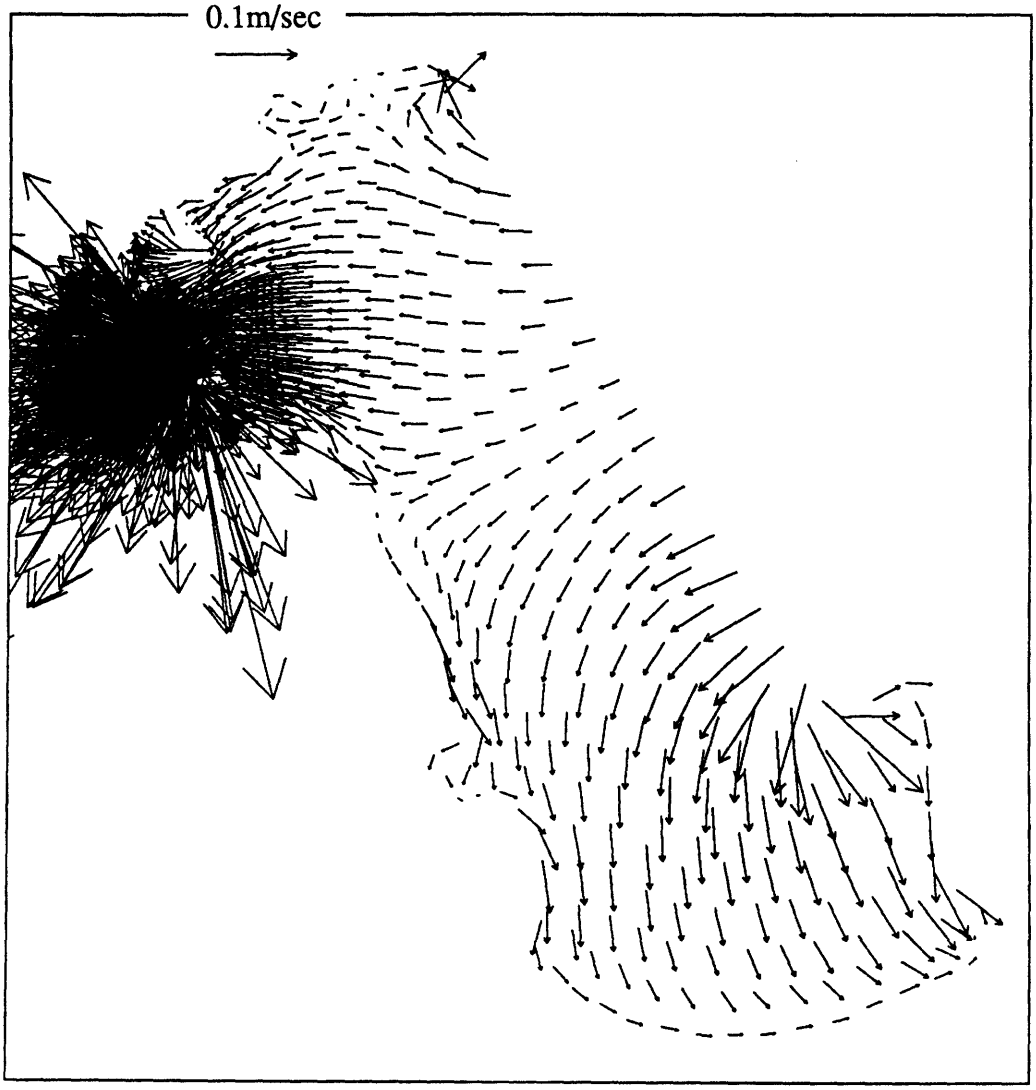

Figure 6-13: Tidally-driven flow field (bottom).

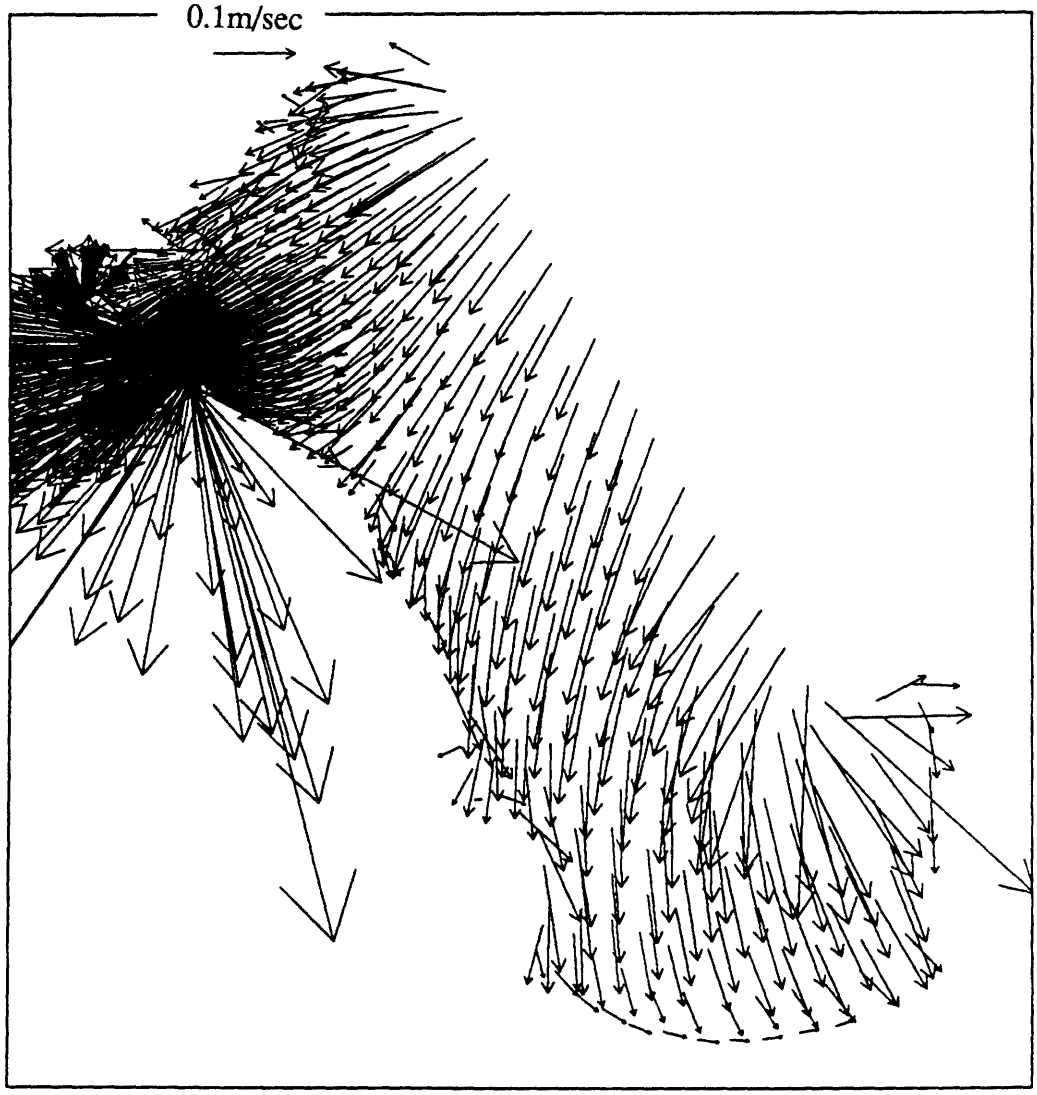

Figure 6-14: Tidally-driven flow field (z = -10m middepth).

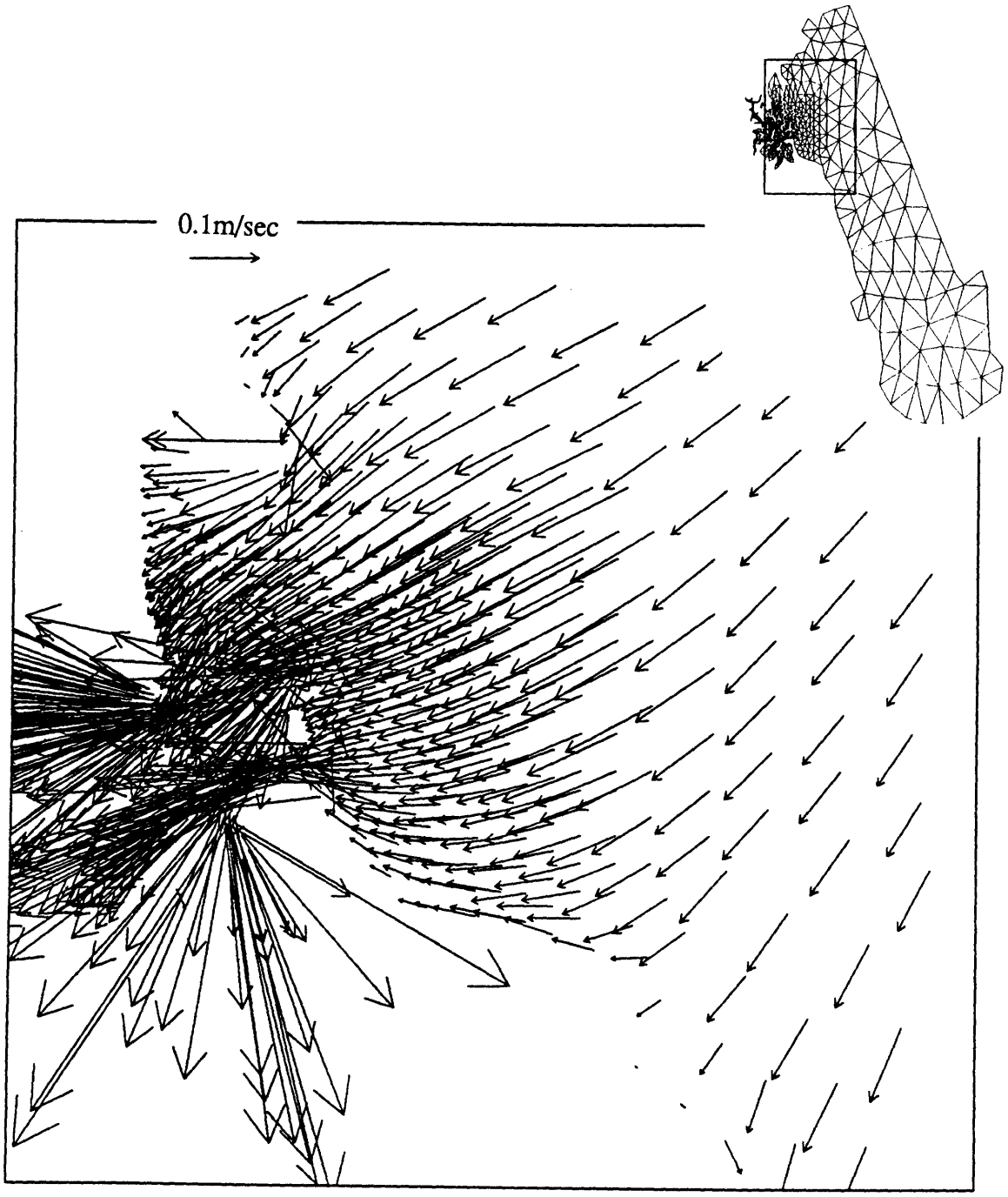

Figure 6-15: Tidally-driven flow field at the vicinity of the outfall (z = -10m mid-depth).

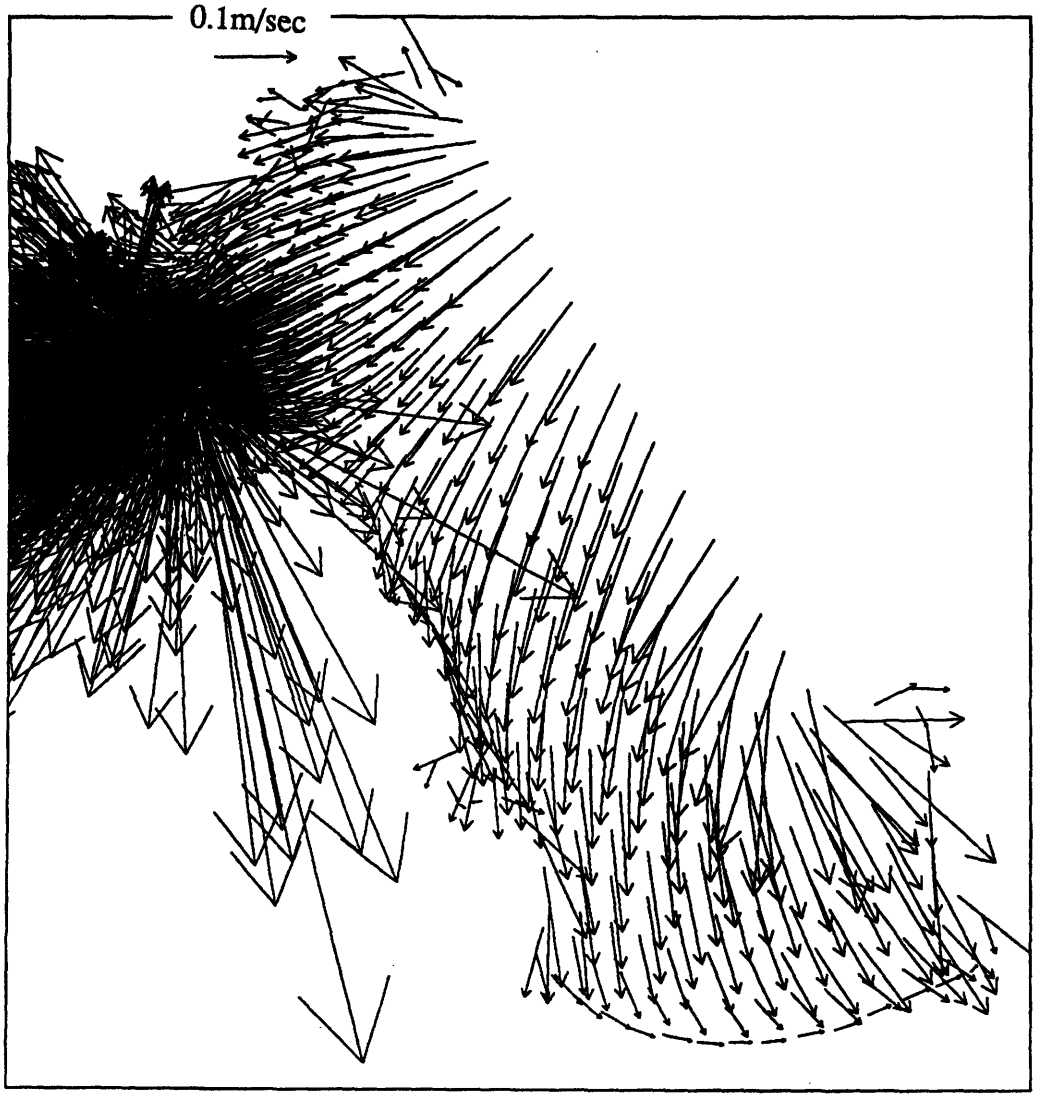

Figure 6-16: Tidally-driven flow field (surface).

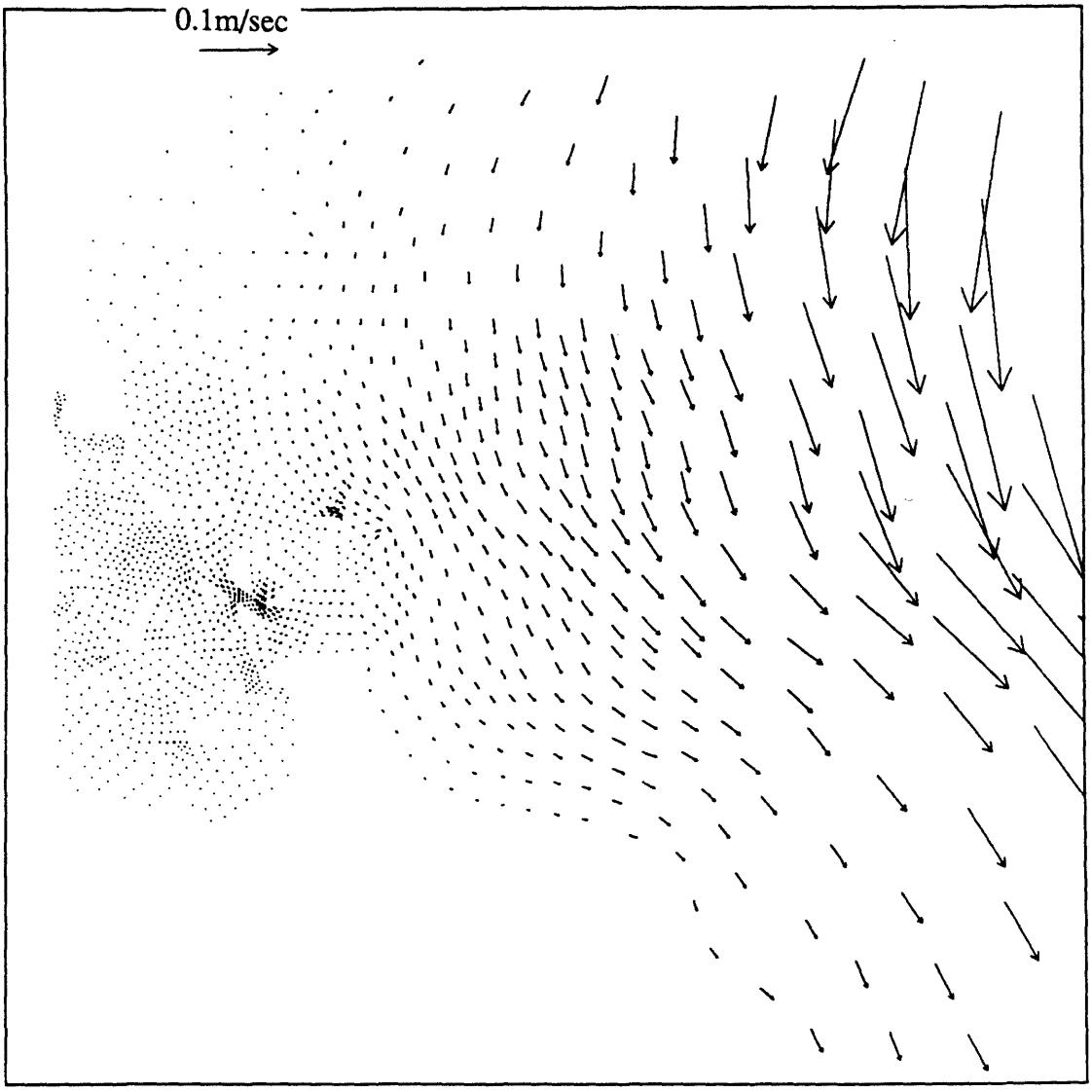

Figure 6-17: Steady baroclinic flow field at the vicinity of the outfall (z = -10m middepth).

$$N\frac{\partial \mathbf{V}}{\partial z} = h\Psi \tag{6.11}$$

$$N\frac{\partial \mathbf{V}}{\partial z} = k\mathbf{V} \tag{6.12}$$

where

$\mathbf{V}$ is the horizontal velocity

$N(x, y, z)$ is the vertical diffusivity

$h\Psi(x, y)$ is the atmospheric forcing

k is the linear bottom stress coefficient

In this study $\Psi = 0$ was set (i.e., no wind). A uniform value of $N = 0.02\frac{m^2}{sec}$ over the domain was used based on the value used by Lynch et al (1991) in the Gulf of Maine study. A sensitivity analysis for N shows that the flow field is very sensitive to the value of N (Fig 6-18 - Fig 6-19) A sensitivity analysis for k shows that only the bottom velocity is sensitive to the value of k. Fig 6-20 shows vertical profiles of the horizontal velocities at the location of the outfall for $k = 0.5\frac{m}{sec}$ and $k = 0.005\frac{m}{sec}$. The value of $k = 0.05\frac{m}{sec}$ was used.

A comparison of simulated horizontal velocities at current meter station 5 with actual measurements are presented in Fig 6-21 and Fig 6-22. The general features seem in reasonable agreement.

Diffusivities

A general way of expressing eddy diffusivities (Csanady, 1973) is

$$K = \tilde{U}L \tag{6.13}$$

where

$\tilde{U}$ is the r.m.s. turbulent velocity fluctuation

L is the (horizontal) length scale of turbulence

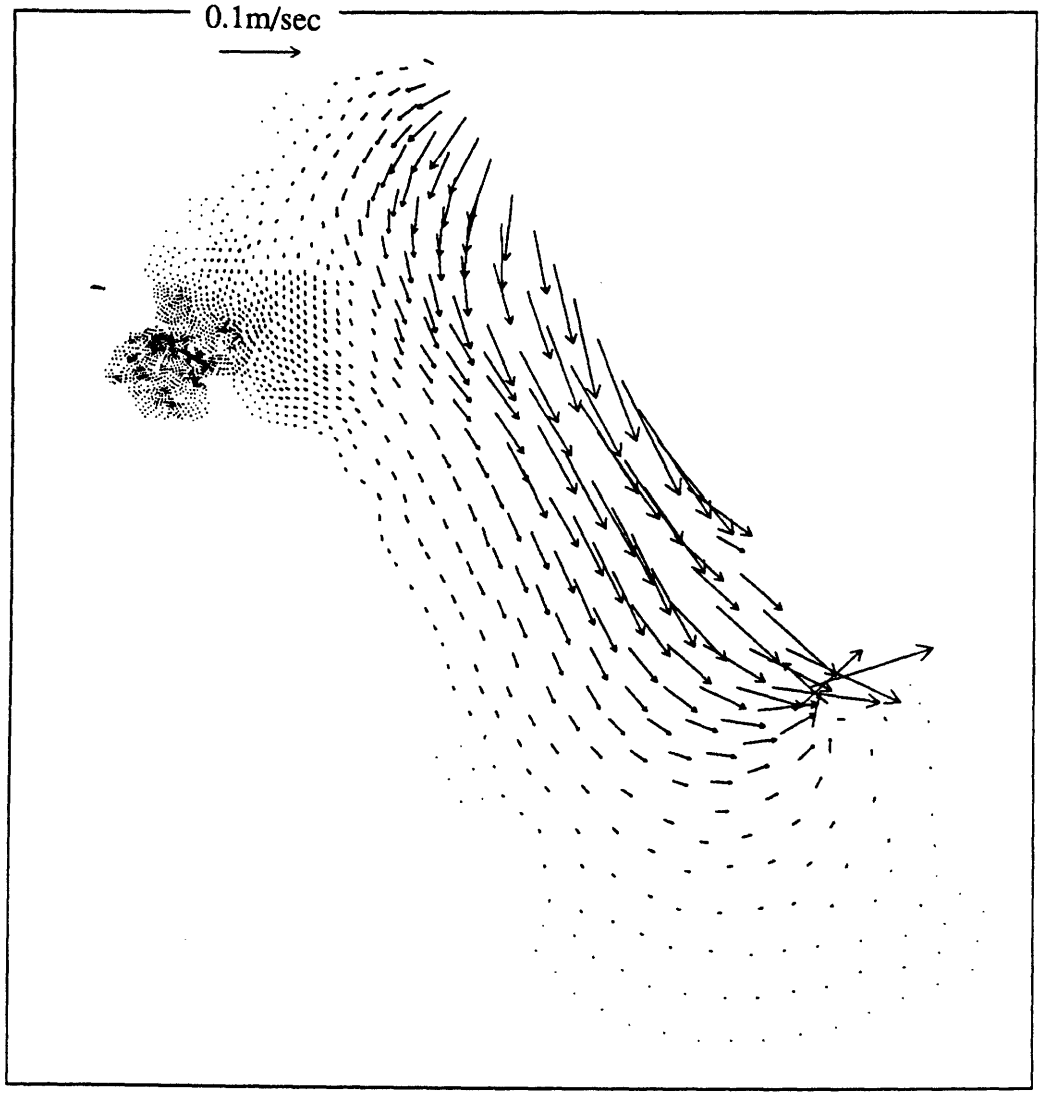

Figure 6-18: Steady baroclinic flow field (middepth) for $N = 0.2$.

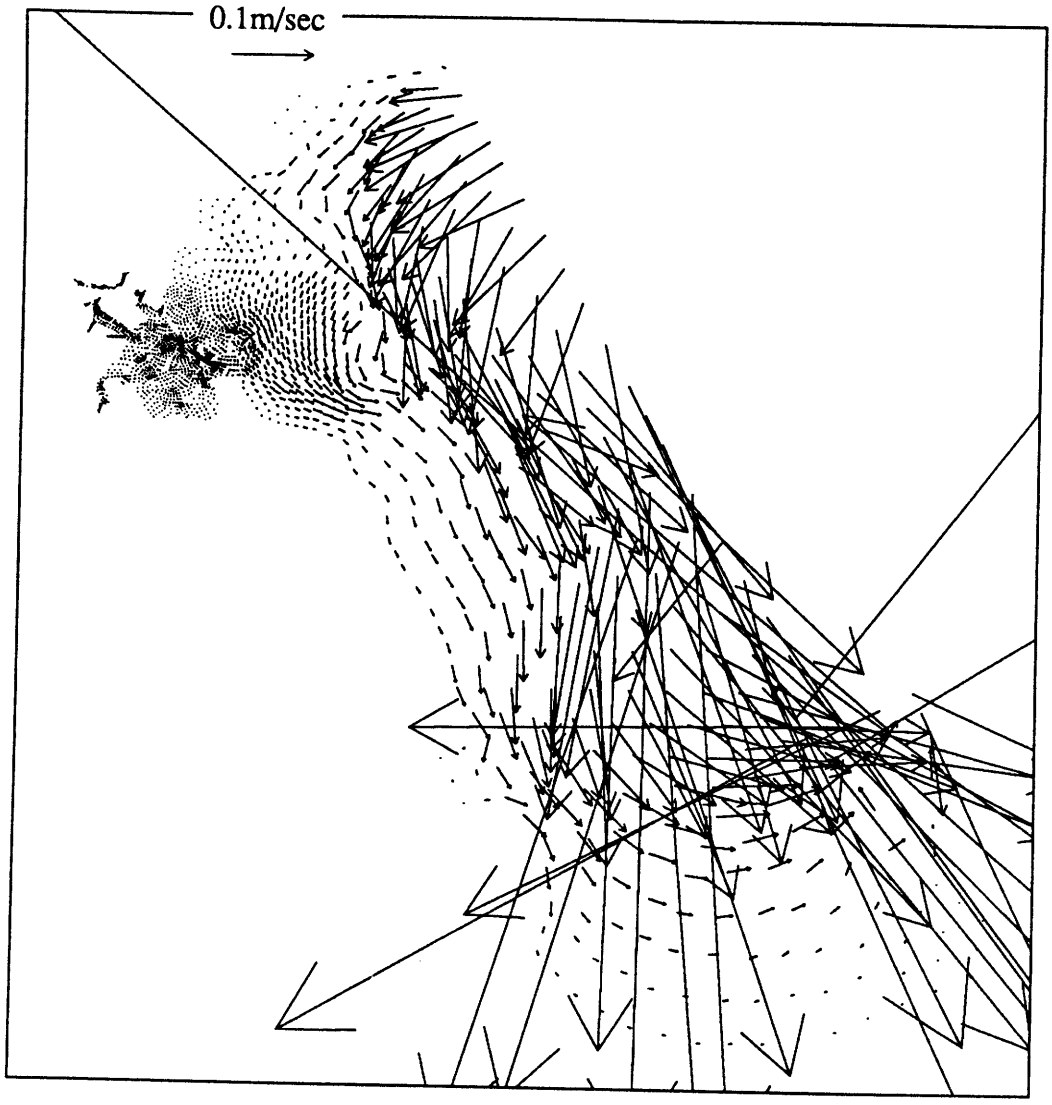

Figure 6-19: Steady baroclinic flow field (middepth) for $N = 0.002$.

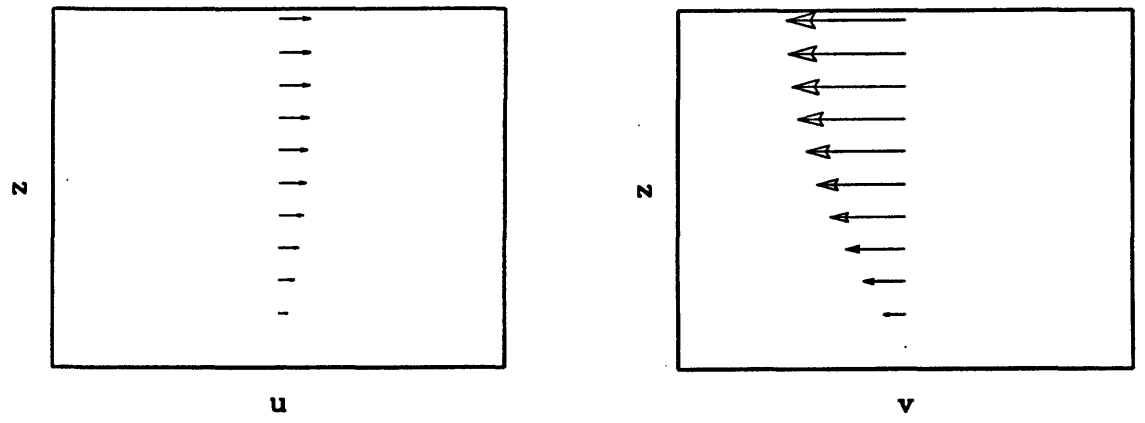

(a)

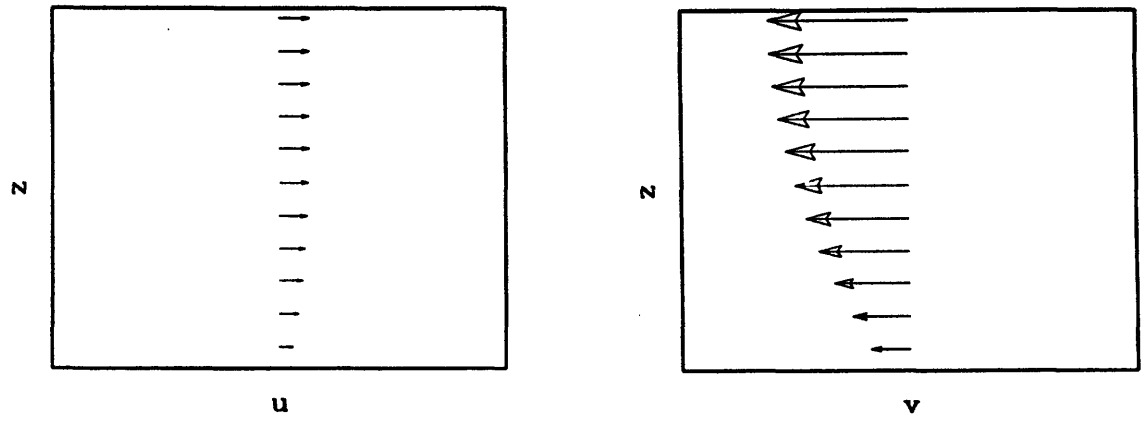

(b)

Figure 6-20: Steady baroclinic flow field (vertical profile of horizontal velocities) for $N = 0.02$. (a) $k = 0.5$, (b) $k = 0.005$

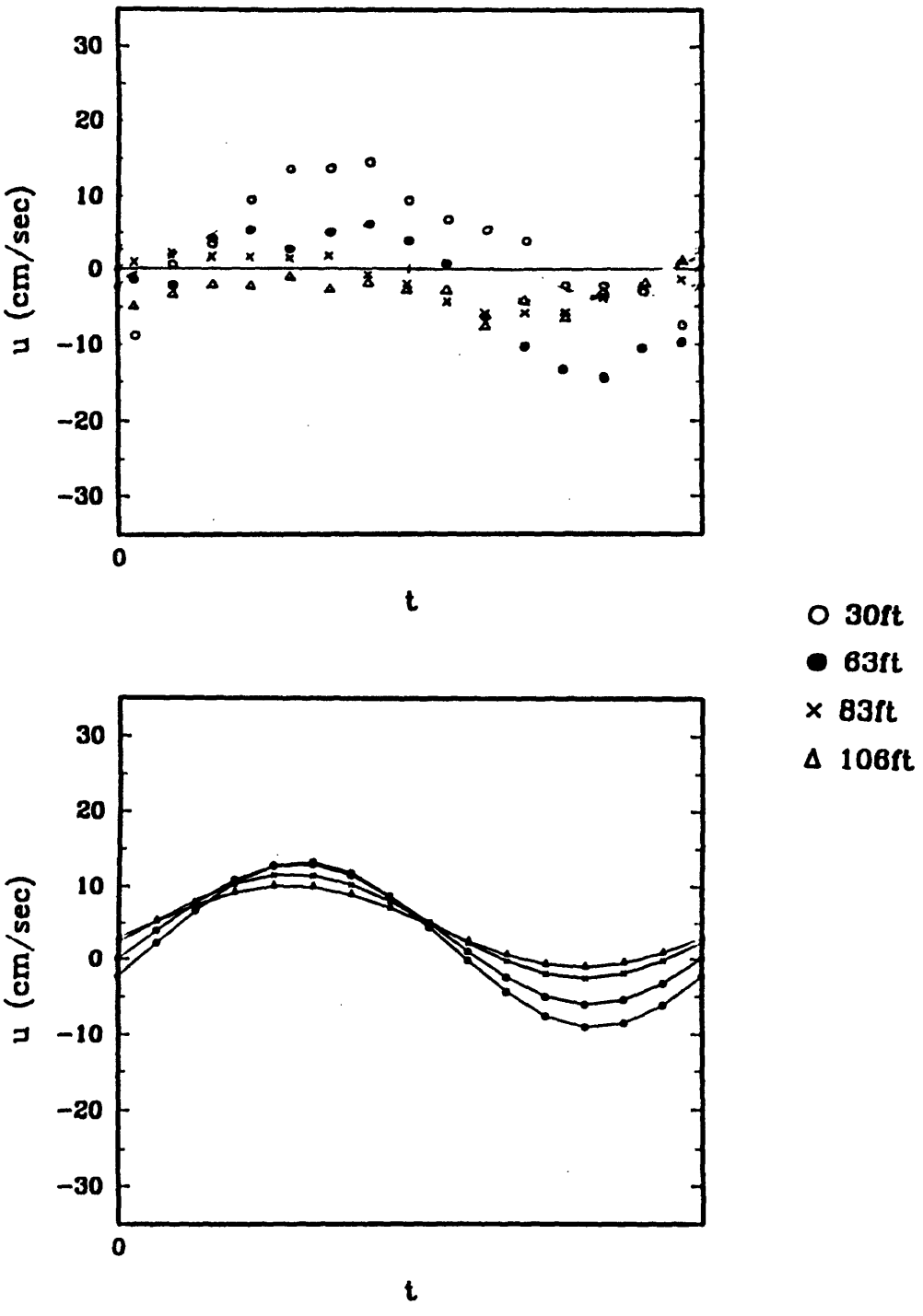

Figure 6-21: Current data at station 5 and HM results for u velocity.

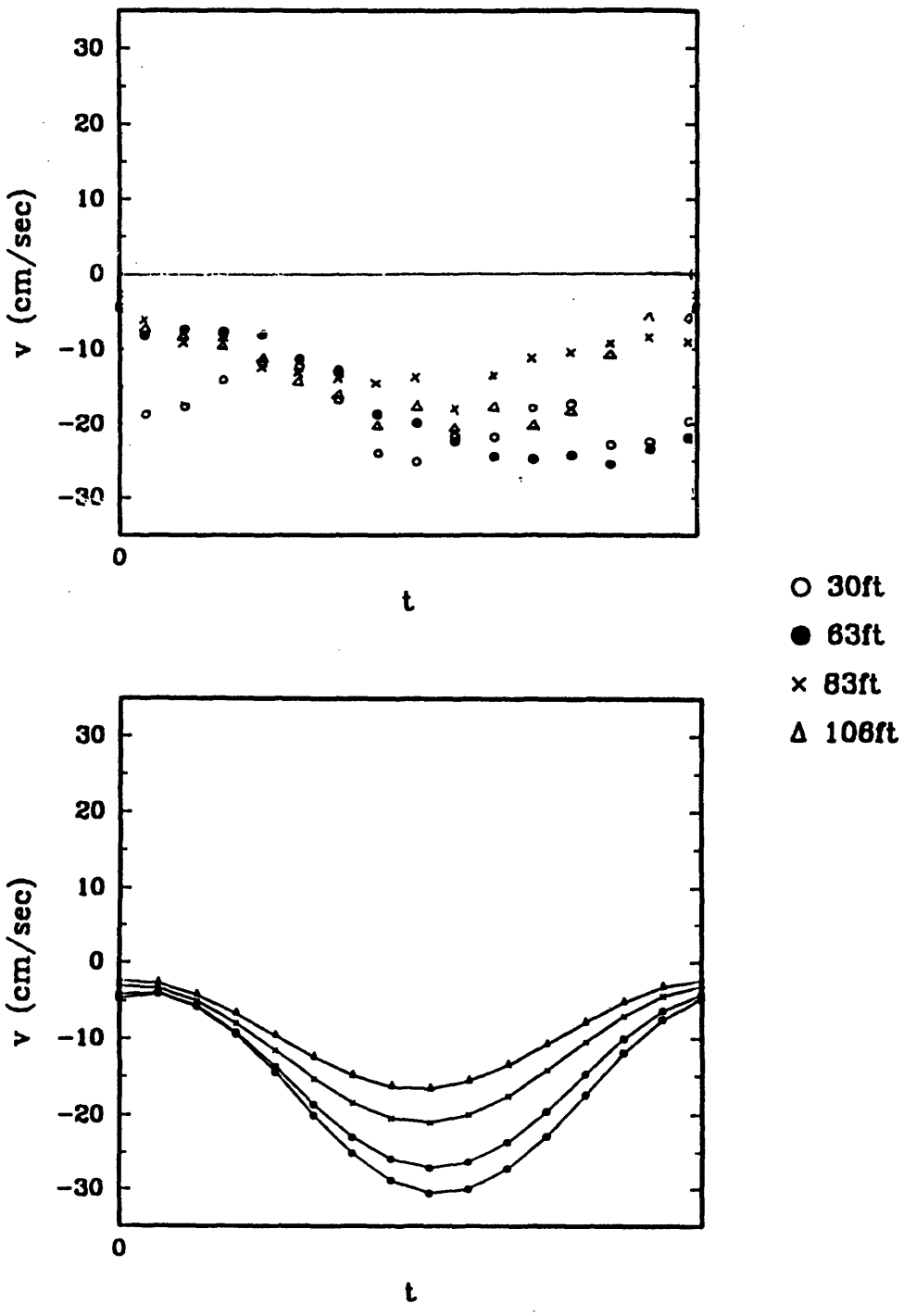

Figure 6-22: Current data at station 5 and HM results for v velocity.

The concept of the length scale of turbulence is not precisely defined. Various investigations (Vreugdenhil, 1975) carried out in boundary layer flows show that far from the wall the length scale tends to an asymptotic value of 0.08 to 0.10 of the pipe radius or the channel depth, which equals an order of magnitude smaller than the size of the biggest eddy. Using the same concept in coastal waters one may argue that L is an order of magnitude smaller than the typical grid size Δ (Deardorff, 1971), i.e.

$$L = c\Delta \tag{6.14}$$

where c is a numerical constant with a value ranging from 0.2 for isotropic turbulence to 0.1 in shear flows. $\tilde{U}$ can be estimated by using such values as ten percent of the local velocity. Taking representative values for Massachusetts Bay of $tildeU = 0.10 \times 0.10m/s = 0.01m/s$ and $L = 0.2 \times 1000m = 200m$ we get $K_x = K_y = 2m^2/s$. The vertical diffusion coefficient $K_z = 0.00001m^2/s$ which is a representative value (Fig 6-23) for the degree of stratification (Koh and Fan, 1970).

Simulations

Experimental data at days 2, 3 and 7 are shown in Fig 6-24 - Fig 6-26. Simulation results for 2, 3 and 7 days after the introduction of particles are shown in Fig 6-27 - Fig 6-34. The results at days 2 and 3 show good agreement with the field data. The simulation results at day 7 differ significantly from the field data. This may be due to the fact that a higher horizontal diffusion coefficient must be used far from the discharge point, where the grid scale is an order of magnitude higher than the grid scale in the vicinity of the source. The subgrid eddy diffusivity was scaled according to the grid scale in the vicinity of the source. The disparity between the field data and the simulations may also be due to the fact, that the velocity field is not well represented due to the diagnostic character of the hydridynamic model.

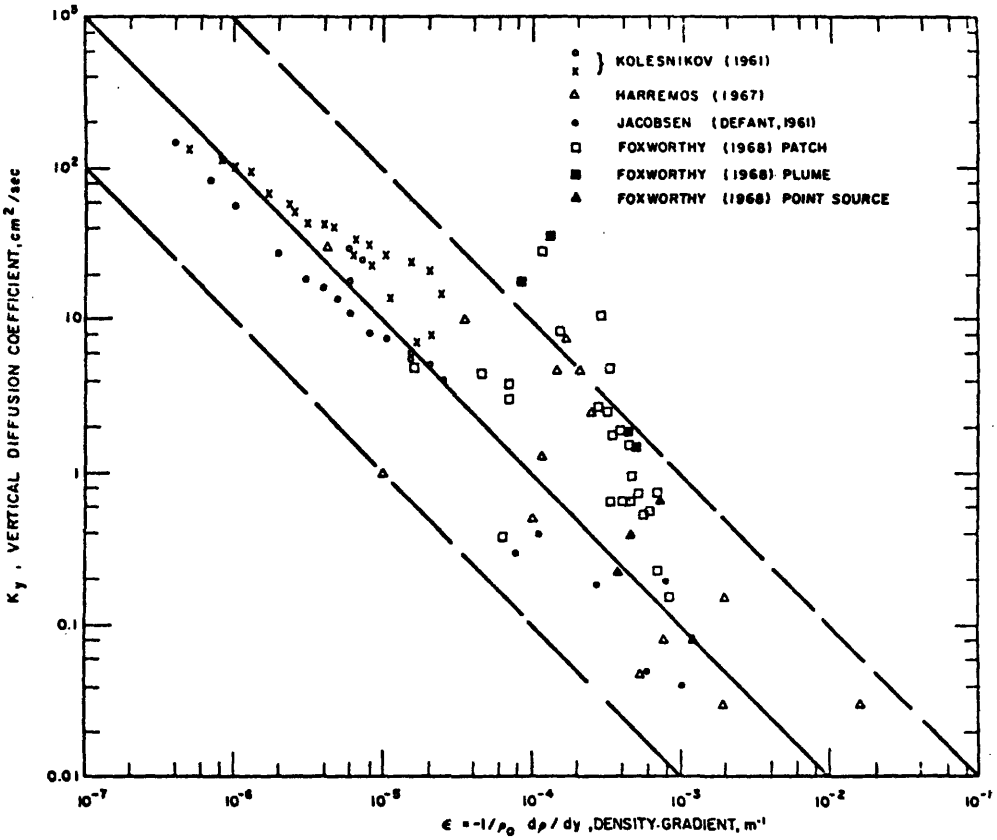

Figure 6-23: Correlation of vertical diffusion coefficient with density gradient

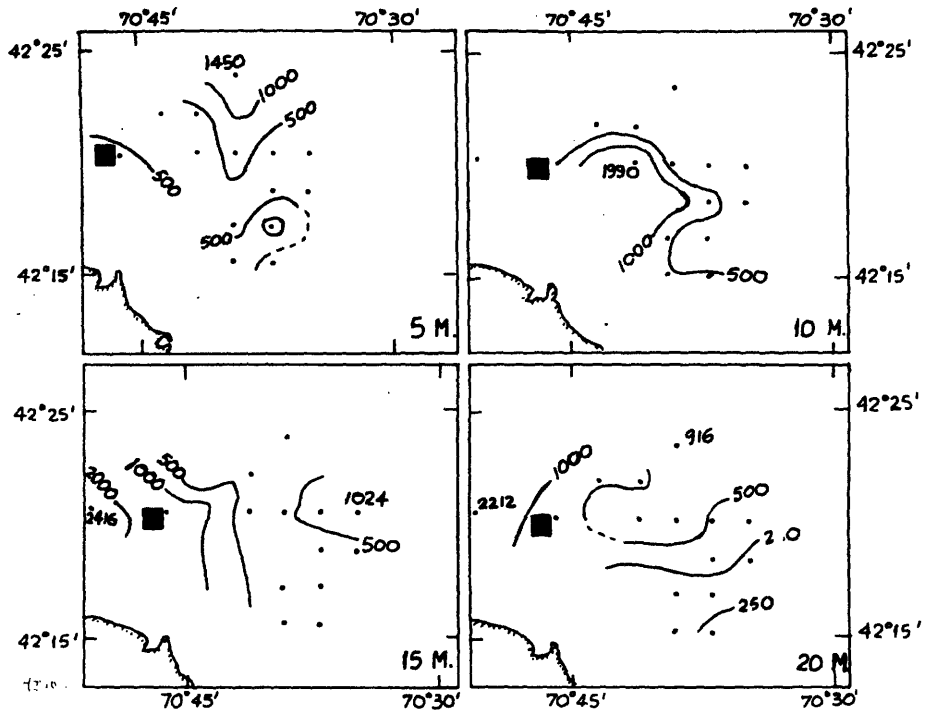

Figure 6-24: Experimental data at Day 2. Concentration contours of ZnS particles/ lt.

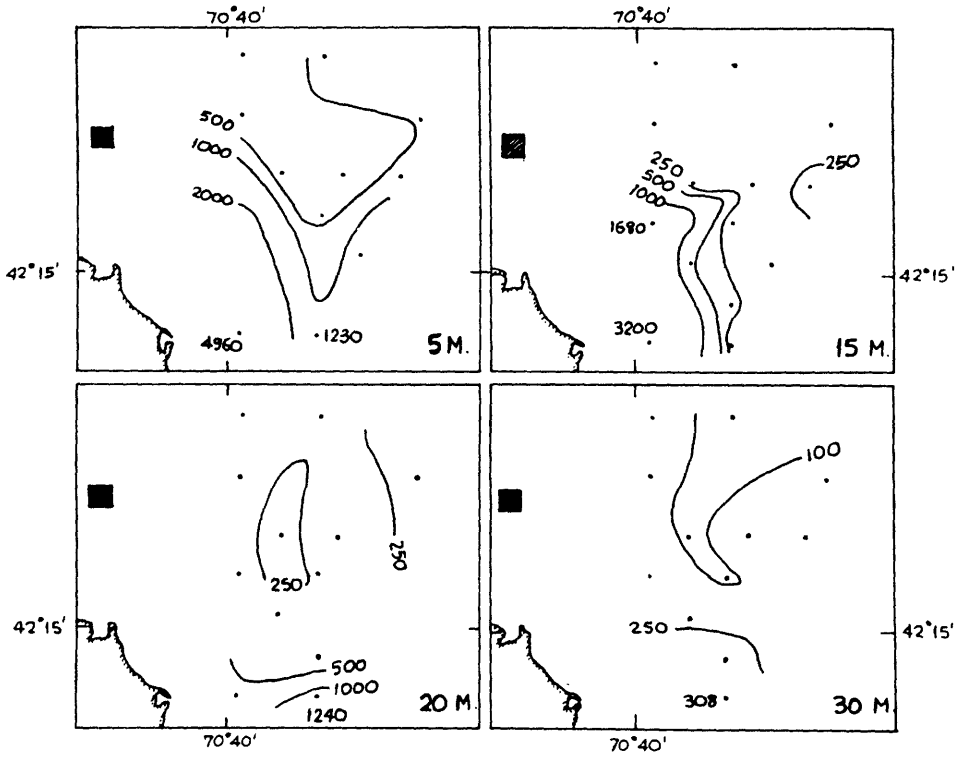

Figure 6-25: Experimental data at Day 3. Concentration contours of ZnS particles/ lt.

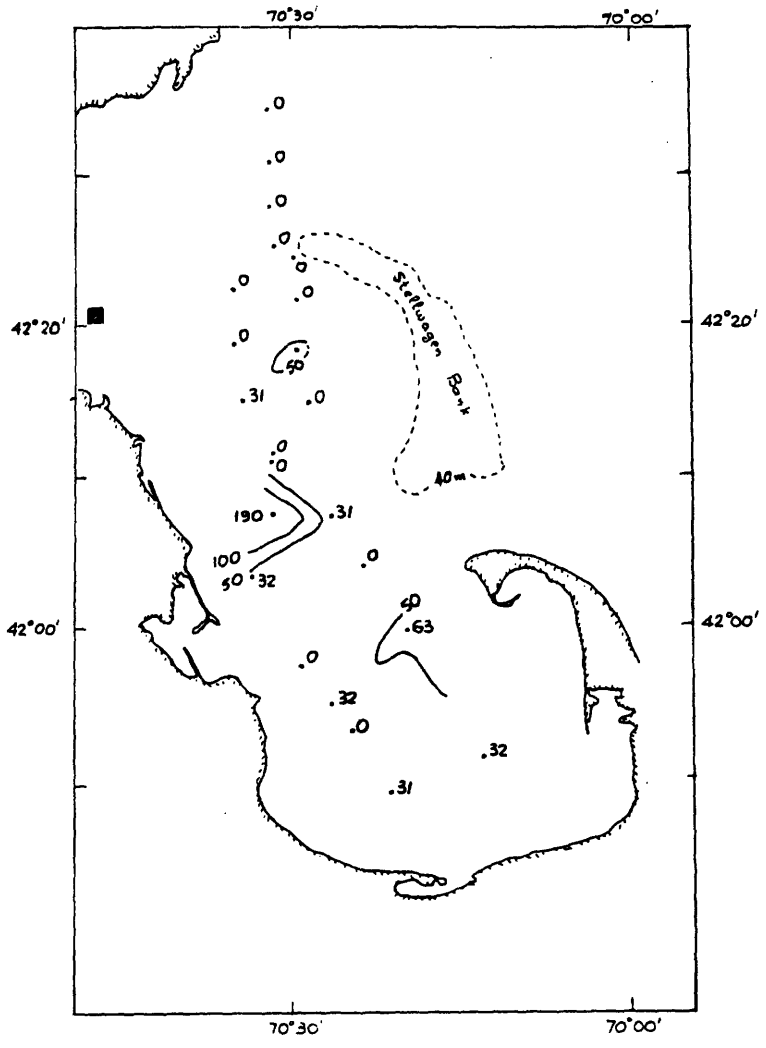

Figure 6-26: Experimental data at Day 7. Concentration contours of ZnS particles/ lt.

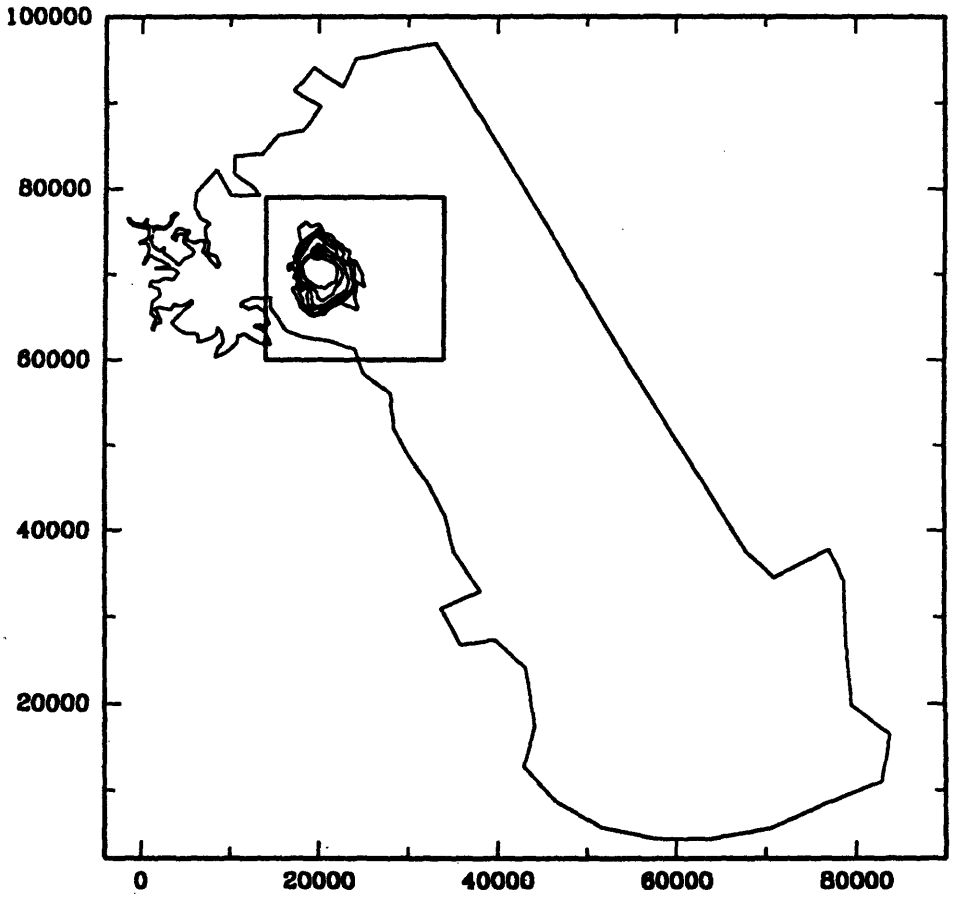

Figure 6-27: Simulation data at Day 2. Depth = -5m. Concentration contours of 10000, 5000, 2000, 1000, 500. and 250 ZnS particles/ lt.

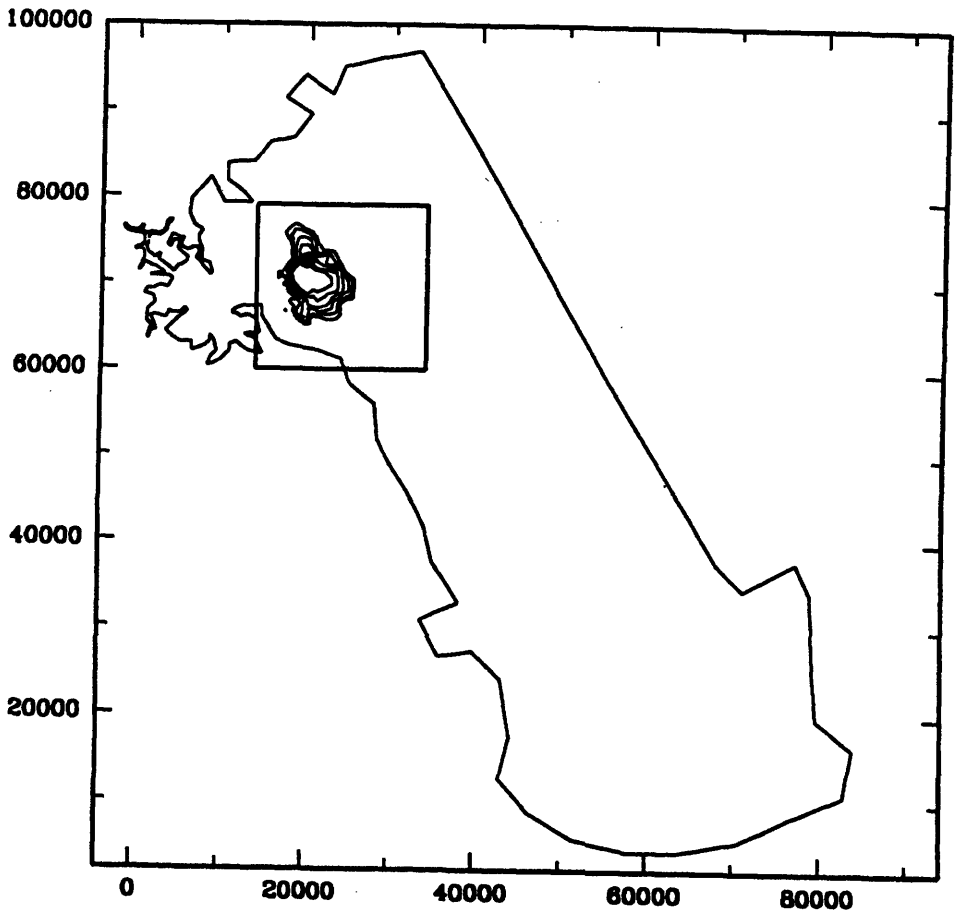

Figure 6-28: Simulation data at Day 2. Depth = -10m. Concentration contours of 10000, 5000, 2000, 1000, 500. and 250 ZnS particles/ lt.

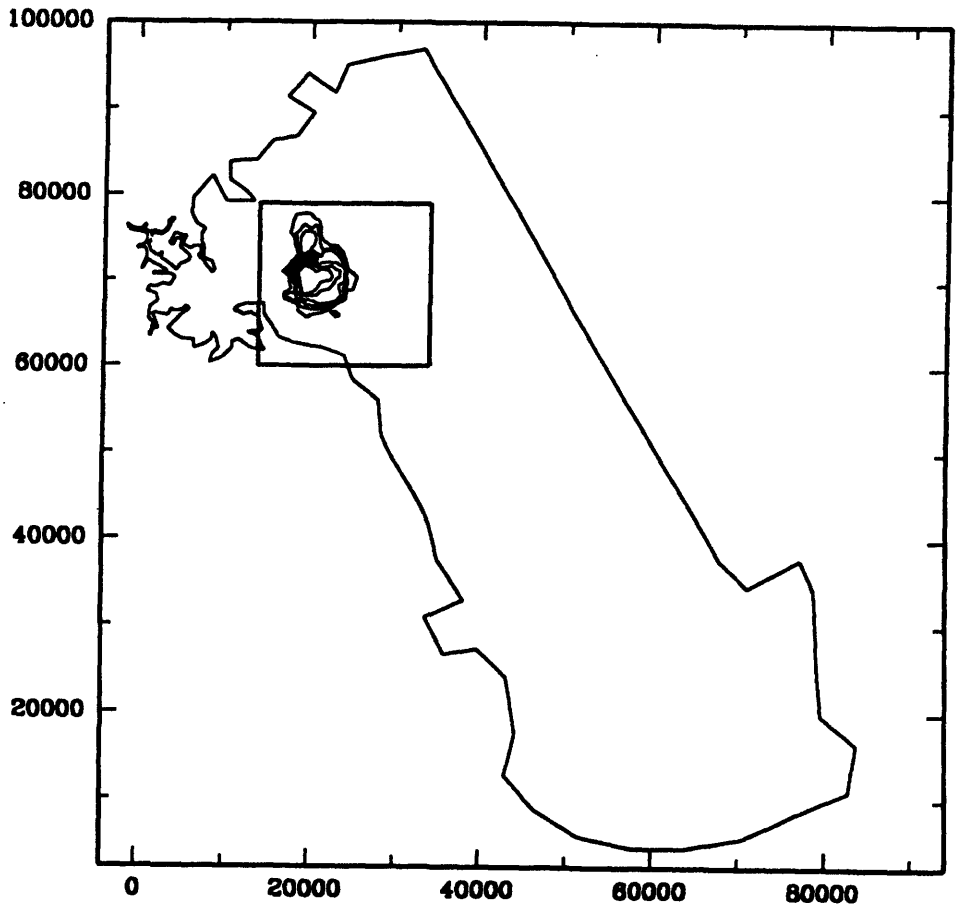

Figure 6-29: Simulation data at Day 2. Depth = -15m. Concentration contours of 10000, 5000, 2000, 1000, 500. and 250 ZnS particles/ lt.

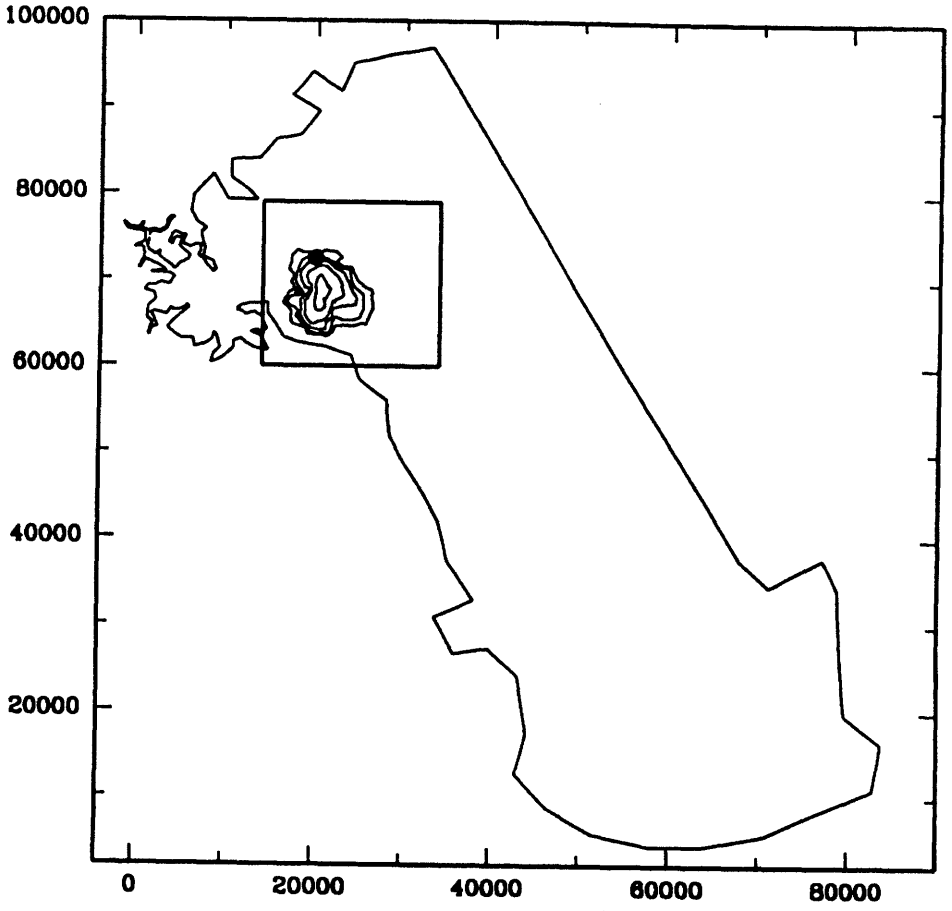

Figure 6-30: Simulation data at Day 3. Depth = -5m. Concentration contours of 5000, 2000, 1000, 500. and 250 ZnS particles/ lt.

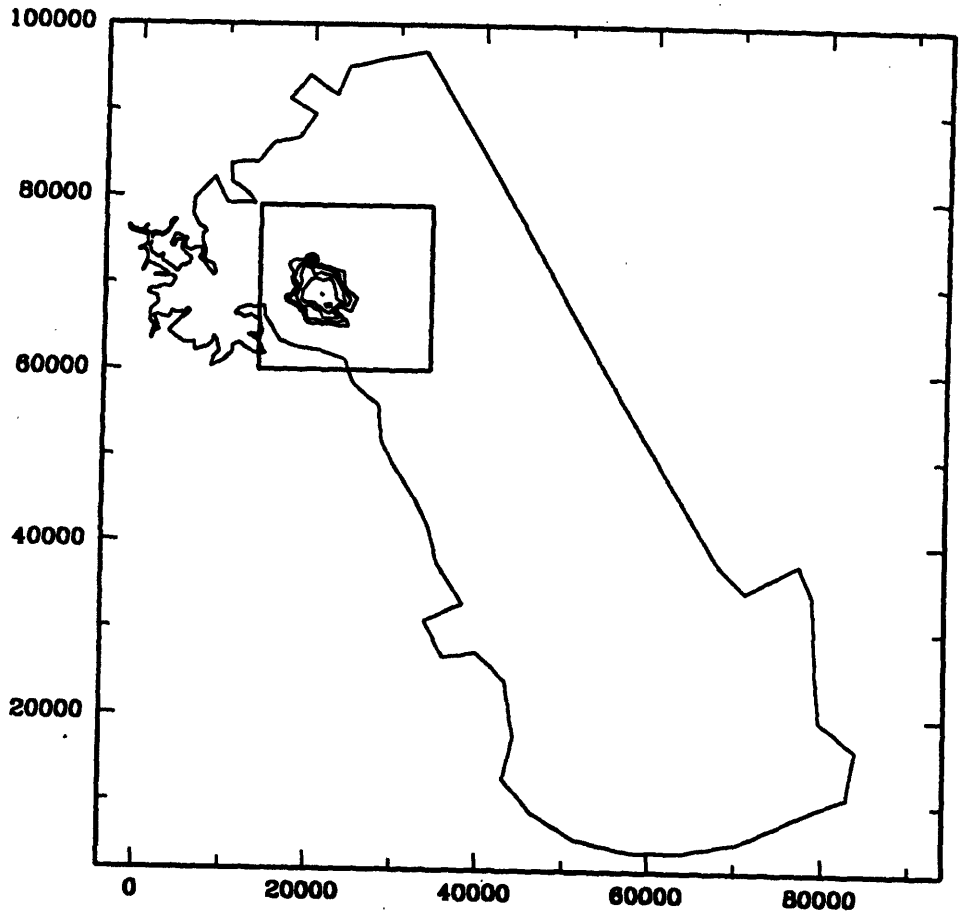

Figure 6-31: Simulation data at Day 3. Depth = -15m. Concentration contours of 5000, 2000, 1000, 500. and 250 ZnS particles/ lt.

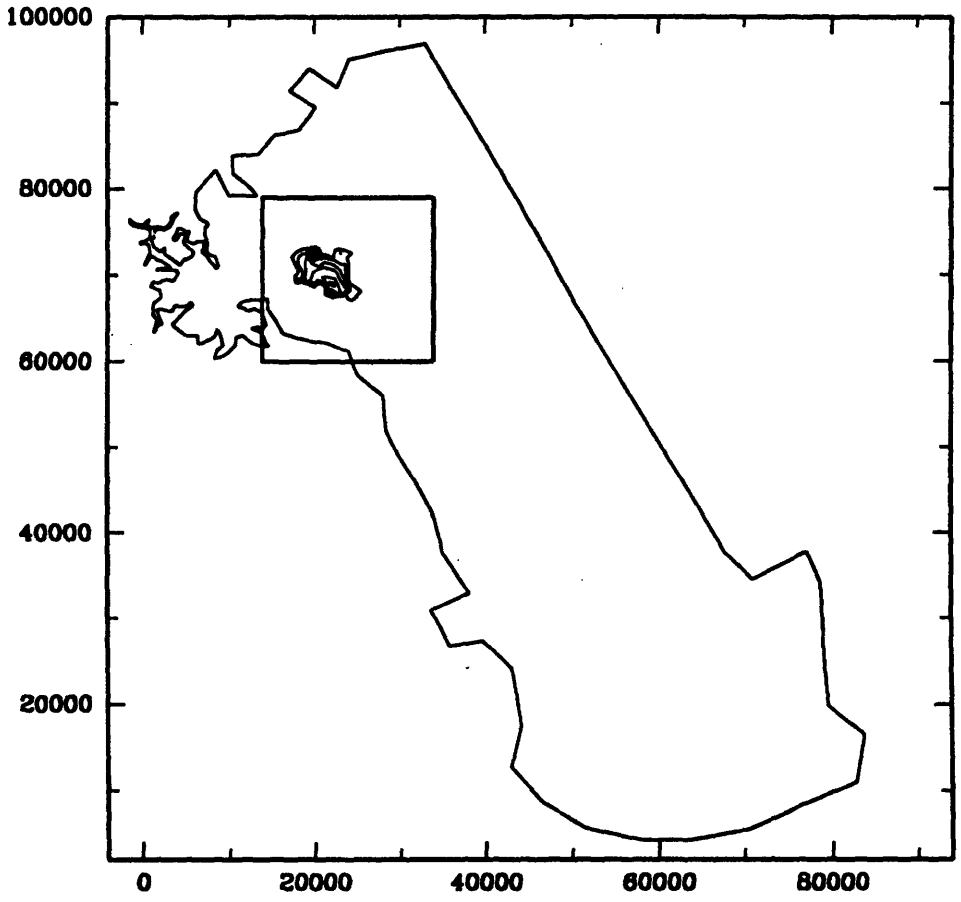

Figure 6-32: Simulation data at Day 3. Depth = -20m. Concentration contours of 2000, 1000, 500. and 250 ZnS particles/ lt.

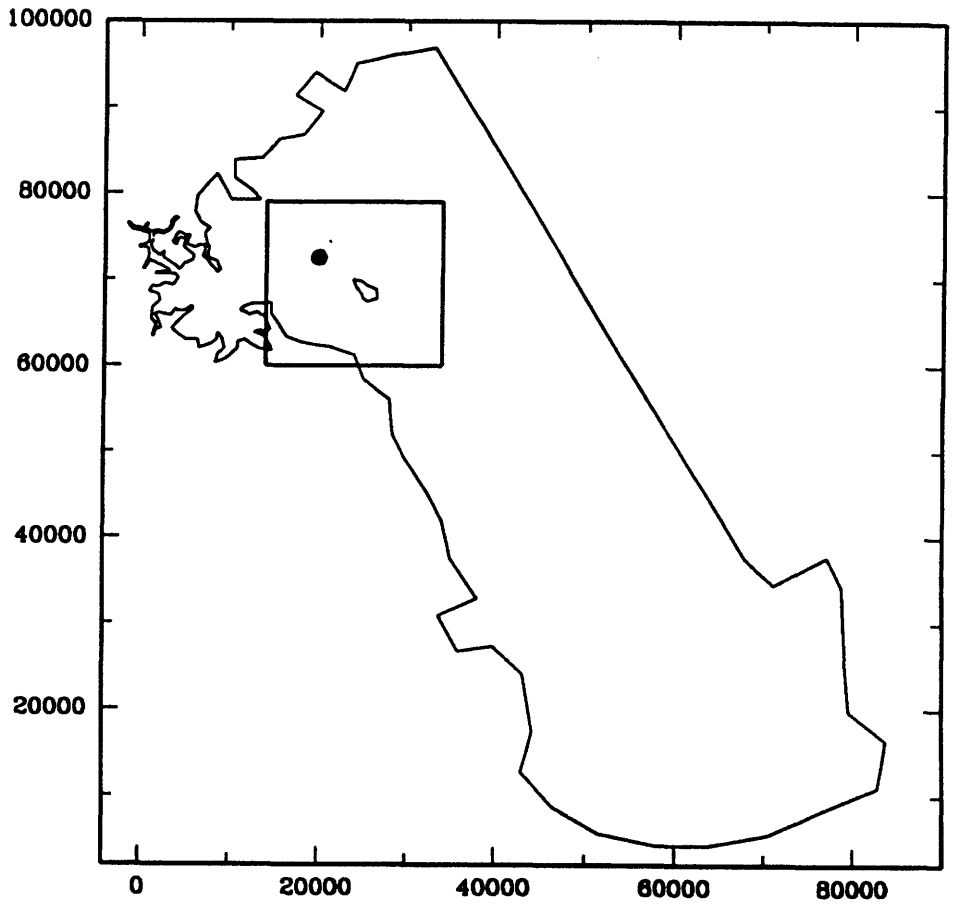

Figure 6-33: Simulation data at Day 3. Depth = -30m. Concentration contours of 250 ZnS particles/ lt.

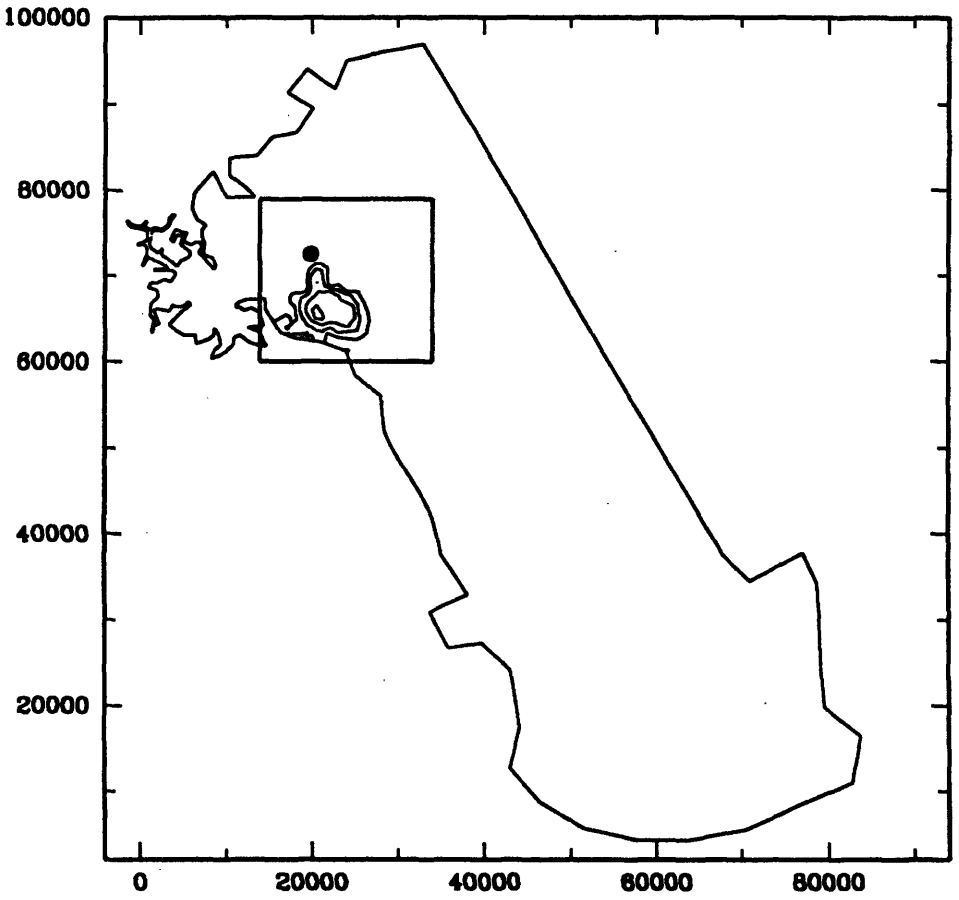

Figure 6-34: Simulation data at Day 7. Depth = -2m. Concentration contours of 2000, 1000, 500 and 250 ZnS particles/ lt.

6.2.4 Demonstration - Application in Massachusetts Bay

Velocity field

The following two components were added to the velocity field generated for the NOMES Experiment (Section 6.2.3):

- The steady state constituent due to the density differences between the well mixed region close to the diffuser (near flow field) and the ambient stratified fluid (Section 6.1). Fig 6-35 shows the resulting velocity field at middepth.
- A vertical steady state velocity component representing the settling velocity of the most slowly settling particles. The reason for this component is explained later.

The maximum current in the vicinity of the outfall is of the order of $0.05m/s$. This results in $F = \frac{u^3}{b} \simeq 0.5$ on Fig 6-2 and so the orientation of the current to the diffuser does not significantly affect S_{in} and z_{tr}. This allows the user to calculate the intermediate flow field only once.

Source Location and Loading

Identifying the sources of fine-grained sediments is not an easy task because they include municipal and industrial wastes, riverine discharge, and open ocean inflow from Mass Bay. Lee (1990) in his 2-D study on contaminated sediment transport in Boston Harbor selected as sources 1) the two existing wastewater treatment plants which contribute fine-grained sediments through sludge disposal and effluent discharges 2) combined sewer overflows 3) dry weather overflow 4) stormwater runoff and 5) direct surface deposition. Since the purpose of this study is to demonstrate the abilities of the developed model only one source is used. The location of this source is chosen to be in the vicinity of one of the proposed locations of the new outfall (Fig 6-36). The discharge rate of $25m^3/sec$ is selected with a loading of TSS of $72mg/l$.

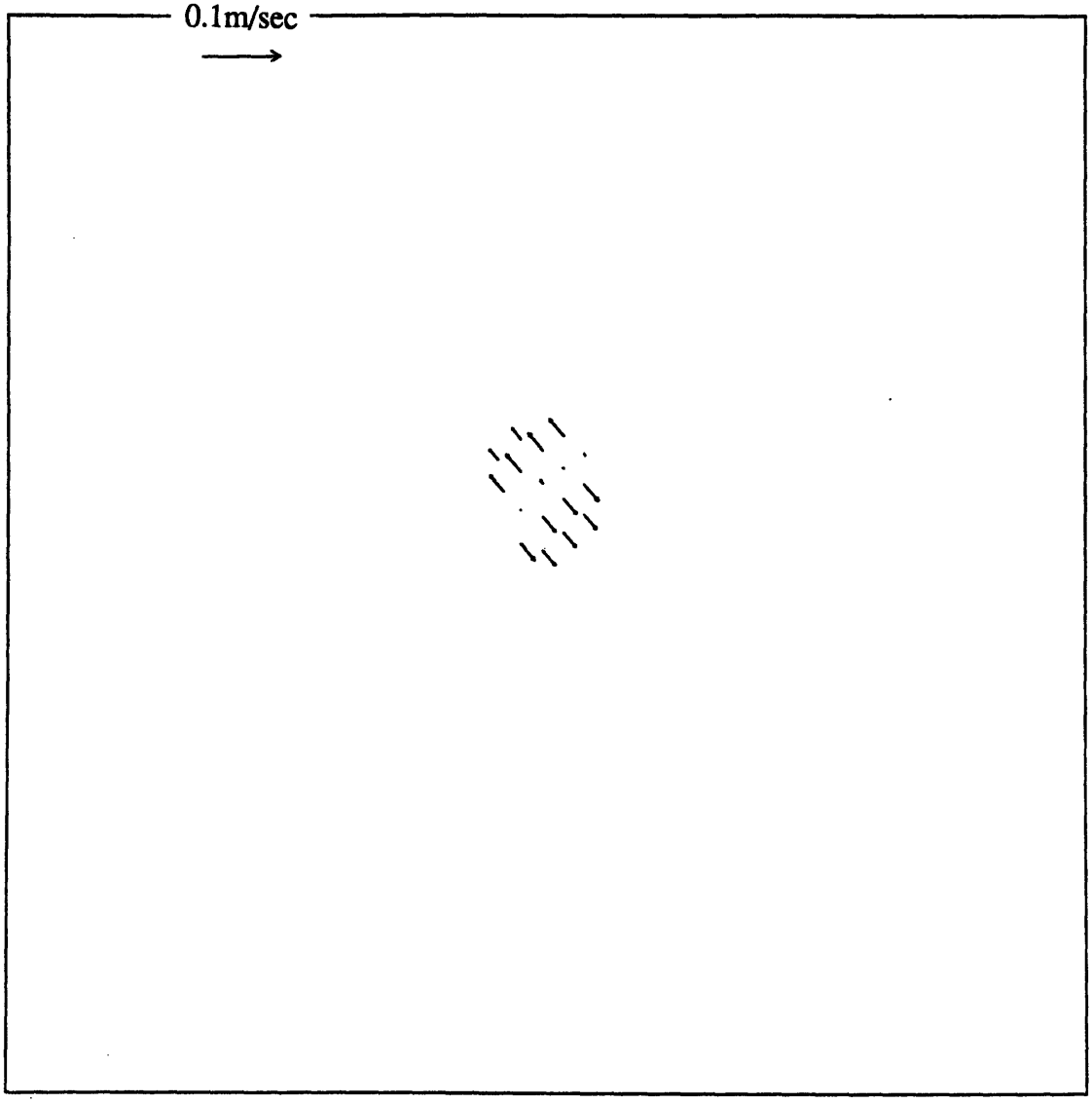

Figure 6-35: Density-driven flow field at the vicinity of the outfall (z = -10m mid-depth).

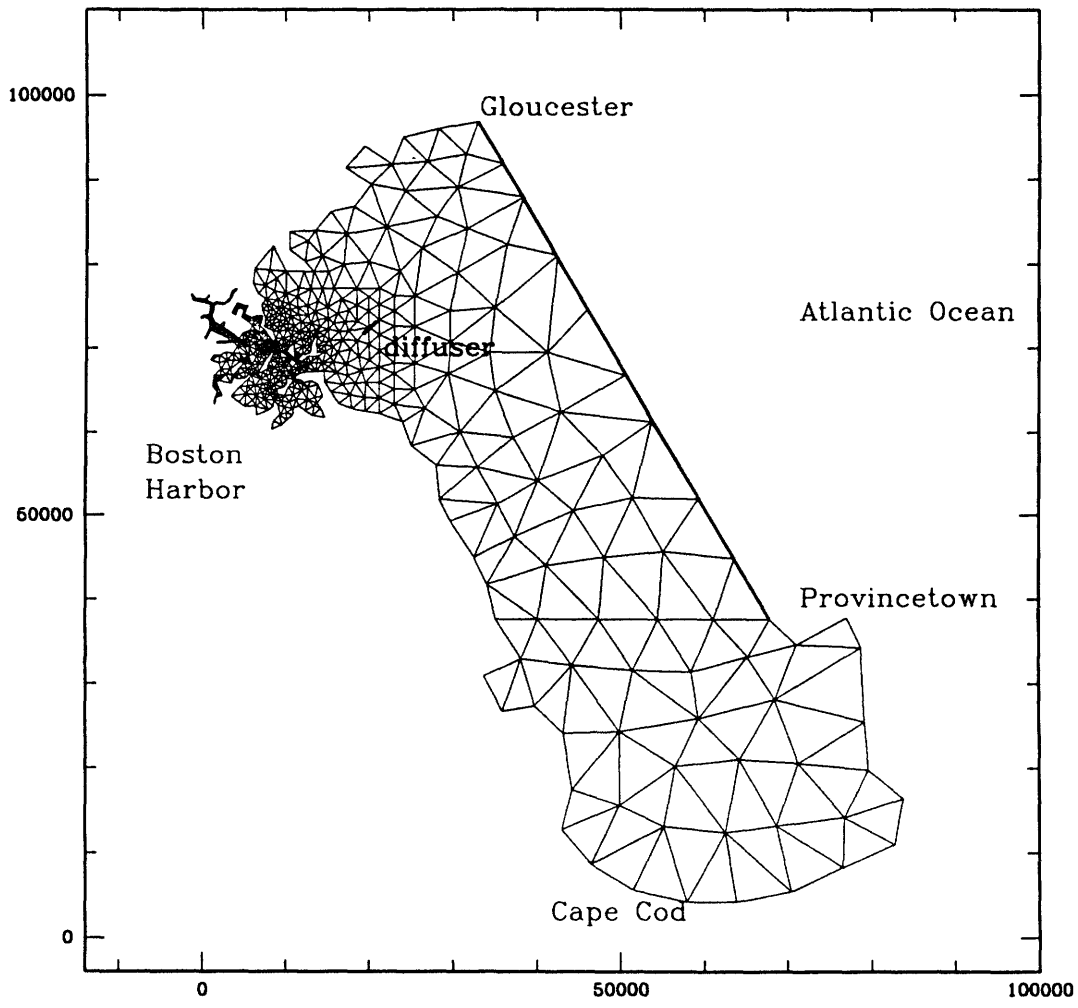

Figure 6-36: Location of diffuser.

Table 6.2: Settling velocities (EPA, 1988)

Percentage	Settling velocity
5	0.001
20	0.0001
35	0.00001
40	do not settle

Simulations

The modeling strategy is the following: Fine grained sediment discharged from the diffuser are modeled by particles whose settling velocities have the distribution shown in Table 6.2 (EPA, 1988). A time step $\Delta t = 3.1h$ is used. At each time step 1000 particles are released that represent 20000kg. These particles are advected based on the velocity field presented before and diffused. The horizontal diffusion coefficient used are $K_x = K_y = 2m^2/s$ and correspond to Peclet numbers of the order of 20 - 200. The vertical diffusion coefficient $K_z = 0.00001m^2/s$ which is a representative value for the degree of stratification (Koh and Fan, 1970). As soon as the particles reach the bottom they stay there and their tracking stops. Using the technique described in Chapters 4 and 5 each batch of the particles that are in the water column is projected onto node concentrations as soon as the standard deviation of its distribution reaches the value of $\sigma_{min} = 1300m$ which lies between one and two times the grid scale around the diffuser. In order to have a more continuous settling a finer settling velocity distribution than the one presented in Table 6.2 was used in the simulations (Table 6.3).

The depth in the vicinity os the outfall is 25m and the trapping level is $z_{tr} = -16.4m$ (Section 6.1.1). Each batch of particles in the particle mode reaches σ_{min} after 14 timesteps and so if vertical velocities are not taken into account a representative cutoff settling velocity of settled particles is of the order of $0.00006m/s$. In order to take into account the settling mechanism of the finer sediments handled in the concentration mode, an average downward vertical velocity w_{av} was superimposed in the velocity field (Fig 6-37). w_{av} must be of the order of $0.00001m/s$. In Fig 6-38

Table 6.3: Settling velocities (finer distribution)

Percentage	Settling velocity
5	0.001
4	0.0009
4	0.0007
4	0.0005
4	0.0003
4	0.0001
7	0.00009
7	0.00007
7	0.00005
7	0.00003
7	0.00001
40	do not settle

- Fig 6-41 a velocity velocity of $-0.00002m/s$ was used, in Fig 6-42 - Fig 6-45 a velocity velocity of $-0.00001m/s$ was used, and in Fig 6-46 - Fig 6-49 a zero settling velocity was used. It is clear that enhanced vertical velocity results in higher bottom concentrations and less elongated plumes due to the fact that horizontal velocities at the bottom are small. Due to the upward velocities in the intermediate flow field the concentrations in the vicinity of the diffuser tend to be uniform. Fig 6-50 show sediment concentration in mg/m^2/yr of all settled particles.

6.3 Discussion

The performance of the developed transport model was tested in two realistic test cases in Massachusetts Bay. The first test case involves the simulation of an instantaneous mass relese. Simulated results were compared with field data. The resulting differences are primarily due to the fact that a diagnostic hydrodynamic model is used. The second test case involves the simulation of a continuous discharge from a location close to the proposed diffuser location. There were no data available for comparison with simulated results. The next step should be the use of a hydrodynamic model, that also solves for temperature and salinity and the comparison of simulated

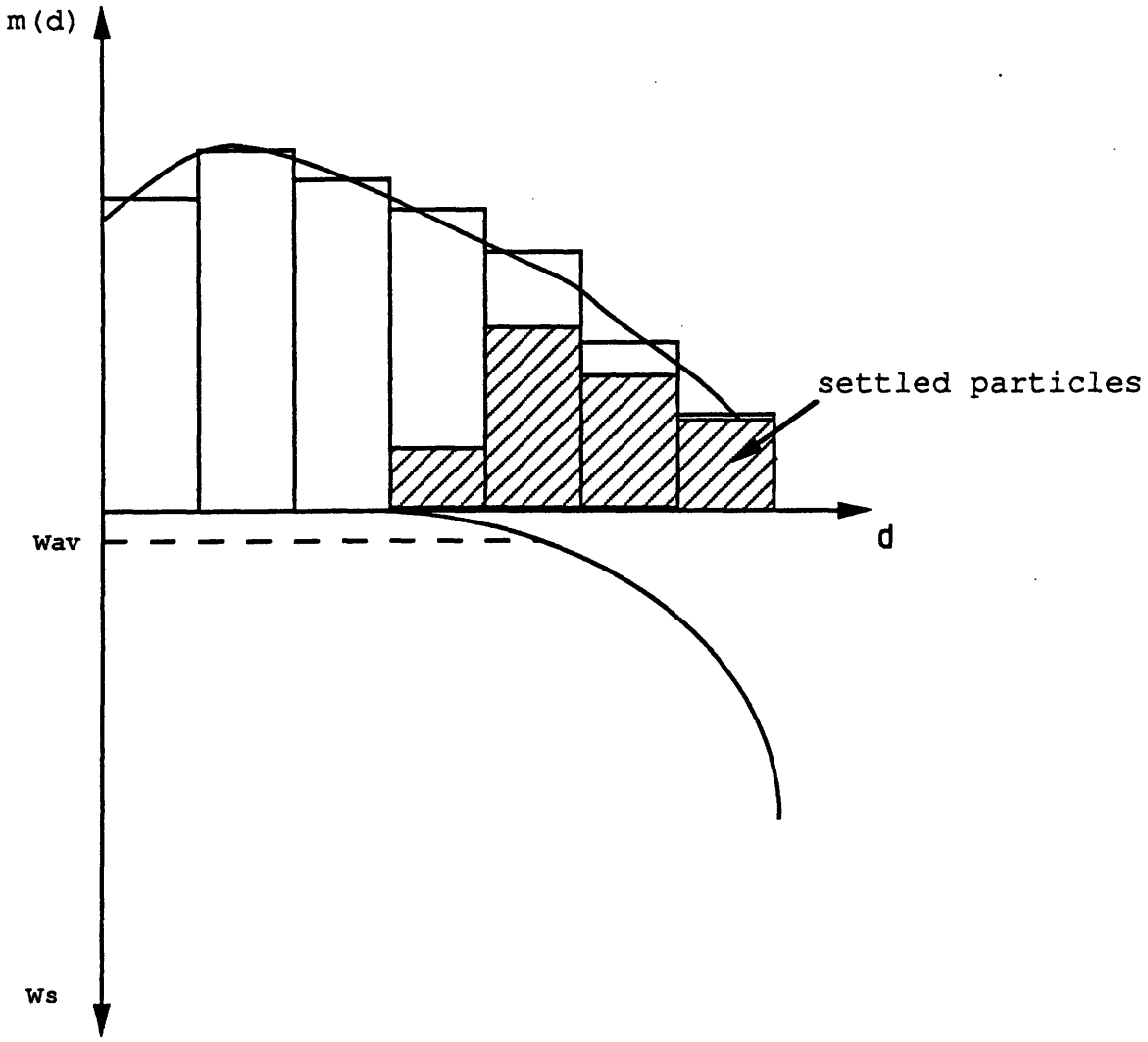

Figure 6-37: Schematic representation of modeling of unsettled particles. d is the particle diameter, m(d) is the mass of particles with diameter d, and w_s are the settling velocities.

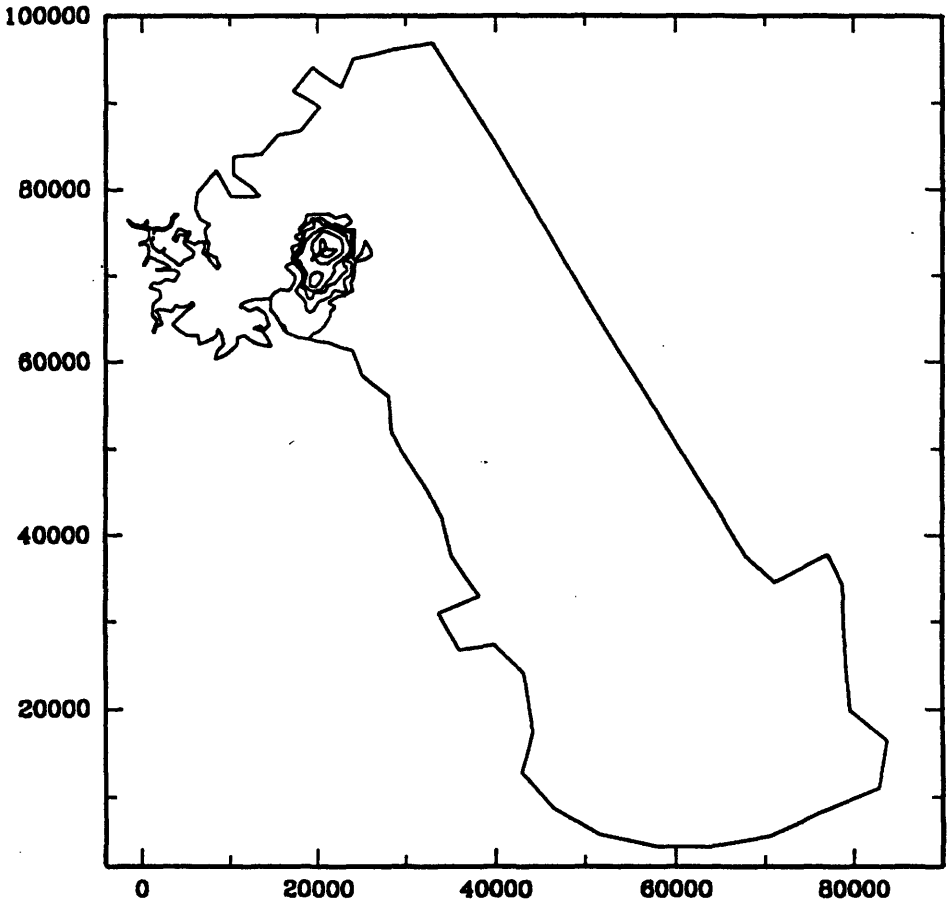

Figure 6-38: Concentration contours of 1., 0.5, 0.2, 0.1, 0.05 and 0.02mg/lt at the bottom at t=15d ($w_{av} = -0.00002m/s$).

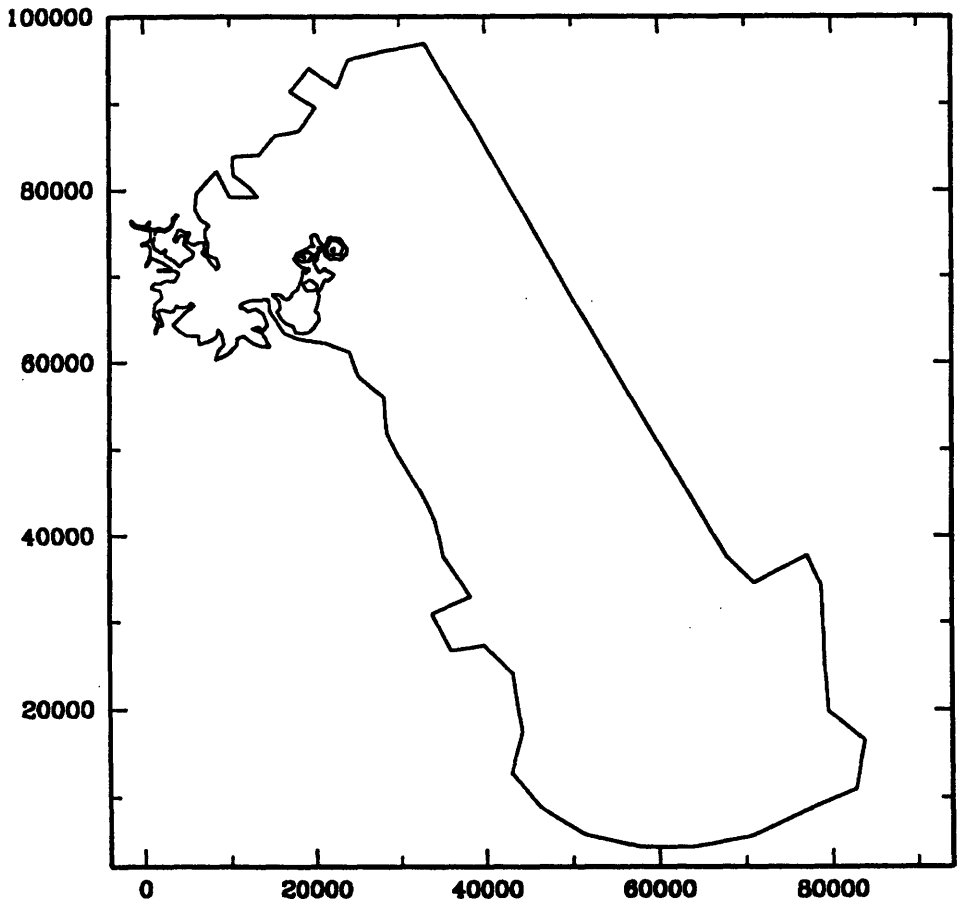

Figure 6-39: Concentration contours of 0.5, 0.2, 0.1, 0.05 and 0.02mg/lt at middepth at t=15d ($w_{av} = -0.00002m/s$).

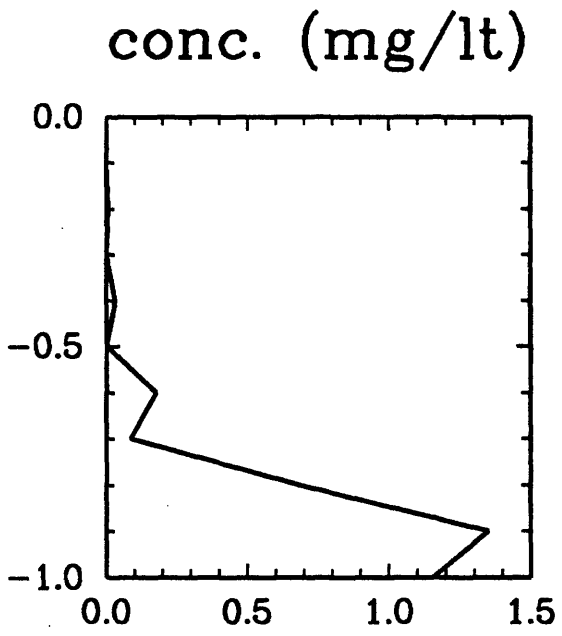

Figure 6-40: Concentration profile (mg/lt) at the location of the diffuser at t=15d ($w_{av} = -0.00002m/s$).

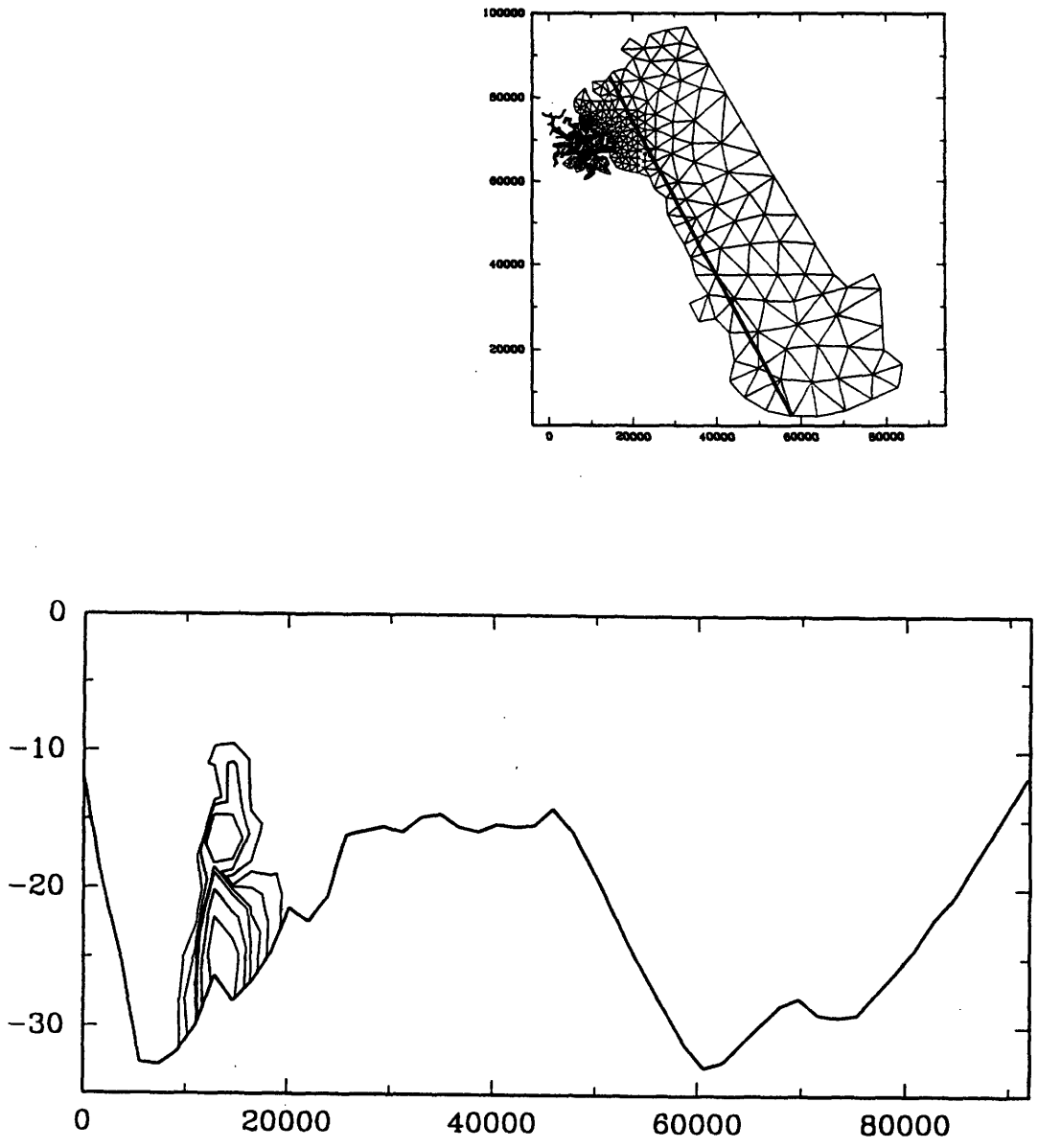

Figure 6-41: Concentration contours of 1., 0.5, 0.2, 0.1, 0.05 and 0.02mg/lt at a londitudinal crossection depicted at t=15d ($w_{av} = -0.00002m/s$).

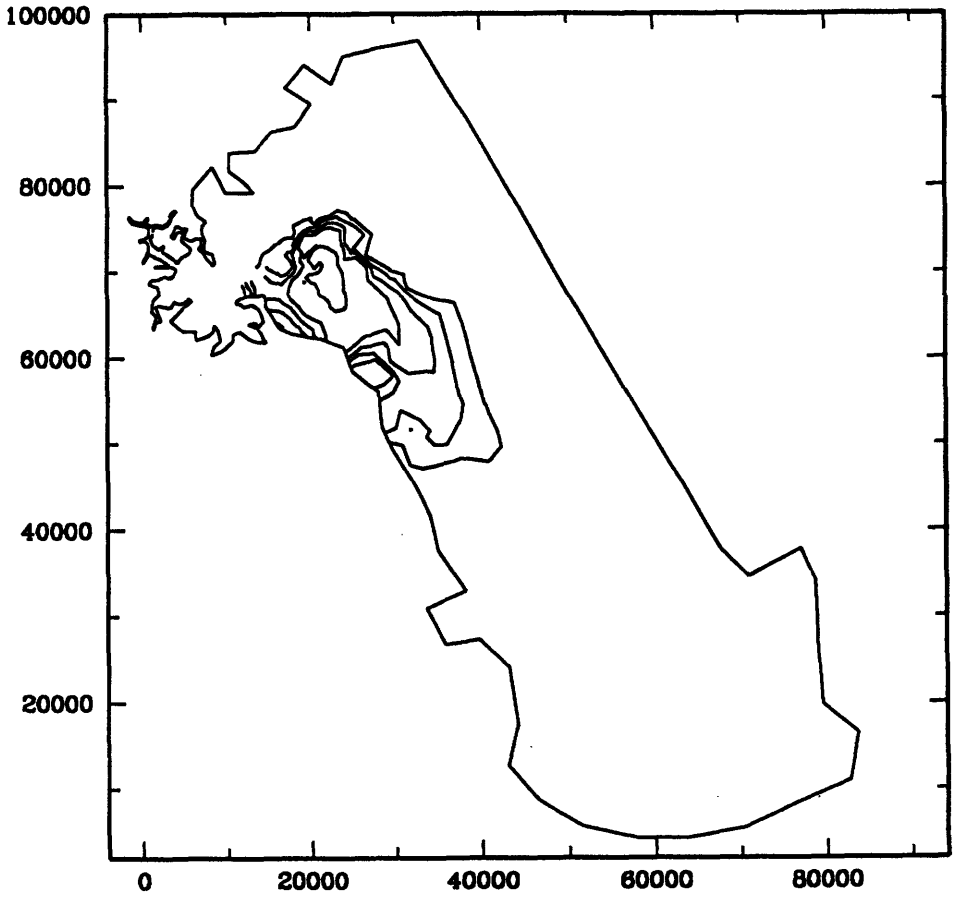

Figure 6-42: Concentration contours of 0.5, 0.2, 0.1, 0.05 and 0.02mg/lt at the bottom at t=15d ($w_{av} = -0.00001 m/s$).

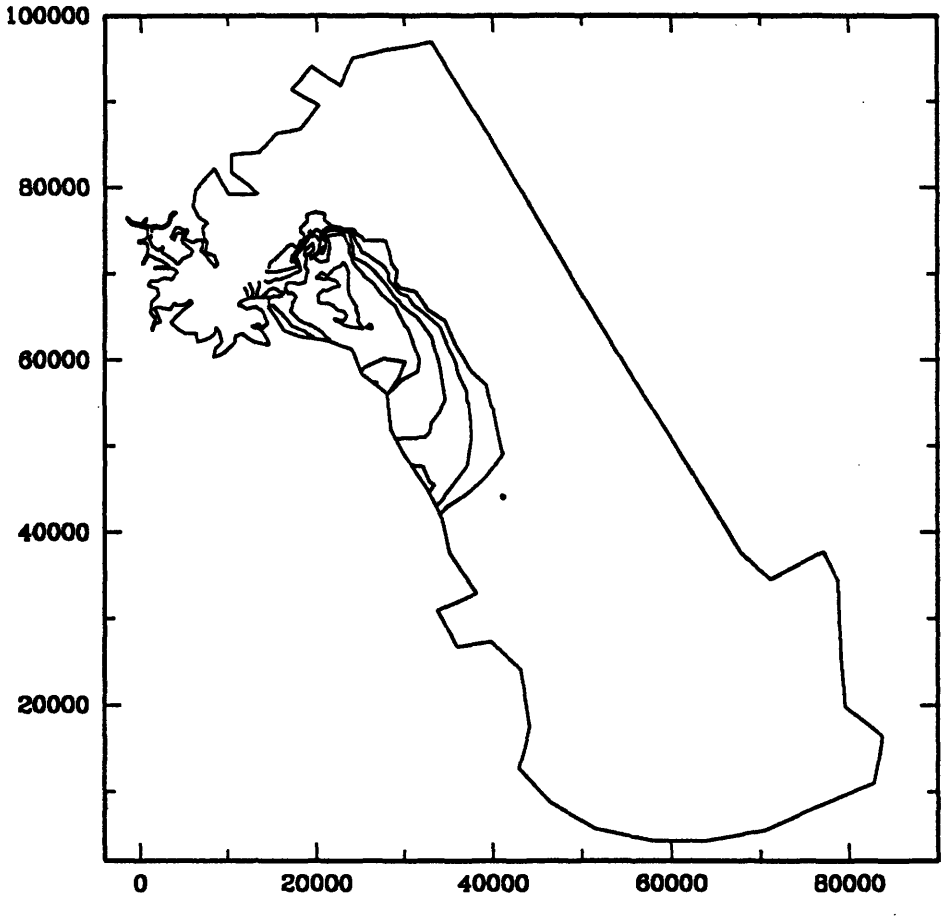

Figure 6-43: Concentration contours of 0.5, 0.2, 0.1, 0.05 and 0.02mg/lt at middepth at t=15d ($w_{av} = -0.00001m/s$).

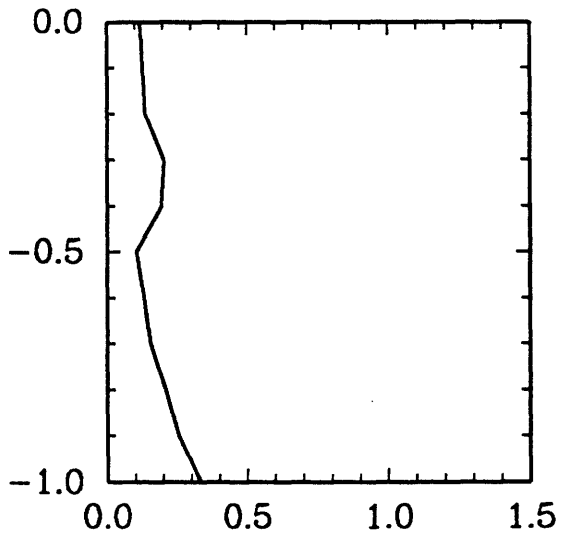

Figure 6-44: Concentration profile (mg/lt) at the location of the diffuser at t=15d ($w_{av} = -0.00001m/s$).

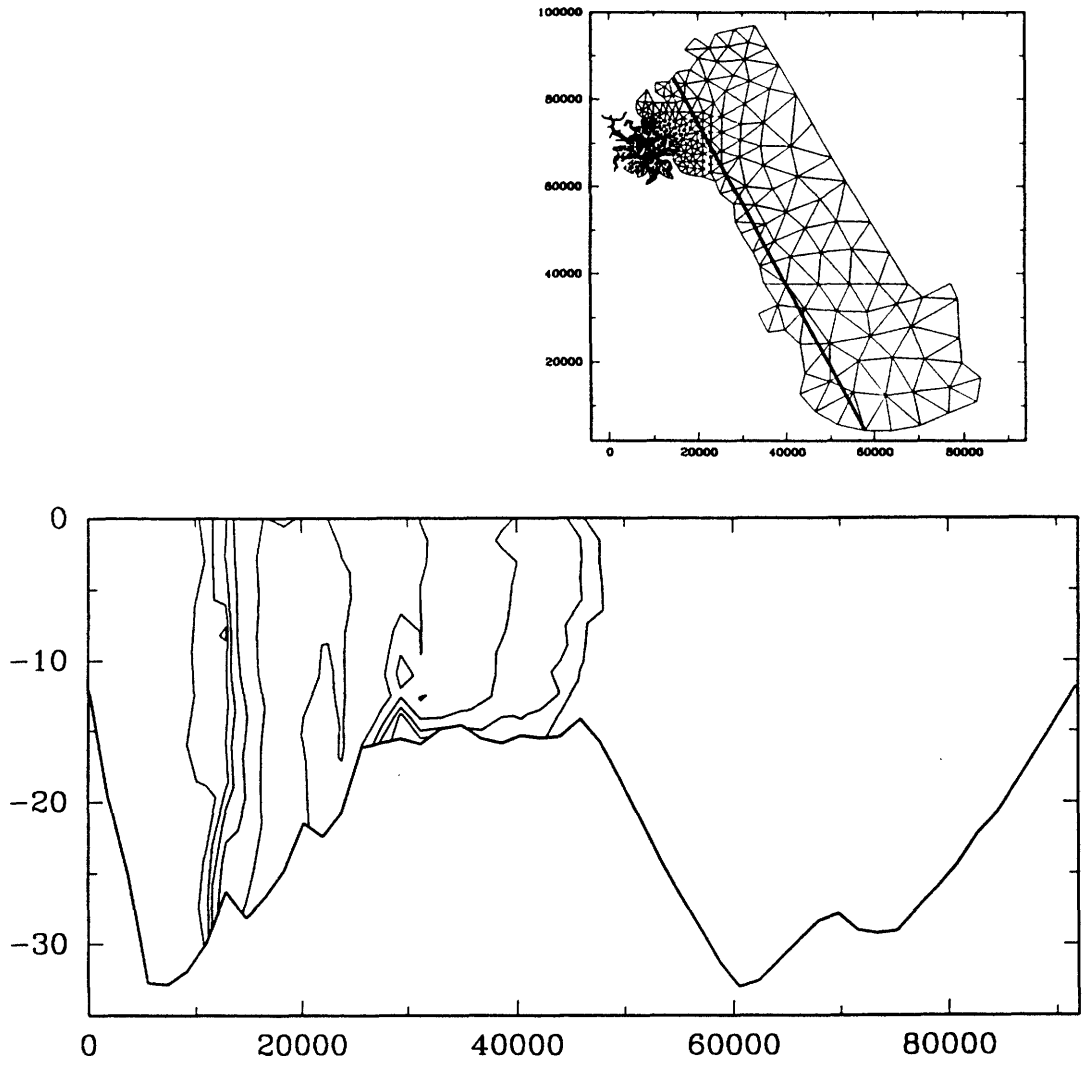

Figure 6-45: Concentration contours of 0.5, 0.2, 0.1, 0.05 and 0.02mg/lt at a londitudinal crossection depicted at t=15d ($w_{av} = -0.00001m/s$).

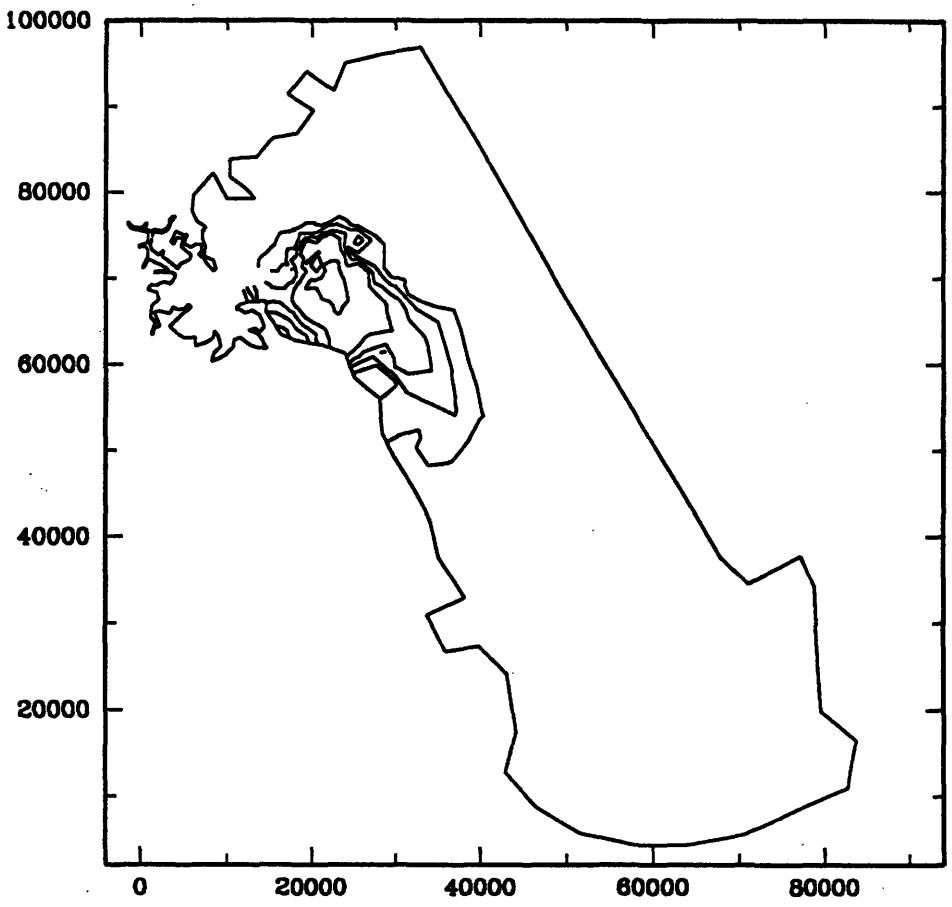

Figure 6-46: Concentration contours of 0.5, 0.2, 0.1, 0.05 and 0.02mg/lt at the bottom at t=15d ($w_{av} = -0.00m/s$).

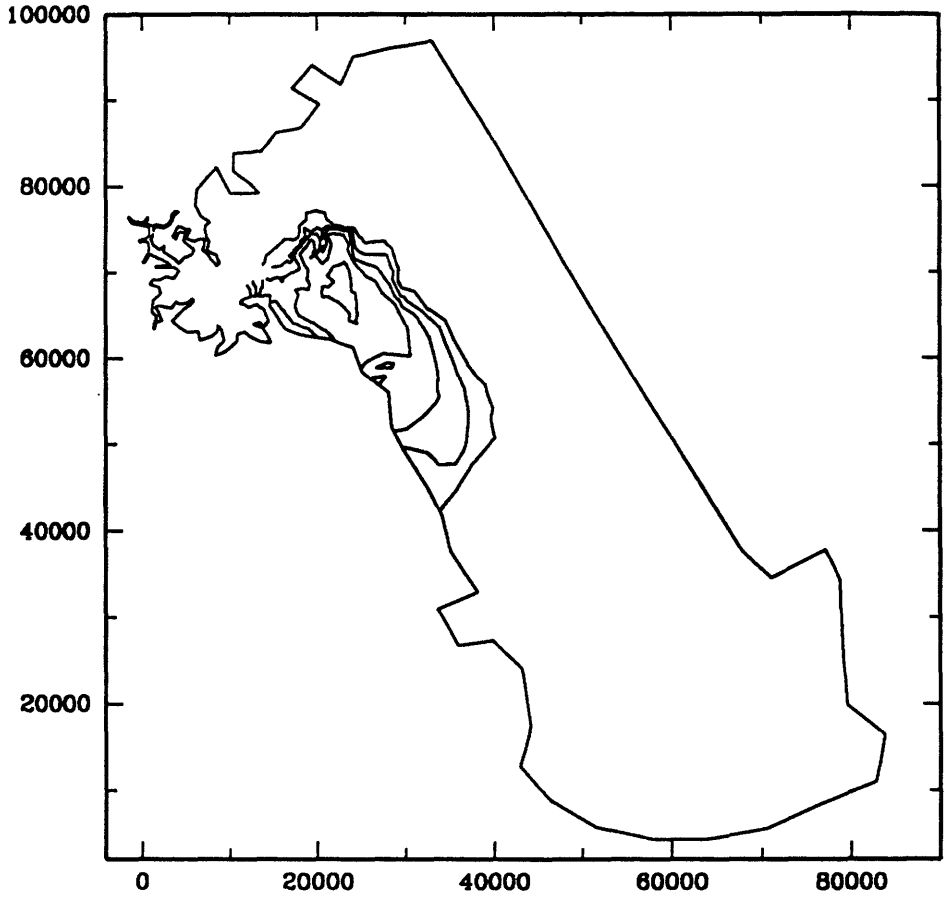

Figure 6-47: Concentration contours of 0.5, 0.2, 0.1, 0.05 and 0.02mg/lt at middepth at t=15d ($w_{av} = -0.00m/s$).

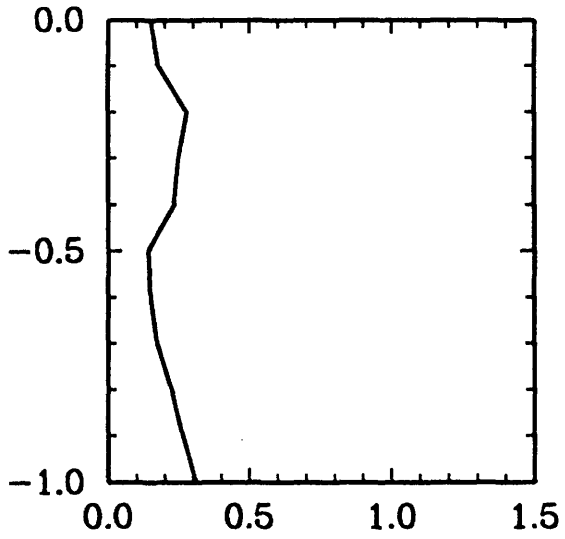

Figure 6-48: Concentration profile (mg/lt) at the location of the diffuser at t=15d ($w_{av} = -0.00m/s$).

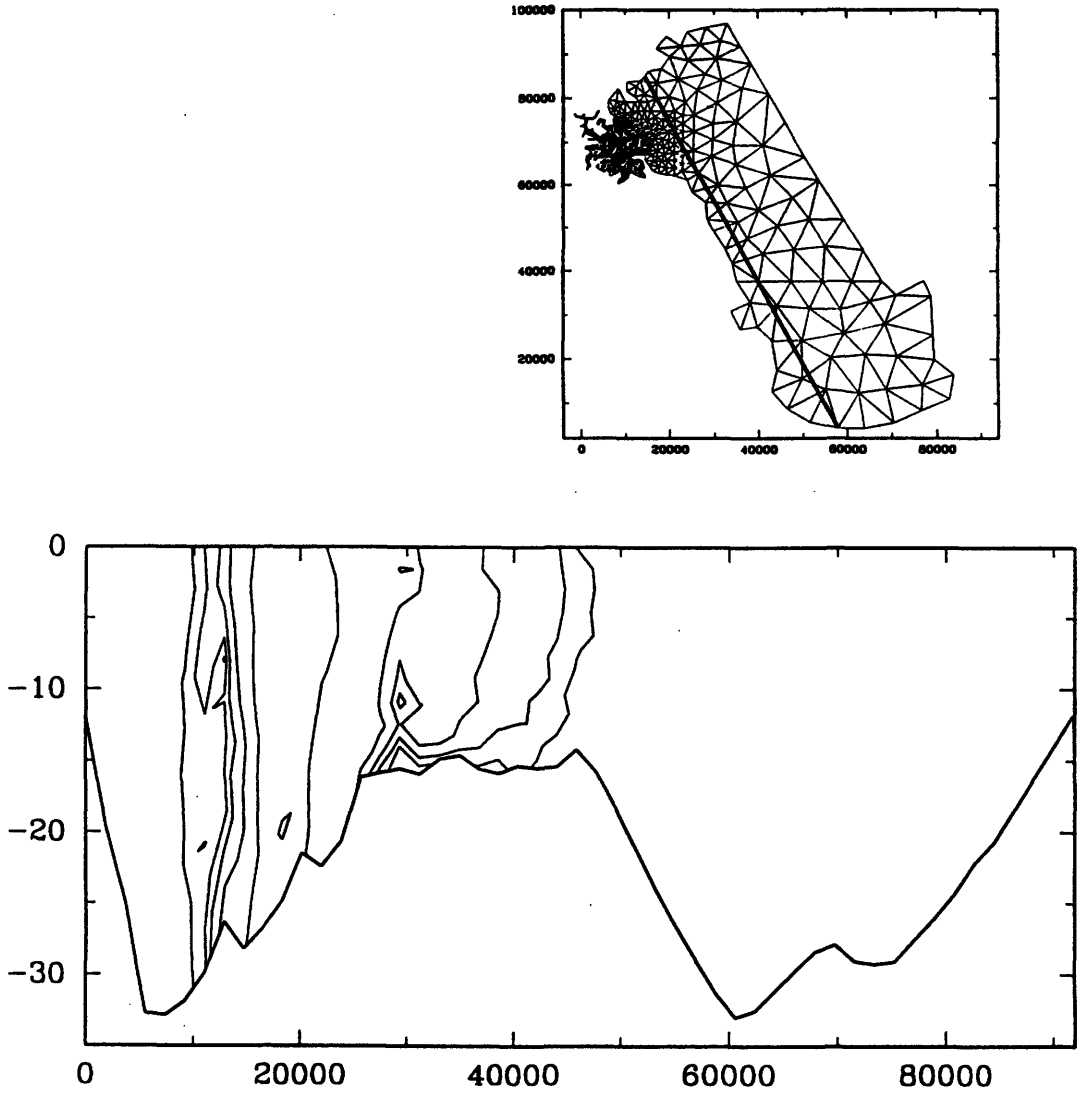

Figure 6-49: Concentration contours of 0.5, 0.2, 0.1, 0.05 and 0.02mg/lt at a londitudinal crossection depicted at t=15d ($w_{av} = -0.00m/s$).

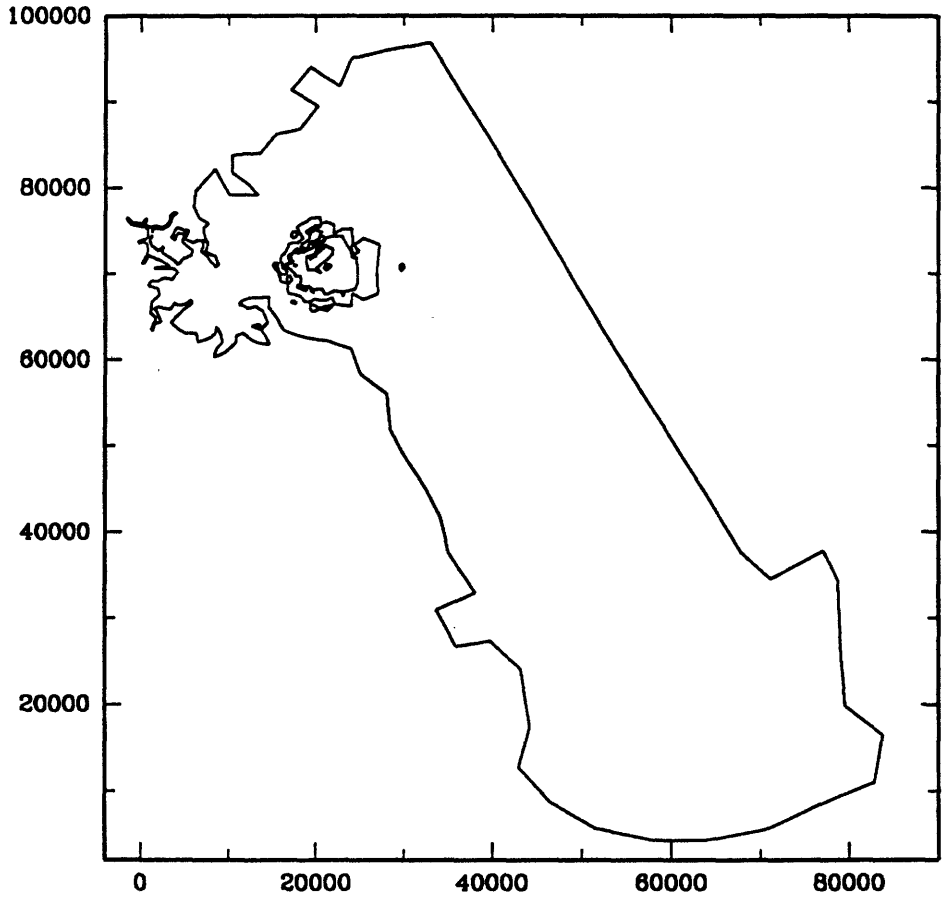

Figure 6-50: Concentrations of all settled sediments of 1000 to 10 g/mm^2/yr (w_{av} = $-0.00001m/s$).

results with field data as soon as there are any available.

6.4 REFERENCES

1. Adams, E. E., R. Kossik, A. E. M. Baptista. Source representation in a numerical model. In Finite Elements in Water Resources (ed. A. Sá da Costa et al.) pp589-598. Proc. of 6th Int. Conf. Lisboa, Portugal, 1986.

2. Baptista, A. M., E. E. Adams, and K. D.Stolzenbach. Eulerian-Lagrangian analysis of pollutant transport in shallow water. Technical Report No. 296. MIT. 1984.

3. Butman, B., and V. Fry. Atlas oftidal elevation and moored current observations in Massachusetts and Cape Cod Bays. 1970-1989. U.S. Geological Survey. Branch of Atlantic Marine Geology. Woods Hole, MA 02543. 1990.

4. Christodoulou, G. C., J. J. Connor and B. R. Pearce. Mathematical modeling of dispersion in stratified waters. R. M. Parsons Laboratory for Water Resources and Hydrodynamics. T. R. No219. MIT. October 1976.

5. Csanady, G. T. Turbulent diffusion in the environment. D. Reidel Publ. Co. 1973

6. Deardorff, J. W. On the magnitude of the subgrid scale eddy coefficient. J. Computational Physics. Vol. 7. Part 1. 1971.

7. EPA. Boston harbor wastewater conveyance system. Vol II. EPA. Region I. Boston, MA. 1988.

8. Garrett, C. J. R., J. W. Loder. Dynamical aspects of shallow sea fronts. Phil. Trans. R. Soc. London A302:563-581. 1981.

9. Helfrich, K. R., and T. M. Battisti. 1991. Experiments on baroclinic vortex shedding from hydrothermal plumes. J. of Geoph. Res. Vol. 96. No C7. pp 12,511-12,518.

10. Jirka, G. H., and R. L. Doneker 1991.Hydrodynamic classification of submerged single-port discharges. J. Hydr. Engrg., 117(9), 1095-1112.

11. Jirka, G. H., and P. J. Akar 1991.Hydrodynamic classification of submerged multiport-diffuser discharges. J. Hydr. Engrg., 117(9), 1113-1128.

12. Lee, J. J. 1990. Contaminant sediment transport in Boston Harbor. S. M. thesis. Dept. of Civil Engineering. MIT. 1990.

13. Lynch, D. R., F. E. Werner, D. A. Greenberg, J. W. Loder. Diagnostic model for baroclinic, wind-driven and tidal circulation in shallow seas. Continental Shelf Research. 1991 (to appear).

14. Muellenhof, W. P., et al. Initial mixing characteristics of muicipal ocean discharges Volume 1: Procedures and applications. Pacific Division Environmental Research Laboratory, Narragansett Office of Research and Development, U. S. EPA, Newport, Oregon 97365. EPA -600/3-85-073a. 1985.

15. Roberts, R. J. W. 1977. Dispersion of buoyant waste discharge from outfall diffusers of finite length. Rep. No. KH-R-35. W. M. Keck Lab. of Hydrauli. and Water Resources. California Institute of Technology, Ca. 183pp.

16. Roberts, R. J. W. 1979. A mathematical model of initial dilution for deepwater ocean outfalls. Proceedings of a specialty conference on conservation and utilization of water and energy resources. San Francisco, CA. Aug. 8-11. Am. Soc. Civ. Eng. pp. 218-225.

17. Roberts, R. J. W., W. H. Snyder, and D. J. Baumgartner. 1989. Ocean outfalls. J. Hydr. Engrg.,ASCE, 115(1).

18. Koh, R. C. Y., and L. N. Fan. Mathematical models for the prediction of temperature distribution resulting from the discharge of heated water into large bodies of water. Tetra Tech, Inc. Pasadena, CA. 1970.

19. Tetra Tech. 1982. Revised section 301(h) technical support document. EPA

430/9-82-011. U. S. Environmental Protection Agency, Office of Water Program Operations, Washington, DC. 208 pp.

20. Vreugdenhil, C. B. and Voogt, J. Hydrodynamic transport phenemena in estuaries and coastal waters: Scope of mathematical models. Symposium on modeling techniques. Modeling '75. San Francisco. September 1975.

Chapter 7

Summary - Future Work

7.1 Summary

The main contribution of this work can be summarized as follows:

- Development of a 3-D Eulerian Lagrangian model for the transport of passive constituents in coastal water bodies.

- Development of a method for the simulation of sources whose extend is small compared to the extend of the grid discretization. This method can be briefly described as follows: Sources are simulated by the release of particles. These particles are advected and diffused according to a particle tracking model. When the standard deviation of their distribution reaches the value σ_{min} which is of the order of the grid scale particles are mapped onto node concentrations and the calculations continue in the concentration mode. A method was developed for interfacing the particle mode with the concentration mode. This method was compared with existing methods and proved to be of the same degree of accuracy and particularly efficient for irregular finite element grids. This methodology for simulating sources is general and could be applied in any case where the modeling of small scale sources is required.

- Development of a method for simulating diffusers in coastal waters. Since the emphasis of this work is on surface water problems the method for simulating sources was applied for the simulation of sea outfalls. The additional issue of representing the flow field in the vicinity of the sea outfall was also analyzed.

7.2 Future Work

This work is primarily concerned with the development of methods in the area of 3-D transport modeling. This section presents some recommendations for further application of the developed model.

- Coupling of the developed 3-D transport model with a stepping HM Due to stability requirements a HM uses time steps of the order of minutes while a TM can use time steps of te order of hours. An extensive literature review of methods used in the past is presented in this study and a new method is proposed for coupling the two models by taking advantage of the Lagrangian character of the calculations. The following is suggested as future work. Implementation of the proposed coupling method in a real case. The Chesapeake Bay study (Dortch, 1990) is the only study where the problem of coupling the HM with the TM was considered. It would be useful to compare the Lagrangian residual method used there with the proposed Eulerian-Lagrangian method by using intratidal and intertidal time steps. The use of intratidal time steps would be of particular interest because the Lagrangian residual method fails to accomodate intratidal time steps due to the Courant number restriction. It would also be interesting to use the proposed method in the case of highly nonlinear coastal bodies or in the vicinity of headlands where the Lagrangian currents fail to represent the residual currents. This would show the superiority of the Eulerian-Lagrangian method from a cost and accuracy point of view.

- Modeling of Intermediate Flow Scale Phenomena The issue here is the modeling of phenomena whose space scale is small compared to the space scale of the

computational domain. The method developed in this research for modeling diffusers could also be used to model phenomena that occur in the intermediate field zone e.g. modeling of sediment settling around the outfall or the modeling of the exchange of constituents in the euphotic zone.

- Utilization of the particle mode The particle tracking mode is used in this research for simulating sources. Particle tracking models can also be used for modeling processes that depend on the behavior of individual particles rather than their aggregation. In a 2-D study (Dimou and Adams, 1989) this feature of a particle tracking model was utilized for modeling the entrainment of larvae through the cooling station of a nuclear power plant at Millstone Point, Connecticut. In this research this ability of the particle mode is demonstrated in an example for settling of particles in Massachusetts Bay.

- Inclusion of Many Sources A challenging aspect of this model from a cost efficiency point of view would be the modeling of several sources. A good example here is the modeling of the combined sewer overflows (CSO) in Boston Harbor.

- Sigma vs. Cartesian Coordinate System In Chapter 2 the advantages and disadvantages of each coordinate system are mentioned. The choice of the coordinate system is left to the HM. In this study a sigma coordinate system was used for compatibility reasons with the available HM. It would be interesting to couple the TM with a cartesian coordinate system HM and compare the results of the two simulations.

- Large Scale Application In this study a demonstration application in Massachusetts Bay was conducted. It is mandatory to test to performance of the model by comparing the results of the simulations with field data.

7.3 REFERENCES

1. Dimou, K. N. and E. E. Adams. 1989. Application of a 2-D particle tracking model to simualte entrainment of winter flounder larvae at the Millstone Nuclear Power Station. Report No. MIT-EL 89-002. Energy Laboratory. MIT.

2. Dortch, M. S. 1990. Three-Dimensional, Lagrangian Residual Transport Computed from an Intratidal Hydrodynamic Model. Technical Report EL-90-11, US Army Engineer Waterways Experiment Station, Vicksburg, MS.